An Electrochemical and Leach Study of the Oxidative Dissolution of Chalcopyrite in Ammoniacal Solutions

---

by

Thandazile Moyo

This thesis is presented in fulfillment of the requirements for the degree of Doctor of Philosophy in Engineering

Faculty of Engineering and the Built Environment

Department of Chemical Engineering

University of Cape Town

April 2016

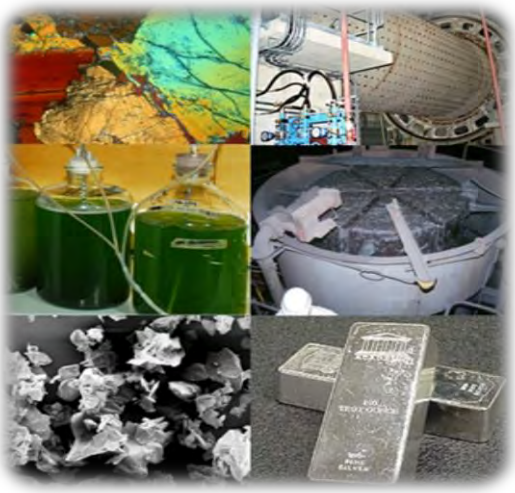

Department of Chemical Engineering

Minerals to Metals Initiative

Abstract

Chalcopyrite is not only the most abundant of the copper sulphides, but also the most stable, making it recalcitrant to hydrometallurgical treatment processes especially in atmospheric leaching. Hence, pyrometallurgical processes are traditionally used to treat chalcopyrite concentrates. However, ore grades are falling and concentration processes are becoming increasingly costly, prompting need to revisit hydrometallurgical treatment processes (especially heap leaching), which are otherwise regarded as relatively economic and environmentally friendly.

Key hydrometallurgical processes for chalcopyrite treatment are ferric sulphate, chloride and ammoniacal systems. The ferric sulphate system does not work well under atmospheric conditions, except in combination with thermophilic microorganisms, whereas the chloride system has only recently been evaluated more seriously for heap leach processes. The ammonia system remains relatively unexplored and most studies date back more than 40 years, but the system has considerable potential for further development.

Ammonia systems can be effectively used to leach copper from chalcopyrite in the presence of an oxidant. The ammoniacal leaching system is heavily reliant on a good surface mass transfer system, hence it being widely studied in high pressure systems where oxygen was accepted to be the oxidant. Leach reactors were designed to use agitation systems which promote the abrasion of an iron based deposit layer thought to passivate the mineral surface. Most research on the ammonia leaching systems has previously been carried out in controlled or bulk leaching studies and only a few used electrochemical studies. A disconnect exits between the two approaches, resulting in different proposed fundamental reaction mechanisms and kinetic understanding.

A fundamental electrochemical and controlled leach study of the oxidative leaching of chalcopyrite in ammoniacal solutions has been undertaken. The study covered the following aspects: a description of the mixed potentials, chemistry and kinetics of the anodic reaction, the cathodic reduction of the oxidants, the formation and effect of surface deposits and lastly a look at how results from electrochemical studies compare to those from the leaching of a similar mineral sample under similar solution conditions.

A detailed study of the mixed potentials on a more or less pure chalcopyrite electrode has shown the redox reactions on the surface of the mineral to be controlled by the oxidation of chalcopyrite and reduction of copper(II). The presence of oxygen has been found to have no significant effect on mixed potentials in ammoniacal solutions in the presence of initial copper(II).

Constant potential and potentiodynamic studies on the anodic reaction have shown the rate of the anodic reaction to increase with an increase in potential in a standard 1M ammonia/ammonium sulphate solution (which buffers at pH 9.6) in exponential fashion supporting conventional Butler-Volmer behaviour with a anodic transfer coefficient of 0.42 and a rate constant k^*_{CuFeS2} of 0.0431 cms^{-1}. Increasing total ammonia increased the rate of reaction only at low concentrations; at higher concentrations increasing total ammonia had no effect on the anodic reaction. An increase of pH at fixed total ammonia concentration showed an increase in reaction rate, but the effect cannot clearly be discerned from the concomitant shift in relative proportion of free NH_3 and NH_4^+.

Coulometric studies have shown the oxidation reaction to proceed via the formation of a thiosulphate intermediate and this to be a 7-8 electron transfer reaction. A surface deposit layer consisting of iron, oxygen and small quantities of sulphur was formed and the sulphur component of this product layer was seen to be gradually depleted during leaching. Anodic currents were found to gradually decrease with time and this was linked to the growth of the surface deposit layer. However, the surface deposit layer did not passivate the anodic reaction; instead, it was proposed that the surface deposit layer adsorbed copper ions and displayed “ohmic” behaviour.

The formation of the surface deposit layer was found to apparently promote the cathodic reduction of copper(II). While reduction of copper(II) was shown to be the primary reduction reaction, the presence of oxygen was seen to promote this reduction reaction through the regeneration of copper(II) in experiments that ran for longer time periods. An apparent accumulation of copper(I) on the mineral surface was seen to adversely affect the rate of the cathodic reaction and thus the overall rate of dissolution. The nature and morphology of the surface layer was found to be significantly influenced by the choice of cation in solution, which was thought to influence primarily the complexation/precipitation of ferric species forming near the surface. The degree of agitation during leach studies influences the rate of leaching due to the fragmentation of surface deposits, which are seen to slow the anodic reaction. A kinetic model has been developed for the anodic and cathodic reactions.

This thesis presents significant new findings regarding the role of the copper(I)/copper(II) redox couple on the oxidative leaching of chalcopyrite. It also highlights the potentially limiting role of the cathodic reactions which have frequently been overshadowed by the focus on chalcopyrite oxidation reactions. Furthermore, the growth of a surface inhibiting layer which cannot be removed in heap leach systems due to the lack of mechanical agitation can now potentially be addressed by looking into the complexation and precipitation characteristics of cations in solution for ammoniacal leach systems.

Acronyms

AAS	Atomic Absorption Spectroscopy
Atm	Atmosphere
BET	Brunauer–Emmett–Teller
BV	Butler-Volmer
CV	Cyclic Voltammetry
EDS	Energy Dispersive Spectroscopy
E_f	formal potential
EIS	Electrochemical Impedance Spectroscopy
E_m	equilibrium potential
EU	European Union
FEG	Field Emission Gun
ICP-OES	Inductively Coupled Plasma Optical Emission Spectroscopy
ICSG	International Copper Study Group
OCP	Open Circuit Potentials
QEMSCAN	Quantitative Evaluation of Minerals by Scanning Electron Microscopy
SCE	Saturated Calomel Electrode
SEM	Scanning Electron Microscopy
SHE	Standard Hydrogen Electrode
SPEM	Scanning Photoelectron Microscopy
UV-Vis	Ultra Violet-Visible Spectroscopy
XPS	X-ray photoelectron spectroscopy
XRD	X-Ray powder Diffraction

XRF	X-ray Fluorescence

Declaration

I know that plagiarism is wrong and hence, I declare that this thesis is my own work and I have duly acknowledged other people's work with an acceptable form of referencing. This thesis has not been submitted before for any degree or examination in any other university.

Thandazile Moyo

14 April 2016

Acknowledgements

It is my pleasure to acknowledge and thank the following individuals and organisations who have kindly assisted in one way or another in the work carried out for the completion of this thesis;

I would like to express my sincere and deep gratitude to my principal supervisor, Professor Jochen Petersen for his guidance, support, tolerance and encouragement throughout the course of my studies. I would like to extend my gratitude to Professor Michael Nicol for his guidance for the duration of this work; I drew inspiration from his years of dedication and commitment to teaching and research in the field of hydrometallurgy.

I would like to acknowledge the input through focused group discussions, of the Bio-Hydrometallurgy group at the Centre of Bio-Engineering Research, UCT. My heartfelt thank you goes to the Hydrometallurgy group UCT for the group discussions carried on around my research topic and special mention to Rahul for proof reading my thesis. Particular thanks to Emmanuel Ngoma for his assistance in the lab. I would like to acknowledge the financial support of the NRF through the Minerals to Metal Initiative and special thanks to Prof J-P Franzidis who took this project on-board.

To my friends, Betina, thank you for cheering me on and reminding me why I started on this journey; Margreth, thank you for sharing in the tears and joys, for hearing me out through the epiphany moments that were and that never were; and all my friends that I have not mentioned by name, your encouragement and prayers are truly appreciated. I express my deep gratitude to my parents, who have not lived to see the dream take shape, but remained an inspiration through every step. I would like to thank my siblings, for believing in me even when I could not believe in myself, and for constantly urging me on. To my husband Eddie and our lovely daughter Angelica, who have been my anchor and campus through it all, I say thank you; this thesis equates to nothing in comparison to you. Lastly, I thank and praise the Lord God, in whose faith this work came to be.

List of publications and presentations

Moyo, T., Petersen J., Franzidis J-P. 2013. The electrochemical oxidation of chalcopyrite in ammonia-ammonium sulphate solutions in the presence of initial cupric ions. Paper presented at the 31st Annual SAIMM Mineral Processing Conference, 6-7 August, Cape Town, South Africa.

Moyo, T., Petersen, J., Franzidis, J-P. and Nicol, M.J. 2014. An electrochemical study of the dissolution of chalcopyrite in ammonia-ammonium solutions. Paper presented at the 7th International Symposium; Hydrometallurgy, 22-25 July, Victoria, British Columbia.

Moyo, T. and Petersen, J. 2016. Study of the Dissolution of Chalcopyrite in Solutions of Different Ammonium Salts. The Journal of The Southern African Institute of Mining and Metallurgy. Vol 115, 509-516

Moyo, T., Petersen, J., Franzidis, J-P. and Nicol, M.J. 2015. An electrochemical study of the dissolution of chalcopyrite in ammonia–ammonium sulphate solutions. Canadian Metallurgical Quarterly, Volume 55 (3), 269-278.

Contents

List of Figures

List of Tables

1 Introduction

1.1 Background

Copper and copper-based alloys are used in a wide range of day to day applications necessary for a reasonable standard of living and hence its continued production and use is essential for society's development (International Copper Study Group, 2015). While demand for copper from world economic powers appears to be decreasing – a decrease of 4% recorded for the European Union (EU) and 1.5% for the Americas; – the worlds emerging economies continue to push up the demand for copper, with China being the leading consumer taking up 45% of the world copper production according to a report by the International Copper Study Group (International Copper Study Group, 2015). It has been projected that the world's demand for copper will continue to grow (AQM Copper Inc, 2015) due to overall urban population increases; which translates to demand for infrastructure and in turn demand for copper required as part of the construction material.

Copper is classified as a chalcophilic element i.e. it has a strong affinity for sulphur in its reduced state, commonly forming sulphide minerals (Dixon, 1979). Chalcopyrite ($CuFeS_2$) is the major source of copper in the world, making up 70% of the world's copper reserves (Fuentes-Aceituno et al, 2008). Traditionally, the mineral has been processed via concentration by flotation, smelting and converting to produce blister copper with a copper content of 98-99% copper. This traditional pyrometallurgical processing route is regarded economically viable for sulphide ores of grades higher than 2% which are upgraded through flotation to concentrate grades between 20 and 30% (U.S. Congress, Office of Technology Assesment, 1987). In the recent years, hydrometallurgy based process routes have gained major interest as an alternative means of processing copper owing to the depletion of high grade ores, and hence a need to economically exploit low grade and mixed grade copper ores. In the present day, pyro-metallurgy plants are equipped with flue gas scrubbers which combat the problems of sulphur dioxide which in the past was commonly cited as part motivation for exploring hydrometallurgy based process options. In the recent years, of major concern are the declining grades of copper ores hence a need to find alternative ways to economically extract the metal. Hydrometallurgy based process routes, specifically through heap leaching, are major contenders as alternative options to economically recover copper from low and mixed grade ores. These also have potential to be viable at either small or large scale production.

Chalcopyrite is not only the most abundant source of copper; it is also recalcitrant to hydrometallurgical treatment processes. Research undertaken in order to enhance the leaching rate of chalcopyrite spans several decades but none the less, no hydrometallurgical process for

chalcopyrite has enjoyed sustained commercial success and many processes have never been attempted at commercial scale. Several hydrometallurgical treatment options have been explored for chalcopyrite, including ferric sulphate (biotic and abiotic), chloride, ammonia and nitrate leaching, as will be discussed in section 2.2. Acid leaching processes, pressurised, biotic and abiotic and mostly at high temperature, have received the most attention from researchers, some of which reached commercialisation stage and these have been reviewed by Dreisinger (2006) who presents the advantages and disadvantages of each process. The most widely studied acid leach systems, the ferric leach system, biotic and abiotic, are characterised by slow leach kinetics and face challenges of low copper recoveries, precipitation of elemental sulphur and high energy requirements for size reduction and mixing. The chloride systems on the other hand, although showing more promising kinetics than the sulphate system, face challenges of corrosion in the plant. Historically, ammoniacal leaching of sulphide ores has been evaluated and showed success, evident from the commercialisation of the Sherritt Gordon (Forward and Mackiw, 1955) process and for chalcopyrite concentrates specifically, Anaconda's Arbiter process (Kuhn et al, 1974).

This thesis focuses on the ammoniacal leaching of chalcopyrite. Ammonia metallurgy has the merits of a high leaching rate, good selectivity, easy purification process, less corrosion and lower reagent consumption for calcareous carbonate gangue (Xi et al, 2011; Shao-hua et al, 2005). Although it has received attention and focus as an area of research in the past, ammoniacal leaching has in the more recent years been overlooked in favour of acid leach systems. The acid leach systems still remain the subject of research to date as researchers have not reached consensus on the causes of the experienced poor leach kinetics or how best to overcome them. This thesis seeks to revisit ammoniacal leaching and build on the work of previous researchers by looking at gaps that may have been overlooked in the past. It is the aim of this study to further elucidate the surface reactions and explain the kinetics of ammoniacal chalcopyrite leaching. Factors such as the commonly reported, but unexplained catalytic effect of copper(II) ions on the anodic reaction (Muzawazi, 2013; Warren and Wadsworth, 1984; Beckstead and Miller, 1977a; Tozawa et al, 1976) and the exact influence and characterisation of the iron-based surface precipitate will be explored. A look into the mechanism of the reaction in light of the findings on the role of copper (II) ions and influence of the so called surface deposit layer will be pursued.

Above and beyond the broad scope to which an understanding of ammoniacal leaching systems is of relevance, its significance has been demonstrated in work on the pre-treatment of Platreef concentrates which were reported to show improved recoveries when pre-leached to remove base metals. The pre-treatment also referred to as pre-leach step, was said to make the precious group

metals in the ore, more amenable to the next stage of leaching (Mwase et al, 2012). Muzawazi and Petersen (2015) then went on to show that this first stage leach could be carried out in ammoniacal solutions thereby combatting the otherwise tedious process of caustic washing the ore heaps to neutralise residual acid that would be left after an acid based pre-leach step, and prevent hydrogen cyanide formation in the cyanide leach stage. Muzawazi and Petersen's (2015) study showed trends consistent with an autocatalytic leaching process, which can be linked back to the reports on the catalytic effect of copper(II) from previous studies (Warren and Wadsworth, 1984; Beckstead and Miller, 1977a; Tozawa et al, 1976).

In the current study, chalcopyrite leaching in ammoniacal solutions will be investigated, looking at the effects of changing various solution parameters as well as the effect of growth of surface deposits on the kinetics of the oxidation and reduction reactions. Furthermore, electrochemistry techniques have gained popularity as a tool to study mineral leaching reactions but little has been done to reconcile results and models from electrochemistry studies to bulk leaching studies, more so, for the ammoniacal leaching of chalcopyrite.

The objectives of this study are to:

- Establish the role of the copper redox couple in the dissolution of chalcopyrite in ammonia-ammonium sulphate solutions.
- Evaluate the mechanism of chalcopyrite leaching in ammonia-ammonium sulphate solutions.
- Determine the deportment of iron and how it contributes to the slow leaching rates.
- Compare the leaching kinetics of chalcopyrite electrochemical leach systems to those in controlled bulk leach systems and establish how the electrochemical studies can be used to understand and predict the controlled bulk leaching of chalcopyrite.

1.2 Thesis lay out

This thesis is divided into 10 chapters and a brief overview of the chapters is given below.

Chapter 2 – presents a detailed review of literature relevant to ammoniacal leaching of chalcopyrite and behaviour of oxidation product species in ammoniacal solutions. This chapter also introduces some fundamental electrochemistry theory relevant to sulphide mineral oxidation.

Chapter 3 – describes the methods and materials used in this study. This section also provides some results analysis methods as well as equipment descriptions were necessary.

Chapter 4 – presents results on mixed potentials and anodic reactions. The influence of varying solution conditions and varying potentials is explored in this chapter.

Chapter 5 – presents results on the cathodic reactions. The influence of various solution conditions and varying potentials on the cathodic reaction is explored in this chapter.

Chapter 6 – presents results on bulk leach studies.

Chapter 7 – The formation of surface deposits on the oxidising chalcopyrite surface are explored in this chapter. The deportment of iron and sulphur is explored and surface deposits are reviewed after both the electrochemistry studies and the controlled leach studies.

Chapter 8 – models for the mixed potential and the dissolution reaction are presented and an overall discussion of all the results is offered.

Chapter 9 – presents the conclusion to the study.

Chapter 10 – recommendations for future work.

2 Literature review

2.1 General aspects of chalcopyrite

Introduction

Copper was one of the earliest metals used by man, dating back to 8000BC (Doebrich, 2009). It occurs as native copper and is also found in many minerals, particularly sulphides (chalcopyrite, bornite, chalcocite and covellite), sulpho salts (enargite), oxides (cuprite) and carbonates (malachite and azurite) (Christie and Brathwaite, 2011). Copper deposits can mostly be grouped into six classes, i.e. porphyry, sediment hosted stratabound, volcanogenic massive sulphide, gabbroid-associated, Native copper and hydrothermal vein and replacement deposits. The porphyry deposits yield about two thirds of the world's copper and are therefore the world's most important type of copper deposit (Doebrich, 2009). In general, these copper deposits which are associated with igneous intrusions are formed by hydrothermal processes i.e. the minerals are precipitated as sulphides from heated waters associated with igneous intrusions.

Occurrence and mineralogy

Chalcopyrite ($CuFeS_2$) is the major source of copper in the world, making up 70% of the world's copper reserves (Fuentes-Aceituno, Lapidus and Doyle, 2008). In the porphyry class, chalcopyrite occurs with bornite, chalcocite and covellite as secondary enrichment ores and is normally associated with galena (PbS), sphalerite (ZnS), molybederite (MoS_2) and pyrite (FeS_2). Gangue minerals usually occur in association with chalcopyrite and can be classified as silicate, limonite, and carbonates. In leaching processes, the gangue class plays a part in influencing reagent consumption rate, thus decisions on the type of reagent to be used can be made based on the knowledge of gangue mineralogy. Gangue minerals may result in excessive reagent consumption, examples being carbonates and limonites for acid leaching processes. Silicates on the other hand are known to have high initial consumption of sulphuric acid but these are also known to regenerate acids through reactions of soluble silicate breakdown products with each other forming various precipitates examples being jarosites, silica and gypsum (Jansen and Taylor, 1999).

While copper is found worldwide, 90% of reserves are located in four areas: the Great Basin of the western United States, the border between Zambia and the DRC, central Canada, and the Andes regions of Peru and Chile (Marianne, 2005). In South Africa, chalcopyrite deposits are found on the Palabora igneous complex, Bushveld Complex and the Uitkomst Complex.

Physical properties of chalcopyrite

Chalcopyrite is not only the most abundant of the copper sulphides, but also the most stable mineral because of its structural configuration, face centred tetragonal lattice (Wang, 2005). Chalcopyrite is also the most refractory to hydrometallurgical processing (Haver, R., Wang, M., 1971). Chalcopyrite crystallises in the tetragonal space group $I\bar{4}2d$ and has a zincblende structure with four-coordinate cations and anions forming distinct corner sharing tetrahedra (Figure 2.1) (Pearce et al, 2006).

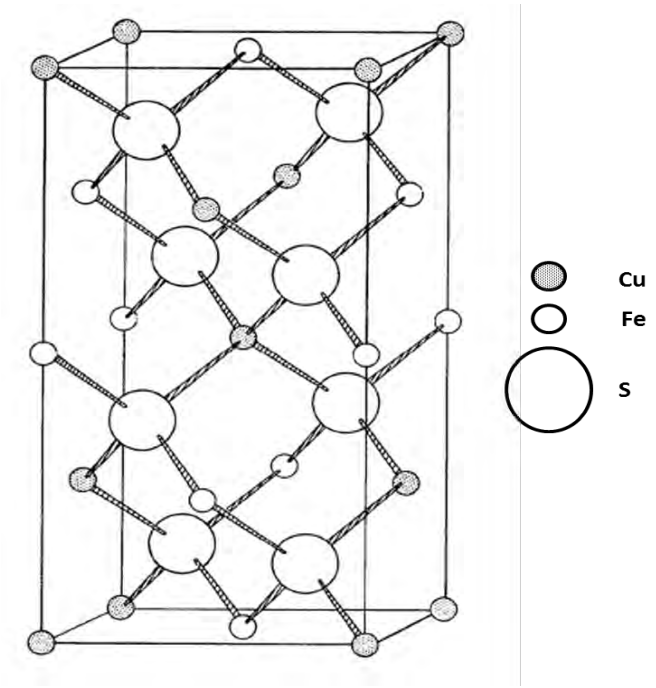

Figure 2.1. Structure of Chalcopyrite. Adapted from Hall and Stewart (Hall and Stewart, 1973)

Pearce et al (2006) discuss the oxidation state of copper and iron in chalcopyrite and provide evidence that the valence formula for chalcopyrite is $Cu^{+}Fe^{3+}(S^{2-})_2$. **Table 2.1** gives a summary of the physical properties of chalcopyrite.

Table 2.1. Physical properties of Chalcopyrite (Compiled from mindat.com, 2015; Geology.com, 2016)

Property	Description
Chemical composition	$CuFeS_2$
Theoretical composition by weight	34.63% Cu, 30.43% Fe, 34.94% S
Hardness	3.5 – 4
Transparency	Opaque
Specific gravity	4.2
Colour	Brassy yellow, tarnishes to iridescent blues, greens, yellow and purples
Streak	Greenish black
Lustre	Metallic
Cleavage fracture	Poor in one direction/uneven
Crystal habit/mode of occurrence	Prismatic sphenoid (wedge shaped) to tetrahedral

Semiconductor properties of chalcopyrite

The semiconductor properties of chalcopyrite can be important in mineral processing and in hydrometallurgy as both processes are influenced by the properties of the mineral surface (Velásquez-Yévenes, 2009). Chalcopyrite is a semi-conductor whose electrical resistivity and type is controlled by deviations from stoichiometry and impurity content and hence its geological environment. Its semi-conducting properties are due to free charge carriers for which three sources may be distinguished (Pridmore and Shuey, 1976);

- Deviation from stoichiometry
- Trace elements in solid solution

- Thermal excitation across the energy gap

2.2 Hydrometallurgy of chalcopyrite

2.2.1 Introduction

Hydrometallurgy involves the use of aqueous media in the extraction of metals. This method has gained major interest in the processing of chalcopyrite owing to the depletion of high grade copper ores, thus prompting the need to exploit mixed and low grade ores. Traditional process routes for chalcopyrite ores involve concentrating, melting and converting. The concentrate is melted slowly and partially oxidised in a flash smelter, to remove remaining gangue and some of the iron and sulphur; the resulting liquid copper-iron sulphide or matte, is then blown with air to oxidise the remaining iron and sulphur, which are respectively slagged off and vented as SO_2 gas (Jones, 1974). Environmental concerns, especially regarding the emission of SO_2 gas, have also been a motivation for the exploration of hydrometallurgy as an alternative method for copper extraction. Hydrometallurgy potentially allows for increased economic exploitation of mixed and low-grade ores, since it is regarded to be less energy and capital intensive in comparison to the traditional pyro-metallurgical processes.

Different approaches to hydrometallurgical treatment of chalcopyrite can be carried out. These include thermal treatment prior to leaching, direct leaching and direct electrochemical leaching (Venkatachalam S, 1991). Direct leaching of chalcopyrite can be carried out in various systems as reviewed by Venkatachalam (1991) and Roman and Benner (1973):

- Sulphate systems – in the presence or absence of micro-organisms
- Chloride systems
- Nitric acid systems
- Cyanide systems
- Ammoniacal systems

Sulphate systems, as reviewed by Klauber (2008), have received the most attention because they are relatively cheap, however, these systems do not work well under atmospheric conditions. Although chloride systems have been found to have higher dissolution rates than the sulphate systems, the sulphate systems have been preferred due to minimal corrosion problems and the ability to regenerate sulphuric acid during electro-winning of the copper (Munoz, 1979). This study will focus on the ammoniacal leaching of chalcopyrite. Motivation for choosing the ammoniacal leaching

system was briefly discussed in section 1.1. Furthermore, ammoniacal leaching of copper ores is a known research area dating back to 1916 where it was applied to leach low grade oxide ores in the Kennecott ammonia leaching plant and in the Calumet and Hecla mines in northern Michigan. Ammonia leaching technologies were later applied to sulphide ores and the Sherrit Gordon process was developed to commercial scale in 1948, becoming a historically recognised milestone in ammoniacal hydrometallurgical processes. Ammonia leach systems received intermittent but considerable research focus until the development of the Escondida process (Duyvesteyn, 1995; Duyvesteyn and Sabacky, 1993) in the 1990s, after which, little research work was done in that area relative to the acid leach systems. The minimal interest in ammoniacal sulphide leaching is thought to have to do with the slow process kinetics which required high operating temperatures and pressures to achieve reasonable recoveries. Radmehr et al (2013) gives a table summarising the most recently researched minerals for ammonia leaching technologies and points out that most of these have been on oxide ores or mattes. This study hopes to develop further understanding of the ammoniacal leaching of sulphides, specifically chalcopyrite, and evaluate how solution parameters and the so-called surface deposit layer influence reaction kinetics. Furthermore, efforts will be made to characterise the surface deposit.

2.2.2 Ammonia chemistry

Ammonia and its salts are highly soluble in aqueous medium. Ammonia's solubility in water is due to its high polarity and its ability to form hydrogen bonds with the water. Ammonia dissolves in water according to equation 2.1.

$$NH_3 + H_2O = NH_4^+ + OH^- \qquad 2.1$$

The OH^- ions give it its basic properties and at equilibrium a substantial amount of ammonia remains in molecular form making it a weak base with a dissociation constant (K_b) of $1.8 \cdot 10^{-5}$ at 25 ˚C which increases slightly with an increase in temperature (Everret and Wynn-Jones, 1938). Ammonium ions (NH_4^+) act as weak acids, dissociating to give a hydrogen ion and ammonia i.e. the reverse of equation 2.1. The ammonium ion is more stable than ammonia at low pH below 9.25 (at room temperature, T_{25}) i.e. in aqueous solution equilibrium of equation 2.1 shifts to the right. At pH 9.25_{T25} the reaction shown by equation 2.1 is at equilibrium.

The combination of ammonia and ammonium salts is known to be a powerful lixiviant used in hydrometallurgical process (Meng and Han, 1996). Together, ammonia and an ammonium salt form a buffer solution well suited for maintaining desired operating pH levels. As previously mentioned, ammonia-ammonium salt solutions have been used as an effective lixiviant in numerous hydrometallurgical processes as evident from the commercially developed Sherrit Gordon process

which treated sulphide concentrates of nickel, cobalt and copper at temperatures of 95-105 °C and air pressure of 800 - 1000 KPa in the 1950s (Forward and Mackiw, 1955); the Arbiter process for recovering copper from chalcopyrite concentrates at 75 - 80 °C in the presence of oxygen at 34.5 – 55.2 Kpa in the 1970s; and the Escondida process which was intended to produce high grade copper concentrates in the 1990s (Duyvesteyn and Sabacky, 1993). Ammonia leaching can be used in non-oxidative, oxidative and reductive leaching (Chmielewski et al, 2009). Ammonia has become more attractive as a lixiviant during the present socio-economic climate due to its low toxicity, low cost and ease of regeneration by evaporation (Meng and Han, 1996). Ammonia processes are ideal when the gangue minerals are acid consuming e.g. with calcareous or dolomitic gangue (Paynter, 1973). Cleaner leach liquors are produced thus facilitating subsequent metal recovery (Bell et al, 1995). Extracting metals from an ammoniacal solution allows the chelating extractant to be readily loaded (Reilly and Scott, 1977). Its selectivity in solubilisation of desired metals has made it attractive as a lixiviant, and this is particularly advantageous in avoiding extraction of iron which is almost invariably present in all copper concentrates (Paynter, 1973). Bromates, chlorates, peroxides, persulfates or oxygen can be used as oxidants in the ammoniacal leaching of chalcopyrite, with oxygen being the least expensive. Leaching of chalcopyrite in ammonia systems has been achieved at commercial scale as evident from the Arbiter Process which had an annual copper production capacity of 36000 tonnes (Havlik, 2008). In the Arbiter Process, chalcopyrite concentrates were leached at 75-80°C in the presence of oxygen (Habashi, 2007). After filtering the solids, the copper was extracted from solution using solvent extraction, stripped by sulfuric acid, and electrolyzed to give metallic copper (Habashi, 2008). The ammonia was regenerated by adding lime to the raffinate and then boiling the slurry. The main reasons for the lack of success of this process were attributed to the technical and economical challenges faced in the ammonia recovery steps (Habashi, 2007).

Ammonia solutions can be used to leach copper sulphides providing the following conditions are observed (Roman and Benner, 1973; Forward and Mackiw, 1955):

- Sufficient oxidising agent is available to react with the sulphide present
- Sufficient NH_3 is present to neutralize the acid formed by the oxidation of the sulphides, the NH_3 in solution should also be sufficient enough to form the higher ammines of copper as well as be available “unbound” to establish equilibrium with the ammines. The “unbound” NH_3 should not be too high as this could result in reduction of the solubility of the ammines.
- Sufficient anions e.g. SO_4^{2-} be present

- The temperature is controlled to provide reasonable reaction rate but not too high as this may cause precipitation of basic salts or insoluble complex ammines.

The disadvantages of ammoniacal leaching are that it is volatile relative to other lixiviants and hence lixiviant losses are incurred although it hydrolyses and the risk of air transport is minimised. Furthermore, extractors so far used for copper recovery from ammonia medium do not have high efficiency (Radmehr et al., 2013).

Chemistry of ammonia-ammonium leaching of chalcopyrite

A typical ammoniacal sulphide leach system can be generalized as shown in equation 2.2 (Stanczyk and Rampacek, 1966):

$$MS + xNH_3 + 2O_2 = M(NH_3)_X SO_4 \qquad 2.2$$

Where M is a metal capable of forming a soluble ammine and x is the number of molecules of NH_3, which varies according to the valence of the metal M. A diagrammatic example for the leaching of a sulphide particle was given by Forward (Forward and Mackiw, 1955) (Figure 2.2); although their illustration was for pentlandite, the principle is generally the same for chalcopyrite.

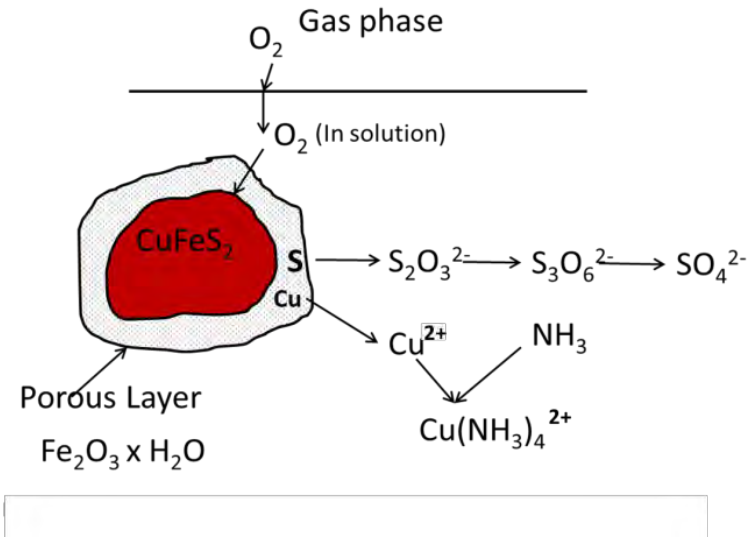

Figure 2.2. Schematic of the leaching of sulphide ore adapted from Forward and Mackiw (1955)

The stoichiometry of ammonia leaching of chalcopyrite has previously been documented (Equation 2.3) (Bell et al, 1995; Beckstead and Miller, 1977a; Roman and Benner, 1973)

$$CuFeS_2 + 4NH_3 + \frac{17}{4}O_2 + 2OH^- = Cu(NH_3)_4{}^{2+} + \frac{1}{2}Fe_2O_3 + 2SO_4^{2-} + H_2O \qquad 2.3$$

Leaching of chalcopyrite in ammonia is possible due to the stabilisation of cupric ion as a tetra-ammine complex. The formation of this complex depends on the concentration of copper and ammonia in solution and the concentration and type of anions present (Roman and Benner, 1973). The leaching process primarily involves the solubilisation of the copper and the oxidation of sulphur and iron. The solubility and stability of the resultant copper ammine ion depends on the concentration of the metal ion in solution, the amount of NH_3 present and on the amount and type of anions present. If ammonia is partially or completely removed from such solutions, for example by boiling, the soluble ammines tend to decompose and the metals precipitate as basic salts (Forward and Mackiw, 1955). This is explained by the equilibrium presented in equation 2.1. Good metals extraction can be achieved at around pH 9.25_{T25} i.e. when equation 2.1 is at equilibrium since both ammonia and ammonium are present thereby minimising possible precipitation of dissolved metal. The sulphide component is oxidised to a soluble species, predominantly sulphate (SO_4^{-2}), together with some lower oxidation state species such as thiosulphate ($S_2O_3^{-2}$), tri-thionate ($S_3O_6^{-2}$) and sulphamate ($SO_3NH_2^-$) (Park et al., 2007b).

The literature survey has found several authors (Park et al, 2007a; Rao and Ray, 1998; Warren and Wadsworth, 1984; Beckstead and Miller, 1977a; Roman and Benner, 1973) who state factors that affect the rate of ammoniacal leaching of chalcopyrite. Although some are specific to the researchers' experimental conditions some of these are inherent to the chalcopyrite-ammonia leaching process.

Hydroxyl ion concentration/pH and Ammonia concentration

The equilibrium of ammonia in aqueous solutions such as the one evaluated in this study is described by equation 2.4.

$$NH_4^+ = NH_3 + H^+ \qquad 2.4$$

Following the ammonia dissociation equation, it will not be possible to increase the pH without increasing the ammonia concentration. The ratio of ammonium to ammonia would follow equation 2.1. The total ammonia is given by the sum of free ammonia and the ammonium ion ($NH_3 + NH_4^+$) and the pH is given by equation 2.5.

$$pH = pK_a + log\frac{[NH_3]}{[NH_4^+]} \qquad 2.5$$

At low pH the larger part of the total ammonia ($NH_3 + NH_4^+$) will be present as ammonium (NH_4^+) and this is expected to result in a decrease in rate of reaction as observed by Guan and Han (1997). The rate of reaction will increase with an increase in pH up to the range of 10.5 – 11.5. Guan and Han

(1997) observed that some oxidants, in their case iodine, start to precipitate with a further increase in pH beyond 10.5. In a study on agitation leaching of chalcopyrite concentrates in the presence of oxygen, Beckstead and Miller (1977a) concluded that the reaction was first order with respect to hydroxyl ion concentration. Warren and Wadsworth (1984) observed a decrease in rest potentials and increase in anodic currents as pH increased at fixed total ammonia concentrations.

Temperature

An increase in temperature has been shown to cause an increase in the rate of reaction, (Guan and Han, 1997; Bell et al, 1995; Beckstead and Miller, 1977a; Tozawa et al, 1976; Stanczyk and Rampacek, 1966). Tozawa et al (1976) and Stanczyk and Rampacek (1966) went on to conclude that practical leaching temperatures should be used since increasing temperature to elevated levels would also result in high vapour pressures of ammonia, water and other reagents. This would affect plant designs (which will need to be designed to handle higher pressures), hence the capital costs. Ammoniacal leaching plants that developed to reach commercial scale (Section 2.2.2), were operated at temperatures in the range 75 – 105 °C.

Ammonium sulphate

Forward and Mackiw (1955), Stanczyk and Rampacek (1966) and Tozawa et al (1976) discuss the importance of the anion during leach reactions, and agree that low sulphate ion concentrations resulted in low reactions rate and hence low recoveries. However, sufficient sulphur is dissolved from the concentrate when sulphide ores are leaching (Forward and Mackiw, 1955). Ammonium sulphate provides the sulphate ion, which is consumed in the formation of $Cu(NH_3)_4SO_4$ according to equation 2.6.

$$Cu(NH_3)_4^{2+} + SO_4^{2-} = Cu(NH_3)_4SO_4 \qquad 2.6$$

The sulphate ions produced from the chalcopyrite leach reaction (Equation 2.3) may result in the lowering of the pH levels of the solution and in turn lower the concentration of free ammonia in solution (Equation 2.5); this will translate to lowered copper recoveries. Park (2007b) studied effect of reagents concentration and noted that for a fixed ammonium sulphate concentration, increasing the ammonium hydroxide concentration resulted in an increase in percentage extraction of copper, while fixing the ammonium hydroxide concentration and varying the ammonium sulphate concentration resulted in marginal increase in percentage extraction. Tozawa et al (1976) proposed that the increased leaching rates of copper minerals observed when ammonium sulphate was

added, could be attributed to the buffer actions of the ammonia and ammonium ion rather than to insufficient SO_4^{2-} in solution to form $Cu(NH_3)_4SO_4$.

Ionic strength

The effect of ionic strength on the ammoniacal leaching of chalcopyrite is not well documented in literature, with Beckstead and Miller (1977a) stating that varying ionic strength by addition of an indifferent electrolyte did not significantly affect reaction kinetics, and Warren and Wadsworth (1984) mentioning the addition of sodium sulphate to increase conductivity but neglecting to report what effect that had on the anodic currents.

Oxygen pressure

The amount of dissolved oxygen in solution and rate of transfer of oxygen from gas phase to liquid phase vary with a variation in partial pressure of oxygen in the gaseous phase. According to equation 2.3, oxygen is necessary for the reaction to proceed. Forward and Mackiw (1955) and Tozawa et al (1976) agreed that in the early stages of leaching, the reaction had high oxygen requirements. Warren and Wadsworth (1984) reported that at low oxygen pressure, empirical order of reaction is approximately 0.5 while at higher oxygen pressures the rate of reaction is much less dependent on oxygen pressure, the reaction order approaching zero (Beckstead and Miller, 1977a). Reilly and Scott (1977) concluded that the reduction of oxygen on the solid surface of the mineral was rate determining under the conditions of their study. Kuhn et al (1974) developed the Arbiter process which did not require high air pressure operations but used oxygen instead of air and specialised agitation techniques to effectively disperse oxygen in leach slurries. It should be noted that a survey of literature indicates acceptance of oxygen as the oxidant in the leaching of chalcopyrite (Muzawazi, 2013; Duyvesteyn and Sabacky, 1993; Warren and Wadsworth, 1984; Beckstead and Miller, 1977a; Tozawa et al, 1976; Kuhn et al, 1974; Forward and Mackiw, 1955).

Initial copper(II) ions concentration

Warren and Wadsworth (1984) found initial copper(II) ions to have no effect on the anodic currents but they observed an increase in the measured rest potentials; the authors concluded that initial copper(II) ions did not directly participate in the redox reaction. In a separate study, Beckstead and Miller (1977a) found initial copper(II) ions to increase the rate of reaction but concluded that it did not directly participate in the redox reaction only serving to catalyse the oxygen reduction reaction. Tozawa et al (1976) also reported increased reaction rates in the presence of initial copper but neglected to comment on what its role may have been. A more in-depth literature survey on the role copper(II) ions in oxidative leaching will follow in section 2.4.1.

Thermodynamics of chalcopyrite ammonia systems

The chemistry of ammoniacal leaching for transition metals and their compounds involves not only oxidation reduction reactions, but complexation equilibria (Meng and Han, 1996). The equilibria can best be described by Pourbaix diagrams which in themselves are plots of the electrochemical equilibrium thermodynamics. Pourbaix diagrams can be referred to as a starting point to establish thermodynamic feasibility of the chalcopyrite ammonia process, they do not provide kinetic information, and this needs to be obtained experimentally. A problem inherent with the direct application of Pourbaix diagrams to kinetic systems is the possible formation of metastable intermediate phases and these phases may be attributed to sluggish solid phase transitions and slow chemical kinetics associated with products reaction (Hiskey and Wadsworth, 1981). A Pourbaix diagram for the chalcopyrite ammonia system is given in Figure 2.3. It can be seen from Figure 2.3 that at around pH 9.6, the most stable copper species at 1M activity and 25°C are $Cu(NH_3)_2^+$ and $Cu(NH_3)_4^{2+}$.

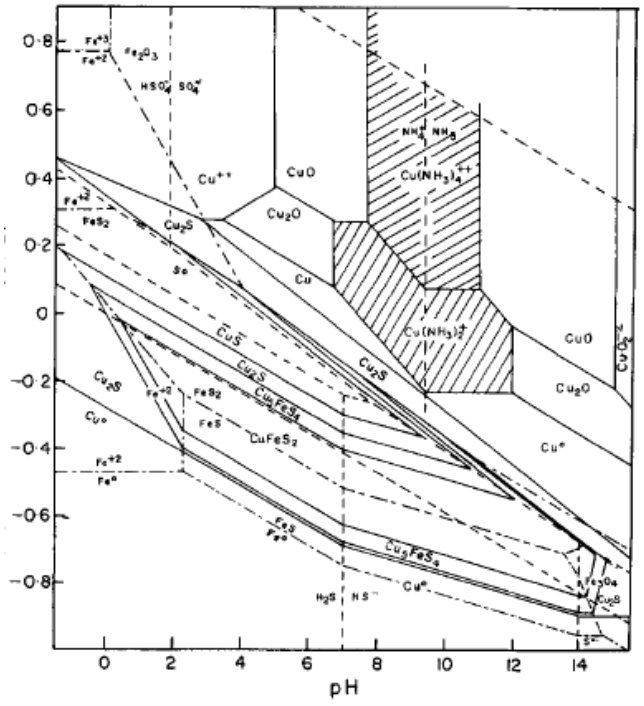

Figure 2.3. Eh-pH diagram of Cu-Fe-S-H_2O system at 25°C all solutes at 0.1M except Cu^{2+}= 0.01, NH_3(pH>9.25) reproduced from direct le aching of sulphide chemistry and applications (Peters, 1976)

Meng and Han (1996) state that the ratio of the $Cu(NH_3)_2^+$ to $Cu(NH_3)_4^{2+}$ relates to the oxidation potential of the system, and they give the equation relating the potential and the ratio as shown below (Equation 2.7)

$$Eh = 0.074 - 0.1182\log(NH_3) + 0.0591\log\frac{[Cu(NH_3)_4^{2+}]}{[Cu(NH_3)_2^{+}]} \quad 2.7$$

Tozawa et al (1976) diagrammatically illustrated the stability regions of the cupric ammine complex as a function of total ammonia and pH after taking into consideration equations 2.8 -2.10.

$$NH_3 + H^+ = NH_4{}^+ \quad 2.8$$

$$Cu(NH_3)_4^{2+} + H_2O = CuO + 2H^+ + 4NH_3 \quad 2.9$$

$$Cu(NH_3)_4^{2+} = Cu^{2+} + 4NH_3 \quad 2.10$$

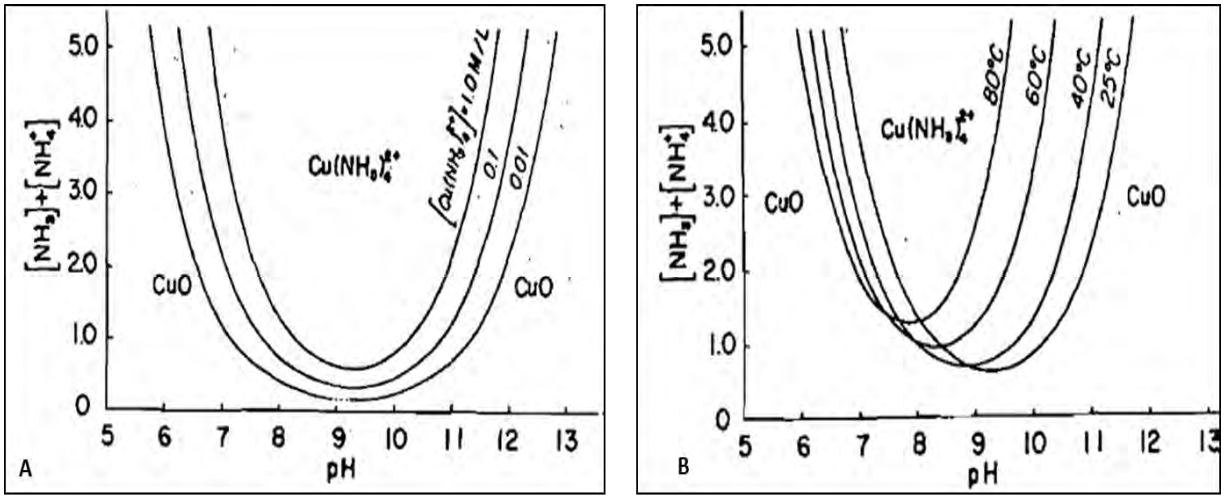

Figure 2.4. $Cu(NH_3)_4^{2+}$ stable regions. Reproduced from On Chemistry of Ammonia Leaching of Copper Concentrates (Tozawa et al, 1976)

According to Figure 2.4a, the stability region of the cupric ammine complex increases with a decrease in concentration of the complex as shown by the wider stability window of the 0.01 M/L compared to the 1 M/L curves. Figure 2.4b shows variations of the stability regions with change in temperature. Similar data could not be found for the cuprous ion which is also known to be stable in ammoniacal solutions.

Speciation in copper-ammonia systems

Copper(I) and copper(II) form neutral anionic and cationic complexes in solution. Aqua-complexed or hydrated copper(I) is very unstable with a reported disproportion constant of $5.4{\cdot}10^5$ (Lamble et al, 1994). On the other hand, hydrated copper(II) can be found in aqueous solution, and the water molecules are easily displaced by ligands to form a more stable copper(II) complex. Ammonia is more polarisable than water hence binds more strongly to copper than water forming a copper-

ammonia complex. Ammonia complexes both the copper(I) and copper(II) forming thermodynamically stable complexes, although the copper(I) ammonia complex will readily oxidise in the presence of even trace concentrations of oxygen.

Copper(I) forms mono-ammine, the diamine and the triammine complex with ammonia, with the diamine being the primary species found in solution. The fact that they are so readily oxidised by air to the intense violet-blue and very stable tetraammine copper cation has probably precluded their detailed study (Lamble et al, 1994). Several thermodynamic models for the copper-ammonia systems have been developed in the presence of different salts and at different temperature and pH windows (Xi et al, 2011; Shao-hua et al, 2005; Trevani et al, 2001; Lamble et al, 1994). Black (2006) presents a detailed literature review of the copper(I) ammonia system and highlights the stability constants of the dormant diamine copper(I) species to be in the range 10.18 – 10.62 in the presence of different anions at 25°C. The author went on to present findings which were also within that range. Further to this, Black (2006) found that the stability constants were independent of the anion in solution while carrying out studies in the presence of sulphate, chloride and perchlorate salts.

At room temperature, the hydrated copper(II) ion, $Cu(H_2O)_6^{2+}$, is known to form distorted octahedral complexes with up to four molecules of ammonia, and a square pyramidal complex when a fifth molecule of ammonia is coordinated (Trevani et al, 2001). The complexation proceeds according to equation 2.11.

$$[Cu(H_2O)_6]^{2+} + nNH_{3(aq)} = Cu(NH_3)_n((H_2O)_{6-n} + nH_2O \qquad 2.11$$

In which n=1 to 5.

Van Wensveen (2010) used Ultra Violet-Visible Spectroscopy (UV-Vis spectroscopy) to study the kinetics of the oxidation of thiosulphate in copper-ammine solutions and found that anions, sulphate, chloride and perchlorate were involved in mixed complex formation with the tetraammine copper(II). In a separate study, Byerley et al (1975; 1973) reported on the formation of a tetraammine copper(II)-thiosulphate intermediate in a study on the oxidation of thiosulphate by copper(II) in ammoniacal solutions. The researchers (Byerley et al, 1975; 1973) went on to propose that thiosulphate oxidation proceeded via the formation of an intermediate oxygen activated tetraammine copper(II)-thiosulphate species. Breuer and Jeffrey (2003) and Van Wensveen (2010) agreed that in the presence of some anions; the anions complexed with the tetraammine copper(II) and this resulted in a reduced rate at which thiosulphate was oxidised. This points to that studies on the chemistry of copper(II) in ammonia solutions must include copper ammonia complexes $Cu(NH)_N^{2+}$ and the copper-salt complexes. A copper(I) and copper(II) speciation tool was developed

for copper ammonia systems at Murdoch University (Nicol, 2013), and it will be used to determine the relevant speciation in the present study.

2.3 Electrochemical principles and their application to leaching studies

Introduction

Ammoniacal leaching of chalcopyrite has been shown to be an electrochemical process (Warren and Wadsworth, 1984; Beckstead and Miller, 1977a; Forward and Mackiw, 1955). This means that the dissolution reaction involves the transfer of electrons between an oxidising and reducing species. Oxidative leaching reactions, such as that of chalcopyrite in the current study, involve the loss of electrons by the mineral which constitutes the anodic reaction; and the simultaneous gain of electrons by the reducing species or oxidant, which constitutes the cathodic reaction. In the ammoniacal oxidative dissolution of chalcopyrite (Equation 2.3), the sulphur in the mineral lattice is oxidised from an oxidation state of -2 to +6, meaning the reactions requires transfer of 8 electrons per sulphur. The 8 electrons would be taken up by two oxygen molecules, and since chalcopyrite has two sulphur atoms; 16 electrons need to be transferred to an oxidant per mole of chalcopyrite oxidised. However, further oxygen requirements may be necessary for the oxidation of the solubilised metals, iron and copper.

One significant advantage is that such reactions can be measured as currents by electronic instruments at a sensitivity which cannot be matched by the conventional chemical analytical methods in terms of amount of metal accumulated in solution. This allows the monitoring of the development of the reactions as they occur, detecting even the dissolution of metals which may subsequently precipitate in solution (Nikoloski, 2002).

Wan et al (1984) highlighted that electrochemical measurements, by design, are limited to initial reaction behaviour and not necessarily describe rate-control phenomena for a leaching reaction that goes to completion. It is necessary that when results of electrochemical measurements are to be compared to those of leaching studies, the extent of reactions and environment under which the reactions occur be similar such that an effective comparison can be achieved.

Dissolution of minerals in aqueous solutions takes place at the mineral-solution interface. For electrochemical processes, it may be represented by half reactions i.e. the oxidation reactions which occur at the anode as well as the reduction reactions, occurring at the cathode. Use of electrochemical techniques allows for the study of reactions at the interface by measuring mineral surface potentials under freely dissolving conditions (when no external power sources are supplied) or by introducing an external source of power to create an electron imbalance resulting in a flow of

electrons as the system tries to re-establish a state of charge neutrality. The techniques relevant to this study are discussed below.

2.3.1 Open circuit potentials

Open Circuit Potentials (OCPs) give the potential at the mineral surface under freely dissolving conditions. This potential is a measure of the equilibrium between solution and mineral surface when no external source of current is applied. OCPs give the potential region for possible reactions on the mineral solution interphase and may thus be used to evaluate the likely changes taking place at the surface of the mineral over time. OCPs are also often referred to as rest potentials, mixed potentials or equilibrium potentials. It is essential to note that these terms do not always refer to the same potential as will be explained below.

Equilibrium potentials are mathematically described by the Nernst equation (Equation 2.12).

$$E = E^0 - \left(\frac{RT}{nF}\right) \ln[\frac{\alpha_{reduced}}{\alpha_{oxidised}}] \quad 2.12$$

This would be valid at the mineral surface in cases where there is a metal/metal ion couple. In a case where a metal sulphide is being oxidised and a metal ion being reduced on the metal sulphide surface, a mixed potential between the metal sulphide and metal ion is established. A mixed potential is established when the system has two half reactions from different redox couples. This is defined as the potential where the sum of the anodic currents is equal to, and opposite the sum of the cathodic current resulting in no net flow of current. Notice has to be taken that this does not describe a situation of lack of reactivity on the mineral surface; rather it is a state of dynamic equilibrium with a net dissolution of the metal sulphide.

These mixed potentials depend upon the properties of the electrode surface (Hiskey and Wadsworth, 1981) and the oxidising power of the solution. The concept of mixed potentials on sulphide minerals in solution is well established and has been the subject of several publications (Nicol and Lázaro, 2002; Holmes and Crundwell, 2000; Nicol, 1993; Kametani and Aoki, 1985; Rand and Woods, 1984; Hiskey and Wadsworth, 1981). It has been qualitatively and quantitavely described by Needes et al (1975) as described below;

Assume a half reaction for the dissolution of a metal sulphide MS

$$MS \leftrightarrow M^{2+} + S + 2e \quad 2.13$$

Coupled to the reduction of Fe(III) on the metal sulphide surface

$$Fe^{3+} + e \leftrightarrow Fe^{2+} \quad 2.14$$

This reaction is schematically represented below (Figure 2.5).

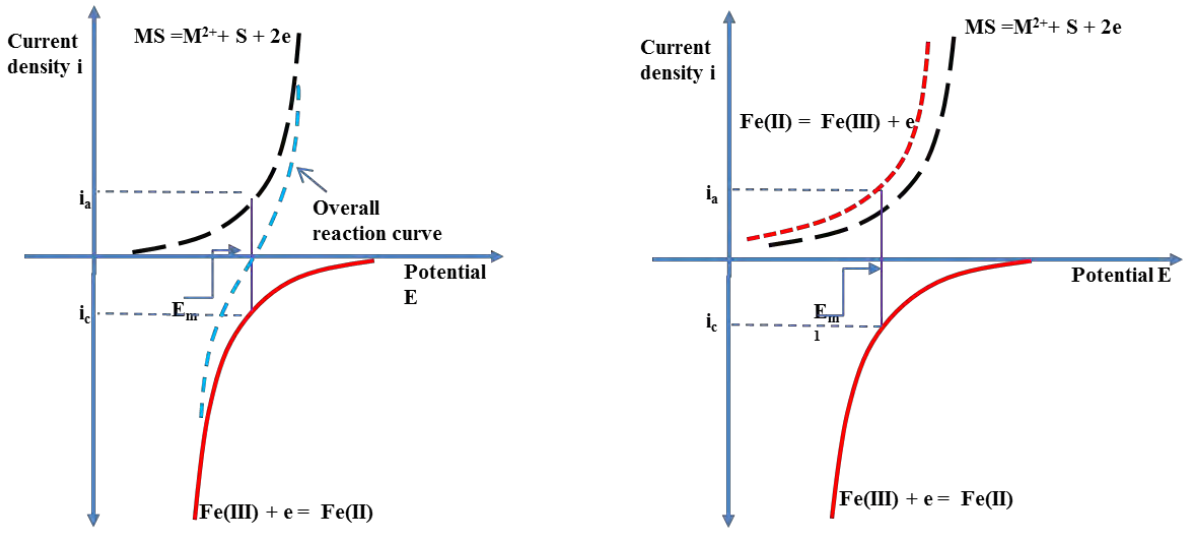

Figure 2.5. Schematic representation of mixed potentials on a metal sulphide in ferric sulphate solutions. Adapted from Nicol and Lazaro (2002)

The first schematic in Figure 2.5 shows oxidation and reduction of the two redox reactions involved, the potential at which the anodic currents are equal and opposite the cathodic currents (Equation 2.15), such that there is a zero net flow of current is referred to as the mixed potential. This schematic also describes a type I mixed potential in which only the anodic and cathodic characteristics of the mineral and oxidant respectively, are significant in the region of mixed potential i.e. in a type I mixed potential system, anodic currents are solely due to the oxidation of the mineral and these anodic currents are equal and opposite to cathodic currents that are also solely due to the reduction of the oxidant.

$$i_a = i_c, i_a - i_c = 0 \qquad 2.15$$

The second schematic illustrates mixed potential for a system which involves more than one anodic reaction; in this case, mixed potential refers to the potential at which the sum of the anodic currents is equal to and opposite the sum of the cathodic currents. This is a type III mixed potentials system in which the anodic branch for the oxidation of the reduced form of the oxidant is such that the current due to this half reaction is considerably greater than that due to the oxidation of the mineral (Nicol, 1993).

The modulus of the current from either the anodic or the cathodic reactions at mixed potential is the exchange current density (Equation 2.16).

$$|i_a| = |i_c| = exchange\ current\ density \qquad 2.16$$

The rate of oxidation of the metal sulphide is analogous to the partial current densities contributed by the metal sulphide to the anodic currents. This can be calculated using the Faraday law (Equation 17).

$$Q = nFe \quad \text{2.17a}$$

$$rate\ of\ oxidation\left(\frac{mol}{cm^2 s}\right) = \frac{i}{nF} \quad \text{2.17b}$$

In which Q is the charge generated, F the Faraday constant (96485 Coulomb mol^{-1}) and n the number of electrons transferred.

2.3.2 Voltammetry

Cyclic Voltammetry (CV) measures the change of current with voltage, whereby potential is increased or decreased linearly with time. A scan rate is set; this refers to the rate at which potential is changed with time. Cyclic voltammetry may be used to identify reduction and oxidation reactions as well as the formal potential of these reactions. Qualitative comparisons can be made of the rate of dissolution in a mixed potential system by comparison of the slopes of the curves at zero current i.e. an analysis of the slopes in the low Tafel region close to mixed potential (Nicol, unpublished). Cyclic voltammograms can be further analysed in line with electrochemistry theory to extract kinetic information for reactions of interest, in this case the anodic dissolution of chalcopyrite in ammoniacal solutions.

When a system is made to shift from mixed potential by the introduction of an external source of electrons, net charge transfers can be achieved. The relationship between the changes in potential caused by the external electron source and the resultant net charge-transfer can be described by the Butler-Volmer equation (Equation 2.18) (Wang, 2000).

$$i = i_0 \left[exp\left\{\frac{-\alpha n F \eta}{RT}\right\} - exp\left\{\frac{(1-\alpha) n F \eta}{RT}\right\}\right] \quad \text{2.18}$$

Where;

- i is the induced current density A cm^{-2}
- i_0 is the exchange current density A cm^{-2} occurring at equilibrium
- α is the transfer coefficient
- n is the number of electrons involved in the half reaction
- F is the Faraday number 96485 C mol^{-1}

- η is the electrode over potential η = $E_{imposed}$ – $E_{equilibrium}$. This is defined with respect to a specific reaction for which the equilibrium potential is known.
- R is the universal gas constant 8.314J $Kmol^{-1}$
- T is the temperature in Kelvins

The Butler-Volmer equation is a sum of the currents from anodic and cathodic half reactions; it relates the current density at a solid solution interphase to potential. Therefore, at sufficiently large over-potentials (additional potential beyond the thermodynamic requirement needed to drive the reaction at a certain rate (Bard and Faulkner, 2001)), one of the exponential terms on equation 2.18 will be negligible compared to the other, thus it may fall of leaving simplified forms of the Butler-Volmer equation e.g. at large negative over potentials $i_c >> i_a$ equation 2.18 becomes equation 2.19.

$$i = i_0 \exp \frac{-\alpha n F \eta}{RT} \qquad 2.19$$

Equation 2.18 can be written out in logarithmic form to give the Tafel equation and plotting log i versus η gives Tafel plots from which values of α may be inferred.

Chronoamperometry

Chronoamperometry is a type of potentiostatic experiment that deals with charge transfer processes at the electrode-solution interface. The output of chronoamperometric measurements is a transient of current density as a function of time. A set potential difference is maintained between the reference electrode and the working electrode. From a chemistry perspective, the current measured reflects the flow of electrons needed to support the active electrochemical processes at rates consistent with the applied potential. Since this technique is based on Faraday's law of electrolysis, equation 2.17a, for a reaction (Equation 2.20);

$$R - (n)e = O \qquad 2.20$$

Equation 2.20 can be used to calculate the unknowns in the reaction.

The shape of the transient can be used to determine the rate limiting step of the processes taking place on the electrode surface (Pugaev, 2011). They can also be used to determine the steady state current density and thus leaching rate at a specified potential. Chronoamperometry can be carried out at intermittent potential steps, by applying a potential for a fixed period of time, leaving the electrode under open circuit and monitoring the potential. This can be repeated a number of times in cycles. The intermittent potential steps technique can be used to determine the extent and rate at

which passivating layers, which are anodically formed on the surface of the mineral, can be removed under non-oxidative conditions (Pugaev, 2011).

While studies on the ammoniacal leaching of chalcopyrite concentrates has been done before (Guan and Han, 1997; Warren and Wadsworth, 1984; Beckstead and Miller, 1977a and 1977b; Reilly and Scott, 1977; Tozawa et al, 1976; Stanczyk and Rampacek, 1966) very little has been carried out using electroanalytical methods described in this section. Warren and Wadsworth (1984) carried out an electrochemical study in which they used cyclic voltammetry to study the anodic reaction sweeping potentials starting from rest potentials to potentials 700 mV above rest potentials. The researchers also presented a few constant potential tests carried out for the purpose of generating sufficient surface product for analysis as well as for the purpose of determining the coulometry of the anodic reaction. While the technique of using potential sweeps in the form of cyclic voltammetry and linear sweep voltammetry is widely used for mineral surface studies and provides invaluable information on surface reactions, it also tends to result in researchers focusing their attention on reactions that occur at potentials that are not typically reached in plant leaching conditions.

In this work, chronoamperometry is used for coulometry purposes i.e. to establish the stoichiometry of the anodic dissolution of chalcopyrite as well as to study in isolation the anodic and cathodic reactions establishing the leaching behaviour of chalcopyrite in extended oxidation experiments.

2.4 Chemistry of the oxidative dissolution of chalcopyrite

This section has briefly been discussed under section 2.2. A more in-depth literature survey of the parameters of interest is addressed in this section. The chemistry of the process has been extensively reported by Forward and Mackiw (1955), Stanczyk and Rampacek (1966) and Tozawa et al (1976).

2.4.1 The role of copper(II) ions in chalcopyrite dissolution

While studying the oxidative dissolution of chalcopyrite in ammoniacal solutions, Beckstead and Miller (1977) reported the cathodic reaction to be that of oxygen reduction. According to their findings, in the absence of oxygen, chalcopyrite did not react with copper(II) additions of up to 10g/L. The authors proposed the cathodic reactions to proceed according to equation 2.21. The authors dismissed the direct reduction of copper(II) on the mineral surface despite observing a near 0.5 order dependence of the rate of reaction on copper(II). It is known that electrochemical reactions follow 0.5 order dependence on concentration of the oxidant hence according Beckstead and Miller's results (1977a), it is possible that copper (II) be the reduced species on the chalcopyrite surface in ammoniacal leaching. Beckstead and Miller (1977a) went on to show a similar order of

the reactions dependence on oxygen partial pressure; they measured the order of reaction to be 0.48 and 0.51 in the presence and absence of oxygen respectively. These similar reaction orders may suggest some form of synergy between oxygen and copper(II) on the overall cathodic reaction but the researchers did not provide clear evidence that it was in fact not copper(II) being reduced and the oxygen catalyzing the copper (II) reduction reaction. Beckstead and Miller (1977a) went on to propose that the oxygen reduction reaction (Equation 2.21) was catalyzed by copper(II) ions. The overall cathodic reaction was then rewritten out as shown in equation 2.21, to indicate no redox involvement of copper(II) i.e. its role was said to be purely catalytic.

$$O_2 + 2H_2O + 4e = 4OH^- \quad 2.21$$

$$O_2 + 2H_2O + Cu^{2+} + 4e = 4OH^- + Cu^{2+} \quad 2.22$$

This conclusion was later supported by Warren and Wadsworth (1984), in that the authors agreed that copper(II) ions played a catalytic role in the dissolution of chalcopyrite. Tozawa et al (1976) reported enhanced leaching rates observed in the presence of copper(II) ions but the authors did not propose a reaction mechanism to explain these observations.

The catalytic role of copper(II) ions in the dissolution of chalcopyrite has been reported by several other researchers for different systems (Elsherief, 2002; Feng and Van Deventer, 2002; Tozawa et al, 1976). Studies carried out on the dissolution of chalcopyrite in acid solutions report iron(III) ions and/or dissolved oxygen to be the active oxidants in sulphuric acid solutions (Hiroyoshi et al, 2001), and Hiroyoshi et al (2004) went on to report on the synergistic effect of copper(II) ions and iron(III) ions on chalcopyrite dissolution in sulphuric acid solutions. Nicol et al (2010) studied the dissolution of chalcopyrite in chloride solutions and reported enhanced leaching rates in the potential window 560-600 mV (SHE) in the presence of copper ions and dissolved oxygen, whereby copper(II) ions were the oxidants. Lundstrom et al (2005) also studied the leaching of chalcopyrite in cupric chloride solutions and reported a critical copper concentration of 9 g/L in the pH range 1-2.5 and temperature 70-90 °C. These findings confirmed conclusion by Jones and Peters (1976), that ferric chloride leaching was in fact, cupric chloride leaching. Oxidative leaching equations have been postulated as shown below.

$$CuFeS_2 + 3Cu^{2+} = 4Cu^+ + Fe^{2+} + 2S^0 \quad 2.23$$

$$CuFeS_{2(s)} + 3[CuCl]^+_{(aq)} + 11Cl^-_{(aq)} = 4[CuCl_3]^{2-}_{(aq)} + FeCl_{2(aq)} + 2S^0_{(s)} \quad 2.24$$

Velasquez (2009) studied the chalcopyrite chloride leaching system and proposed a two-stage process in which non-oxidative dissolution occurs followed by an oxidative dissolution step as shown

in equations 2.25-2.28. This suggests an indirect involvement of copper(II) ions in the chalcopyrite chloride dissolution system.

$$CuFeS_2 + 4H^+ = Cu(II) + Fe(II) + 2H_2S \quad 2.25$$

$$CuFeS_2 + 2H^+ = CuS + Fe(II) + 2H_2S \quad 2.26$$

$$H_2S + 2Cu(II) = 2Cu(I) + S + 2H^+ \quad 2.27$$

$$2Cu(I) + \frac{1}{2}O_2 + 2H^+ = 2Cu(II) + H_2O \quad 2.28$$

It is apparent that the role of copper(II) ions in the chloride system has been quite extensively investigated. Akin to the chloride system; in ammoniacal solutions copper(I) ions are also stable, hence reactions that involve the reduction of copper(II) ions to copper(I) ions are feasible, provided the thermodynamic requirements of the process are met. The possibility of the involvement of the copper(I)/copper(II) redox couple is thus considered well worth evaluating for the chalcopyrite ammoniacal systems. Literature on chalcopyrite copper(I)/copper(II) ammonia systems could not be found but other ammonaical systems involving the copper(I)/copper(II) couple will be reviewed. While copper(II) is generally stable is aqueous solutions, copper(I) is susceptible to autoxidation and disproportionation but forms stable complexes with ligands such as chloride, iodide, ammonia, cyanide and imidazole. This makes application of cupric leaching limited to solutions in which copper(I) is stable hence cannot be applied to the widely researched sulphate leaching of chalcopyrite. It has however been shown in acid leaching that presence of the copper(I)/copper(II) redox couple improved leaching (Hiroyoshi et al, 2004; Dutrizac, 1992), this was done in the presence of chloride ions which can complex hence stabilize copper(I).

The role of copper(II) ions as an oxidant in ammoniacal solutions has been extensively studied by Byerley et al (1975; 1973) and van Wensveen (2010), who studied the oxidation of thiosulphate ions by copper(II) ions in the presence and absence of oxygen. These authors agree that the mechanism of this homogeneous oxidation reaction differs in the presence of oxygen. Under their conditions of study, Byerley et al (1973) found the oxidation of thiosulphate to be first order with respect to copper(II) ions, van Wensveen (2010) suggested a more complex rate equation at higher copper(II) ions concentrations. Byerley et al (1973, 1975), reported that with respect to the $(SO_4)^{2-}$ formation process, the role of the copper(II) ions species is to complex both the O_2 and $(S_2O_3)^{2-}$, providing a mechanism for electron transfer and allowing O_2 to interact via an ionic mechanism (Figure 2.6).

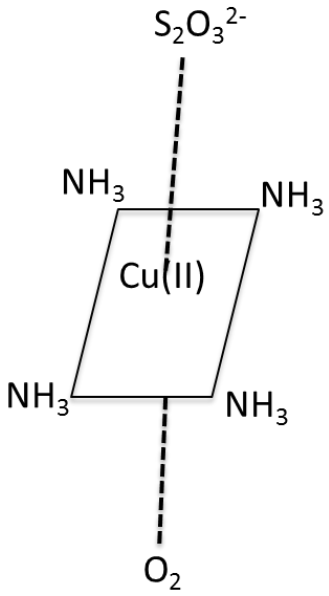

Figure 2.6. Schematic of the thiosulphate-copper(II)-oxygen complex redrawn from (Byerley et al 1975)

In a separate study, Koyama et al (2006) provided further evidence that copper(II) ions are an effective oxidant in ammoniacal solutions when they leached copper from printed circuit boards in the absence of oxygen. The authors observed that the concentration of copper(I) ions increased with time while that of copper(II) ions decreased. They proposed that the reaction occurs according to equation 29.

$$Cu + Cu(NH_3)_4^{2+} = 2Cu(NH_3)_2^{+} \qquad 2.29$$

Koyama et al (2006), went on to report decreased rates of leaching when $Cu(NH_3)_2^+$ was added to the initial leach solutions. Black (2006) studied the thermodynamics of the aqueous copper-ammonia-thiosulphate system and reported the speciation of copper(I) ions in solutions of high ammonia concentrations such as those produced in copper leaching to include the following species: $Cu(NH_3)_2^+$ as the abundant species; $Cu(NH_3)_3^+$ whose concentration increases with an increase in total ammonia and small quantities of $Cu(NH_3)^+$. Black's work(2006), which was aimed at obtaining relevant thermodynamic data for copper(I) ions and copper(II) ions species under experimental conditions that approximate those of gold leaching processes using thiosulphate, identifies the different copper(I) ions and copper(II) ions species present in an ammoniacal solutions. Van Wensveen (2010), Trevani et al (2001)and Black (2006) found the most prevalent copper(II) species in ammonia solutions at pH above 9.5 to be the tetraammine while the most prevalent copper(I) species is the diamine. The formation constant of the tetraammine-copper(II) and diamine-copper(I) are given by Richardson (1997) to be $6.3 \cdot 10^{10}$ and $1.3 \cdot 10^{2}$ respectively.

The role of copper(II) ions as an oxidant in mineral leaching in ammoniacal solutions has been extensively studied in gold processing (Van Wensveen, 2010; Cheng, 2003; Rajib et al, 1997). Rajib-Dasgupta et al (1997) studied the electrochemical behaviour of gold in ammoniacal solutions using various oxidants and suggested the rate of oxidation to be in the order $Cu(II)>Co(III)>O_2>H_2O_2$. The authors found the gold oxidation to be of order 0.38 with respect to copper(II) ions, and copper(II) ions were found furthermore to have no effect on the anodic current, while increasing the rate of reaction. They also found $Cu(NH_3)_4^{2+}$ and O_2 to have a synergistic effect on the dissolution rate of gold.

The possible role of Cu(II) as an active oxidant is apparent in leaching systems as outlined above. In chalcopyrite dissolution, the thermodynamic requirements of the process are such that it would be necessary that the potential window for the oxidation of the mineral be lower than that of the copper(I)/copper(II) redox couple and this is satisfied in the operating range of most chalcopyrite ammoniacal leaching studies found in literature. It has thus been considered worthwhile to evaluate the role of copper(II) ions in the oxidative dissolution of chalcopyrite in ammonia-ammonium sulphate solutions.

2.4.2 The Deportment of Iron

One of the stated advantages of ammoniacal leaching is the selective dissolution of copper over iron. The iron is reported to form a barrier on the mineral surface which then alters the dissolution kinetics of the mineral (Beckstead and Miller, 1977b; Stanczyk and Rampacek, 1966; Forward and Mackiw, 1955). The presence of an iron based surface layer has been widely reported by researchers in the ammoniacal dissolution of chalcopyrite (Guan and Han, 1997; Warren and Wadsworth, 1984; Beckstead and Miller, 1977a; Beckstead and Miller, 1977b; Stanczyk and Rampacek, 1966; Forward and Mackiw, 1955), however researchers have not reached a consensus on the actual composition of this product layer and how it is formed. Limited literature on the formation of the product layer could be found and this was in most instances not supported with any data. The presence of an iron based surface product is obviously visible and has also been observed during the course of the current study.

Passivation effect of the iron product

Passivation of chalcopyrite refers to its loss of reactivity associated with an increase in potential. This is a widely reported phenomenon under both acid and alkaline leaching (Pugaev, 2011; Córdoba et al, 2009; Tshilombo and Dixon, 2003; Bell et al, 1995; Hackl, 1995; Beckstead and Miller, 1977b). Forward and Mackiw (1955) suggested that sulphide minerals, chalcopyrite in this case, react with oxygen, water and ammonia to produce soluble salts in such a way that the iron present in each

mineral particle is converted to hydrated iron oxide in situ with the result that the particles, when leaching is complete, consist of hydrated iron oxide pseudomorphic with the original mineral. Beckstead and Miller (1977b) discuss the nucleation and growth of a haematite passivating layer, stating that this occurred on the anodic sites thus limiting the overall reaction by limiting the anodic reaction and that agitation up to 3000rpm increased the rate of reaction possibly by abrading off the haematite layer and exposing more of the "anodic sites". The issue of separating the leaching reaction to have anodic sites and cathodic sites as referred to by Beckstead and Miller (1977b) and other researchers (Santos et al, 2008; Habashi and Bas, 2014; Santos et al, 2008) , is in itself subject of controversy with Crundwell (Crundwell, 2013) having argued against the possibility of having physically separate anodic and cathodic sites, citing that this would imply possibility of flow of electrons through the bulk material.

The contradiction between Forward and Mackiw's work (1955) and Beckstead and Miller's work (1977b) is that Beckstead (1977b) looks at the nucleation and growth of the Fe product and identifies it as haematite while Forward and Mackiw (1955) looks at an ion substitution mechanism resulting in an iron product atypical of chalcopyrite. In a study on the surface oxidation of chalcopyrite in alkaline solutions, Yin et al (2000) worked in alkaline sodium tetra-borate solutions, at a pH of 9.2 and reported that the iron in the top layer of chalcopyrite oxidised forming a monolayer of $Fe(OH)_3$ and Fe_2O_3 while the copper and sulphur remained unoxidised in the original chalcopyrite crystal structure forming a phase they designated as CuS_2^* which together with the $Fe(OH)_3$ and Fe_2O_3 retarded the oxidation of the mineral.

Chandra and Gerson (2014) studied the surface speciation of freshly fractured chalcopyrite when exposed to oxygen or water or both oxygen and water using high-spartial-resolution scanning photoelectron microscopy (SPEM). The authors found no evidence of sulfoxy species and reported presence of Fe(III)-O after 50 min of exposure to oxygen only. On exposure to both oxygen and water, Fe(III)-O/OH^x/SO_n^y species were found on the mineral surface. The kinetics of these reactions were not reported, however the conclusion that there was an iron based surface product was apparent.

In a separate study Stanczyk and Rampacek (1966) found chalcocite (Cu_2S), covellite (CuS) and bornite (Cu_5FeS_4) to leach more readily than chalcopyrite under similar solution conditions. The authors attributed the lowered reaction extent of chalcopyrite to the formation of a haematite reaction product on the surface of chalcopyrite while bornite, which also contains iron was said to contain insufficient iron for it to have any significant effects on the reaction kinetics. In the development of the Sherrit-Gordon process, critical agitation speeds were reported and these are

said to have allowed for the abrading of the haematite layer thus improving leaching rates. Also, in the Arbiter process, intense mixing is done to achieve good oxygen transfer rates as well as to abrade the haematite phase from the surface unleached chalcopyrite, thus exposing a fresh surface for reaction. The role of the iron based surface product on passivating the chalcopyrite surface is reported to be similar to the passivation observed on the same mineral by a protective sulphur layer or jarosites in ferric sulphate leaching.

Due to the limited amount of literature available on the behaviour of iron in the chalcopyrite ammonia system, reference will be made to other studies involving iron oxidation. Kim et al (1991) studied the active passive behaviour of sintered iron in ammoniacal ammonium carbonate solutions at pH= 9.7 and reported that surface films were formed on the bulk iron during air exposure or immersion in ammoniacal solutions. The surface films were characterised by XPS. When immersed in ammoniacal solution open circuit potentials in the range 0.04-0.09 V (SHE) were reported, and the authors did not detect any dissolution of iron at these potentials. The XPS results and transients obtained during cathodic reactivation of the iron suggested that an air formed Fe_3O_4 was responsible for the observed behaviour. In another study, Lee et al (1985) studied the anodic dissolution of iron in ammoniacal ammonium carbonate solutions and reported that under the conditions of their study, iron exhibited three general regions (active, passive and oxygen evolution) in addition to a cathodic loop. The active regions were in the potential range -0.65 to -0.4 V (SHE) while the passive region was in the range -0.33 to 1.0 V (SHE). The observed cathodic loop was attributed to oxygen discharge.

2.4.3 Iron chemistry

Beckstead and Miller, (1977b) who proposed the most widely documented chalcopyrite dissolution equation suggested that the iron from chalcopyrite is oxidized to a ferric state, valence of +3 (Equation 2.3), this ferric iron could be considered a natural reaction product if it was accepted that iron in chalcopyrite is already in a +3 valence state as proposed by Pearce et al (2006).

Warren and Wadsworth (1984) reported significant amounts (3-20%) of ferrous iron in the product film. The authors postulated that a ferrous iron intermediate was formed, this can be readily oxidised to ferric, and the oxidation can be achieved even by traces of dissolved oxygen. Aside from the work of Warren and Wadsworth (1984), the presence of ferrous iron has not previously been reported for chalcopyrite leaching systems but is however possible especially when reference is made to the Caron process in which iron is first oxidised to ferrous which is in turn oxidised to ferric iron as per equations 2.30 and 2.31.

Due to limited literature on the deportment of iron in ammoniacal leaching of chalcopyrite, reference will be made to the behaviour of iron in the Caron process. The Caron process, has been described as the oxidative dissolution of pre-reduced iron based nickel-cobalt-copper in ammoniacal carbonate solutions at atmospheric temperature (Caron, 1950). At a pH of about 9.8 in ammoniacal solutions the dominant dissolved iron species is the ferrous tetra-ammine ion, and the dissolution reaction has been postulated to occur according to equation 2.31 (D'Aloya and Nikoloski, 2012; Roy, 2010; Nikoloski and Nicol, 2006; Nikoloski, 2002; Osseo-Asare and Asihene, 1979).

$$Fe + 4NH_3 \rightarrow Fe(NH_3)_4^{2+} + 2e \qquad 2.30$$

$$FeNi + O_2 + 8NH_3 + 2H_2O = Fe(NH_3)_2^{2+} + Ni(NH_3)_6^{2+} + 4OH^- \qquad 2.31$$

The ferrous ammine is oxidized in aerated solutions to form ferric, which does not form ammines and is thus precipitated as $Fe(OH)_3$ releasing the ammonia (Equation 2.32).

$$Fe(NH_3)_2^{2+} + \frac{1}{4}O_2 + 2OH^- + \frac{1}{2}H_2O = Fe(OH)_{3(S)} + 2NH_3 \qquad 2.32$$

Nikoloski (2002), showed that iron is prone to passivation in solutions typical of those used in practice and confirmed its occurrence in leaching reactors of a commercial scale in the Caron process. Passivation was shown to occur due to the formation of an oxide layer at potentials which can be attained in the presence of high concentrations of dissolved oxygen and/or other oxidants such as Co(III) ions (Nicol et al 2004).

Das and Anand (1995) studied the precipitation of iron oxides from ammonia ammonium sulphate solutions and found the precipitation of iron in the presence of oxygen to show a positive dependence on temperature in the range 343-363 K and a negative dependence on total ammonia at concentrations of 6.97-10.5 M with initial ferric concentrations of 1-13 gL^{-1}. The researchers found the nature of iron oxide precipitate to be sensitive to temperature, total ammonia and ferric iron concentrations under the conditions of their study. Asselin (2011) reported that Fe(II) ammines are only thermodynamically stable under reducing conditions and concluded that they were unlikely to be formed if oxygen was present. Asselin (2011) presented quasi equilibrium Pourbaix diagrams for the Fe-NH_3-H_2O system (Figure 2.7). According to the diagram, $Fe(OH)_3$ is the species presents at noble potentials across all pH ranges while $Fe(OH)_2$ is present only at pH above 11.

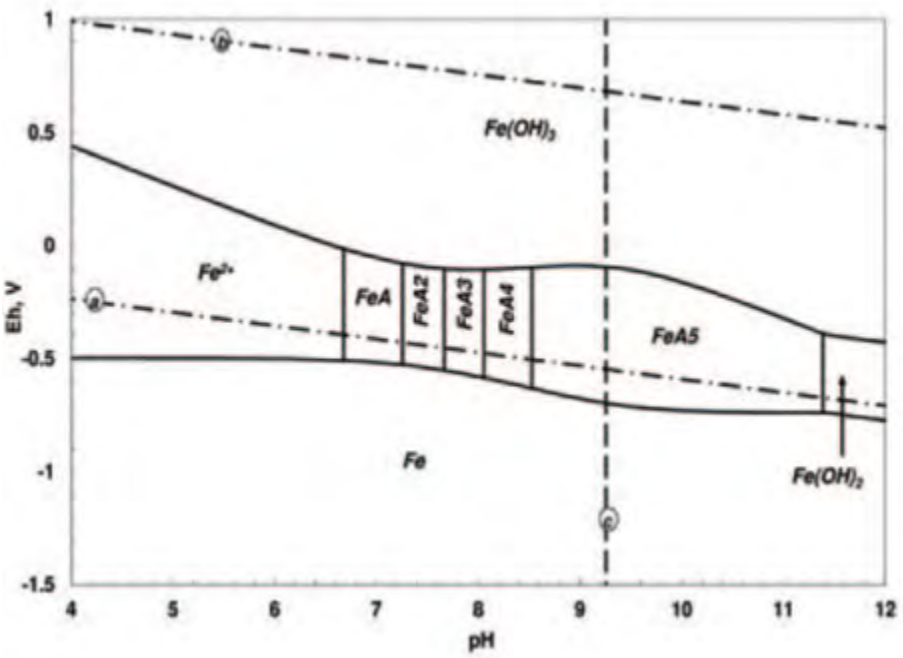

Figure 2.7. Quasi equilibrium pourbaix diagram Fe-NH_3-H_2O @ 298 K. [Fe] = 10^{-3} $[NH_3]_{Total}$ = 6 M. FeA_n represents the ammino-iron(II) species where "n" is the number of NH_3 ligands in the complex. (Source: Asselin, 2011).

Klocke and Hixon (1972) , speak of substantial amounts of iron in the ferrous state being soluble in high strength ammoniacal solutions (4.5-8.5 mols of NH_4OH per litre) while in dilute solutions the said iron was not soluble. The researcher carried out their study under chloride, sulphate and carbonate salts and their results were similar regardless of the choice of ammonium salt with the soluble iron species being found to be $Fe(OH)_2$ at pH 9.3-9.7. Leussing and Kolthoff (1952), in a study to determine the solubility product of ferrous hydroxide and the ionisation of the aqua-ferrous iron, found evidence of the formation of ammino-iron(II) complexes. Contrary to Klocke and Hixon (1972) who required high strength ammonia solutions and high iron concentrations, Leussing and Kolthoff (1952) report their work at 0.1 M Ferrous hydroxide in solutions between 0.1 M and 1 N ammonium chloride. The authors are however in agreement that solubility increased with an increase in ammonia concentrations.

Caldeira et al (2008) investigated the carbonate effect on pyrite oxidation in alkane solutions and identified (using diffuse reflectance infrared spectroscopy) iron carbonate compounds as one of the products of pyrite oxidation. The authors explain the increased oxidation rate typically observed on pyrite in carbonate solutions to possibly be due to the formation of Fe(II)-CO_3 complexes, the buffering effect of the carbonate and the fact that complexation with bicarbonate/carbonate provides a stronger Fe(III)/Fe(II) redox couple increasing the iron(III) ions solubility. The authors also produced predominance diagrams showing the existence of stable and metastable iron species

present in the iron carbonate system (Figure 2.8). The diagram shows solid and soluble Fe(II)-carbonate complexes [GR1$CO_{3(S)}$, $Fe(OH)_{2(S)}$, $FeCO_3^{0}{}_{(aq)}$, $Fe(CO_3)_2^{2-}{}_{(aq)}$ $Fe(OH)CO_3^{-1})_{(aq)}$] formed at pH range 6-12.

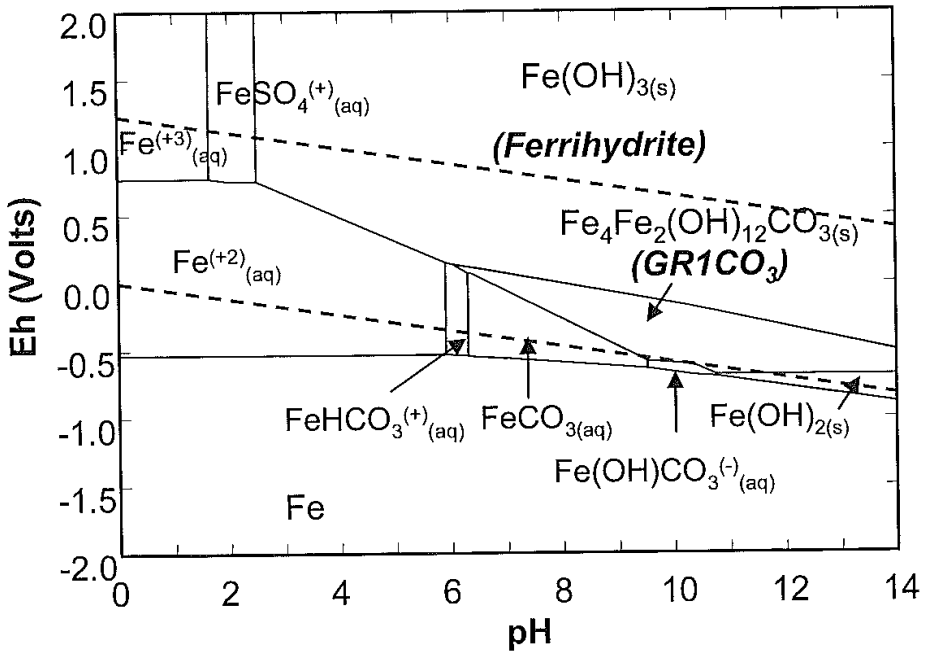

Figure 2.8. Eh-pH diagram for the metastable Fe-S-CO_3-H_2O system at 25°C showing stability regions for the ferrihydrite $Fe(OH)_{2(S)}$, GR1CO_3 ($Fe_4Fe_2(OH)_{12}CO_3$) and Fe(II)-carbonate complexes regions. Reproduced from Caldeira et al (2008).

In the presence of sulphate irons, the ferrous ammine may precipitate as $Fe(NH_3)_4SO_4$. Hydrolysis of this can occur according to equation 2.33 (Das and Anand, 1995).

$$Fe(NH_3)_4SO_4 + 2H_2O = Fe(OH)_2 + 2(NH_4)_2SO_4 + 2NH_3 \qquad 2.33$$

In the presence of oxygen ferric compounds can be formed (Equation 2.34) and these can be dehydrated to give haematite (Equations 2.35 and 2.36). In general, the nature of iron oxide precipitants is reliant on solution conditions. Das and Anand (1995) found crystalline magnetite to form in solutions at 6.97 M total ammonia, 13 g/L ferrous iron at temperatures between 70 and 90°C, while crystalline haematite was formed at even higher total ammonia 6.97-11 M but at lower ferrous iron concentrations 1 g/L, and temperature of 90° C. In a separate study, Wang et al (2007) were able to precipitate ammoniojarosite at around 95°C in solutions containing 165 mM ammonium ions.

$$Fe(NH_3)_4SO_4 + 10H_2O + O_2 = 4Fe(OH)_3 + 4(NH_4)_2SO_4 + 8NH_3 \qquad (2.34)$$

$$2Fe(OH)_3 = Fe_2O_3.3H_2O \qquad (2.35)$$

$$Fe_2O_3.3H_2O = Fe_2O_3 + 3H_2O \quad (2.36)$$

2.4.4 Sulphur chemistry

The oxidation state of sulphur ranges from S^{-2} in sulphides to S^{6+} in sulphate, i.e. during chalcopyrite oxidation a possible eight electron transfer per sulphur is possible. Sulphur exhibits oxidation states of -2, 0, +2, +4 and +6. In aqueous solutions, the form in which anions containing sulphur occur is largely dependent on pH. At low pH reduced sulphur may be present as undissociated H_2S while at high pH it would be present as HS^- and at very high pH as S^{2-}. Oxidised sulphur may be present as HSO_4^- in strong acid but SO_4^{2-} prevails in pH ranges of natural water (Hem, 1960). The application of redox potentials to evaluation of reactions involving sulphur is complicated because oxidation or reduction of sulphur through chemical agents alone is commonly very slow, with sulphate and sulphide commonly existing for a long time at Eh levels where they are not expected to be stable (Hem, 1960). Hamilton and Woods (1981) investigated the surface oxidation of pyrite and pyrrhotite and reported that the formation of sulphur was restricted to the order of a monolayer at pH 9.2-13. They also found that the proportion of sulphate formed increased rapidly with an increase in potential. This is in agreement with a report by Filmer et al (1979), who found sulphur to be formed on the surface of copper sulphides in ammonia solutions, however restricted to pH range 10-10.5, above which the sulphur was then oxidised according to equation 2.37. Filmer also found that the formation of sulphur from CuS and Cu_2S improved in their stated pH window under highly oxidising conditions and proposed that this sulphur did not come from the disproportionation of sulphur-compounds in solution but rather from solid state reactions according to equation 2.38.

$$2S + 3O_2 + 4OH^- = 2SO_4^{2-} + H_2O \quad 2.37$$

$$Cu_yS = yCuS + (1-y)S \quad 2.38$$

In a separate study, Chander et al (1992), reported that a sulphur rich layer was exposed when iron in pyrite dissolved by complexation with EDTA. This observation was in agreement with that of Buckley and Woods (1987) who reported that initial oxidation of sulphide minerals proceeds through progressive removal of metal atoms leaving the sulphur species largely unaltered. Warren and Wadsworth (1984) studied the electrochemical oxidation of chalcopyrite in ammoniacal solutions and reported an amorphous surface product but also stated that in some instances, when testing the surface product, they observed the presence of elemental sulphur. The researchers also reported that the electrolyte showed positive results for elemental sulphur and they concluded that the film and electrolyte contained intermediate sulphur species capable of forming elemental sulphur by disproportionation. Their conclusion contradicted that of Filmer et al (1979) which was

that the sulphur they observed in copper sulphide leaching came from solid state reactions. Warren and Wadsworth (1984) tested the sulphur species they found and identified it to be orthorhombic sulphur.

Possible formation of polysulphide intermediates in ammonia systems has previously been reported and is widely accepted for sulphide mineral leaching (Arbiter and McNulty, 1999; Warren and Wadsworth, 1984; Filmer et al, 1979; Tozawa et al, 1976; Forward and Mackiw, 1955). Thermodynamically, aqueous polysulphide solutions are unstable and sulphur dissolved as polysulphide decomposes to thiosulphate $S_2O_3^{2-}$ in accord with net consumption of dissolved sulphur (Litch and Davis, 1997), equation 2.39. In the presence of an oxidant, the thiosulphate oxidises to sulphate.

$$4S_{dissolved} + 4OH^- \xrightarrow{yields} S_2O_3^{2-} + 2HS^- + H_2O \qquad 2.39$$

Figure 2.9 shows the metastable Eh-PH diagram of an S-H_2O system at 25 °C and 1M sulphur. According to the diagram, elemental sulphur will be stable in a very narrow window around pH 9-9.5 and potentials; the typical pH window for ammoniacal sulphide leaching.

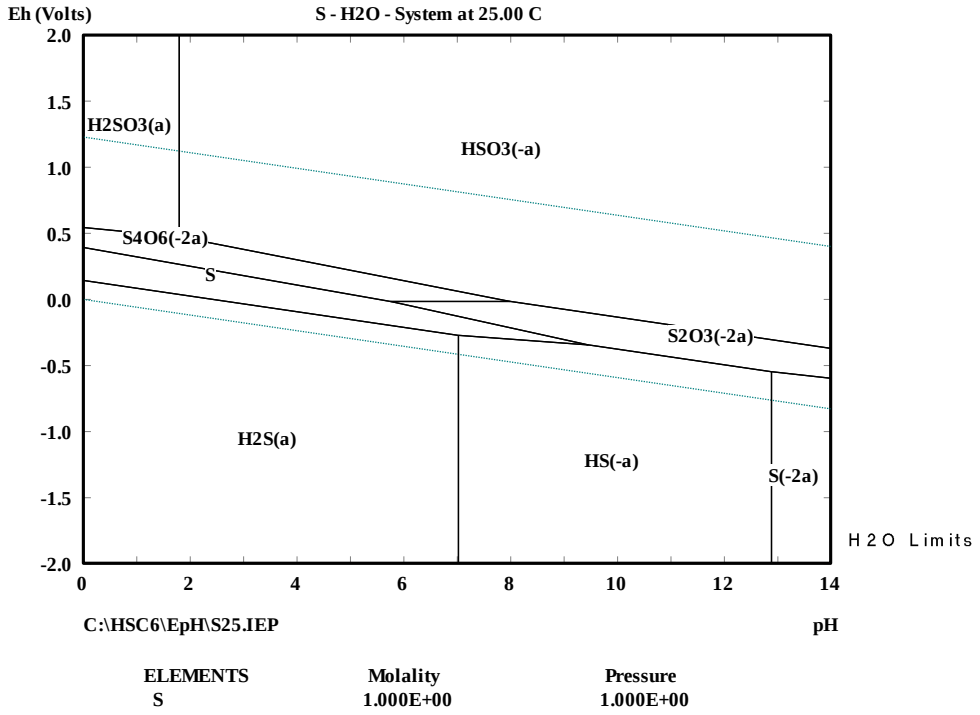

Figure 2.9. Metastable Eh-Ph diagram for the S-H_2O system at 25°C. [S] =1 M. Generated using HSC Chemistry 6

2.4.5 Deportment of sulphur in chalcopyrite oxidation

The deportment of sulphur in the electrochemical leaching of chalcopyrite is not extensively reported. Researchers have reported that the oxidation reaction is complicated by the fact that the sulphide is not directly oxidised to sulphate but goes through intermediates such as thiosulphate, polythionate and sulphamate, all of which are present in varying amounts (Warren and Wadsworth, 1984; Beckstead and Miller, 1977b; Tozawa et al, 1976; Forward and Mackiw, 1955).

The role of sulphate ions in ammoniacal leaching

In ammonia-ammonium sulphate solutions, the ammonium sulphate is generally added for its buffering effect on the pH. Muzawazi (2013) investigated the influence of different ammonia salts on the leaching of base metals in a platreef ore concentrate and found ammonium carbonate to have better buffering effects due to its double buffer properties as well as to give better metal recoveries over a 5 day period. The choice of anion present in leaching solutions was reported to be important by Forward and Mackiw (1955), as this anion and the amount of NH_3 will determine the stability of the dissolved metal in solution. Literature gives contradicting reports on the effect of sulphate ion concentrations in the ammoniacal leaching of chalcopyrite. Tozawa et al (1976), Abiter and McNutty (1999) and Stanczyk and Rampacek (1966) found that copper extraction rates increase in the presence of sulphate ions with Ek et al (1982) reinforcing the need to use a sulphate based buffer system because he had found the ammonium sulphate to eliminate the build-up of the oxidised phase around the leaching particle. Contrary to this, Rao and Ray (1998) reported that sulphate ions did not have any beneficial effect in the leaching of chalcopyrite. For an ore containing, chalcopyrite and other copper sulphides, Duyvesteyn (1995) reported that the initial rate of copper dissolution is constant at high levels of ammonium sulphate i.e.>80 g/L but the final extraction is a function of applied ammonium sulphate concentration.

2.5 Problem statement and research approach

Literature survey has indicated that ammoniacal leaching of chalcopyrite is a technically viable process. Ammoniacal processing was researched and developed to bench and commercial scale in the 20th century most of which were decommissioned due to non-specified technical problems. In the present day, the need to resort to treating low and mixed grade ores which cannot be economically processed through the traditional pyrometallurgical processes has grown and this further prompts the need for further research into hydrometallurgical based treatment processes. Ammoniacal leaching has not received much attention relative to the acid systems, especially ferric sulphate leaching, despite the fact that ammoniacal systems have shown promise in the past. The leaching reaction has been reported to be promoted by the presence of copper(II) ions but their

exact role has not been reported with researchers taking a rather simplistic explanation stating that copper(II) ions catalyse the reaction. Problems relating to growth of a surface deposit layer (thought to be related to the iron species in chalcopyrite) on the leaching chalcopyrite surface as well as poor oxygen mass transport have been cited as explanation for the slow leach kinetics. Not much research has been done to evaluate the formation of this surface deposit layer and relate it to observed kinetics. Furthermore, the nature of this surface deposit layer remains controversial. The leaching reaction has mostly been studied through bulk leach tests with only a few studies carried out using electrochemical techniques. Electrochemical techniques provide a tool that can analyse reactions at high sensitivity, typically not achieved in in bulk leach tests and have been demonstrated to be capable of providing invaluable information pertinent to surface reaction mechanism and kinetics. These techniques have been employed widely in the study of chalcopyrite acid leaching but little has been done towards showing how well the results from bulk leach studies and electrochemical studies corroborate.

It is the objective of this thesis to establish the role of copper(II) ions in the leaching reaction; to determine the deportment of iron from the leaching chalcopyrite and to characterise the surface deposit layer and determine how it affects the leaching reaction. This will lead to establishing the leaching mechanism of chalcopyrite in ammoniacal solution. And lastly, effort will be made to establish how well electrochemical techniques can be used to predict bulk leaching kinetics.

The following hypotheses have been formulated and will be tested;

- The oxidation reaction proceeds through electron transfer from the oxidising sulphur in the chalcopyrite to an intermediate copper(II)-oxygen complex formed in solution.
- The formation and nature of the surface deposit layer is influenced by anions present in solution as well as by the mechanical and fluid dynamic environment in which the leaching reaction proceeds.

The approach to this study will be as follows;

- Carry out electrochemical tests which will be split into;
    1. Measuring chalcopyrite's rest potentials in varied solution conditions in the presence and absence of oxygen.
    2. Carry out cyclic voltammetry tests in the anodic and cathodic direction starting from rest potential.

3. Carry out constant potential tests in solutions that do not contain a chemical oxidant. The tests will be run at potentials corresponding to the rest potentials measured in 1 above.
4. Do surface analysis to identify the surface deposits formed in the electrochemical tests in different solution conditions.

- Carry out controlled leach tests
  5. Run bulk leach tests.
  6. Do surface analysis and chemical analysis on the leach residue.

3 Materials and Methods

Introduction

The bulk of this work was carried out using electrochemical studies, through the measurement of open circuit potentials, generation of cyclic voltammograms and chronoamperometric tests. Controlled leached tests were done as additional work to allow for the generation of sufficient surface product as well as to provide data to allow comparison of controlled leaching to electrochemical oxidation tests.

3.1 Materials

3.1.1 Chalcopyrite sample

A sample of natural chalcopyrite was supplied by VWR International, Wards Natural Science. The sample originated from Durango, Mexico. The purity of the sample was confirmed through XRD, XRF and QEMSCAN analysis. XRD analysis (**Figure 3.1**) of the mineral sample showed a small impurity peak at the 31 2-theta scale but this was indicated to be a trace impurity after quantitative analysis of the XRD data which indicated the sample to be 100% chalcopyrite. Results from a chemical analysis of the sample using Inductive Coupled Plasms Optical Emission Spectroscopy (ICP-OES) and LECO indicated 32.0% Cu, 30.5% Fe, 33.4% S, 2.4% Zn, and 1.2% Ca. QEMSCAN analysis of the sample indicated it to be 95% chalcopyrite, with small amounts of sphalerite, calcite and quartz (**Table 3.1**). XRF indicated presence of 0.2% silica, 1% zinc and 0.7% lead in the sample. Thus, the sample was accepted as being of high purity.

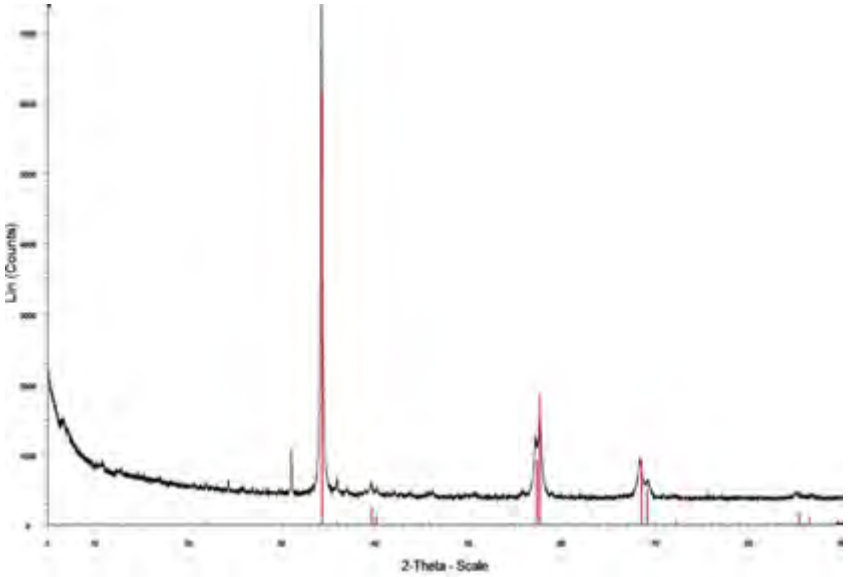

Figure 3.1. XRD spectra for Chalcopyrite sample used in the study

Table 3.1. QEMSCAN results for chalcopyrite sample.

Mineral	% Composition
Chalcopyrite	95.24
Sphalerite	3.32
Calcite	1.30
Chlorite	0.11
Other sulphides	0.03

3.1.2 Electrode preparation

Chalcopyrite working electrode

Electrodes were prepared by cutting the mineral into cuboid shapes about 15 mm long. These were mounted on brass stubs with conductive silver epoxy (Advanced Laboratory Solutions) and the assembly then imbedded in non-conductive epoxy resin and left to dry. Subsequently, the electrode stub was attached to an electrode holder comprising of a copper connector embedded in non-conductive epoxy resin (Figure 3.2), the electrode assembly could then be threaded onto a rotating disk motor. The electrode surface was subjected to a series of polishing stages on SiC abrasive paper of 1200 grit size, then on 1 µm, 0.3 µm and 0.05 µm aluminium oxide prior to each experiment except where stated. This was done to ensure a homogenous chalcopyrite surface was exposed to the solution in each test and that any form of surface oxides had been removed. Two electrodes cut from the same chalcopyrite sample were used through the course of the studies and the exposed surface areas of the two was measured to be 0.4277 cm^2 and 0.3604 cm^2 using imagej® for image analysis of photographs of the electrode surface.

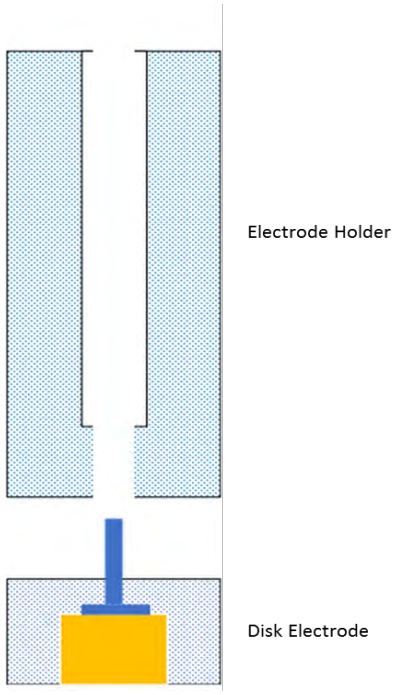

Figure 3.2. Schematic of the working electrode showing the chalcopyrite stub and the electrode holder.

Reference Electrode

A Saturated Calomel reference Electrode (SCE) supplied by Metrohm was used for all experiments. The potential of the reference electrode was routinely checked against that of a master silver/silver chloride electrode which was stored separately and not used for any day to day laboratory test work. All potentials in this work are reported against the Standard Hydrogen Electrode (SHE) by adding 241 mV to the measured potentials.

Platinum wire (Auxiliary electrode)

An auxiliary electrode was fabricated by soldering a 30 mm platinum wire to a copper wire 0.5 mm in diameter. The assembly was then embedded in non-conductive epoxy resin leaving 20 mm of the platinum wire exposed on the front end and an equal length of copper wire exposed on the opposite end (**Figure 3.3**).

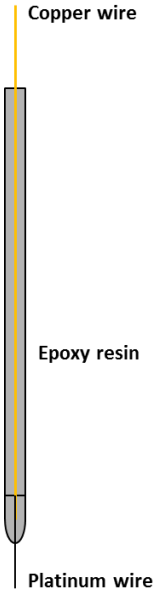

Figure 3.3. Schematic of the fabricated auxiliary platinum electrode

3.1.3 Test solutions preparation

Test solutions were prepared from distilled, deionised water and analytical grade $CuSO_4.5H_2O$ (Merck), NH_4OH (25%, Merk), $(NH_4)_2SO_4$(Merk), $(NH_4)_2CO_3$(Sigma Aldrich®), NH_4ClO_4(Sigma Aldrich®), H_2SO_4(Merk)and NaOH(Merk). NH_4OH was the solvent in all cases except where stated otherwise and it was mixed with an ammonium salt of choice at a ratio of 1:1 ratio on the ammonium ion, e.g. 1 M NH_4OH : 0.5 M $(NH_4)_2SO_4$ or 1 M NH_4OH : 1 M NH_4ClO_4. Ammonia concentrations are reported based on total ammonia i.e. (NH_3+NH_4^+). In experiments requiring the addition of copper at the start of the experiment, the copper was added by dissolving CuSO4.5H2O in the ammonia-ammonium salt solutions. The NH_3 consumed by complexation with added copper (II) was replaced by the addition of stoichiometric amounts of ammonium hydroxide. pH levels were maintained within (range) by addition of either H_2SO_4 or NaOH in all tests unless otherwise stated.

Preparation of copper(I)-diammine solutions

Copper(I) solutions were prepared by reacting copper(II) from copper sulphate in solution with powdered metal copper in an air tight container under nitrogen in solutions of excess ammonia. Copper(I) would be formed according to reaction equation 3.1.

$$Cu^0 + Cu^{2+} = 2Cu^+ \qquad 3.1$$

Nitrogen was first bubbled through solutions of ammonia-ammonium sulphate to remove oxygen, the depending on the desired copper(I)/copper(II) ratio, copper metal powder was introduced into the reactor and the reactor once again sealed. This reaction was carried out in the reactor in which

the subsequent electrochemical test was carried out. Once all copper metal powder had reacted completely and metal particles were no longer seen to settle when stirring stopped, it was assumed that the reaction had reached completion and desired copper(I)/copper(II) ratios had been achieved. The electrochemical experiment was run subsequent to this copper(I) generation reaction.

3.1.4 Electrochemical tests

A 250 mL thermostatted cell (supplied Metrohm) was used to carry out all the electrochemical measurements. 80 mL of test solution (except otherwise stated) were added into the cell and temperature was regulated via the thermostatted jacket. Either oxygen (99.99%) or nitrogen was bubbled into the electrolyte for 10 min prior to starting the experiments. Subsequently, the electrodes were put in place and the desired test was started. Bubbling was continued throughout the experiment, taking caution to ensure gas bubbles did not accumulate on the chalcopyrite electrode surface.

Preliminary tests were conducted in which either oxygen or nitrogen was bubbled into solutions of the same volume and similar composition to those used in the tests to assess the rate of saturation. Figure 3.4 shows the degree of oxygen saturation of a solution of 1 M total ammonia containing 5 g/L copper(II) at different temperatures. The graph clearly shows that there was very little change in dissolved oxygen after 5 min with the solution at 25°C having reached saturation in that time frame. Tests of sparging the solutions with nitrogen showed that the percentage saturation of the solutions with oxygen decrease to less than 1% in just under 3 minutes.

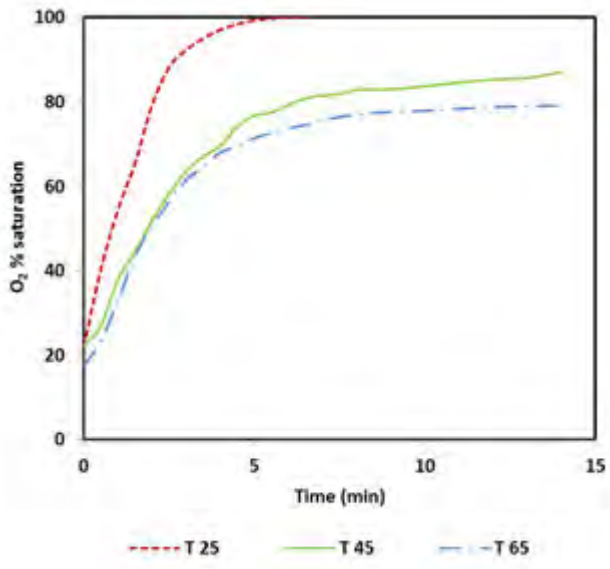

Figure 3.4.% oxygen saturation in 1 M (NH_3+NH_4^+), pH 9.6±0.15 in the presence of 5 g/L initial Cu(II).

A schematic of the configuration and a picture of the cell set up are shown in Figure 3.5. A Gamry Series G 300/750 Potentiostat was used for all the tests.

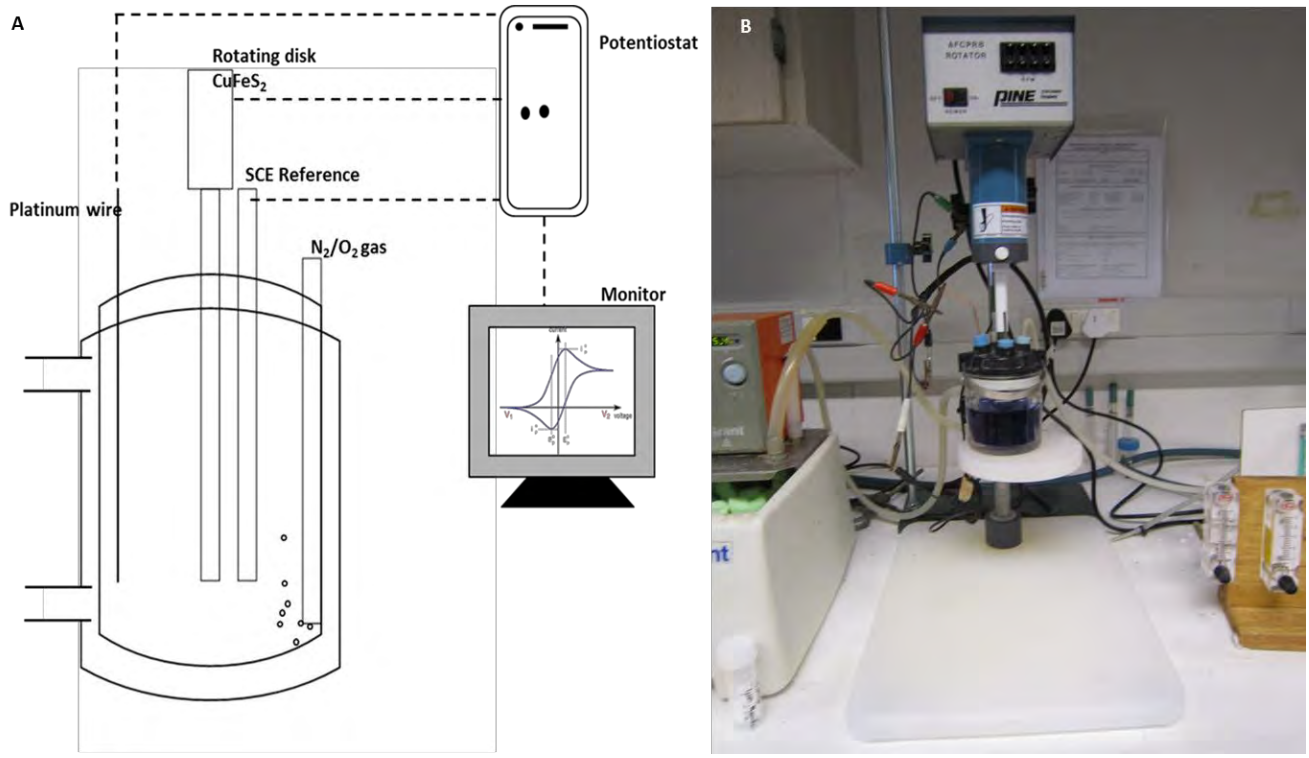

Figure 3.5. A-Schematic of electrochemistry tests set up. B- Image of the laboratory set up showing the cell and electrodes.

Open circuit or rest potential tests

Open circuit potentials were run on the test solutions described above. The electrodes were allowed to equilibrate (kept at open circuit) with the solution for 30 minutes in all cases except were longer equilibration periods were desired. Potential time transients were recorded, and the values reported and discussed in the results section are the final potentials measured after the 30 minutes equilibration period except where stated otherwise. In each test, a freshly polished chalcopyrite electrode was used (see section 3.1.2).

Cyclic voltammograms

Cyclic voltammograms were generated immediately after the measurement of the open circuit potentials except where stated otherwise, i.e. a freshly polished chalcopyrite electrode was allowed to equilibrate for 30 minutes prior to the start of each cyclic voltammogram. The voltammograms were generated at a scan rate of 1 mV/sec. The forward (anodic) sweep limit was set to 300 mV above rest potential and then swept back to cathodic potentials set to 250 mV below the rest

potential. Where more than one sweep was desired, a second forward sweep was done immediately after the cathodic sweep. This allowed for observation of currents due to oxidation of species generated during the preceding cathodic sweep. Additional sweeps were done which started at rest potential sweeping in the negative direction to potentials 250 mV below rest potential, then reversing this to values 300 mV above rest potential.

Chronoamperometric tests

Anodic tests

Chronoamperometric tests where run on freshly polished electrode surfaces without allowing the electrode the 30 minute initial equilibration in solutions that *had no* initial copper(II). Experiments were carried out by fixing the potential at values measured in the rest potential tests described above (after 30 min) and at values in the vicinity of the rest potentials up to ±100 mV in solutions without initial copper(II). It should be reiterated that chronoamperometric tests were done in solutions of similar composition to which the corresponding rest potentials were measured but in the *absence* of copper(II) ions. At rest potential, there is no net flow of current but a setup such as the one described in this passage allowed for the isolated measurement of anodic currents corresponding to anodic contributions at rest potential i.e. dissolution current densities of chalcopyrite at rest potential. The current response of the electrode was measured for 2 hours unless stated otherwise. Where coulometric calculations were intended, the tests were run for either 5 hours or 22 hours in 30 mL of solution. At the end of the experiment the solutions were analysed in triplicate for copper using Inductively Coupled Plasma Optical Emission Spectroscopy (ICP-OES) described in section 3.2.1.

Cathodic tests

Tests were done by setting the potential to arbitrarily chosen cathodic potentials within the vicinity of the rest potential of the chalcopyrite. Prior oxidation of the electrode was done for an hour at 255 mV (unless otherwise stated) and subsequently followed by switching to cathodic potentials and observing current response for 2 hours, bringing total run time for each test to 3 hours. Cathodic tests were carried out in solutions containing initial copper(II) at varied concentrations in the presence/absence of oxygen. The electrode was polished prior to the start of each experiment.

3.1.5 Leaching tests

A similar sample to that used in making the disc electrode was used. The sample was micronized (81% passing -75 µm). Prior to each experiment, the sample was washed in sulphuric acid to remove an oxide layer which had been indicated to be present from preliminary tests. The sample was rinsed by flushing in distilled water, dried and weighed prior to the start of each experiment. Thermostatted 500 mL reactors were used for the tests (Figure 3.6). Test solutions were introduced into the reactor and temperature allowed to equilibrate. Either oxygen (99.99%) or nitrogen was bubbled into the electrolyte for 10 min prior to starting the experiments and a blanket of the gas then maintained over the solution through the entire experiment. The chalcopyrite sample was then added and this was considered to be the time at which the experiment started. Magnetic stirrers were used for agitation purposes. Starting pH of the solutions was 9.6±0.15 from the buffer of the ammonia ammonium sulphate. This was measured at each sampling point and when it was found to have dropped below acceptable values, ammonia solution was used to bring it up to the desired point.

Additional controlled leach tests were carried out on 5 mm x 5 mm x 5 mm pieces of chalcopyrite in 3 M total ammonia–ammonium sulphate solution, pH 9.6±0.15 at 25°C in two reactors (Reactors A and B). Reactor A had glass beads added which allowed for the abrasion of the surface product from the chalcopyrite blocks, while reactor B had no beads in it. The leaching experiments went on for a period of 5 days, allowing for significant amounts of surface product to be generated. Magnetic stirrers were used; this was adequate to keep the sample in swirling motion but could not suspend the sample in solution. The leach residue was analysed i.e. both the debris from reactor A and the remaining unleached chalcopyrite.

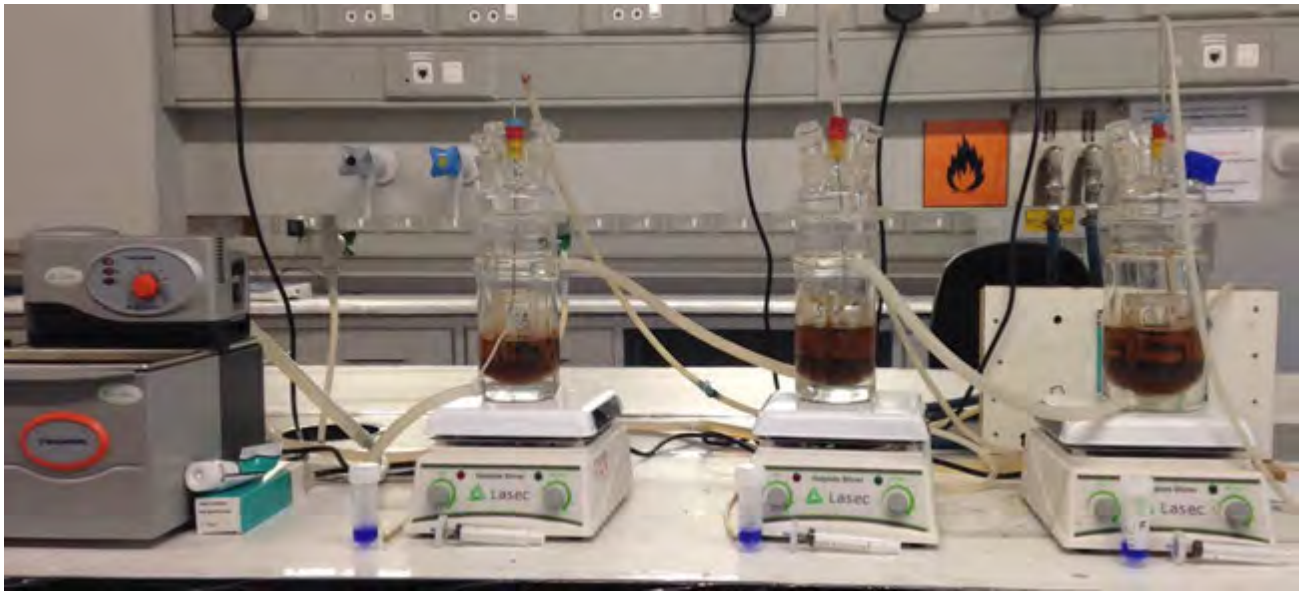

Figure 3.6. Leaching reactors for the bulk leaching tests

3.2 Analytical Techniques

3.2.1 Chemical Analysis

Acid digestion of solids

A chemical analysis was done on the chalcopyrite sample prior to and post leaching. This required acid digestion of the sample prior to ICP or AAS analysis. 50 mg of sample was placed in a mixture 6 mL of concentrated Hydrochloric Acid (HCl), 2 mL concentrated Hydrofluoric Acid (HF) and 2 mL concentrated Nitric Acid (HNO_3). Digestion was carried out in a MarcsXpress (CEM) microwave oven at 1600 W, 180°C for a total time of 30 minutes.

Atomic Absorption Spectroscopy (AAS)

AAS was used to quantify the copper and iron in solutions after controlled leach tests as well as on digested leach residues. The technique quantifies chemical elements based on the absorption of optical radiation by free atoms in gaseous state. A Varian SpectrAA 110 model was used for the analysis.

Inductive Coupled Plasms Optical Emission Spectroscopy (ICP-OES)

This type of analysis was employed to quantify copper from solutions used in electrochemical tests after 5 or 22 hours oxidation at fixed potentials (potentiostatic tests done for Coulometry purposes). Samples from these tests contained low concentrations of copper which may have been below the

detection limits of AAS analysis. The technique relies on atomic emission generated by a combustion flame. A Varian 730-ES model was used for the analysis.

3.2.2 Mineral and surface deposit layer analysis

X-ray powder diffraction (XRD)

XRD is a rapid analytical technique primarily used for phase identification of a crystalline material (Dutrow and Clark, web page). This technique was used for the analysis of chalcopyrite samples prior to leaching as well as for the analysis of leach residue. The XRD spectra was collected using a Bruker D8 Advance powder diffractometer with Vantec detector and fixed divergence and receiving slits with Co-Ka radiation at a scan of 10 – 90 2-Theta. The phases were identified using Bruker Topas 4.1 software (Coelho, 2007) and the relative phase amounts (weight%) were estimated using the Rietveld method.

Since it was expected that the leach residue would be largely amorphous, the samples were first analysed to identify and quantify any crystalline phases present. This was then followed by a procedure in which the same leach residue sample was spiked with a known quantity of crystalline phase material then reanalysed so as to quantify the non-crystalline phase. 0.03565 g of corundum (crystalline material) was used to spike 0.32085 g of the leach residue.

Scanning Electron Microscopy (SEM) and Energy Dispersive Spectroscopy (EDS) Analysis

This technique analyses the surface of materials employing the use of a focused beam of high-energy incident electrons which are rastered across the surface of a sample. Interactions between the electron beam and atoms at various depths within the sample will cause the release of electrons which can be then be collected with a suitable detector. A Nova Nano Field Emission Gun (FEG) SEM was used carry out the measurements. SEM provides information on the external elemental composition and morphology/texture of a solid sample. The technique was employed to analyse the surface of the electrode prior to and post leaching in a bid to identify the surface deposit and establish how its morphology differed from that of the unleached surface. Residue from bulk leach tests were also subjected to this form of analysis. Energy Dispersive Spectroscopy (EDS) works in conjunction with the SEM for the elemental characterisation of the samples. EDS allows for the identification of elements and their relative proportions. The interaction between the electron beam and sample as described in the SEM, produces various emissions, amongst which is X-rays. An EDS detector separates characteristic X-rays of different elements into an energy spectrum and EDS system software is used to analyse the energy spectrum in order to determine the abundance of specific elements (Goodge, 2016). The EDS spectra were collected using an Oxford Instruments X-

MAX 20 mm^2 silicon drift (SDD) at beam energy of 20 keV. The electron penetration depth for the instrument is given by equation 3.2.

$$R = \frac{4120}{\rho} E^{1.265-0.0954lnE} \qquad 3.2$$

In which R is the penetration (microns), E is the primary electron energy (MeV) and ρ is the absorber density (gcm^{-3}). The electron penetration on chalcopyrite with a density of 4.18 gcm^{-3} was determined to be 30.1 µm.

Quantitative Evaluation of Minerals by Scanning Electron Microscopy (QEMSCAN)

QEMSCAN measures the mineralogical variability of a solid sample based on its chemistry at a micrometre scale. It employs an integrated use of electron beam technology SEM, EDS and back scattered electron (BSE) to allow for an automated analysis of mineral samples. A QEMSCAN 650F, using a field emission gun-scanning electron microscope (FEG-SEM) and equipped with two Bruker 4010 SDD detectors was used. Chalcopyrite samples were analysed prior to and post leaching in order to confirm purity of the mineral prior as well as identify changes in nature of the mineral surface post oxidation. Leached ore samples from the bulk leach studies were dried and mounted into epoxy resin. Leached blocks (Section 7.4) were also mounted similarly but in such a manner that a cross section of the mineral sample could be viewed during analysis.

Malvern Particle Analysis

A particle size distribution for the sample was done using Malvern particle analysis equipment Malvern 2000 and the Malvern Hydro 2000 models. Figure 3.7 shows a Malvern particle size distribution curve for the chalcopyrite sample prior to leaching.

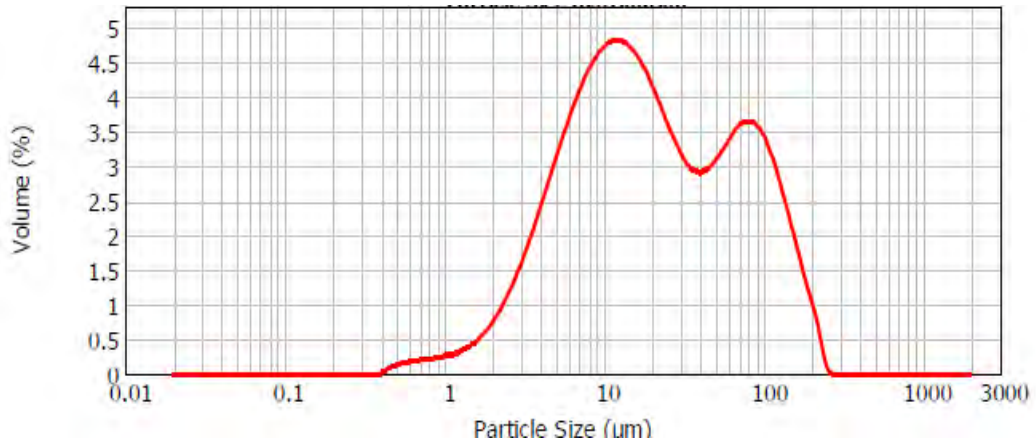

Figure 3.7. Malvern particle size distribution of the chalcopyrite sample.

Brunauer–Emmett–Teller (BET) Surface analysis

Physisorption tests were done in order to characterise the surface of chalcopyrite prior to and post leaching. The surface area and pore volumes were determined using a Micromeritics Vac Prep 061 and a Micromeritics Tristar II 3020.

3.2.3 Results analysis methods

Arrhenius plots

The Arrhenius equation (Equation 3.3) was used to calculate activation energy in all instances.

$$k = Ae^{\frac{-Ea}{RT}} \quad 3.3$$

In which k is the initial rate of reaction reported as current densities μAcm^{-2} or $gL^{-1}D^{-1}$.

A is the pre-exponential factor.

Ea is the activation energy (J)

R is the universal gas constant (8.314 $Jmol^{-1}K^{-1}$)

T is the absolute temperature (K)

Equation 3.3 is linearised to get equation 3.4 and the slope of a plot of Ln k versus 1/T is equal – Ea/R.

$$\ln k = -\frac{Ea}{RT} + lnA \quad 3.4$$

Compensation for iR drop

IR compensation, as the name suggests, compensates for errors made in measured currents due to resistance across the solution. The electrolyte used for the tests was conductive however, it was necessary to do iR compensation when measured current densities were high such as in cathodic reduction tests. Resistance of the solution was determined by taking the inverse of the slope of the linear part of the cyclic voltammetry curve at potential about 50 mv above rest potential. At such high regions, it is expected that the resistance due to the electrochemical reaction has become constant and the solution resistance is what changes. The true potential on the mineral surface was

then calculated from Ohm's law (Equation 3.5) for every data point along the potential current transient.

$$V = IR \tag{3.5}$$

Conversion of leaching rate to charge

Where necessary, the rate of leaching from bulk leach tests was converted to charge density, similarly current densities from constant potential tests were also converted to charge density. Leaching rates were converted starting from the unit of g/hour and taking the following steps;

i. Convert ghr^{-1} to $molhr^{-1}$ by dividing by the molar mass of copper(II) 63.55 g.
ii. Multiply the leaching rate $molhr^{-1}$ by the number of electrons transferred per mol of dissolved chalcopyrite measured as dissolved copper in solution to get the number of mols of electrons transferred per hour in the test.

Taking a basis of 1 hour

iii. Multiply the mols of electrons transferred in 1 hour in ii) above by the number of coulombs per mole of electrons, 96485 $Cmol^{-1}$.
iv. Since samples are different sizes, divide answer to iii) by total surface area of sample to get answer as a charge density with units of Ccm^{-2}.
v. The charge density from iv can be divided by the time 3600 seconds to give current density.

4 Rest Potential and Anodic Reaction Results and Discussion

4.1 Rest potentials

The oxidative leaching of sulphides has been established to be an electrochemical process (Elsherief, 2002; Hiskey, 1993; Biegler and Horne, 1985; Warren and Wadsworth, 1984; Biegler and Swift, 1979; Beckstead and Miller, 1977a; Reilly and Scott, 1977; Forward and Mackiw, 1955), as such it is expected that the rate of leaching will be dependent on potential. The dissolution of chalcopyrite in conditions of industrial interest occurs at open circuit potential (also referred to as rest potential or mixed potential), where the potential of the electrode is not imposed by an external source such as a potentiostat (Olvera et al, 2015). Thus, studies of rest potentials and the dissolution current densities of chalcopyrite at the measured rest potentials form the core of this work considering we are looking to understand the reactions that chalcopyrite undergoes under freely dissolving conditions. For the purpose of this thesis, rest potentials will be referred to as mixed potentials from hereinafter. It is interesting to note that a vast amount of work in literature on the application of electrochemical techniques focuses mostly on voltammetry studies (Vasquez et al, 2011; Elsherief, 2002; Biegler and Horne, 1985; Warren and Wadsworth, 1984; Warren et al, 1982; Biegler and Swift, 1979; Jones, 1976) leaving this very significant aspect of mixed potentials measurements mostly unexplored.

Mixed potentials have been measured by recording the potential of a rotating disk chalcopyrite electrode in the absence and presence of initial copper(II) ions at varied concentrations in ammonia-ammonium sulphate solutions at 1 M [NH_3+ NH_4^+], 25°C, 1600 rpm and pH 9.6±0.15 unless otherwise stated. These allow us to establish the relevant operating potential region for the anodic oxidation of chalcopyrite in the specified solution conditions. Figure 4.1 shows typical trends of the measured mixed potentials over a 30 minute period at different initial copper(II) concentrations in the presence and absence of oxygen. It was observed that the potential increased rapidly during the first 200 seconds, there after the rate of increase became more gradual, almost levelling out when observed over a 30 minute period. This change from a rapid increase to a more gradual increase suggests that steady-state is being reached between the mineral surface and solution. However, when measurements were taken over longer periods of time (Figure 4.2), it becomes apparent that these curves do not level out entirely; rather the potential continues to increase with time in a more or less linear manner i.e. steady state is in fact not attained. This is indicative that either the surface of the mineral or solution conditions at the surface of the mineral are gradually changing. In these tests, the electrode was rotating at 1600 rpm. At such high rotation speed, the concentration of oxidising species at the surface of the mineral should be maintained uniform for the duration of the

tests, therefore, the observed continuously increasing potentials suggest that the mineral surface was changing, possibly through growth of a surface film. Presence of such a surface film affects the electrochemical characteristics of the electrode. The nature and stability of the film are discussed in Section 7.

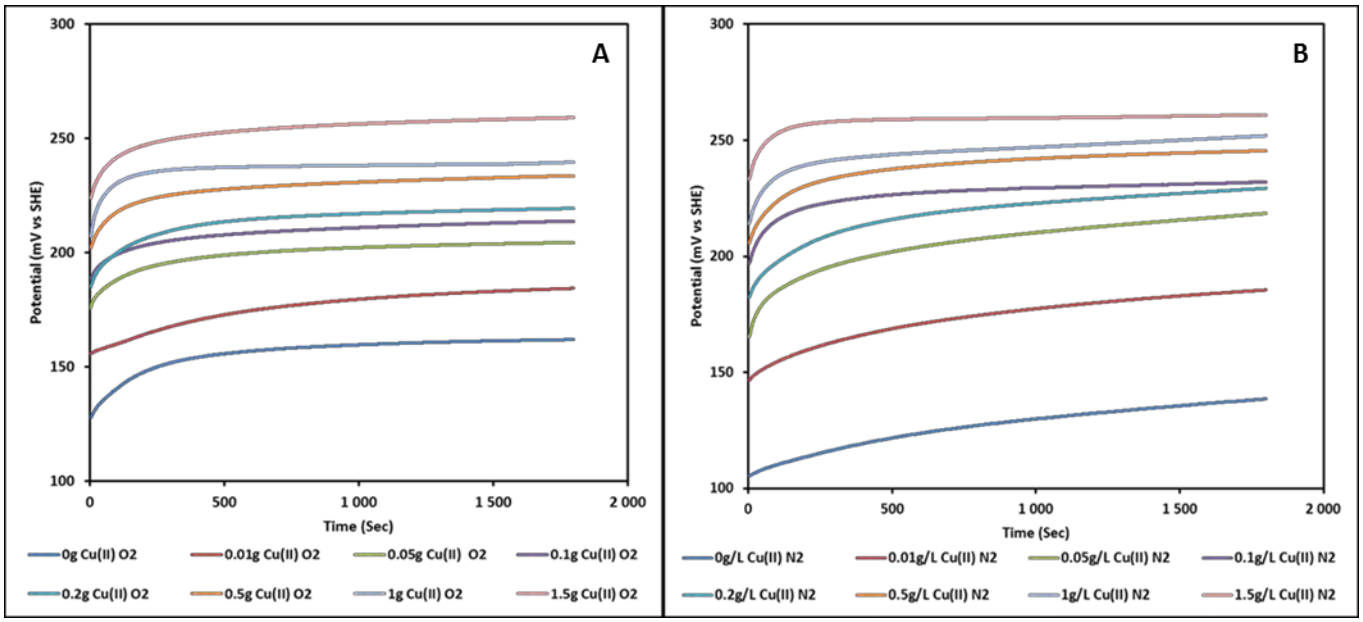

Figure 4.1. Mixed potential in ammonia-ammonium sulphate solutions at 1 M (NH_3+NH_4^+), 25°C, 1600 rpm, pH 9.6±0.15 in the presence (A) and absence (B) of oxygen at varied initial Cu(II) concentrations.

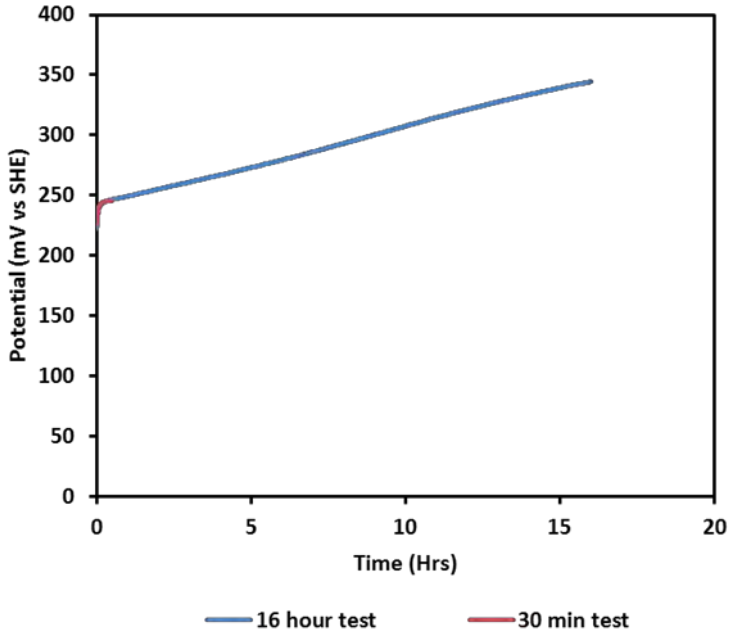

Figure 4.2. Chalcopyrite mixed potential in ammonia-ammonium sulphate solutions at 1 M (NH_3+NH_4^+), 25°C, 1600 rpm, pH 9.6±0.15 under nitrogen.

4.1.1 Bulk solution potential versus chalcopyrite mixed potential

It is important that the difference between solution potential and mixed potential be understood before we go into the detailed description and discussion of the results. Nicol and Lazaro (2002) discuss the role of E_h measurements in the interpretation of the kinetics and mechanisms of the oxidation and leaching of sulphide minerals. The authors highlight how solution potential (E_h) differs from the potentials measured on the mineral surface and in the proximity of the mineral surface thereby making apparent how errors can be made when one assumes the solution potential to be the mineral surface potential when using these measurements to interpret sulphide mineral leaching kinetics. Power and Ritchie (1983) and Nicol (1993), provide more detailed background theory on mixed potentials (E_m) and solution potential (E_h), providing further insight on the differences between the two and how they can be manipulated to give information on sulphide mineral surface reactions in solution.

Figure 4.3 shows the difference between solution potential and the mixed potential (after 30 minutes at open circuit) in an ammonia-ammonium sulphate buffered system at 1M [NH_3+ NH_4^+], 25°C, 1600 rpm, pH 9.6±0.15 in the presence and absence of oxygen. The pH of the solutions at higher initial copper(II) concentrations (> 2 g/L), was adjusted using ammonium hydroxide in order to ensure a consistent amount of uncomplexed ammonia in all the tests. Solution potentials were higher than mixed potentials in all the experiments in the presence of initial copper(II) without any copper(I) in solution under nitrogen. Similar trends where observed under oxygen, except solution potentials were notably higher than those observed under nitrogen and remained fairly consistent, not being affected by an increase in initial copper(II) concentrations. The measured mixed potentials were found to be reproducible within 10 mV except for those measured at zero initial copper(II) under nitrogen. This lack of reproducibility was attributed to the fact that there is no substantial cathodic reaction occurring i.e. the potential is not poised.

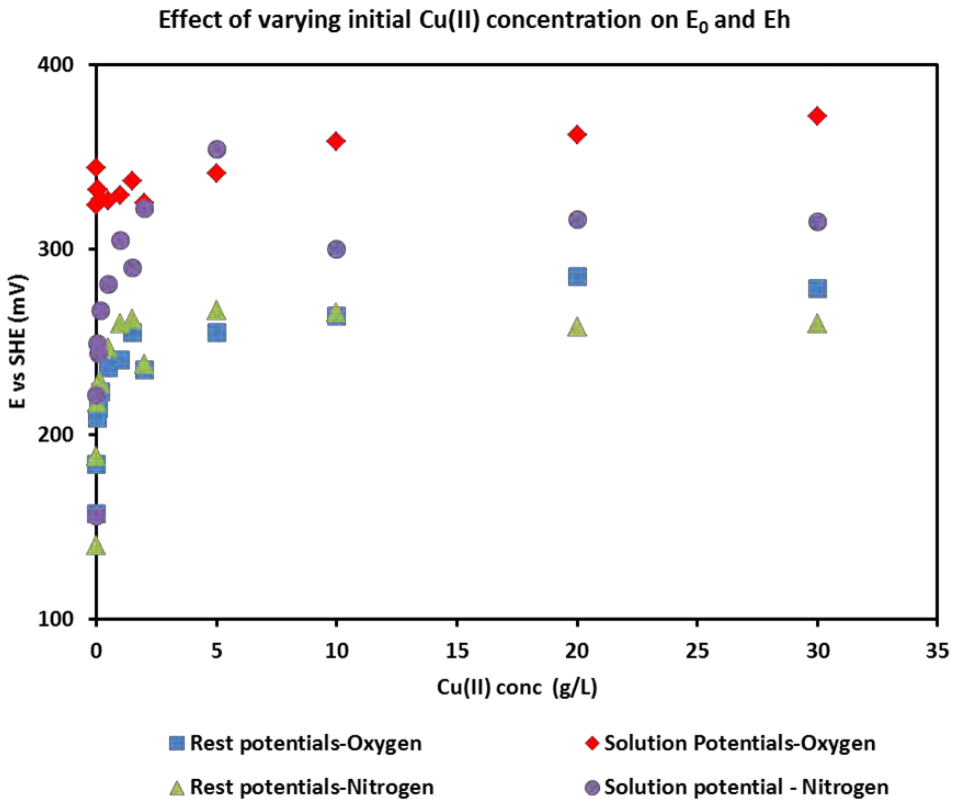

Figure 4.3. Rest and solution potentials of chalcopyrite in ammonia-ammonium sulphate solutions at 1 M (NH_3+NH_4^+), 25°C, 1600 rpm, pH 9.6±0.15 in the presence and absence of oxygen.

Figure 4.4a shows chalcopyrite mixed potentials and solution potentials in ammonia-ammonium sulphate solutions at 1M [NH_3+ NH_4^+], 25°C, pH 9.6±0.15, 1600 rpm under nitrogen in the presence of copper(I) and copper(II) and Figure 4.4b shows potential time transients of the mixed potential in similar solution conditions in the presence and absence of copper(I) at fixed copper(II) concentration. The mixed potentials and solution potentials (Figure 4.4a) were observed to be similar, which suggests that in the presence of copper(I) the use of solution potential to interpret leaching kinetics may be possible. However, it should be noted that in this case, this was possible under nitrogen only, because copper(I) readily oxidises in the presence of even trace concentrations of oxygen. Mixed potentials in the presence of both initial copper(I) and copper(II) (Figure 4.4b) were about 20 mV lower than those measured when there was only copper(II) in solution.

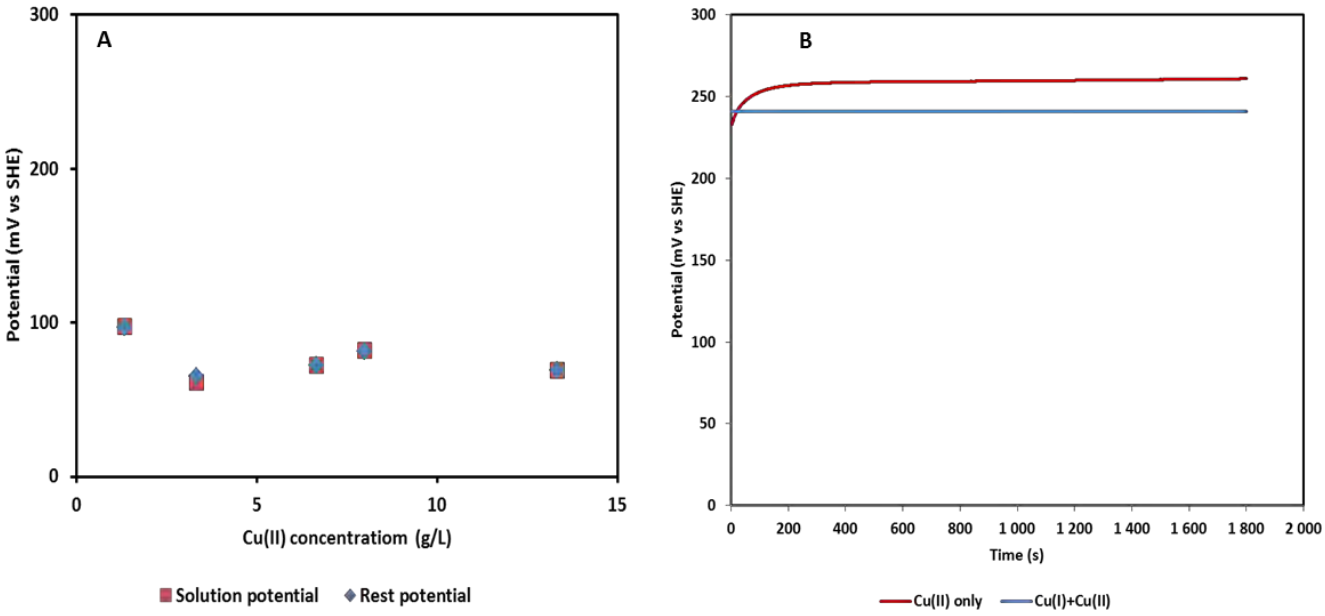

Figure 4.4. A - Rest and solution potentials of chalcopyrite in ammonia-ammonium sulphate solutions at 1 M (NH_3+NH_4^+), 25°C, 1600 rpm, pH 9.6±0.15, in the presence of equimolar Cu(I) and Cu(II) under nitrogen. B – rest potentials over a 1800 sec in solutions containing Cu(II) only (red curve) and in solutions containing equimolar Cu(II) +Cu(I)(blue curve).

In the presence of copper(I) in solution, mixed potentials were observed to be similar to solution potentials (Figure 4.4), suggesting that when copper(I) concentrations are not negligibly small, mixed potentials were controlled by the copper(II)/copper(I) redox couple. This phenomenon is diagrammatically illustrated by Figure 4.5 which shows how the presence of copper(I) contributes to the anodic currents. It can be seen (Figure 4.5) that at the mixed potential, currents due to the oxidation of copper(I), contribute significantly to the anodic currents with those of the oxidation of the chalcopyrite being rather small. This is similar to the illustration of the ferric ferrous iron system given in Figure 2.5. It is reiterated that at the mixed potential, the sum of the anodic currents is equal to the sum of the cathodic currents resulting in no overall current flow. Needes et al (1975) discussed the electrochemical model for the leaching of uranium dioxide and, according to their model, the observed similarity of mixed potentials and solution potentials in the presence of initial copper(I) qualifies this as a type (III) system, in which the contribution of the rate of the anodic reaction becomes negligible in determining the mixed potential i.e. mixed potentials fall close to the equilibrium potential of the copper(II)/copper(I) redox couple.

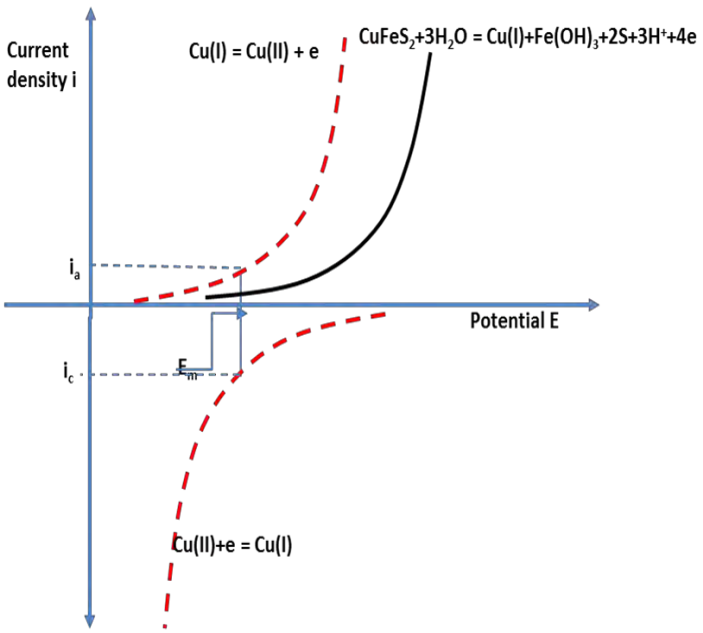

Figure 4.5. Mixed potential schematic of chalcopyrite oxidation by copper(II) showing the effect of significant copper(II) concentrations.

Table 4.1 shows some of the data from Figure 4.4a, measured mixed potentials and solution potentials and includes calculated solution potentials for similar solution conditions. The calculated potentials were determined using the Nernst equation and a formal potential of 100 mV (Bard and Faulkner, 2001) for the copper(II)/copper(I) complexed with ammonia. It can be seen that the calculated values approximate the measured values indicating that in the presence of sufficiently large quantities of copper(I), mixed potentials are governed by the copper(I)/copper(II) couple.

Table 4.1. Measured rest and calculated solution potentials of chalcopyrite in 1 M (NH_3+NH_4^+), 25°C, 1600 rpm, pH 9.6±0.15 in in nitrogen and different ratios of copper(I)/copper(II)

Concentration g/L			Potential (mV)		
Cu(I)	Cu(II)	Total Cu	E_m versus SHE	E_h versus SHE	Calculated E_h
1.33	1.33	2.67	97	97.15	100
4	8	12	81.2	82	82.2

4.1.2 Effect of oxygen on mixed potentials

The effect of oxygen on the leaching of chalcopyrite has previously been evaluated through bulk leach studies (Beckstead and Miller, 1977a; Forward and Mackiw, 1955; Reilly and Scott, 1977; Tozawaet al, 1976) and been found to increase the rate of chalcopyrite dissolution. In bulk leach studies, the dissolution of chalcopyrite occurs at the minerals mixed potential. Thus, the effect of oxygen on mixed potentials is evaluated in this section.

Mixed potentials have been measured in the presence and absence of oxygen with the final mixed potential values recorded after 30 minutes. It was observed that the potentials measured in the presence of oxygen were found to be similar to those measured in the absence of oxygen (under nitrogen). A plot of the mixed potentials against the log of the copper(II) concentration gives a linear fit with the points for oxygen lying on the same line as those under nitrogen within acceptable experimental reproducibility i.e. ± 10 mV (Figure 4.6) under similar solution conditions. This suggests that the presence of oxygen has a negligible effect on the mixed potentials, i.e. oxygen reduction occurs at a rate much lower than that of copper(II) on the chalcopyrite surface under these conditions.

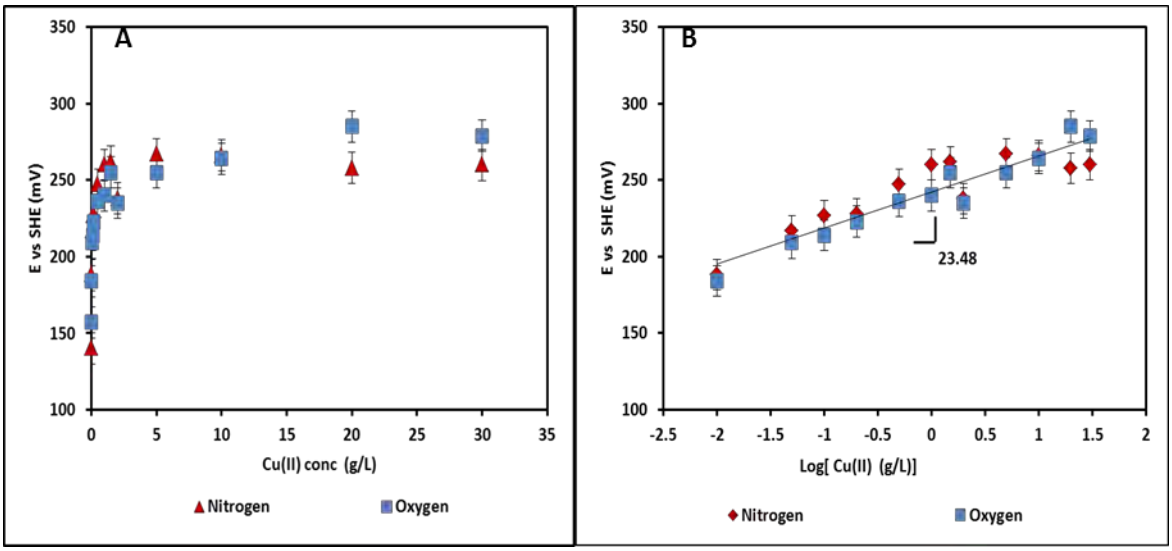

Figure 4.6. Chalcopyrite mixed potential in ammonia-ammonium sulphate solutions at 1 M (NH_3+NH_4^+), 25°C, 1600 rpm, pH 9.6±0.15 in the presence/absence of oxygen at varied initial copper concentrations. A- is a plot of rest potential versus Cu(II) concentration and B is a plots of the same data against the natural logarithm of Cu(II) concentration.

4.1.3 Effect of copper(II) ions on mixed potentials

Mixed potentials were measured in the absence of initial copper(II) and in the presence of varied initial copper(II) concentrations. Under both oxygen and nitrogen, mixed potentials (measured after the electrode was left to equilibrate for 30 minutes as described in the methodology) were found to increase with an increase in initial copper(II) concentration (Figure 4.3 and Figure 4.6). This is

expected and can be explained using the mixed potential model, i.e. it is expected that as the copper(II) concentration increases, the cathodic curve will shift to the right resulting in an increase in mixed potentials, as shown schematically in Figure 4.7. Lundstrom et al (2005) reported similar observations while leaching chalcopyrite in cupric chloride media, where the copper(I)/copper(II) redox couple is also thermodynamically stable. They (Lundstrom et al; 2005) found the increase in potentials with an increase in copper(II) concentrations to follow the Nernst equation with a slope of 60 mV/decade.

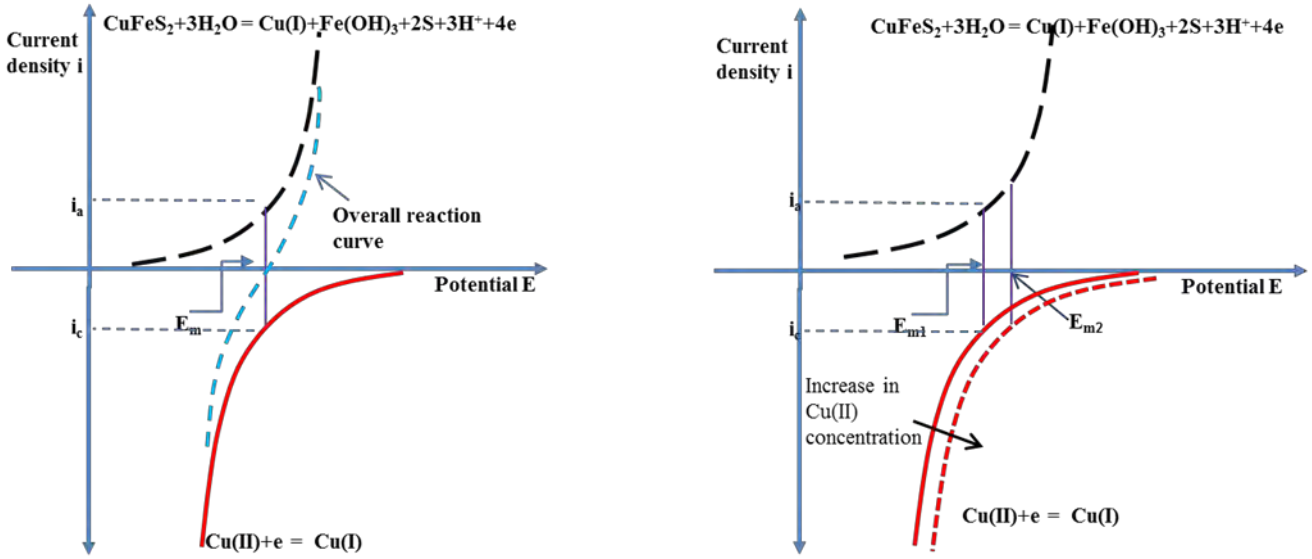

Figure 4.7. Mixed potential schematic of chalcopyrite oxidation by Copper(II) showing the effect of increasing Copper(II) concentration.

4.1.4 Effect total ammonia on mixed potentials

The total ammonia concentration was varied and its effect observed on the mixed potentials. Mixed potentials decreased with an increase in total ammonia (Figure 4.8) when measured at 25°C, pH 9.6±0.15 under nitrogen. This is consistent with observations made by Warren and Wadsworth (1984) who varied the total ammonia concentrations while fixing pH, at pH 10.3 and pH 9.2 and in both instances observed a decrease in mixed potentials.

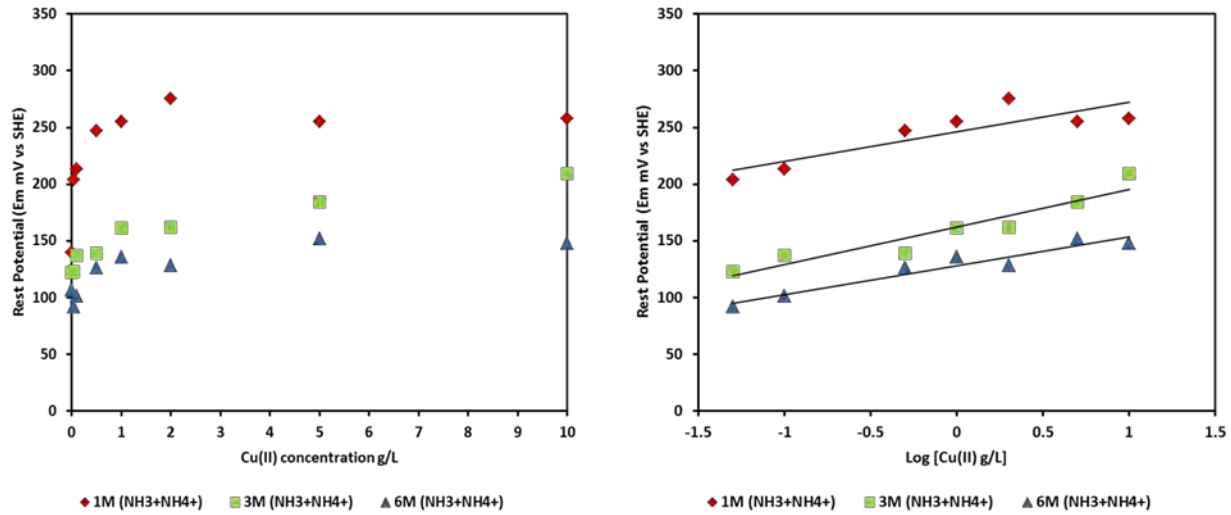

Figure 4.8. Chalcopyrite mixed potential in ammonia-ammonium sulphate solutions at 1M (NH_3+NH_4^+), 25°C, 1600 rpm, pH 9, 9.6 and 10 (±0.15) under nitrogen at varied initial copper concentrations

Thermodynamically, it is expected that the mixed potentials would decrease with an increase in free ammonia concentration as predicted from the Nernst equation for the copper(II)/copper(I) couple (Equation 2.7, Meng and Han, 1996) and that for chalcopyrite oxidation (Equation 4.1). Thus the observed decrease in mixed potentials with pH is expected for the solution conditions reviewed in the current study.

$$E_m = E_0 + \frac{0.059}{n}\log\frac{[Cu(NH_3)_4^{2+}]}{[NH_3]^4} \qquad 4.1$$

4.1.5 Effect of pH on mixed potentials

It is not possible to vary pH without varying ammonia concentration, so to test for the effect of pH changes, total ammonia was maintained constant at 1 molar but the ammonia to ammonium ratio was allowed to vary. An increase in pH resulted in a decrease in mixed potentials (Figure 4.9); this is expected considering increasing OH^- concentration results in an increase in free ammonia (Equation 2.4). This decrease in mixed potentials was consistent with results reported by Warren and Wadsworth (1984), who also observed a decrease in mixed potentials when they increased pH between pH 8.3 and 11.

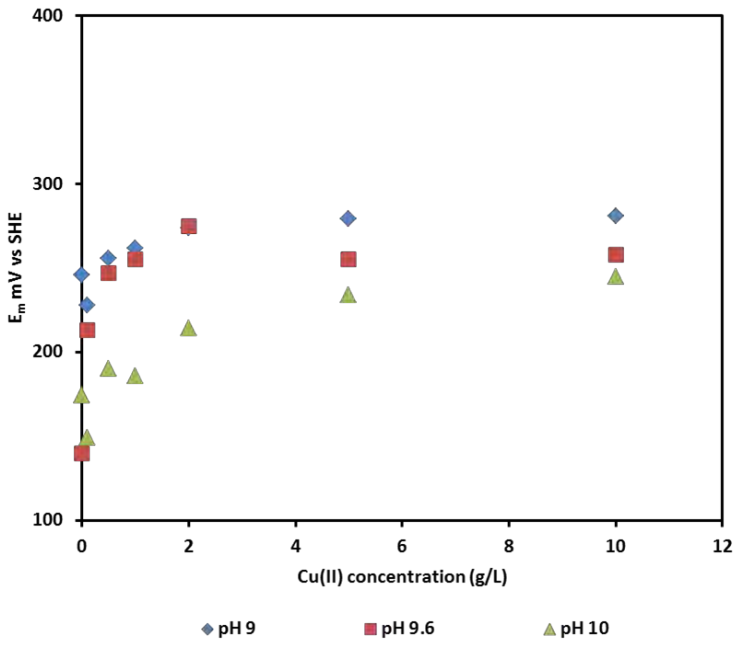

Figure 4.9. Chalcopyrite mixed potential in ammonia-ammonium sulphate solutions at 1M (NH_3+NH_4^+), 25°C, 1600 rpm, pH 9, 9.6 and 10 (±0.15) under nitrogen at varied initial copper concentrations

4.2 Anodic reactions

A distinction needs to be made between the oxidative dissolution reaction (equation 2.3), and the anodic dissolution reaction (Equation 4.2 (Beckstead and Miller, 1977a) and Equation 4.3 (1997; Warren and Wadsworth, 1984)). The oxidative dissolution equation encompasses both the anodic and cathodic reactions and has a zero net accumulation of electrons while the anodic dissolution reaction is a half-reaction.

$$CuFeS_2 + 4NH_3 + 19OH^- = Cu(NH_3)_4^{2+} + 1/2\ Fe_2O_3 + 2SO_4^{2-} + 19/2\ H_2O + 17\ e \qquad 4.2$$

$$CuFeS_2 + 4\ NH_3 + 9\ OH^- = Cu(NH_3)_4^{2+} + Fe(OH)_3 + S_2O_3^{2-} + 3\ H_2O + 9\ e^- \qquad 4.3$$

In section 4.1, mixed potential results were discussed. At mixed potential, the anodic reaction and cathodic reaction occur simultaneously. This section looks at the anodic reaction, and how it is influenced by solution conditions. The anodic reaction is evaluated primarily at the mixed potential and potentials close to the mixed potential.

4.2.1 Effect of oxygen

Oxygen reduction, as discussed in section 2.4, has previously been established to be the cathodic reaction of interest (Warren and Wadsworth, 1984; Beckstead and Miller, 1977a; Reilly and Scott, 1977; Forward and Mackiw, 1955). Therefore it is considered important to establish its effect on the chalcopyrite anodic dissolution reaction. The effect of oxygen on the anodic reaction has been

studied on the chalcopyrite surface using chronoamperometric tests at the mixed potentials measured in section 4.1.2 as well as using cyclic voltammetry.

For the chronoamperometric tests, the potentiostat was set to maintain the mixed potential, as measured in the presence of initial copper(II) and the current response of the chalcopyrite electrode was then recorded. The chalcopyrite electrode was subjected to solutions conditions similar to those in which the set mixed potential was measured, but in the *absence* of initial copper(II). In the absence of oxygen, the described set-up allowed for the isolated measurement of the anodic currents at mixed potential, i.e. the dissolution current density of chalcopyrite at the mixed potential. The curves give valuable information on the oxidation rate of the anode at a particular potential as well as allows for the determination of the stoichiometry of the oxidation reaction when coupled to chemical analysis of the products. Figure 4.10 shows the general trend of the chronoamperometric tests for the anodic reaction. A sharp decrease in anodic currents is observed during the first 5 -10 minutes, and this was followed by what appears as steady state currents but has in fact been established to be a less gradual decrease over longer times (Figure 4.11). It is expected and accepted in literature (Warren et al 1982; Biegler and Swift, 1979) that the current would spike at the onset of the experiment then decrease rapidly to currents significantly lower than the initial current. Aspects to do with the continued gradual decrease in anodic currents will be explored in detail in chapter 8 where they are discussed in relation to the formation of a surface deposit layer. In Figure 4.11, an increase in current density was observed after 0.5 hours to about 2 hours. This was not seen to be consistent across all the curves and thus it is suspected that this increase in current may have been due to an inclusion being exposed on the mineral surface.

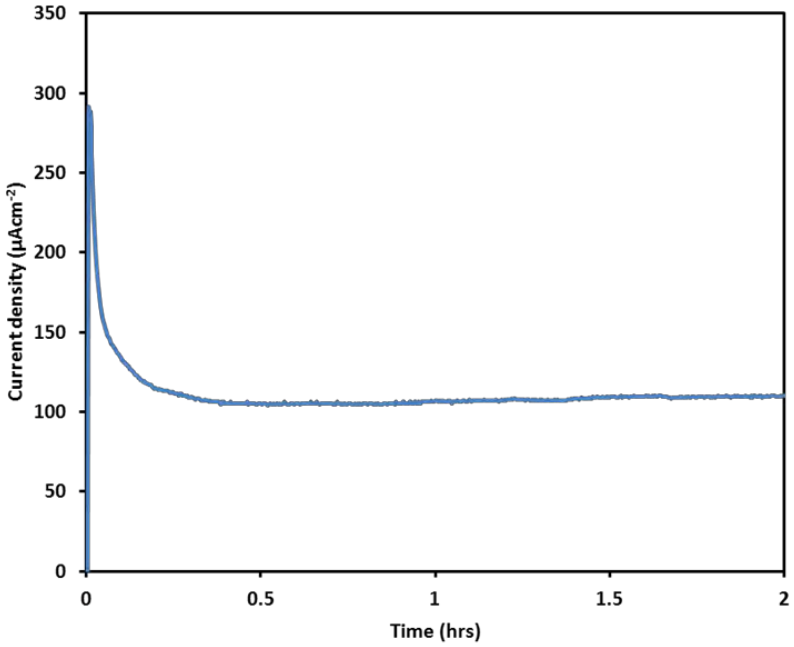

Figure 4.10. Chronoamperometry test, potential set at 255 mV SHE in 1 M (NH_3+NH_4^+), 25°C, 1600 rpm, pH 9.6±0.15 under nitrogen. The set potential is the mixed potential measured in similar solutions in the presence of 5 g/L Cu(II)

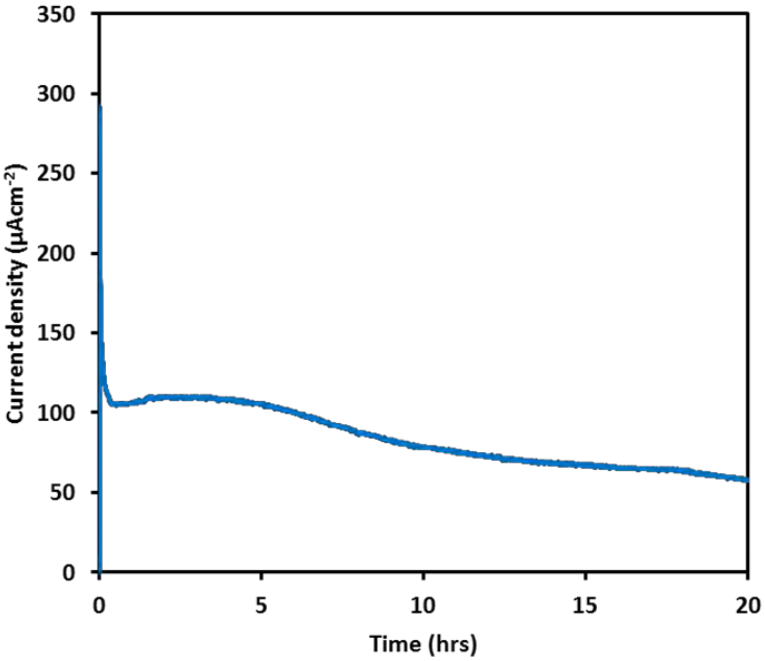

Figure 4.11. Chronoamperometry test, potential set at 255 mV SHE in 1 M (NH_3+NH_4^+), 25°C, 1600 rpm, pH 9.6±0.15 under nitrogen. The set potential is the mixed potential measured in similar solutions in the presence of 5 g/L Cu(II).

Note the longer duration of this test.

The effect of oxygen on anodic currents was investigated by running a chronoamperometric experiment for 1.5 hours under nitrogen then stopping nitrogen supply and introducing oxygen (Figure 4.12). Preliminary tests had indicated that the partial pressure of oxygen would increase within the vessel and the solution would be saturated with oxygen in just less than 10 minutes. It was observed that introducing oxygen did not result in any significant change or increase in the anodic currents.

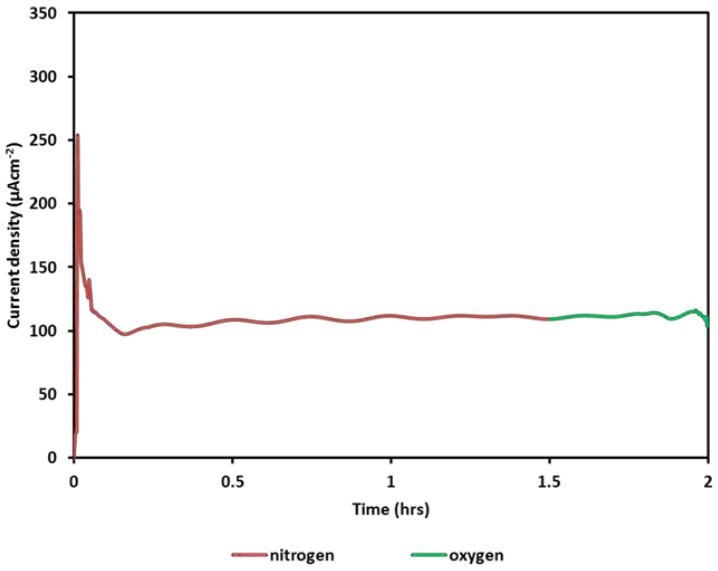

Figure 4.12. Chronoamperometry test, potential set 255 mV SHE in 1 M (NH_3+NH_4^+), 25°C, 1600 rpm, pH 9.6±0.15 under nitrogen. The set potential is equivalent to the mixed potential measured in similar solutions in the presence of 5 g/L Cu(II). Test started under nitrogen and the gas was switched to oxygen.

Figure 4.13 shows plots of log to base 10 of the current density (after 2 hours) measured in the presence and absence of oxygen. The current densities were observed to be similar for either gas and the data gives a linear fit with an R^2 value of 0.97.

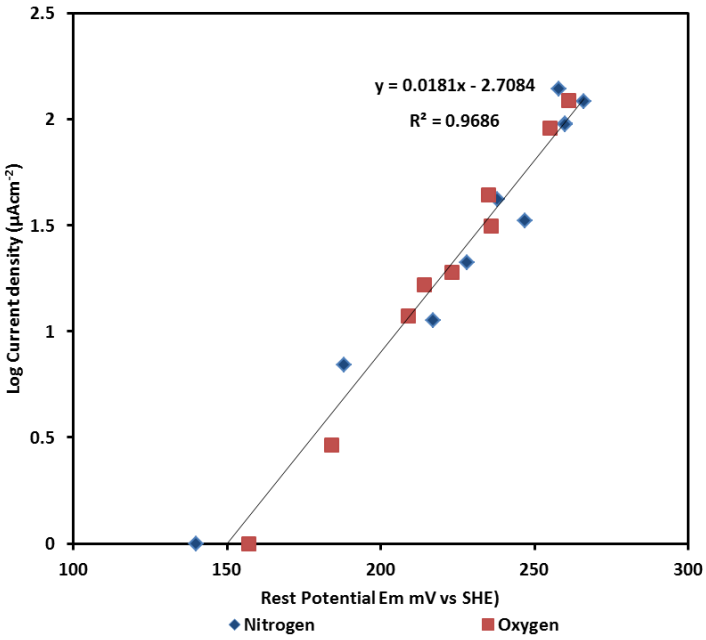

Figure 4.13. Log of current density after 2 hours measured at the equivalent mixed potentials for various initial copper(II) concentrations. Chronoamperometric curves were generated in the presence and absence of oxygen in 1 M (NH_3+NH_4^+), 25°C, 1600 rpm, pH 9.6±0.15.

From these results, it is apparent that oxygen had a negligible effect on anodic currents under the conditions of this study. The effect of oxygen on the anodic reaction has not previously been documented in literature, with the only other study that investigated the isolated anodic reaction having been carried out by Warren and Wadsworth (1984) under nitrogen.

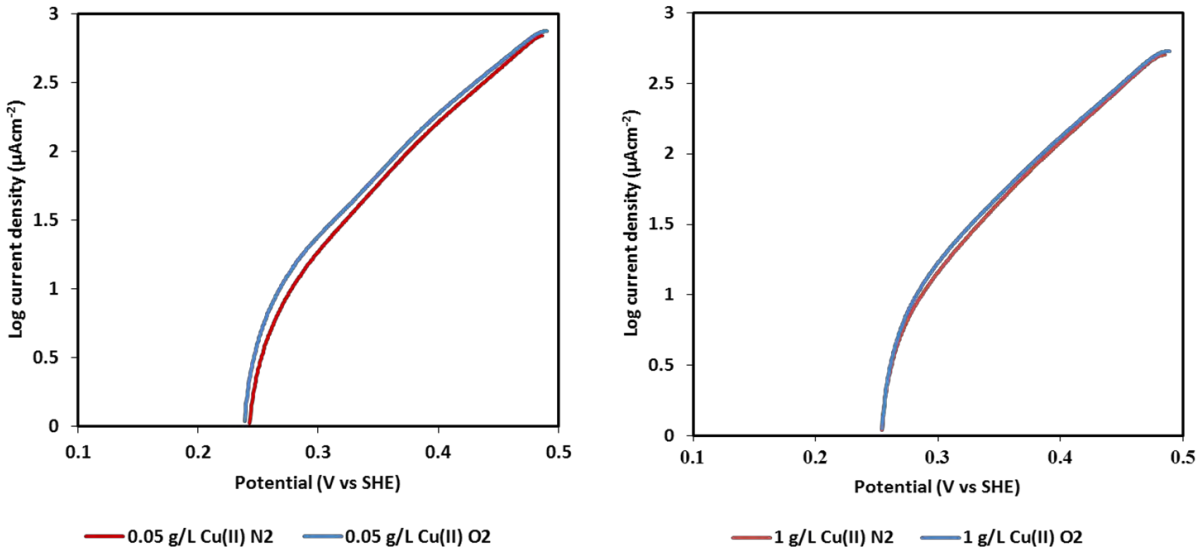

Figure 4.14. Tafel plots of chalcopyrite oxidation at 0.05 g/L copper(II) and 1 g/L copper(II) in the presence and absence of oxygen at 1 M (NH_3+NH_4^+), 25°C, 1600 rpm, pH 9.6±0.15

Figure 4.14 shows Tafel plots of chalcopyrite oxidation measured from potential sweeps in the presence and absence of oxygen at 0.05 g/L and 1 g/L initial copper(II). It can be seen that the presence of oxygen did not have a significant effect on the anodic curves, even in tests carried out when initial copper(II) was present in solution. Koyama et al (2006) has shown the oxidising power on elemental copper in oxygenated ammoniacal solutions to follow the order $Cu(II)/Cu(I)>O_2/H_2O$. This is in agreement with the findings in this study in that when both copper(II) and oxygen are present in ammoniacal solutions, copper(II) is the more effective oxidant. In a study on the oxidation of thiosulphate in ammoniacal solutions containing copper(II) and dissolved oxygen, Byerley et al (1975; 1973), proposed a mechanism of oxidation in which oxygen interacted with the thiosulphate via a copper(II) species which was to say, oxygen did not directly oxidise the thiosulphate but was necessary for the reaction to proceed. Although this applied in a homogeneous system, it is interesting in that it presents a reaction mechanism which requires both copper(II) and oxygen to be present in solution.

4.2.2 Effect of potential on the anodic reaction

The effect of potential on the anodic reaction has been evaluated by running chronoamperometric tests in ammoniacal solutions, in the *absence* of added copper(II) ions, with the potentiostat set at the mixed potentials measured in section 4.1. Notice that the mixed potentials in section 4.1 were measured in solutions that contained initial copper(II). By fixing the potential at the mixed potentials measured in the presence of initial copper(II), then measuring the current response of the electrode immersed in solutions *without* initial copper(II), we are able to;

i. Evaluate the influence of potential on anodic currents
ii. Relate the observed influence of potentials from i above to the mixed potentials of chalcopyrite in solutions containing copper(II).

It is worth reiterating that taking the approach described above, allows for the measurement of the isolated anodic currents i.e. dissolution current densities of chalcopyrite at the set potential which in the case of this study is the mixed potential measured in section 4.1.

Figure 4.15a presents plots of current density (after 2 hours of oxidation) as a function of potential (corresponding mixed potentials measured in the presence of initial copper(II) ions), and Figure 4.15b presents the same current densities as a function of initial copper(II) concentrations. It can be seen that anodic current densities increased with an increase in potential. Figure 4.15b also shows an outlier at 1.5 g under nitrogen, and this was considered to be an unnormally and may be due an inclusion on the mineral surface. In electrochemical processes, current density is analogous to rate of reaction as discussed in section 2.3, thus the current density/rate of the anodic reaction have

been shown to increase with potential. This increase of anodic current densities with potential has been reported by Warren and Wadsworth (1984), however, the authors also reported that the current densities showed some current peaks and dips which they said were due to the formation a number of passive intermediate layers. In the current study, as can be seen from Figure 4.14 and Figure 4.15, no such peaks or dips in current densities were observed.

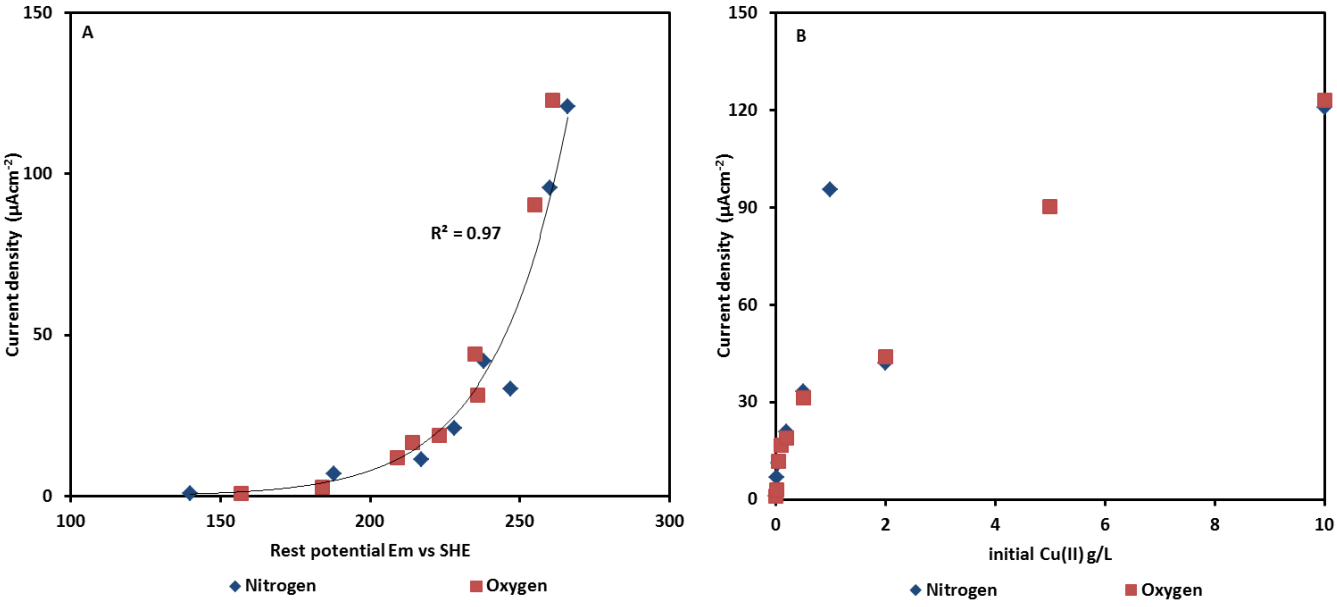

Figure 4.15a-Effect of copper (II) on anodic current density after 2 hours in 1 M (NH_3+NH_4^+), 25°C, 1600 rpm, pH 9.6±0.15 in the *presence* and *absence* of oxygen . 4.15b- is the same data shown on 4.15a, this time plotted against the mixed potentials measured in the presence of copper(II)

4.2.3 Effect of copper(II)

Copper(II) ions have previously been reported to increase the rate of ammoniacal leaching of chalcopyrite, and as discussed in section 2.4.1, in most cases these increased rates of leaching are reported as observations without explanation as to how they are achieved, while in some studies, the role of the copper(II) is said to be purely catalytic (Beckstead and Miller, 1977a). Thus, the exact role of copper(II) in the ammoniacal leaching of chalcopyrite remains unclear and will be evaluated in this section by looking at the effect of varying initial copper(II) concentration on anodic current densities.

The effect of copper(II) on the oxidation of chalcopyrite was evaluated through chronoamperometric tests. The chronoamperometric tests were run as described earlier in solutions that did not have initial copper(II), but in this case, copper(II) was added into the solution during the course of the experiment. Figure 4.16 shows chronoamperometric curves run at 255 mV, neither test solutions contained copper(II) at the start of the experiment. In the course of the experiments,

0.025 g and 0.05 g of copper(II) was added into respective test solutions as 5 mL and 10 mL of a 5 g/L copper(II) solution (added solutions were similar in composition to test solutions but included 5 g/L copper(II)). A decline in anodic current was observed upon addition of the copper(II) solutions and after reaching minimum values which appeared to vary with the amount of copper introduced, currents densities began to increase again gradually. Current densities declined by 19 μAcm^{-2} and 14 μAcm^{-2} when 0.05 g and 0.025 g of copper(II) were added respectively. This decrease in current density is expected at potentials close to the mixed potential and is due to the simultaneous reduction of copper(II) i.e. a simultaneous cathodic reaction. The decrease with time of the copper(II) concentration and the increase in the copper(I) concentration results in a subsequent slow increase in anodic current due to both oxidation of the mineral and of copper(I).

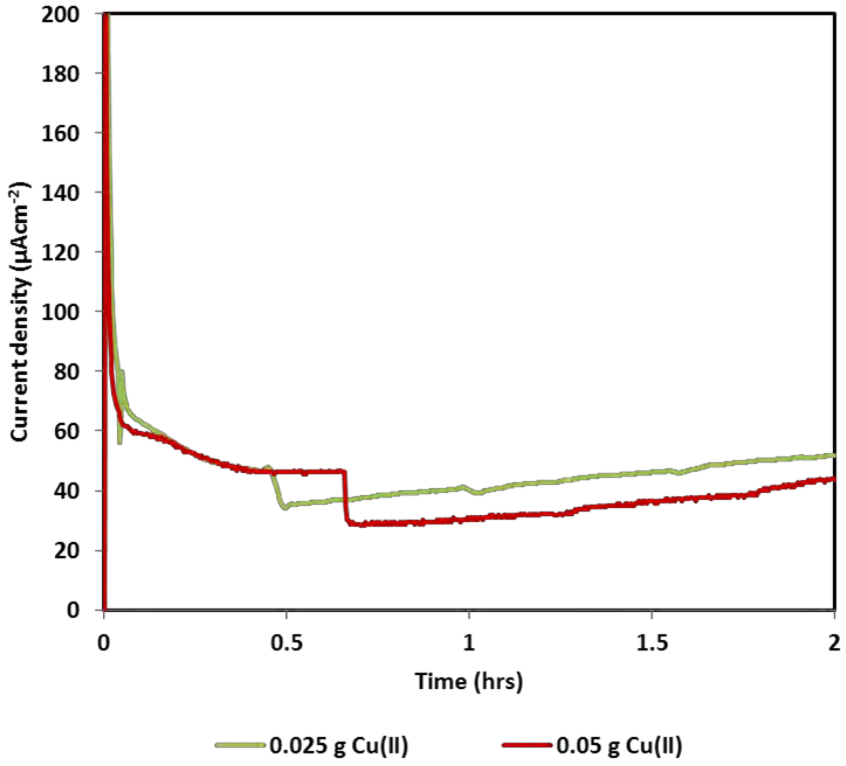

Figure 4.16. Chronoamperometric test, potential set at 255 mV in 1 M (NH_3+NH_4^+), 25°C, pH 9.6±0.15 under nitrogen

4.2.4 Effect of total ammonia and pH

Figure 4.17 shows the anodic current densities observed during potential sweeps at a scan rate of 1 mV/sec in solutions of varied total ammonia in the absence of initial copper(II). Anodic current densities were relatively low at 1 M total ammonia at all potentials, and the current densities were not significantly affected by an increase in total ammonia from 3 M to 6 M. Figure 4.18 shows the anodic current densities of chalcopyrite in solutions of varied total ammonia concentrations in the presence of 5 g/L initial copper (II). It can be seen that anodic current densities were not significantly

affected by total ammonia at low potentials between 3 and 6 M, but increasing total ammonia resulted in an increase in current densities at high potentials. The most dramatic increase in anodic current densities was observed between the 1 M and 3 M total ammonia. It should be pointed out that in all these studies the free ammonia available in solution was in excess of that required for the complexation reaction.

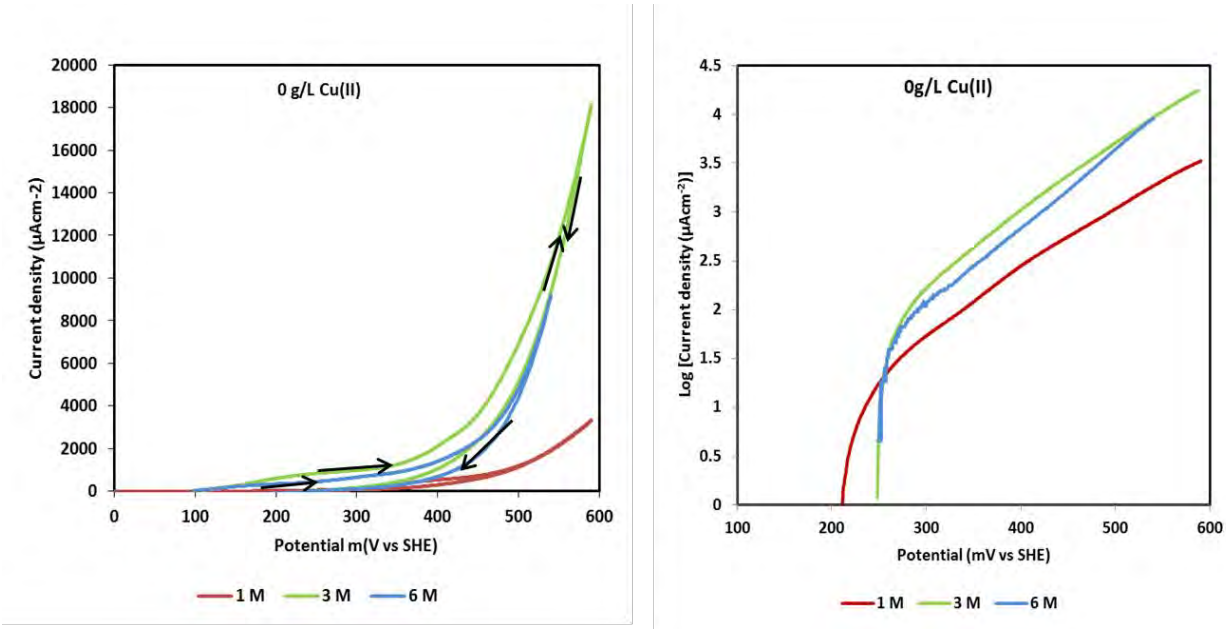

Figure 4.17. Cyclic voltammogram and Log current density-potential plots measured in solutions of varied total ammonia, 25°C, pH 9.6±0.15, no initial Cu(II), under nitrogen at a scan rate of 1 mV/sec

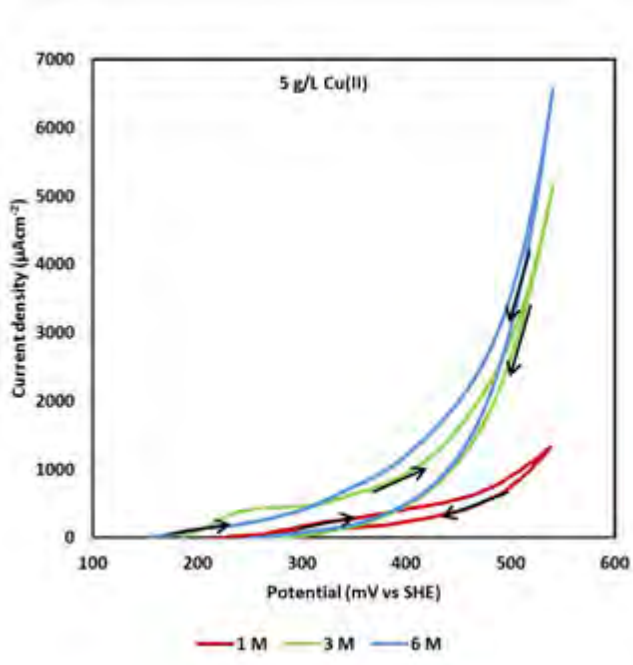

Figure 4.18. Cyclic voltammogram measured in solutions of varied total ammonia, 25°C, pH 9.6±0.15, 5 g/L initial Cu(II), under nitrogen at a scan rate of 1 mV/sec

Warren and Wadsworth (1984) evaluated the effect of ammonia on the anodic reaction and reported increased anodic currents at a pH of 9.2 and low free ammonia 0.028 to 0.468 M. At high free ammonia, 1 M to 4.32 M and pH 10.24, the researchers (Warren and Wadsworth, 1984), reported no dependence on free ammonia at high potentials. Warren and Wadsworth (1984) neglected to mention the apparent lower anodic currents observed at 1 M free ammonia at all potentials but their reported lack of dependence was true for currents observed between 1.61 and 4.32 M free ammonia.

It is expected that in the presence of varied copper(II) concentrations in solution, the species distribution of ammonia and ammonium ions in solution would change due to some free ammonia being taken up in the complexation of copper(II) forming cupric ammine. Table 4.2 shows the concentration of free ammonia available in solutions of varied total ammonia at varied initial copper(II) concentrations calculated using thermodynamic data and spreadsheets developed by Nicol at Murdoch University (Nicol, 2013). As expected, the concentration of free ammonia increases with an increase in total ammonia at fixed initial copper(II) concentrations, but decreases with an increase in initial copper(II) at a fixed total ammonia concentration. In a 1 M solution, increasing copper(II) concentrations from 0 g/L to 10 g/L results in the uptake of 63% of the free ammonia present and smaller changes in free ammonia are observed when similar calculations are done at 3 M and 6 M with an uptake of 22% and 11% of the initial free ammonia respectively.

It is proposed that there is a minimum threshold concentration of free ammonia below which increasing free ammonia results in an increase in anodic current densities and maximum concentration above which further increases in free ammonia does not promote anodic currents.

Table 4.2. Concentration of free ammonia in solutions of different total ammonia at varied copper(II), 25°C, at pH 9.6±0.15.

Initial Cu(II) g/L	Free NH_3 mol/L		
	1 M	3 M	6 M
0	0.6	1.81	3.61
2	0.53	1.73	3.54
5	0.41	1.61	3.42
10	0.22	1.42	3.23

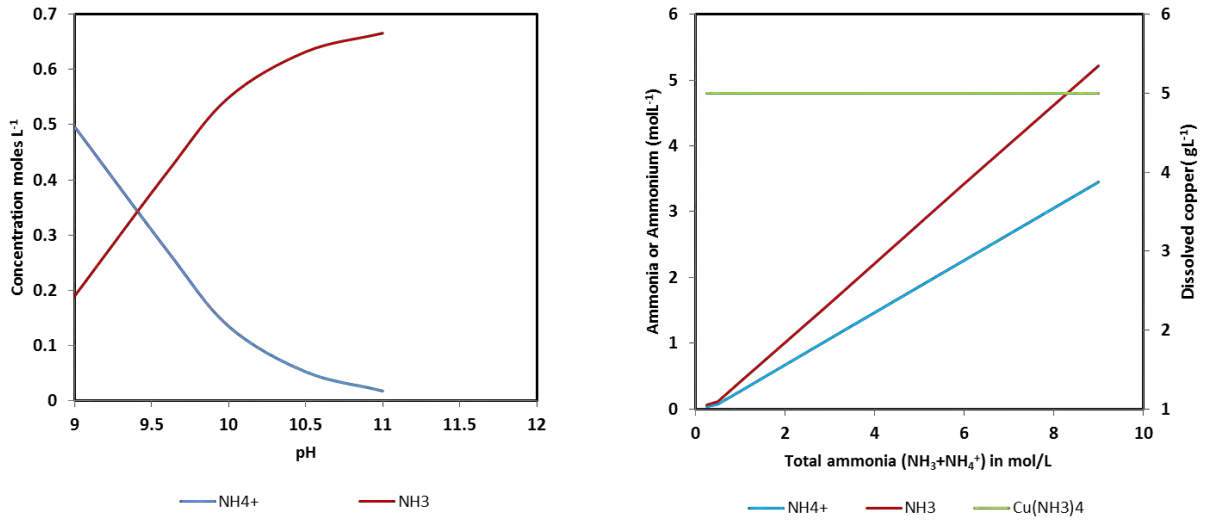

Figure 4.19. A- Ammonia and ammonium species distribution as pH changes at 1 M (NH_3+NH_4^+), 5 g/L copper(II), 25°C. B- Species distribution of ammonia, ammonium and dissolved copper at different total ammonia concentrations at pH 9.6±0.15, 5 g/L copper(II).

Figure 4.19b shows a species distribution of free ammonia, ammonium and copper(II) in solution (5 g/L) at 25°C, pH 9.6 and varied total ammonia concentrations (Nicol, 2013). The amount of soluble copper is constant at all total ammonia concentrations between 0.25 M and 9 M, but the concentration of free ammonia available for further complexation (with any copper that may come into solution during leaching reactions) is significantly lower at low total ammonia concentrations. Following the speciation diagram (Figure 4.19), one could infer that at fixed solution pH, increasing total ammonia in solutions that already have sufficient uncomplexed ammonia would not cause a significant effect on the rate of chalcopyrite leaching. However, if total ammonia was to be increased in solutions that had insufficient uncomplexed ammonia then an increase in anodic currents would result. This would explain the observed increase in anodic currents from 1 M to 3 M and the insignificant changes seen thereafter.

It should be pointed out that there is no consistency in the manner that ammonia effects are discussed in literature, with some scholars referring to total ammonia (Warren and Wadsworth, 1984) while other scholars refer to it just as ammonia (Tozawa et al 1976) with no indication whether this refers to total or free ammonia, and also neglecting to mention the amount of copper in solution, thereby leaving the reader without clarity on the quantity of ammonia available for complexing with copper(II) from the dissolving chalcopyrite. Guan and Han (1997) studied the anodic oxidation of gold in ammoniacal solutions using copper(II) as an oxidant and reported that the reaction was zero order with respect to ammonia and 0.3 with respect to copper(II) but pointing out that increasing ammonia concentration promoted the anodic reaction while supressing the cathodic

reaction. In Figure 4.20a and Figure 4.20b, the order of reaction with respect to total ammonia and to free ammonia was determined using slopes of the polynomial fits to data presented in Figure 4.17 at 300 mV. It is clear that using total ammonia allows for a reasonable approximation of the order of reaction with respect to free ammonia. At 1 M total ammonia or 0.413 M free ammonia, the reaction order was found to be 1.7 and 1.76 respectively and at 3 M total ammonia or 1.61 M free ammonia the reaction order was found to be 0.1 and 0.09 respectively. No comparison could be made to literature values because literature studies report on the order of reaction with respect to ammonia on the overall leaching reaction while this section focuses on the anodic reaction.

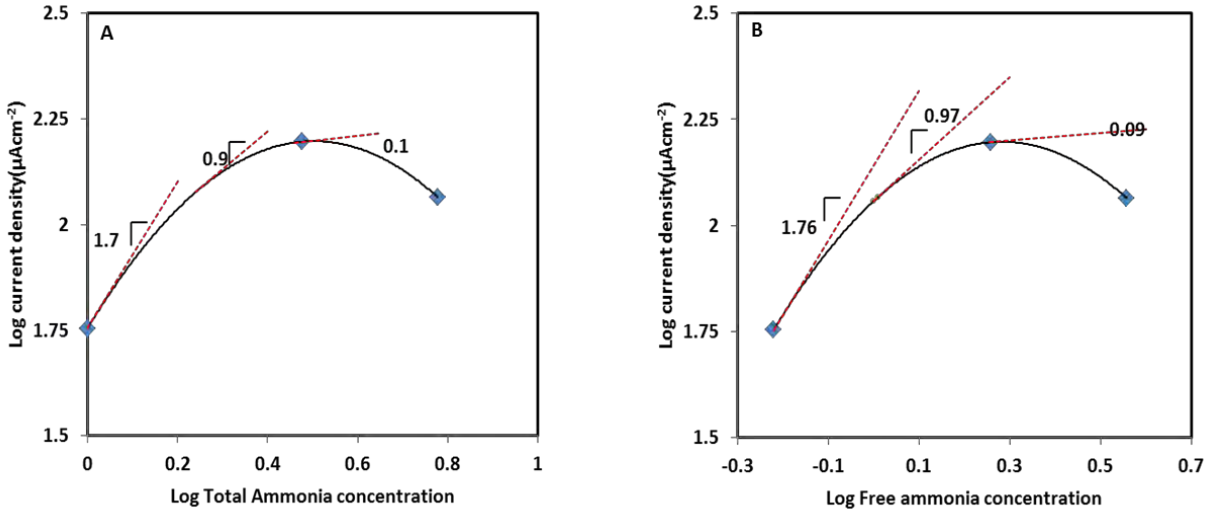

Figure 4.20. Log-Log plot of anodic current densities versus total ammonia and Log-Log plot of anodic current densities free NH_3 concentrations in solutions with no initial copper(II) at 25°C, 1600 rpm, pH 9.6±0.15 in the absence of oxygen.

4.2.5 Effect of pH

Anodic current densities were seen to increase with an increase in pH (Figure 4.21), and this is consistent with findings presented by Warren and Wadsworth (1984) who observed increased currents when pH was increased. The reaction order was determined using a second order polynomial fit and the gradient at different points in the curve determined Figure 4.21b. At the lowest pH studied, pH 9, the reaction order was determined to be 0.54 which does not agree with the first order dependence reported by Warren and Wadsworth (1984) working in similar solution conditions. It is reiterated that very limited literature could be found on the anodic reaction with most studies reporting on the overall leaching reaction. At pH 10 the reaction order was determined to be 0.02 and it will be reasonable to report this as a zero order dependence on pH. Looking at Figure 4.19a, it can be seen that the pH range 9-10, used in this study, falls in the transition from first to zero order for ammonia and increasing pH directly results in increasing ammonium concentrations yet lowering the ammonium concentration.

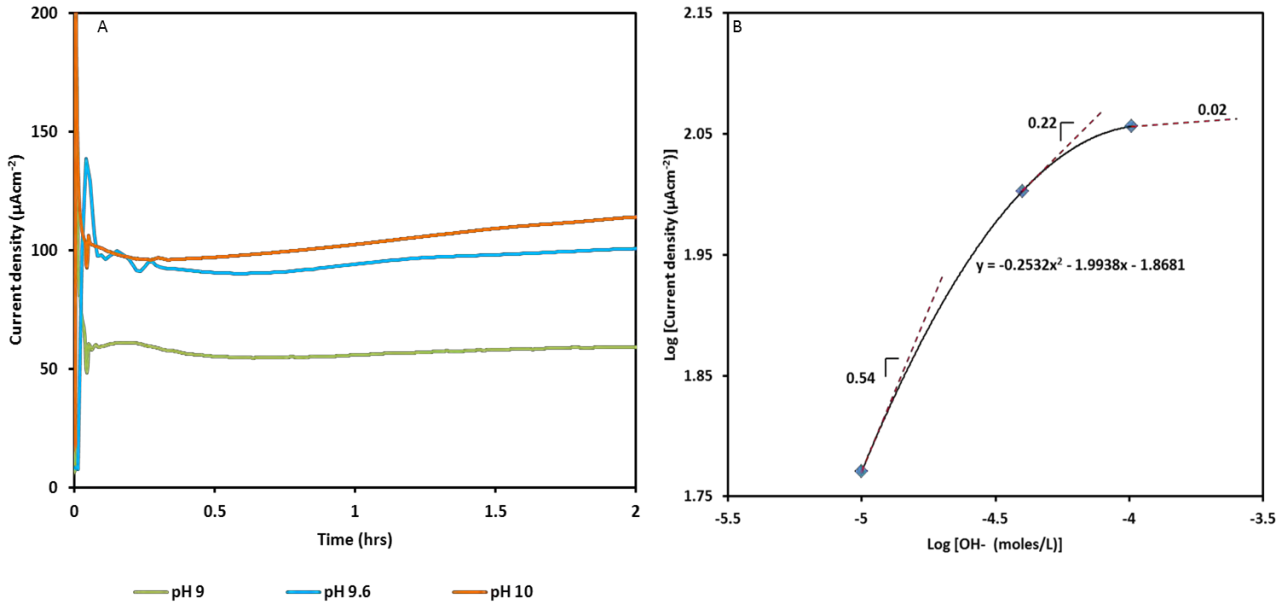

Figure 4.21. A – Current time transients of chalcopyrite oxidation at pH 9, 9.6 and 10 with the potentials set to 279 mV, 255 mV and 234 mV (corresponding to mixed potentials measured in similar solutions in the presence of initial copper(II) presented in Figure 4.9. B - Log plot of anodic currents versus OH^- concentrations in 1 M (NH_3+NH_4^+), 25°C, 1600 rpm, pH 9.6±0.15 in the absence of oxygen.

4.2.6 Coulometry

The stoichiometry of the anodic reaction was determined using Coulometry and calculating the amount of charge transferred together with an analysis of the electrolyte at the end of each test. The charge passed in a test was calculated by integrating the current density time plots such as the ones presented in Figure 4.10 and Figure 4.16 (the rest of the curves are presented in the appendix section (Appendix 3)). The copper released over this period was determined using ICP analysis. Tests were run for periods of 5 h or longer in solutions in order to ensure the amount of copper was sufficient for detection. The potential for these fixed potential tests was in each case set to the potentials corresponding to the mixed potential of chalcopyrite as measured in the presence of 5 g/L copper(II) at 1600 rpm. Further tests were run at potentials in the vicinity of these mixed potentials, i.e. measured mixed potential up to ±100 mV. The number of electrons transferred per molecule of chalcopyrite dissolved (measured as copper in solution) was calculated using the Faraday Law of electrolysis (Equation 2.17a).

A similar number of electrons, average 7.4 and 7.2 were transferred per molecule of chalcopyrite under oxygen and nitrogen, respectively, at potentials and periods shown in (Table 4.3 and Table 4.4). These values are not consistent with the anodic reactions equation 4.2 (Beckstead and Miller, 1977a) nor equation 4.3 (Guan and Han, 1997; Warren and Wadsworth, 1984) which require more charge per unit of copper dissolved.

Table 4.3. Determination of number of electrons transferred per copper under nitrogen at mixed potential and within the vicinity of this mixed potential in 1 M (NH_3+NH_4^+), 25°C, pH 9.6±0.15 under nitrogen.

Duration of test (H)	E_m (mV versus SHE)	Total Cu from ICP (mol)	Total charge Q (C)	n(e)=Q/F	No of electrons/mole Cu
5	206	5.93E-06	0.131	1.36E-06	7.6
5	230	1.26E-05	0.288	2.99E-06	7.1
20	255	4.44E-05	2.615	2.71E-05	7.6
22	255	4.69E-05	2.567	2.66E-05	7.1
5	260	1.32E-05	0.261	2.71E-06	6.8
5	306	3.52E-05	0.744	7.71E-06	7.6
22	306	1.13E-04	5.957	6.17E-05	6.9
22	306	1.02E-04	5.459	5.66E-05	6.9

Table 4.4. Determination of number of electrons transferred per copper in the presence of oxygen at mixed potential and within the vicinity of this mixed potential in 1 M (NH_3+NH_4^+), 25°C, pH 9.6±0.15.

Duration of test (H)	E_m (mV versus SHE)	Total Cu from ICP (mol)	Total charge Q (C)	n(e)=Q/F	No of electrons/mole Cu
5	240	1.16E-06	0.255	2.64E-06	7.6
22	244	5.70E-05	3.135	3.25E-05	7.1
22	244	4.56E-05	2.763	2.86E-05	7.9
5	271	5.55E-05	1.152	1.19E-05	7.2
5	281	8.60E-05	1.727	1.79E-05	6.9
5	326	4.88E-05	1.106	1.15E-05	7.8
5	340	6.30E-05	1.316	1.36E-05	7.2

The results suggest that possibly thiosulphate is the product of oxidation of sulphide and that copper(I) or copper(II) are the primary products of anodic oxidation at the potentials studied as shown in equations (4.4) and (4.5).

$$CuFeS_2 + 4\ NH_3 + 6\ OH^- = Cu(NH_3)_2^+ + Fe(NH_3)_2^{2+} + S_2O_3^{2-} + 3\ H_2O + 7e^- \quad 4.4$$

$$CuFeS_2 + 4\ NH_3 + 6\ OH^- = Cu(NH_3)_4^{2+} + Fe(NH_3)_2^{2+} + S_2O_3^{2-} + 3\ H_2O + 8e^- \quad 4.5$$

Considering the solution concentrations of OH^- are much lower than those of the NH_3, the equations could be written differently, e.g. equation 4.4 can be written as shown below (Equation 4.6).

$$CuFeS_2 + 10\ NH_3 + 3H_2O = Cu(NH_3)_2^+ + Fe(NH_3)_2^{2+} + S_2O_3^{2-} + 6NH_4^+ + 7e^- \qquad 4.6$$

It is likely that subsequent oxidation of copper(I) to copper(II) and iron(II) to iron(III) (as a hydroxide) by dissolved oxygen will occur as non-faradaic reactions close to the electrode surface. The proposed reaction products agree with that of Warren and Wadsworth (1984) and Gaun and Han (1997), who also proposed the formation of a thiosulphate intermediate established experimentally at the mixed potential of dissolution in their respective studies. Despite not being able to account for it in the stoichiometry they proposed for the anodic reaction, Warren and Wadsworth (1984) identified iron in the oxidation state of +2 on the surface of their mineral which supports the formation of $Fe(NH_3)_2^{2+}$ proposed in this study (Equations 4.4 and 4.5).

Activation energy

The effect of temperature on the ammoniacal leaching of chalcopyrite has been discussed in section 2.2. Mixed potentials were measured in solutions at 1 M total ammonia and 1 g/L initial copper(II) under nitrogen and were found to be, 260, 271 and 273 mV at 25, 35 and 45°C respectively. The anodic current densities corresponding to the measured potentials are shown in Figure 4.22 and these have been used to calculate the activation energy.

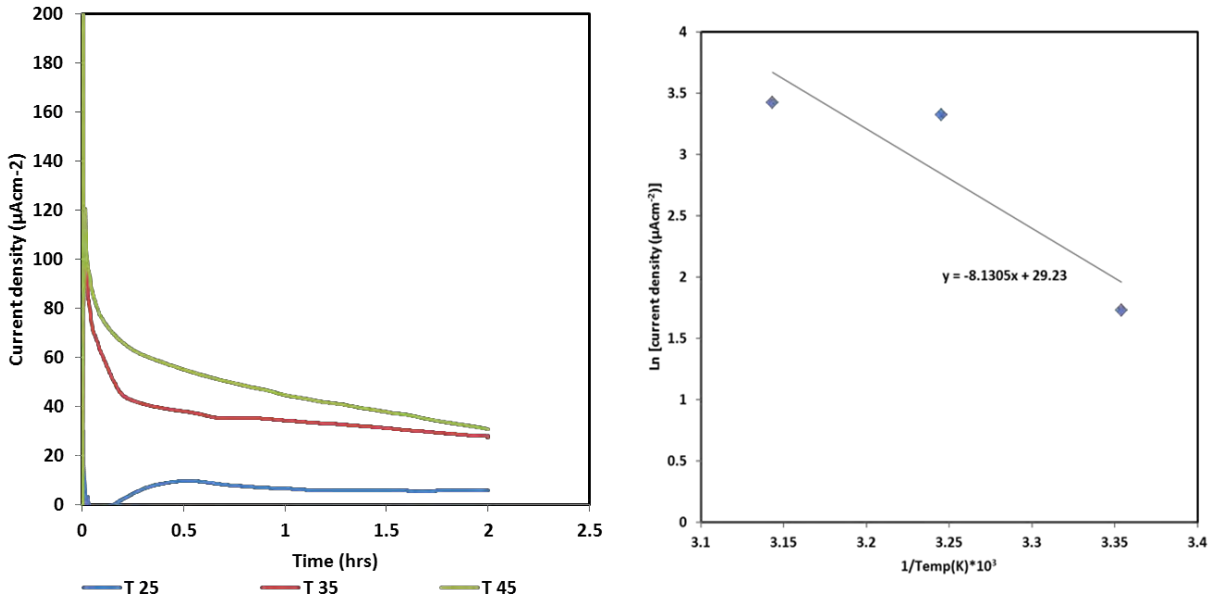

Figure 4.22. Reaction rate over 2 hours versus inverse of absolute temperature in 1 M (NH_3+NH_4^+), pH 9.6±0.15 under nitrogen

To calculate the activation energy for the anodic reaction, the Arrhenius equation (Equation 3.2) has been used.

The y-intercept from Figure 4.22 gives ln A, Ea =67.6 kJ/mol, which suggests that the reaction is controlled by the chemical surface reaction. It is pointed out that only 3 data points were used to come to the conclusions on activation energy calculation through this thesis, thus these values are accepted as guidelines rather than absolute.

4.2.7 Effect of choice of ammoniacal salts

The nature of the anion in solution was evaluated by carrying out additional tests in solutions buffered using ammonium carbonate and ammonium perchlorate. The aim of these tests was to evaluate the influence of anions on the formation of surface deposits as will be discussed in Chapter 7. This was motivated by observations of presence of sulphur in the surface deposit layer and since in a sulphate system, one could not distinguish if the observed sulphur was adsorbed onto the precipitate from solution or was from the oxidising chalcopyrite, it was considered necessary to work in solutions that did not contain initial sulphate.

Table 4.5 shows mixed potentials of chalcopyrite after 30 minutes, and the corresponding amounts of charge passed when potentials was fixed at the measured mixed potential for 2 hours, in the different ammonia buffered solutions at 1M total ammonia, 25°C, 1600 rpm, pH 9.6±0.15 under nitrogen. The lowest mixed potentials were observed in the ammonia-ammonium carbonate solutions at 228 mV while the highest mixed potentials were measured in the ammonia ammonium sulphate solutions at 255 mV.

Table 4.5. Mixed potentials measured after 30 min and the amount of charge passed when potentials were set to the measured mixed potential for 2 hours in various ammonia-ammonia salt buffered solutions at 1M (NH_3+NH_4^+), 25°C, 1600 rpm, pH 9.6±0.15 under nitrogen at 5 g/L initial copper(II) concentrations.

Ammonium Salt	E_m (mV)	Charge passed in 2 h
CO_3^{2-}	228	258.7
SO_4^{2-}	255	246.6
ClO_4^-	254	182

The dissolution current densities of chalcopyrite at the mixed potentials reflected in Table 4.5 were measured as described in the methodology. Figure 4.23 shows the current time transients for the

different ammoniacal solutions. Currents were observed to be highest in ammonia-ammonium sulphate solutions in the initial stages of the oxidation curves, but these were also seen to decline rapidly to values below those of currents measured in ammonia-ammonium carbonate solutions. The obvious decline in currents observed in ammonia-ammonium sulphate solutions is indication of continued growth of an inhibiting layer on the mineral surface, and the fact that, in ammonia-ammonium carbonate solutions currents only decrease slightly suggests that any form of inhibition taking place on the mineral surface is occurring significantly slower than that occurring in sulphate solutions. The currents in ammonia-ammonium perchlorate solutions were found to be the lowest and the rate of decline of currents was lower than that observed in sulphate solutions

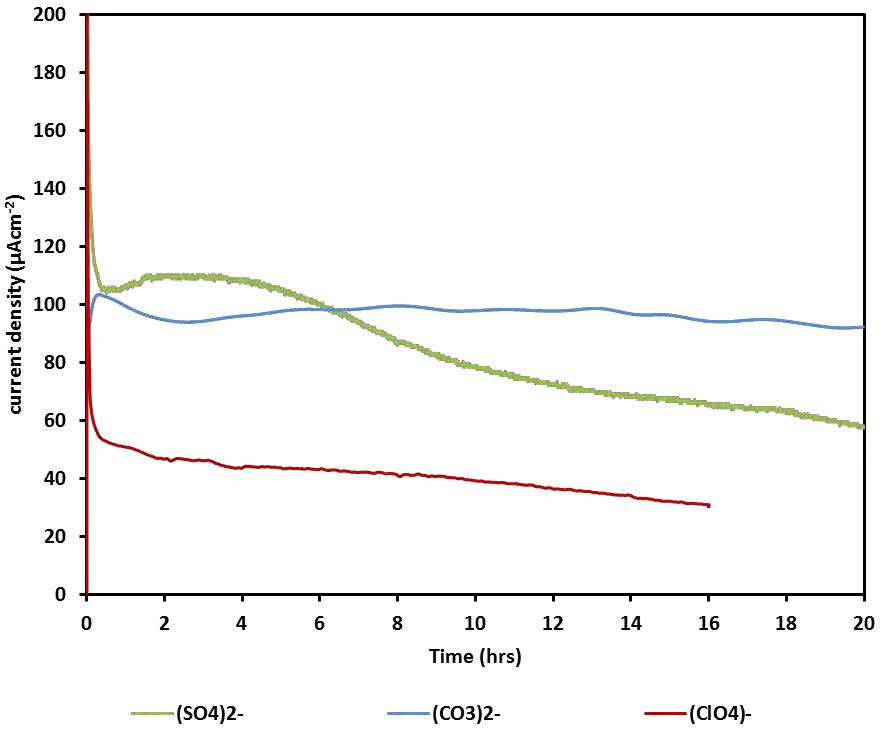

Figure 4.23. Chronoamperometric test, potential set at mixed potentials measured in 1 M (NH_3+NH_4^+), 25°C, pH 9.6 ±0.15 under nitrogen in varied ammonia-ammonium salt buffered solutions.

Coulometry of the anodic reaction in the different ammonia-ammonium buffer solutions was determined from the charge passed in the chronoamperometric tests and copper assays of the solutions at the end of each test. Table 4.6 summarises the results.

Table 4.6. Determination of number of electrons transferred per mole of copper at mixed potential.

Duration of test (h)	Ammonium salt	E_m (V versus SHE)	Total Cu from ICP ppm	Total charge Q (C)	n(e)=Q/F	No of electrons/mol Cu
22	Carbonate N_2	0.231	2.876	2.751	2.85E-05	7.9
5	Carbonate N_2	0.231	2.007	0.6351	6.58E-06	7
22	Sulphate N_2	0.26	2.824	2.615	2.71E-05	7.6
5	Perchlorate N_2	0.255	1.136	0.309	3.20E+00	4.7
5	Perchlorate N_2	0.255	1.708	0.473	4.90E-06	4.9

In the carbonate system, an average of 7.4 electrons were transferred per molecule of chalcopyrite dissolved (measured as copper in solution) similar to the average of 7.2 that was found for the sulphate system (section 4.2.6). This once again, supports the formation of a thiosulphate intermediate (Equation 4.7) and suggests that the copper and iron are in the cuprous and ferrous state with any subsequent oxidation occurring as non-Faradaic reactions. The perchlorate, on the other hand, had approximately 5 electrons transferred per molecule of chalcopyrite, suggesting the formation of elemental sulphur and the formation of cupric and ferric (Equation 4.8), i.e. the oxidation of the iron and the copper take place as faradaic reactions.

$$CuFeS_2 + 4\ NH_3 + 6\ OH^- = Cu(NH_3)_2^+ + Fe(NH_3)_2^{2+} + S_2O_3^{2-} + 3\ H_2O + 7e^- \quad 4.7$$

$$CuFeS_2 + 4\ NH_3 + 3\ OH^- = Cu(NH_3)_2^+ + Fe(OH)_3 + 2\ S + 5e^- \quad 4.8$$

4.3 Discussion

Electrochemical experiments have shown copper(II) to be the primary oxidant in the oxidative dissolution of chalcopyrite in the presence and absence of oxygen at 25°C. Increasing copper(II) concentrations has been shown to result in increased mixed potentials and since chalcopyrite leaching is a potential driven reaction, this increase in potential translated to increased anodic currents. Figure 4.15a showed how anodic current densities varied with potential and Figure 4.15b showed how the current densities presented in Figure 4.15a related to the initial copper(II) potentials at which the potentials were measured. The results indicate that under freely dissolving conditions i.e. mixed potentials, chalcopyrite oxidation increases with an increase in concentration

of the oxidant. In electrochemical reactions, current densities/rate of oxidation is known to vary linearly with the square root of copper(II) concentration(Section 2.4.1). This is shown in Figure 4.24.

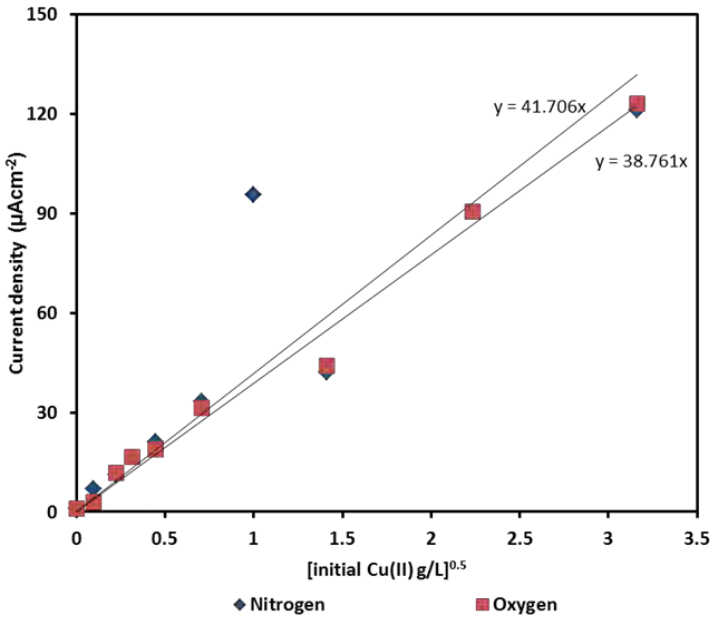

Figure 4.24. Current density versus square root of initial copper concentration in 1 M (NH_3+NH_4^+), 25°C, 1600 rpm, pH 9.6±0.15 in the presence and absence of oxygen.

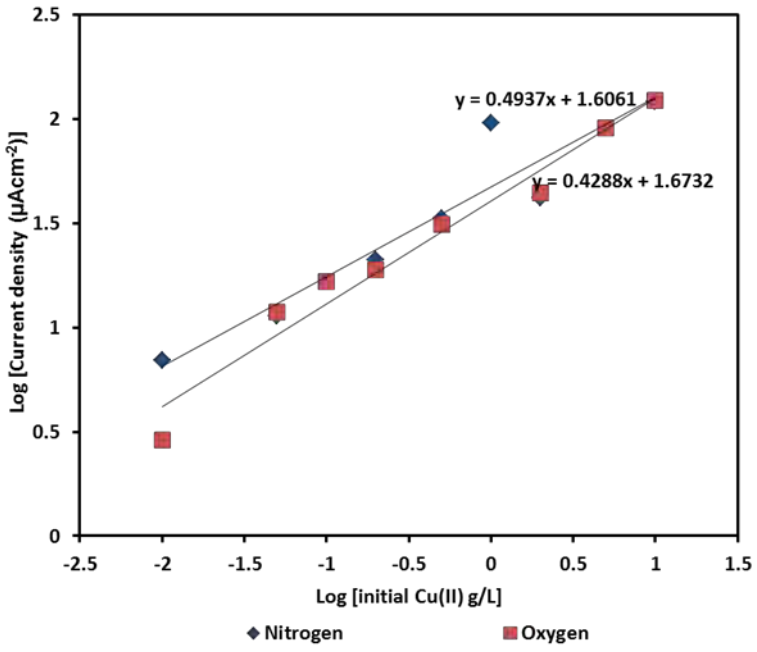

Figure 4.25. Log-log plot of oxidation currents versus initial copper concentrations in 1 M (NH_3+NH_4^+), 25°C, 1600 rpm, pH 9.6±0.15 in the presence and absence of oxygen.

The reaction order of the oxidation reaction with respect to copper(II), at mixed potentials was determined from the results presented in Figure 4.15. The order of the reaction was found to be 0.49 under nitrogen and 0.43 under oxygen (Figure 4.25). Crundwell (2013) reviewed the order of reactions for a large number oxidative and reductive dissolution reactions and found that most of the values were consistently close to 0.5 for the oxidant and -0.5 for the reductant despite vast variations in experimental conditions for the different studies. Beckstead and Miller (1977a), in a leach study, reported that the chalcopyrite oxidation reaction was not significantly affected by initial copper(II) at low concentrations, but reported 0.5 order with respect to copper(II), at high concentrations. Tozawa et al, (1976) reported on the increased rate of chalcopyrite leaching in ammoniacal solutions observed in the presence of cupric but suggested the role of copper(II) to be purely catalytic. Byerley el al (1975) proposed a reaction mechanism in which an intermediate species is formed in which a tetraammine copper(II) has one axial O_2 and one axial thiosulphate (S_2O_3) (Figure 2.6), the role of the cupric ammine being that of complexing both the oxidant (O_2) and reductant (S_2O_3), thus providing a mechanism for electron transfer between the oxygen and thiosulphate. While their study (Byerley el al, 1975) was carried in a homogeneous system, it is referred to as demonstration of the role of copper(II) as an oxidant in ammoniacal solutions. A reaction proceeding in this manner would require that both oxygen and copper(II) be present in solution, suggesting that synergy exists between the oxidising species present. Contrary to the work by Byerley et al (1975), Koyama et al (2006), in similar solution conditions, suggested that tetraammine copper(II) directly oxidised the surface of copper showing the reaction to proceed in the absence of oxygen. Several studies in gold leaching (Cheng, 2003; Aylmore and Muir, 2001; Rajib et al, 1997) have shown copper(II) to be the surface oxidant in thiosulphate gold leaching. In cupric chloride media, Lundström et al (2007) found copper to be the oxidant and reported a critical copper(II) concentration of 9 g/L below which changes in copper(II) did not significantly affect chalcopyrite's dissolution rate.

The presence of oxygen has been shown to have no significant effect on mixed potentials (Figure 4.6) and the corresponding dissolution currents of chalcopyrite at the mixed potentials (Figure 4.13). In the context of a leaching reaction, this as mentioned earlier occurs at mixed potential, oxygen has been reported to result in increased rates of leaching (Beckstead and Miller, 1977a, Forward and Mackiw, 1955; Tozawa et al, 1976). Beckstead and Miller (1977a), who studied chalcopyrite leaching in ammonia-ammonium sulphate solutions similar to those used in the current study and reported a half order reaction with respect to oxygen at low oxygen concentrations and zero order at high concentrations. The researchers (Beckstead and Miller, 1977a) went on to say that this half order dependence on oxygen was not affected by the presence of copper(II) ions. Forward and Mackiw

(1955) reported on the high requirements of oxygen that were necessary during the early stages of leaching of fresh sulphides. The researchers (Forward and Mackiw, 1955) attributed the high oxygen requirements to its use for the oxidation of the sulphide as well as the oxidation of thiosulphate in solution, suggesting that under the conditions of their study, oxygen became depleted and the rate of reaction became limited by the dissolution of oxygen at the gas-liquid interface. Forward and Mackiw (1955) went on to report that as the reaction neared completion, oxygen demand became less and other rate controlling factors became more significant. The researchers did not comment on the effect of the presence of alternative redox couples in solution, such as the copper(I)/copper(II) couple (coming from the oxidising chalcopyrite). Tozawa et al (1976) also reported on the increased rate of copper extraction from chalcopyrite when oxygen partial pressure was increased up to 3 $kgcm^{-2}$, above which further increases in oxygen partial pressure had no apparent effect. This is in agreement with Beckstead and Miller's (1977a) findings in that dependence on oxygen concentrations was not very apparent at high oxygen partial pressures. In chloride systems in which copper(I) is also thermodynamically stable, it is accepted that that copper(II) can oxidise the mineral surface, and iron(III) or dissolved oxygen regenerates the oxidant (Senanayake, 2005). Thus, considering that in the system under review the same redox couple is thermodynamically stable, it is reasonable to postulate that the role of oxygen is to regenerate the copper(I) rather than be the primary oxidant on the surface of the mineral.

4.4 Conclusion

Electrochemical experiments have shown copper(II) to be the primary oxidant in the oxidative dissolution of chalcopyrite in the presence and absence of oxygen at 25°C. Increasing copper(II) concentrations has been shown to result in increased mixed potentials and since chalcopyrite leaching is a potential driven reaction, this increase in potential translated to increased anodic currents. The presence of oxygen has been shown to have no significant effect on anodic currents and thus, the hypothesis that copper and oxygen form an intermediate complex which then oxidises chalcopyrite has been shown not to be true. Increasing pH resulted in lower mixed potentials but promoted the anodic reaction in the pH range 9-10. The anodic reaction was of order 0.53 with respect to OH^- at the lower pH range evaluated pH 9 - 9.6 and at the high end pH 9.6-10, the reaction was not dependent on pH. The order of reaction with respect to free ammonia was 0.94 at low free ammonia and 0.2 order at high total ammonia. The anodic reaction is proposed to occur via the formation of copper(I), iron(II) and thiosulphate intermediates which are postulated to be further oxidised in solution as non-faradaic reactions. Choice of anion influences the anodic currents, with SO_4^{2-} showing the highest current densities which however, tend to gradually decline with time while

CO_3^{2-} showed current densities that are lower than those seen in SO_4^{2-} solutions but were shown to attain steady state. The anodic reaction has been shown to be surface reaction controlled.

5 Cathodic reactions

During the leaching process, both cathodic and anodic reactions occur on the surface of the mineral. Since oxidative leaching is a redox reaction, this study would not be complete without exploring the cathodic reactions. The reduction reactions of interest are those involving the reduction of the oxidant which has previously been identified as oxygen (Warren and Wadsworth, 1984; Beckstead and Miller, 1977a; Reilly and Scott, 1977; Forward and Mackiw, 1955). Contrary to this, section 4.1 of this thesis explored the mixed potentials on the surface of chalcopyrite and identified the reduction of copper(II) as the primary reduction reaction on the mineral surface under the conditions of this study. This section explores the reduction reactions on the surface of chalcopyrite at cathodic potentials in the vicinity to the mixed potentials. The cathodic reactions have been studied using cyclic voltammetry and potentiostatic tests. Potentiostatic experiments allow for the isolation of the cathodic reaction by fixing the potential to values negative of measured mixed potentials and we can then monitor the current response in varied solution conditions. Effect of oxygen, potential, copper(II) concentration, prior oxidation of the mineral surface have been explored.

5.1 Effect of prior-oxidation

The effect of oxidising the electrode prior to running cathodic tests was evaluated. Oxidation of chalcopyrite in ammoniacal solutions is associated with the build-up of a deposit on the surface of the mineral (Guan and Han, 1997; Meng and Han, 1996; Beckstead and Miller, 1977b; Reilly and Scott, 1977; Forward and Mackiw, 1955). It was desired to test if the presence of the surface deposit layer had any influence on cathodic currents. The electrode was pre-oxidised at different potentials for one hour. The potential was immediately switched from the oxidising potential and set to a cathodic potential at 191 mV, and the current response was then observed for 2 hours. Figure 5.1 shows cathodic currents observed in these experiments. A fourth curve (blue) is shown and this was without any prior anodisation. It was observed that increasing the potential at which the electrode was pre-anodised resulted in subsequent cathodic current densities becoming more cathodic. It is brought to the reader's attention that cathodic currents are negative. Thus, when values of cathodic currents are becoming more negative, it means there is an increase in cathodic currents or the currents can be said to be more cathodic. The graphs show that upon switching to negative potentials, there was a sharp cathodic increase in currents, which is due to the charging of the electrical double layer on the mineral surface and thereafter, currents become less cathodic, then appear to be increasing cathodically especially on the curve prior oxidised at the high anodic potential 275 mV. The reader is reminded that these cathodic tests were carried out in solutions

containing initial copper(II) and for which the mixed potential as measured in section 4.1, was 255 mV.

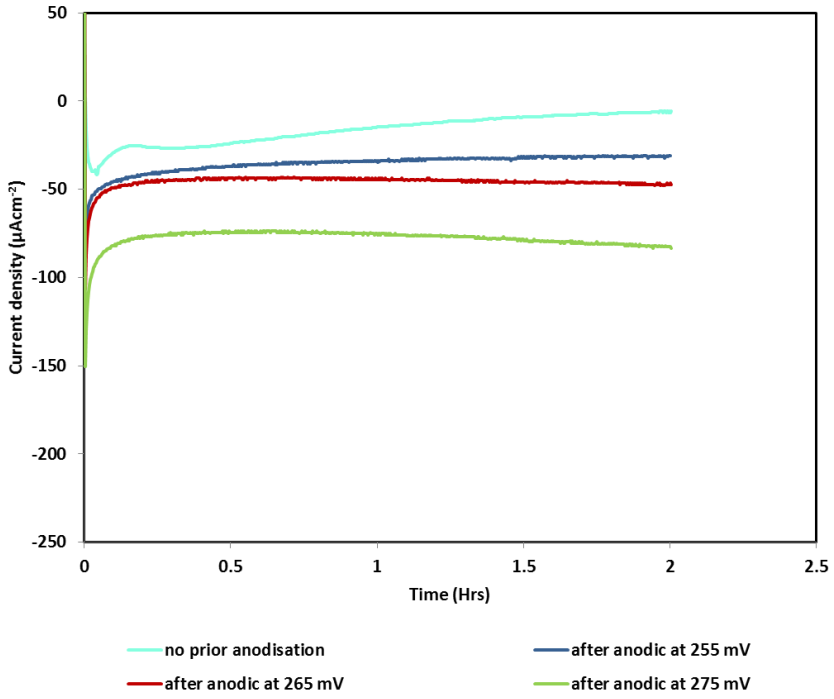

Figure 5.1. Cathodic current densities at 191 mV generated after 1 hour of oxidising the electrode at varied anodic potentials in 1 M (NH_3+NH_4^+), 25°C, 5 g/L initial Cu(II) pH 9.6±0.15 under nitrogen.

Figure 5.2 shows cathodic current densities at 191 mV generated after the electrode was oxidised at 255 mV for different durations. Current densities were observed to be more cathodic, showing an increase of ≈ 100 µAcm^{-2} when the electrode had been pre oxidised for 5 hours compared to when it had been prior oxidised for an hour.

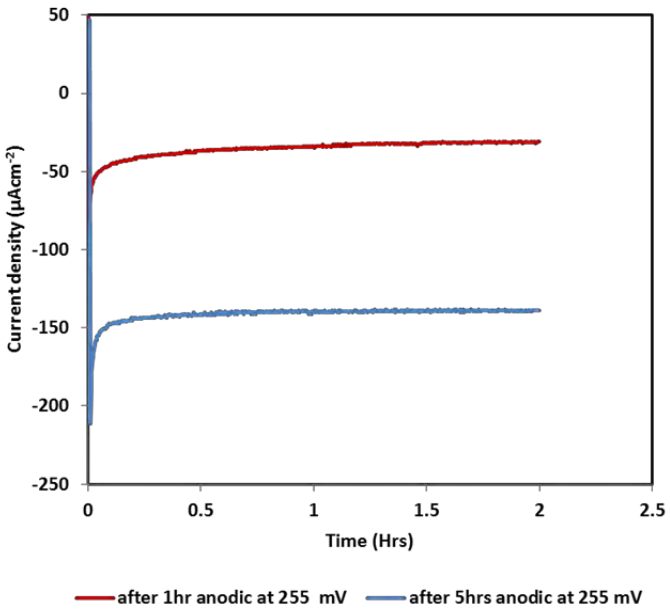

Figure 5.2. Cathodic current densities at 191 mV generated after 1 hour and 5 hours oxidation of the electrode at an anodic potential of 255 mV in 1 M (NH_3+NH_4^+), 25°C, 5 g/L initial Cu(II) pH 9.6±0.15 under nitrogen.

Thus, although increasing the anodic potential during prior oxidation, and increasing the duration of oxidation at a fixed anodic potential are expected to result increased growth of the surface deposit layer, an increase in cathodic currents was observed. Further cathodic test results presented in this section were all done on chalcopyrite surfaces that had been prior-oxidised for 1 hour at 255 mV; the reason for this was the consideration that in real leaching systems, reduction reactions are unlikely to occur on unoxidised mineral surfaces.

5.2 Effect of potential

Similar to the anodic reaction, the cathodic reaction is potential driven, thus it is expected that the rate of this reaction will increase as potentials become more negative. Figure 5.3 shows chronoamperometric test results, showing cathodic currents at different potentials in 1 M total ammonia at 25°C in the presence of 5 g/L initial copper(II) at a pH of 9.6. Currents are seen to increase cathodically as the potentials become more negative as would be expected. Cyclic voltammetry results (Figure 5.4) in which the potential was scanned at a rate of 1 mV/sec cathodically from the mixed potential after the mineral electrode was left to equilibrate for 30 min in the desired solution (257 mV in 1 g/L and 122 mV in 0 g/L solutions) to -8.5 mV (SHE) shows similar results i.e. current densities are observed to increase cathodically with a decrease in potentials in the presence of an oxidant, 1 g/L copper(II) in solution. In the absence of an oxidant (Figure 5.4), no significant cathodic currents were observed. In the constant potential tests, the current-time transients show a sharp cathodic increase in currents, followed by a decline to reach

steady state within the first 5 minutes. The sharp initial current peaks are common to all the constant potential tests and are due to the charging of the double layer.

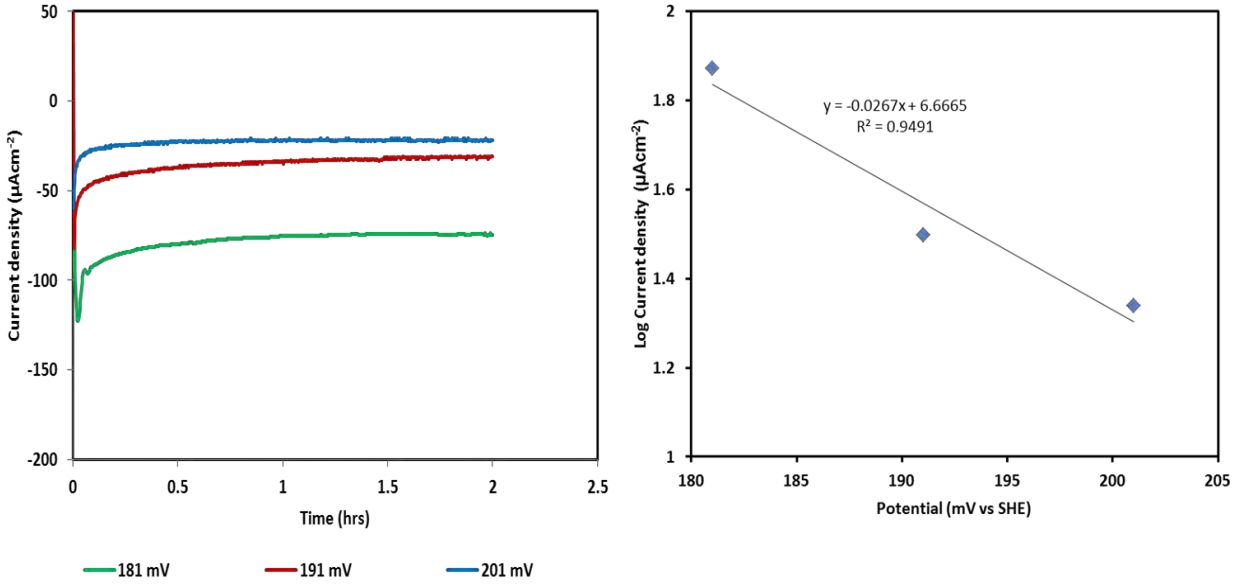

Figure 5.3. Chronoamperometric tests in 1 M (NH_3+NH_4^+), 25°C, 5 g/L initial Cu(II) pH 9.6±0.15 under nitrogen at various cathodic potentials. Electrode was pre-oxidised for an hour prior to each test.

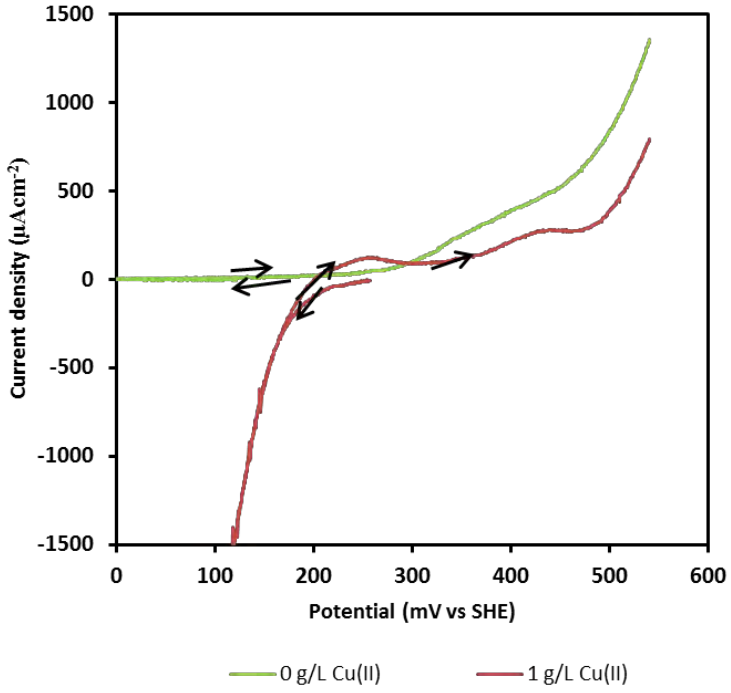

Figure 5.4. Cyclic voltammograms starting from mixed potential sweeping cathodically to 8.5 mV then forward to 540 mv in 1 M (NH_3+NH_4^+), 25°C, 5 g/L initial Cu(II) pH 9.6±0.15under nitrogen.

5.3 Effect of oxygen on cathodic currents

Results from anodic tests (Chapter 4) conclusively showed that the anodic reactions were not significantly affected by the presence of oxygen. However, it is known that both oxygen and copper are possible electron acceptors in the leaching reaction, and in most batch leach processes the reaction starts off with solutions that do not contain any copper(II). Furthermore, while anodic tests indicate that oxygen is not the primary oxidant, it does not conclusively show whether or not oxygen would be involved in the overall reaction. This section looks at the involvement of oxygen in the reaction from a cathodic perspective.

The effect of oxygen on cathodic current densities was evaluated by potentiostatting under nitrogen for an hour then switching to oxygen for another hour with all other parameters held constant. In the absence of initial copper(II), introduction of oxygen was observed not to result in significant changes in cathodic current densities (Figure 5.5). It would have been expected that the cathodic current densities would become more cathodic if oxygen was reduced at these potentials.

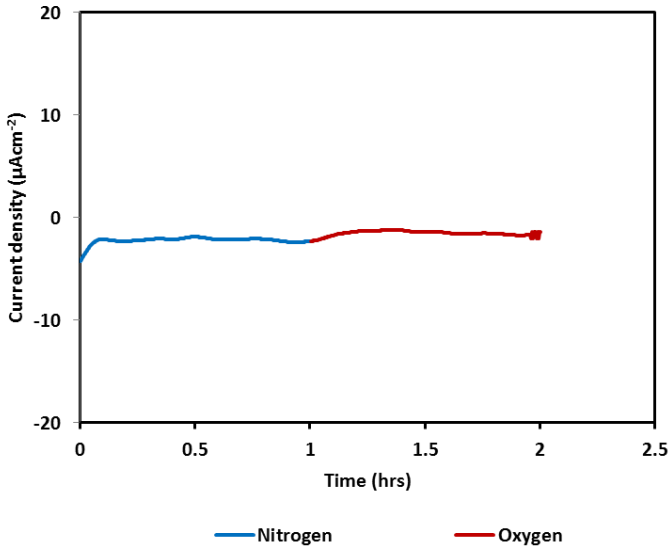

Figure 5.5. Chronoamperometric tests in 1 M (NH_3+NH_4^+), 25°C, pH 9.6±0.15 cathodic potential set at 191 mV the blue curve ran under nitrogen for an hour and the gas was switched to oxygen (red curve) for another hour.

However, in the presence of initial copper(II), introducing oxygen was observed to result in currents gradually becoming more cathodic (Figure 5.6), hinting at a slow kinetic process occurring on the mineral surface, with the current density dropping lower in an exponential fashion. The magnitude of the changes appeared to be related to the initial copper concentrations, the effect of switching from nitrogen to oxygen gas supply on current densities was calculated as a gradient. A gradient of -31 $\mu Acm^{-2}h^{-1}$ was calculated in 1 g/L solutions compared to -42 $\mu Acm^{-2}h^{-1}$ calculated in 5 g/L

solutions. The observed step changes after an hour were 7.01 µAcm^{-2} in the presence of 1 g/L copper(II), and 12.3 µAcm^{-2} in the presence of 5 g/L copper(II).

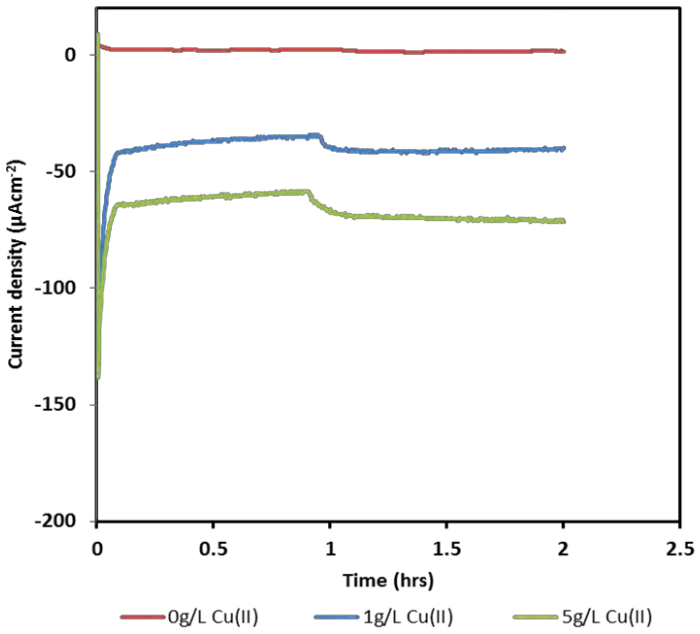

Figure 5.6. Chronoamperometric tests in 1 M (NH_3+NH_4^+), 25°C, pH 9.6±0.15 cathodic potential set at 191 mV at 0, 1 and 5 g/L initial copper(II) concentrations. Experiment started under nitrogen and oxygen was introduced after 1 hr.

Figure 5.7 reproduces the 5 g/L curve (green curve) from Figure 5.6 and also shows another 5 g/L curve (black curve) which ran at the same potential (191 mV) in which the test ran for the 2 hour duration under nitrogen *without* introducing oxygen. The change in the observed current densities is apparent with the presence of oxygen promoting cathodic current densities after 2 hours at -70.76 µAcm^{-2} compared to the current densities observed under nitrogen only that were at -49.95 µAcm^{-2}.

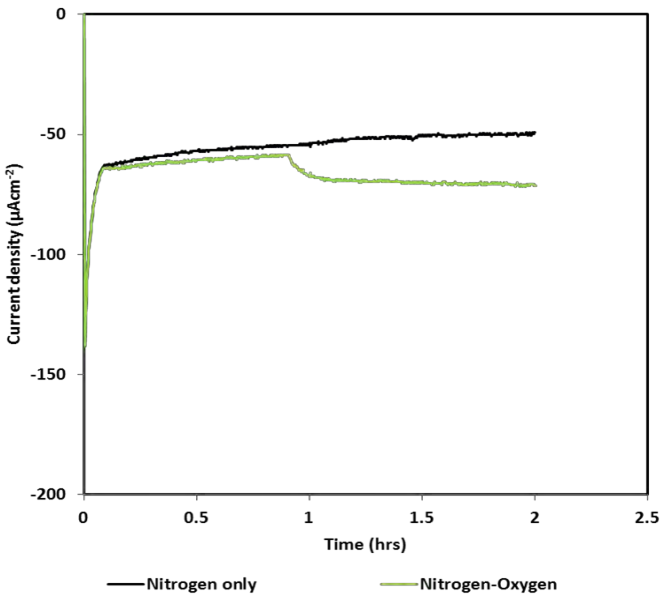

Figure 5.7. Chronoamperometric tests in 1 M (NH_3+NH_4^+), 25°C, pH 9.6±0.15 cathodic potential set at 191 mV at 5 g/L initial copper(II) concentrations with and without oxygen introduced after about 1 hour.

Oxygen has previously been accepted as the oxidant on the chalcopyrite surface ((Duyvesteyn, 1995; Duyvesteyn and Sabacky, 1993; Warren and Wadsworth, 1984; Beckstead and Miller, 1977a; Kuhn et al, 1974; Forward and Mackiw, 1955). Use of oxygen as an oxidant requires that oxygen be present at the solution-mineral interface. Kuhn et al (1974) developed an ammoniacal leaching process based on the improvement of agitation to increase surface oxygen mass transfer by preventing continuous growth of a surface deposit layer on the mineral surface and also improved oxygen mass transfer rate through the solution. Peters (1987) talks of oxidation on the mineral surface occurring by dissolved oxygen or "surrogate oxidants" which he defines as oxidants that are created by the consumption of oxygen. The solubility of oxygen in water and models of its solubility have been the subject of many publications (Geng and Duan, 2010; Tromans, 2000; 1999; Peters, 1987; Narita et al, 1983). Tromans (1999) presents a model for oxygen solubility in aqueous solutions and according to this model, oxygen solubility in water at 1 atm oxygen pressure is about 0.0012 molal/atm at 298 K. While Tromans (2000; 1999) show this solubility to vary with temperature and pressure between 1 and 10 atm and 298-612 K, Narita et al (1983) reported that the solubility of oxygen is essentially independent of both temperature (over the range 298–348 K) and the oxygen partial pressure (over the range 0.1–1.0 atm). Tromans, 2000; Peters, 1987; Narita, Lawson et al, 1983, agree that the ratio of solubility of oxygen in the electrolyte solutions to that in pure water decreases as the concentration of the electrolyte increases with Tromans (2000) reporting that the solubility could be lowered to about 0.4 times that of pure water.

Peters (1987) went on to state that oxygen arriving at the mineral surface is not reactive enough under inorganic conditions to be reduced at leaching rates typically observed because electrochemical reduction rate of oxygen is too slow. The slow kinetics of oxygen reduction are a widely reported phenomenon and have been subject of research mainly in fuel cell studies (Wy et al, 2012; Liang et al, 2011; Song and Zhang, 2008; Zhang et al, 2005; Kinoshita, 1992) where the use of platinum group metals is employed to accelerate the reaction. The slow oxygen reduction kinetics explains the insignificant cathodic currents observed when no initial copper(II) was present in solution leaving dissolved oxygen as the only species that could be reduced. Preliminary tests (section 3.1.3) in which oxygen was bubbled (at the same flow rate as that used in the tests) into solutions similar to that used in the tests reported in this thesis, showed that the solution was 79% saturated with oxygen after 2 minutes and reached 100% saturation in 5 min. Results from these preliminary tests suggest that the apparent lack of significant changes in the observed cathodic currents in solutions that did not contain copper (II) (Figure 5.5) was not due to the poor solubility of oxygen in solutions used for this study. This is further confirmed in Figure 5.6, where introducing oxygen into solutions containing copper(II) was immediately followed by changes in cathodic currents.

Results from this section agree with those of the anodic tests and are further confirmation that in the presence of copper(II), oxygen reduction is not the primary reduction reaction occurring of the surface of chalcopyrite. Peters's (1987) idea of surrogate oxidants sounds more plausible at this stage, considering presence of both oxygen and copper(II) was observed to promote cathodic currents thereby indicating some synergistic effects of the two electron acceptors. The apparent differences in magnitude of cathodic currents increase with an increase in copper(II) concentrations will be discussed in in the next section where effect of initial copper(II) concentrations on cathodic currents will be discussed.

5.4 Copper(II) concentration and mass transfer effects

Contrary to literature (Warren and Wadsworth, 1984; Beckstead and Miller, 1977a; Tozawa et al, 1976; Forward and Mackiw, 1955), it has been established that copper(II) is not a catalyst, rather, it is the primary oxidant in the oxidative dissolution of chalcopyrite in ammoniacal solutions. The reduction of copper(II) occurs according to equation 5.1 written out using the most stable cupric ammine species in the pH range (pH 9- pH 10) used in this study.

$$Cu(NH_3)_4^{2+} + e = Cu(NH_3)_2^{+} + 2NH_3 \qquad 5.1$$

Figure 5.8 shows the effect of copper(II) concentration on cathodic potentials at 191 mV pH 9.6. In each case, the electrode was anodised for an hour at 255 mV prior to the cathodic test, the potential was then immediately switched to a cathodic potential set at 191 mV in similar solutions but of varied initial copper(II) concentrations. Current densities became more cathodic in the presence of copper(II) changing from ≈ 0 μAcm^{-2} in the absence of initial copper(II) to -29 μAcm^{-2} in the presence of 1 g/L copper(II). Varying copper (II) concentrations appeared to promote the cathodic reaction, however only marginal increases were observed between when initial copper(II) was increased from 1 g/L to 2 g/L and no further increases were observed beyond 5 g/L .

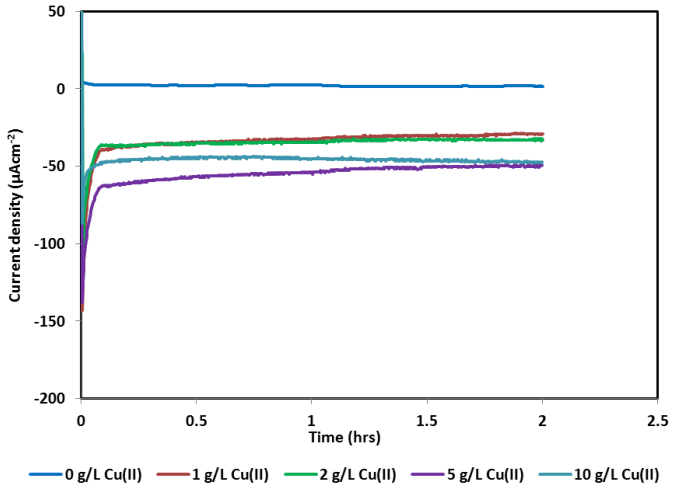

Figure 5.8. Chronoamperometric tests in 1 M (NH_3+NH_4^+), 25°C, pH 9.6±0.15 cathodic potential set at 191 mV at various initial Cu(II) concentrations under nitrogen. In each case, the electrode was oxidised for an hour at 255 mv prior to the start of each test.

Figure 5.9 shows cathodic branches from cyclic voltammograms in which potential was scanned anodically from mixed potential to 300 mV above mixed potential (to pre-oxidise the electrode) then reversed to 250 mV below mixed potential at various initial copper(II) concentrations. At the lowest initial copper(II) concentrations (0.05 g/L and 0.2 g/L), the current densities become mass transfer limited at below 100 mV while a small peak was observed at 95 mV. At initial copper(II) concentrations above 0.2 g/L, no cathodic current limitations were observed in the potential range studied.

Figure 5.10a. shows a cyclic voltammogram where potential was swept anodically from mixed potential to potentials 300 mV above mixed potential then the sweep was reversed up to cathodic potentials 250 mV less than the mixed potentials. This was immediately followed by the start of another sweep which started at the end point of the first cycle i.e. at 250 mV negative of mixed potential and swept up to 300 mV above mixed potential. Figure 5.10b. shows plots of only the

second cycles generated in a manner similar to that of Figure 5.10a. An anodic peak is apparent in all the second sweeps starting at around 200 mV. The peak is probably due to the oxidation of a species formed at cathodic potentials and it is seen to increase with an increase in initial copper(II) concentration. This peak was not observed in solutions in which initial copper(II) was not present in solution (Figure 5.4). The peaks are taken to be due to the oxidation of copper(I) (Equation 5.2) generated from the reduction of copper(II) during the first sweep. It could be expected that the peak sizes would increase with an increase in initial copper(II) as one would expect more copper(II) to have been reduced at high concentrations thus generating more copper(I) on the mineral surface. The transient nature of the sweep will result in the curve reverting to its normal anodic trajectory once oxidation of all residual copper(I) has been completed. It is important to note that for the copper(I) to be available for re-oxidation, it must have been held on the mineral surface and not dispersed into the bulk solution.

$$Cu(NH_3)_2^{+} + 2NH_3 = Cu(NH_3)_4^{2+} + e \qquad 5.2$$

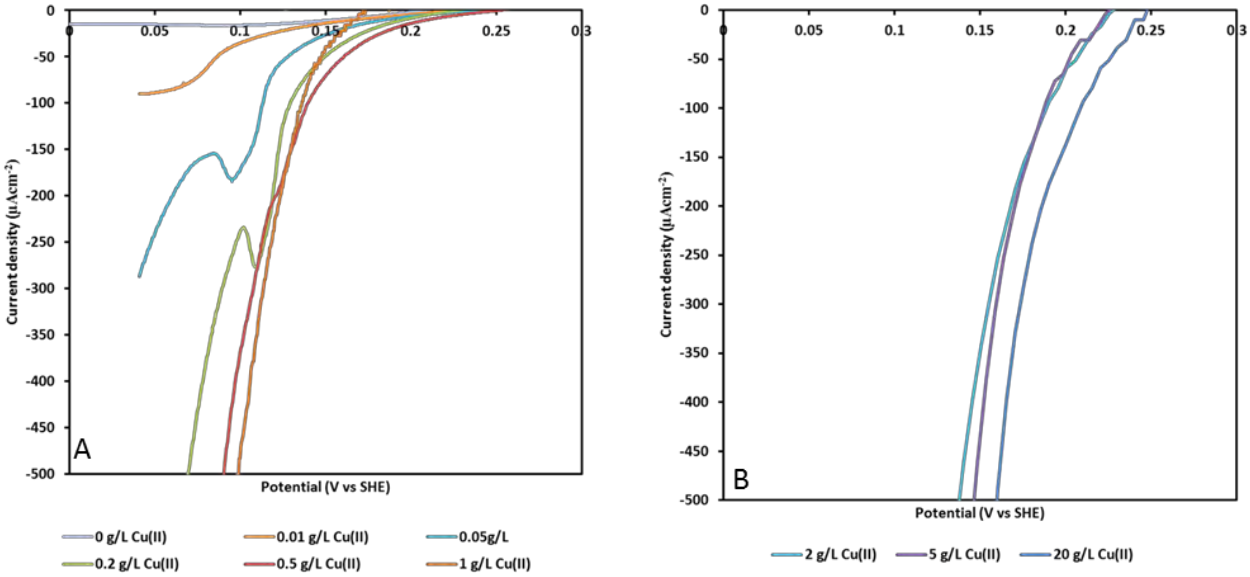

Figure 5.9. Cyclic voltammograms showing only the cathodic branch. Sweep started at mixed potential and swept anodically to 300 mV versus mixed potential then cathodically to 250 mV versus mixed potential in 1 M (NH_3+NH_4^{+}), 25°C, pH 9.6±0.15 at various initial Cu(II) concentrations under nitrogen. A and B follow the same methodology, graphs were separated to avoid having too many curves on one graph.

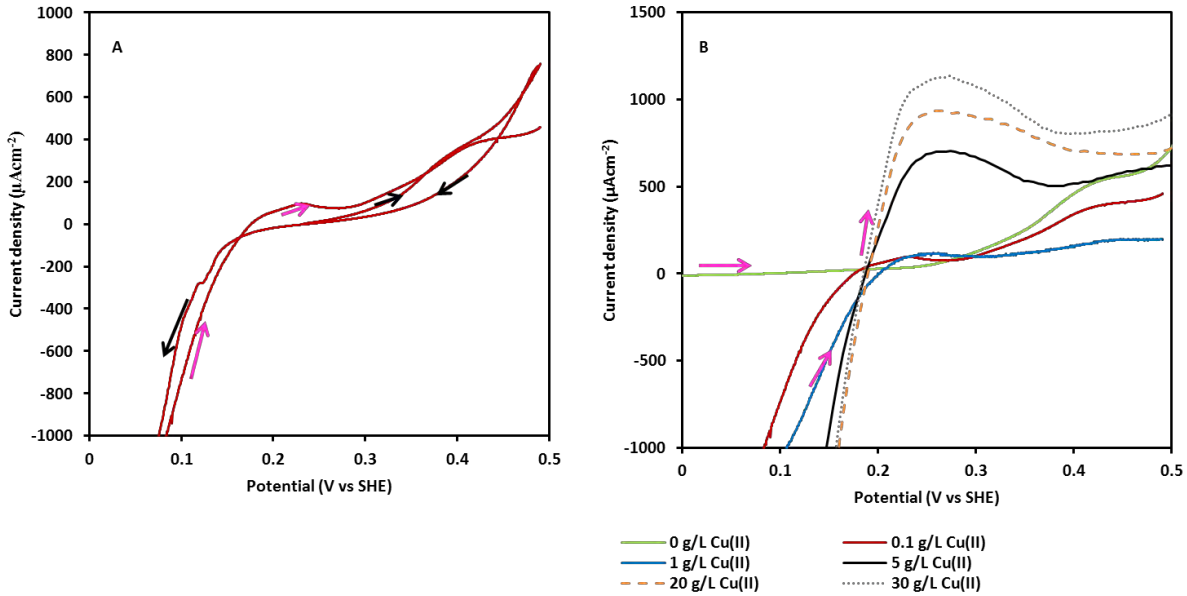

Figure 5.10. Cyclic voltammograms generated at a scan rate of 1 mV/sec in 1 M (NH_3+NH_4^+), 25°C, pH 9.6±0.15 at various initial Cu(II) concentrations under nitrogen. A shows a complete cyclic voltammogram starting with an anodic sweep form mixed potentials as indicated by arrows black arrows indicate first cycle pink arrows indicate 2nd sweep starting at 250 mv negative of mixed potential. B shows only part of second cycles generated in the same manner as demonstrated in A.

Figure 5.11 shows a current density-time plot at a fixed potential (191 mv) in 1 M (NH_3+NH_4^+), containing 5 g/L initial copper(II), during which the rotation speed of the electrode was varied in steps. Cathodic current densities decrease when rotation speed is lowered from 1600 rpm to 200 rpm. It was observed that after each step, the current densities quickly levelled off showing no further decrease until agitation speed was increased once more. This suggests the presence of limiting current densities (i_L) at each rotation speed. Limiting current densities refers to the maximum attainable current densities i.e. the reaction cannot go faster than i_L because the transport process in the electrolyte bulk is incapable of supplying the electron acceptor to the interface at a faster rate (Bockris et al, 2000). A plot of the current density versus the square root of the rotation speed according to the Levich equation for mass transport to a rotating disk gives a straight line going through the origin (Figure 5.12). This suggests that a reversible mass transport controlled reaction is taking place on the surface of the electrode. There were no deviations from linearity observed, even at the highest agitation speed of 4400 rpm.

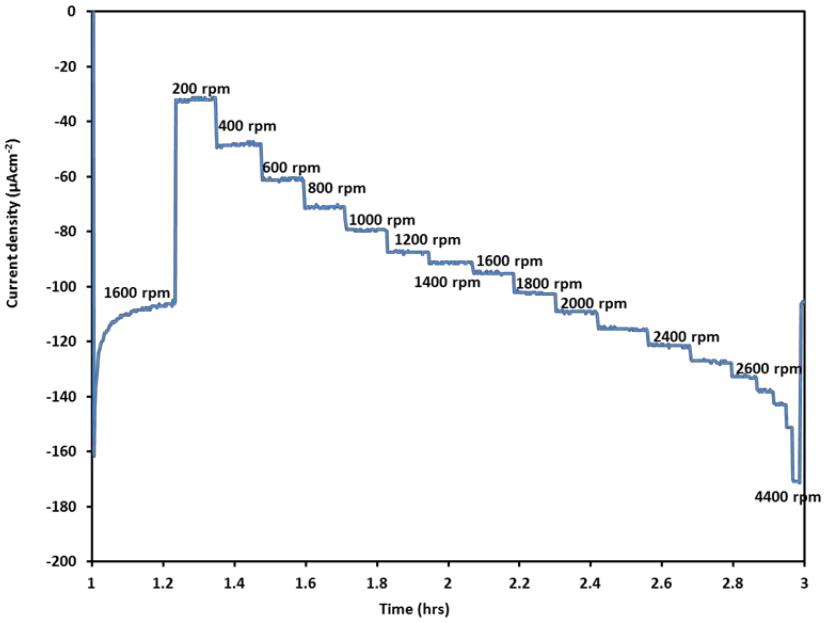

Figure 5.11. Chronoamperometric tests in 1 M (NH_3+NH_4^+), 5 g/L Cu(II), 25°C, pH 9.6±0.15.20 cathodic potential set at 191 mV at varied agitation speeds.

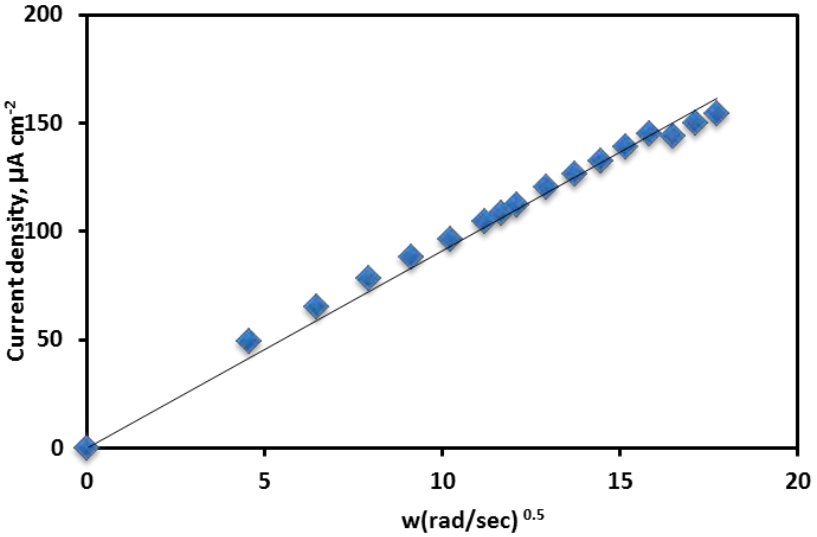

Figure 5.12. Plot of current density versus square root of agitation speed at 255 mV in 1 M (NH_3+NH_4^+), 25°C, 1600 rpm, pH 9.6±0.15 under nitrogen.

The diffusion coefficient for copper(II) was found to 3.94 x 10^{-9} cm^2s^{-1} which is 3 orders of magnitude lower than the 5 x 10^{-6} cm^2s^{-1} expected for the concentrations used in this test (Hinatsu and Foulkes, 1989) .

$$i_L=0.62nFAD^{2/3}\omega^{1/2}\,\nu^{-1/6}C_b \qquad 5.3$$

where;

i_L limiting current density (Acm^{-2}))

n number of electrons transferred

F Faraday ($Asmol^{-1}$)

A area of the electrode (cm^2)

D diffusion coefficient (cm^2sec^{-1})

ω angular velocity ($rads^{-1}$)

v kinematic viscosity ($cmsec^{-1}$)

Since the potential in these tests was set at a value not too far from the mixed potential, the oxidation of copper(I), i.e. the product of the reduction reaction (Equation 5.1) can occur and this has been shown in the sweeps on Figure 5.10. Thus, the currents from this oxidation reaction contribute to the (overall) measured cathodic currents resulting in the observed mass transfer limitations possibly being related to the migration away from the electrode surface of the copper(I) making it unavailable for oxidation.

Note that current densities due to the oxidation of copper(I) are positive and if summed with the negative cathodic current densities from the more prominent reduction reaction, the result is that the measured cathodic current densities will be less negative or less cathodic than would otherwise have been measured in the absence of interference from the oxidation reaction. This is illustrated in Figure 5.13, which shows a simulation (Appendix 2) in which the red curve (measured) shows the current densities measured by the instrument and the green and blue curves show the true cathodic curve and the curve for oxidation of copper(I) respectively. The measured current densities are a summation of the true reduction current densities and the oxidation of copper(I) which occurs in the same potential region. A detailed model of the cathodic currents is presented in appendix 1.

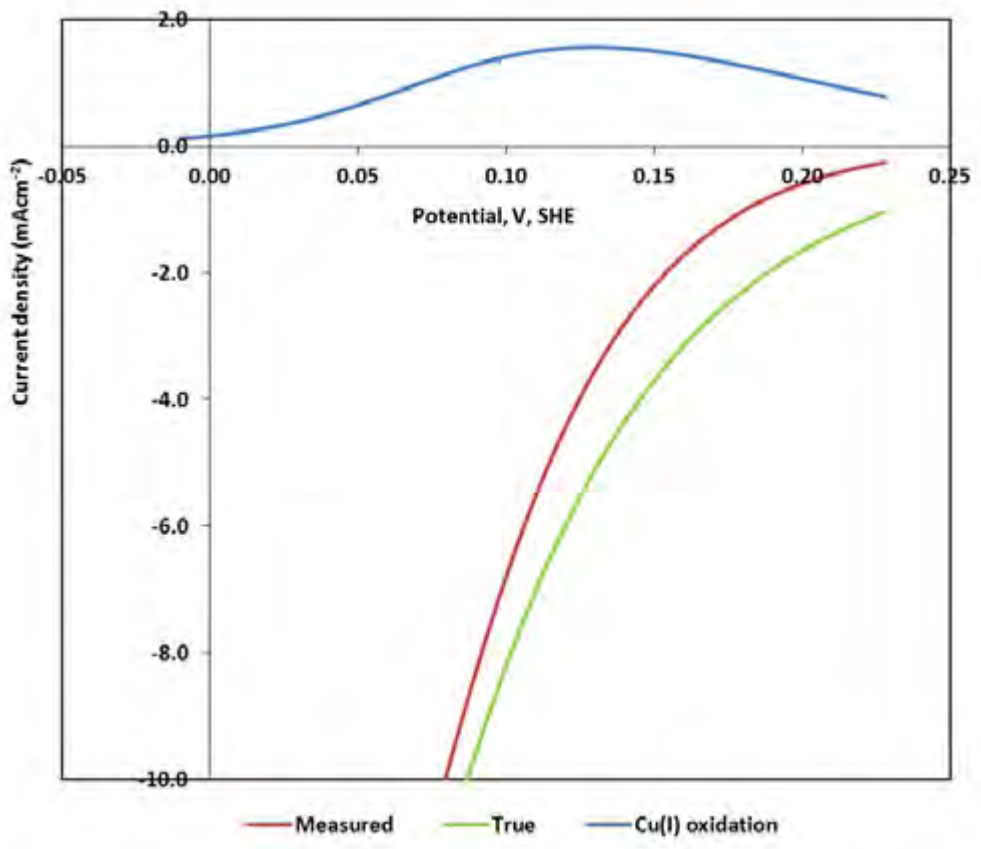

Figure 5.13. Simulation of current densities during in the cathodic reduction of copper(II) on chalcopyrite at 1600 rpm in 5 g/L copper(II) solutions.

5.5 Effect of total ammonia and pH

The effect of total ammonia and that of pH on the cathodic reaction has been evaluated at different cathodic potentials. The electrode was first pre-oxidised for an hour at 255 mV, then kept at varied cathodic potentials for two hours. Figure 5.14 shows how cathodic current densities recorded after 2 hours varied with an increase in pH between pH 9 and pH 10. The figure also shows how the current densities at different pH values varied with potential.

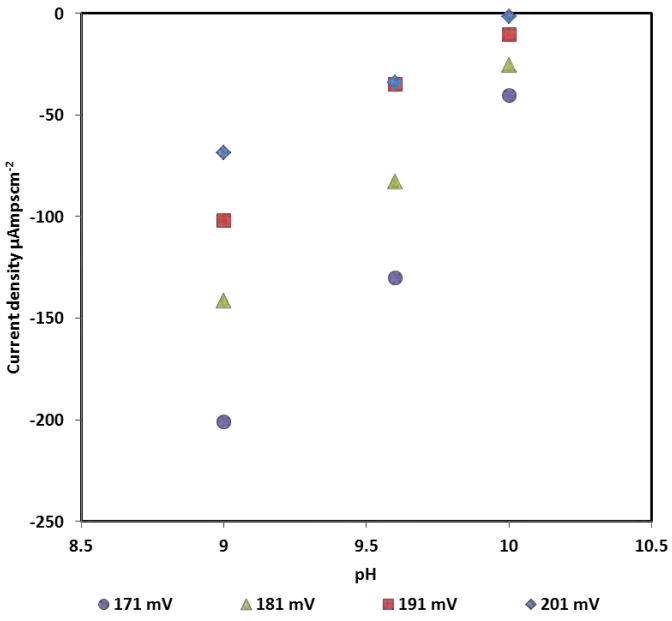

Figure 5.14. Effect of pH on cathodic currents at varied potentials and varied pH in 1 M (NH_3+NH_4^+), 1 g/L Cu(II), 25°C, 1600 rpm, under nitrogen. In each case, the electrode was pre-oxidised for 1 hr at 255 mV.

Figure 5.15 shows log current density versus potential plots of cathodic current densities on the chalcopyrite surface at varied pH. It was observed that increasing pH above 9.6 did not cause significant changes in cathodic current densities at the less negative potentials i.e. 100 mV to 200 mV, however cathodic current densities at pH 9 were higher than those observed at pH 9.6 and pH 10 (Figure 5.15). The result trends from Figure 5.15 are in line with the constant potential data presented in Figure 5.14.

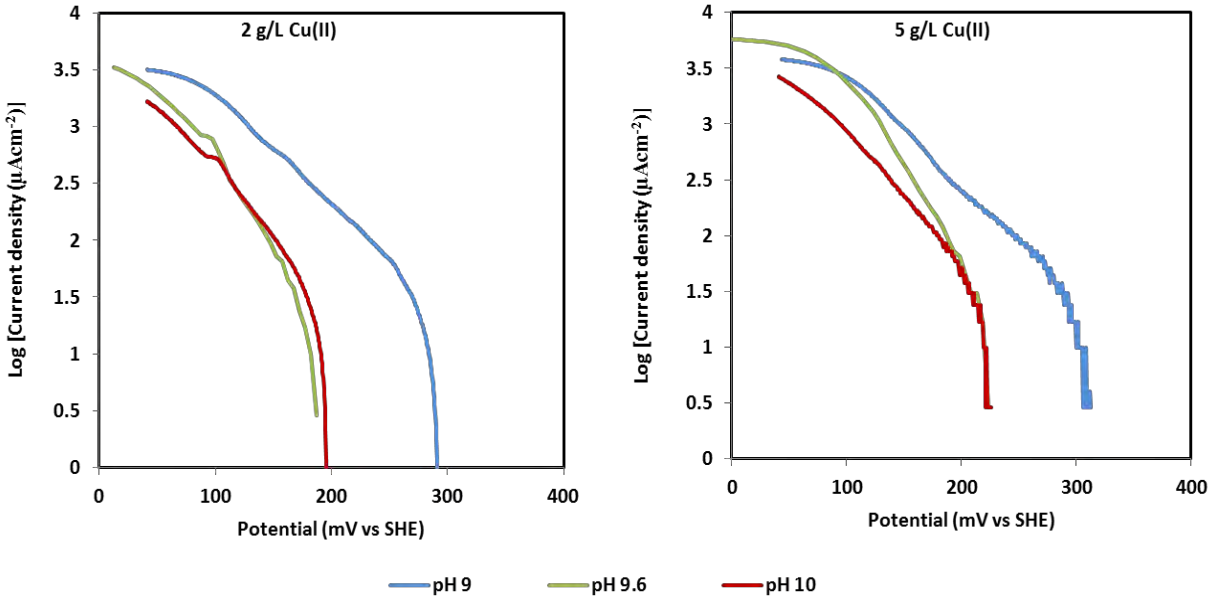

Figure 5.15. Log current density-potential plots of chalcopyrite at 1 M (NH_3+NH_4^+) at 25°C, 1600 rpm, varied pH under nitrogen in solutions containing 2 g/L and 5 g/L initial Cu(II) at a scan rate of 1 mV/sec. In each case, the electrode was pre-oxidised by sweeping anodically to 300 mV above mixed potential

The rate of the cathodic reaction decreases with increasing pH and negative reaction orders were determined as shown in Figure 5.16. A concentration profile of copper(II) at different total ammonia concentrations was shown in Figure 4.19 and it is apparent that it did not vary significantly with changes in total ammonia. However, it is known that the species distribution of the different copper(II)-ammine species will vary with changes in pH and total ammonia (Togrinson and Hathaway, 1968; Tomlinson et al., 1969; Hathaway and Tomlinson, 1970; Trevani et al , 2001; Pavelka and Burda, 2005; Van Wensveen.C, 2010).

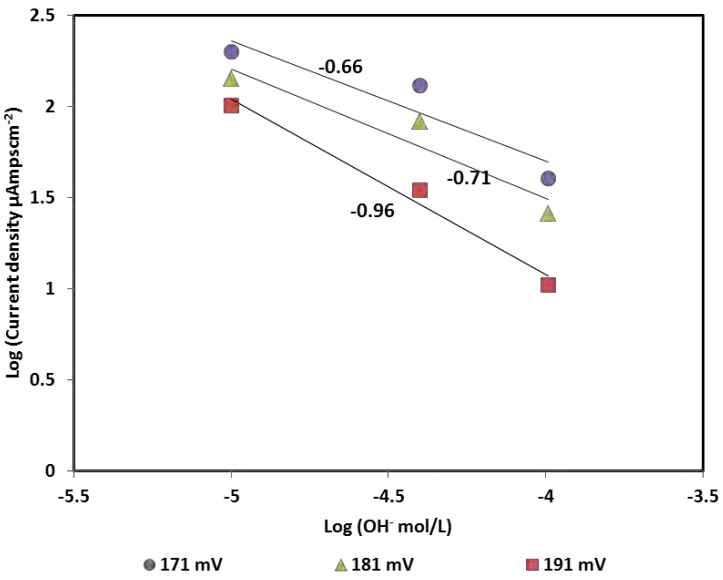

Figure 5.16. Log-Log plot of current density versus hydroxyl ion concentration at different potentials in 1 M (NH_3+NH_4^+), 1 g/L Cu(II), 25°C, 1600 rpm, pH 9.6±0.15 under nitrogen.

A concentration profile of tetra- ammine-copper(II) ($Cu(NH_3)_4^{2+}$) at different pH and total ammonia is shown in Figure 5.17. It can be seen that concentrations of tetra-copper(II)-ammine decrease only slightly with increase in pH and total ammonia. Because the tetra-copper(II)-ammine concentration changes are so small, i.e. less than 0.01 $molL^{-1}$; it is not expected to cause the observed decrease in cathodic current densities. On the other hand, Figure 5.18 shows concentration profiles of tri-ammine-copper(II) ($Cu(NH_3)_3^{2+}$), and it can be seen that concentrations of this species decrease significantly with an increase in total ammonia; $Cu(NH_3)_3^{2+}$ concentration changes by an order of a magnitude between 1 M and 6 M total ammonia. Changes in pH seem to affect the tri-ammine-copper(II) at low pH, but showed no significant effect at high pH and this is consistent with the results presented in Figure 5.14 and Figure 5.15. Thus, although the tetra-ammine-copper(II) species is the most dominant and has been accepted as the oxidising species in the ammoniacal leaching of other minerals (Aylmore and Muir, 2001; Senanayake, 2005a; 2005b; Marsden and Ian House, 2006), results from the current study suggest that tri-ammine-copper(II) is probably the active species. The tri-amime-copper(II) species is not widely studied while the tetra-ammine and the penta-ammine copper(II) have enjoyed researchers attention. Itoh et al (1998) identified tri-ammine-copper(II) complexes as active species in the hydrolysis of phosphate esters and attributed this to the structural configuration of the tri-ammine-copper(II) complex. It is pointed out that no further test work was carried out to identify the exact copper(II) ammine species on the mineral surface but deductions were made based on observed changes in current densities with pH and total ammonia. It would have been expected that current densities show no dependency on pH within the pH range

of the current study, if it is assumed that all copper(II) species present in solution were acting as the oxidising species. The observed negative dependence on pH is thus considered to be related to the concentration profile of tri-copper(II)-ammonia species in solutions of different pH.

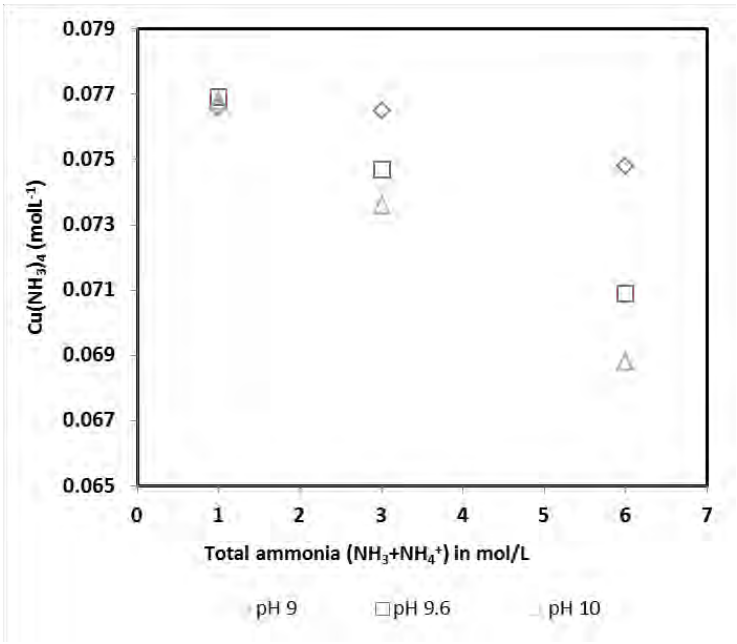

Figure 5.17. Concentration profile for $Cu(NH_3)_4^{2+}$ in solutions of different total ammonia and different pH in solutions containing 5 g/L Cu(II).

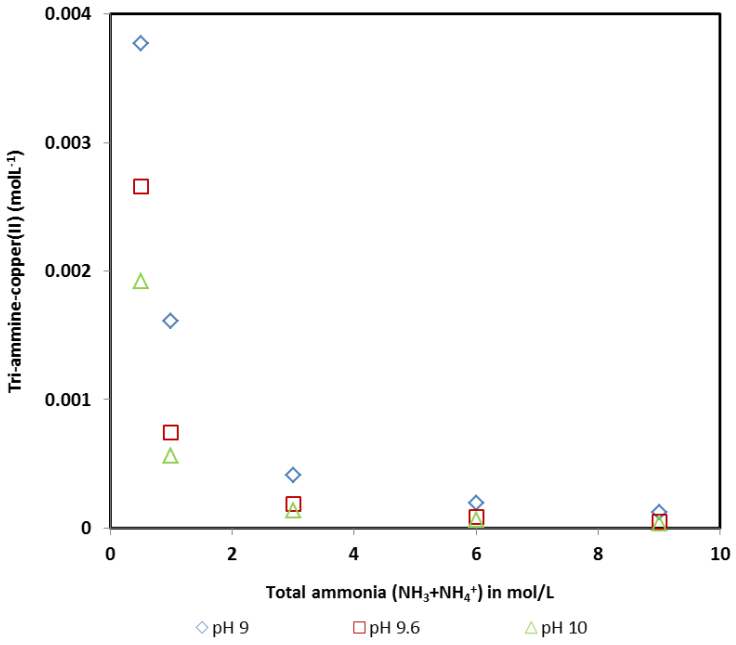

Figure 5.18. Concentration profile for $Cu(NH_3)_3^{2+}$ in solutions of different total ammonia and different pH in solutions containing 5 g/L Cu(II)

Effect of total ammonia

Tests to evaluate the effect of total ammonia were carried out at three total ammonia concentrations, 1, 3 and 6 M. Figure 5.19 shows that at similar potentials, the current densities became less cathodic with an in increase in total ammonia from 1 M to 3 M (NH_3+NH_4^+). In fact, current densities were only cathodic at 1 M (NH_3+NH_4^+), there-after becoming anodic at 3 and 6 M (NH_3+NH_4^+). The observations made on Figure 5.19 also suggest a negative dependency on total ammonia.

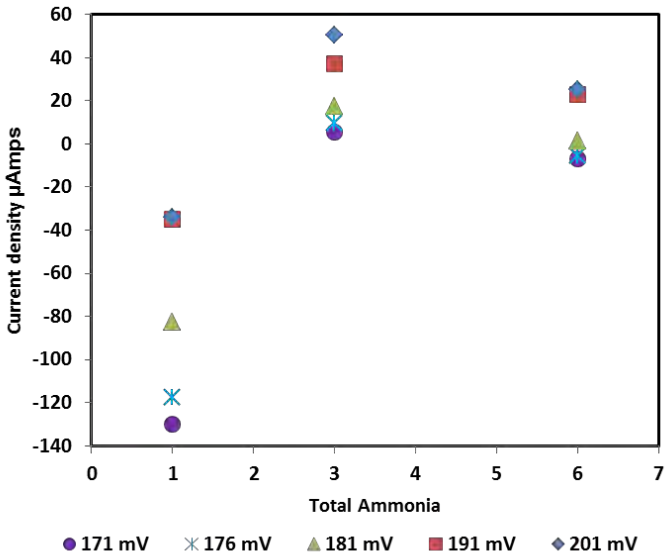

Figure 5.19. Effect of total ammonia on cathodic currents at varied potentials and varied total ammonia (NH_3+NH_4^+), 1 g/L Cu(II), 25°C, 1600 rpm, pH 9.6±0.15 under nitrogen. In each case, the electrode was pre-oxidised for 1 hr at 255 mV.

It can be seen from Figure 5.14 and Figure 5.19 that as pH and total ammonia increased, cathodic currents became less negative with Figure 5.19 showing positive or anodic currents at all potentials evaluated in 3 M and 6 M total ammonia solutions. These positive currents are explained with reference to the mixed potentials of chalcopyrite as reported in section 4.2.4.

- Mixed potentials of chalcopyrite were observed to decrease with an increase in both total ammonia and pH

This implies that by fixing the potential and observing the resultant current densities in solution conditions of varied total ammonia or pH, caution has to be exercised when choosing the set potential. The set potentials have to be sufficiently low such that, even when the mixed potentials decrease as has been shown in Figure 4.8 and Figure 4.9, the set potential remains lower than the

mixed potential and results in negative current densities. The mixed potentials of chalcopyrite at 1 M, 3 M and 6 M total ammonia, 1 g/L initial copper were presented in section 4.1.4 and are 255 mV, 161 mV and 136 mV (SHE) respectively. While all the chronoamperometric tests (Figure 5.19) in the 1 M solutions were measured at potentials below chalcopyrite's mixed potential in similar solutions i.e. they were measured at potentials that generated cathodic currents; it can be seen that even at the lowest potential evaluated (171 mV); the chalcopyrite electrode in the 3 M and 6 M solutions was actually at potentials positive of the mixed potential and hence generated the positive currents observed.

Figure 5.20 shows cyclic voltammograms generated by sweeping the electrode surface at a scan rate of 1 mV/sec at cathodic potentials. The results show that cathodic current densities increased with an increase in total ammonia between 200 mV and 300 mV in the presence of ≤2 g/L copper(II) in solution. At the more negative potentials, below 100 mV, an inverse effect of total ammonia on cathodic currents was observed. In the presence of ≥ 5 g/L copper(II), 1 M total ammonia still showed the lowest cathodic currents between 200 mV and 300 mV; however the 3 M total ammonia solutions showed higher currents than the 6 M total ammonia solutions.

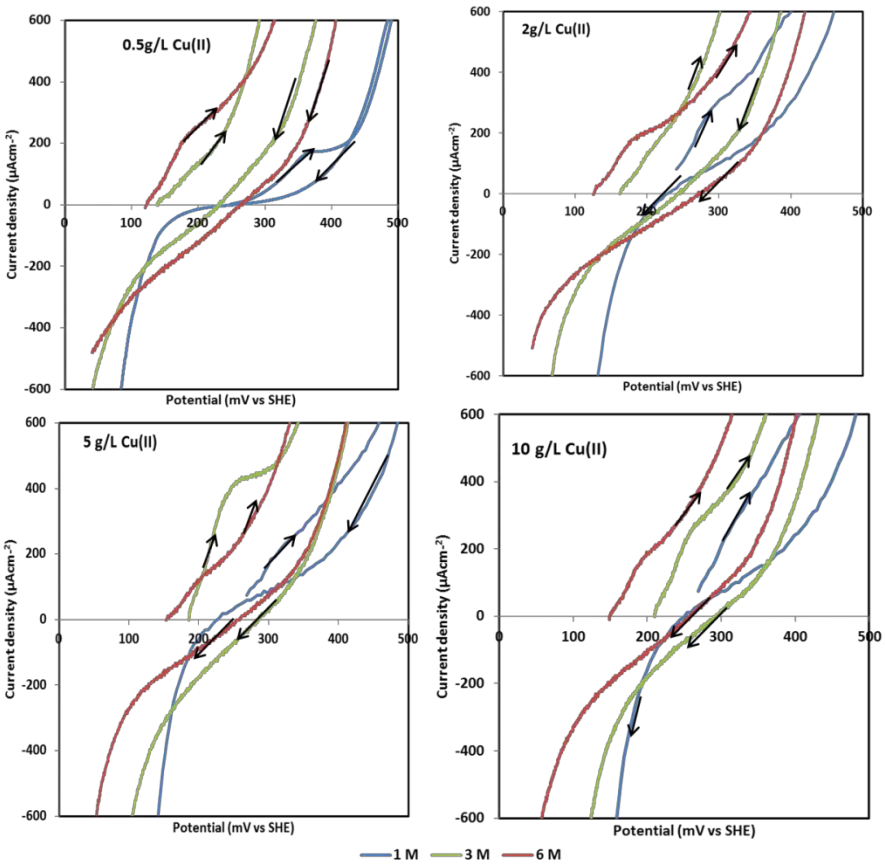

Figure 5.20. Cyclic voltammograms of chalcopyrite at varied total ammonia (NH_3+NH_4^+) at 25°C, 1600 rpm, pH 9.6±0.15 under nitrogen in solutions containing 0.5 g/L, 2 g/L, 5 g/L and 10 g/L initial Cu(II) at a scan rate of 1 mVsec^{-1}. In each case, the electrode was pre-oxidised by sweeping anodically to 300 mV above mixed potential.

5.6 Effect of agitation on cathodic sweeps

Figure 5.21a shows the effect of agitation speed on current densities at 50 rpm, 400 rpm and 1600 rpm in 1 g/L copper(II) solutions at 1 M (NH_3+NH_4^+), 25°C, pH 9.6±0.15 under nitrogen. Mixed potentials (Table 5.1) were not significantly affected by the rotation speed. The limiting currents at potentials below about 100 mV at 50 rpm and 400 rpm and at about 50 mV at 1600 rpm were due to mass transport limitations on copper(II). This provides further confirmation that the Levich like behaviour shown in Figure 5.11 could not have been due to mass transport limitations on the copper(II) since that test was run at 191 mV, which is higher than the 50 mV at which mass transport of copper would be expected under similar test conditions.

Figure 5.21b shows current response when sweeping anodically from the negative limit shown in Figure 5.21a. Anodic current densities are higher at lower agitation speeds with the 50 rpm and 400 rpm showing their first anodic peaks currents to be around 210 µAcm^{-2} compared to the curve at 1600 rpm which has a first peak current of around 150 µAcm^{-2} also accompanied by a negative shift in potentials. This was considered to be related to the rate of mass transfer of copper(I) formed

during the cathodic phase of the sweep. At high rotation speed the copper(I) is transported more rapidly than it would be at low agitation speed, hence it is not available for re-oxidation. This dependence on mass transport has been demonstrated in constant potential tests (Figure 5.11) in which reduction of copper(II) on the chalcopyrite surface showed Levich-like dependence on rotation speed at current densities well below current densities expected for copper(II) reduction. The effect of increasing agitation speed on cathodic currents is similar to that of introducing oxygen (Figure 5.6) in that both instances result in the currents becoming more cathodic. The net effect is similar but it is achieved differently. Agitation transports the copper(I) away making it unavailable for oxidation while introducing oxygen results in the in situ oxidation of the copper(I) thus making it unavailable to be oxidised in a faradaic reaction.

Table 5.1. Mixed potentials measured after 30 minutes in 1 M (NH_3+NH_4^+), 25°C, pH 9.6±0.15 under nitrogen

Rotation speed (rpm)	Mixed potential mV (SHE)
50	264
400	261
1600	264

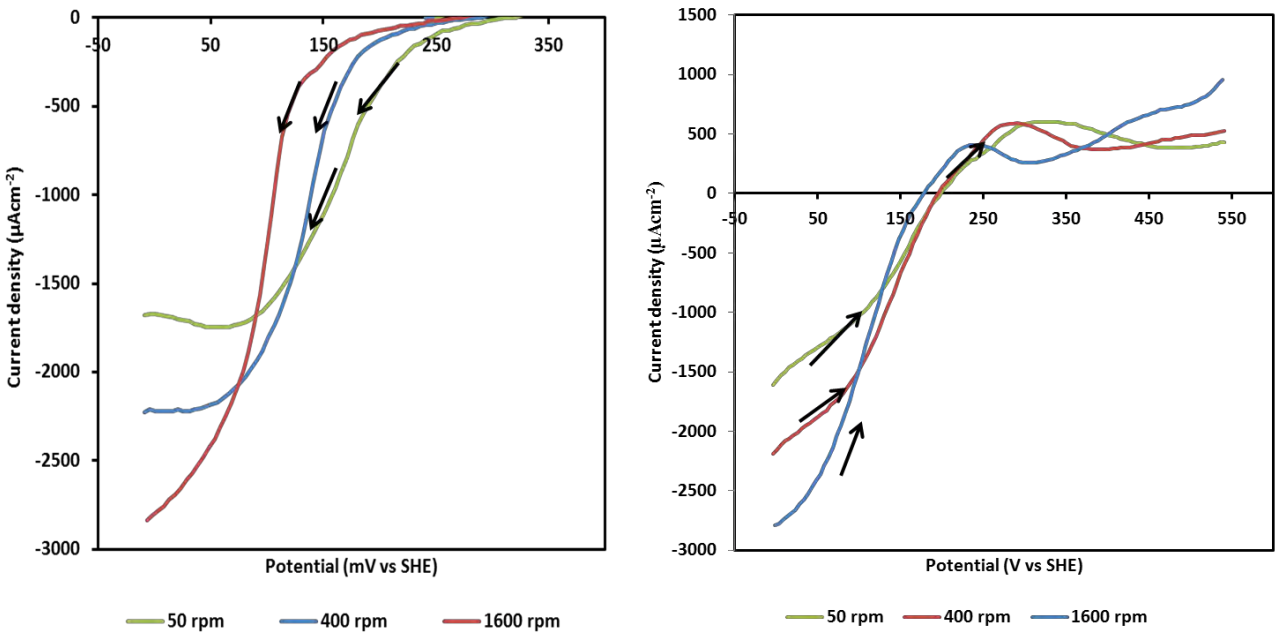

Figure 5.21. Cyclic voltammograms in 1 M (NH_3+NH_4^+), 25°C, 1600 rpm, 1 g/L Cu(II), pH 9.6±0.15 under nitrogen

Activation energy

The activation energy of the cathodic reaction was determined from the data presented in Figure 5.22. Figure 5.22 shows cathodic branches of cyclic voltammograms measured in 1 M total ammonia at 25°C, pH 9.6±0.15 under nitrogen. Figure 5.22a shows the data as measured from the instrument and Figure 5.22b shows the same set of data after correcting for IR drop as described in the methodology (Section 3.2.3). Since it is our contention that these curves represent a summation of current densities due to the cathodic reduction of copper(II) and the currents due to the oxidation of the generated copper(I) as illustrated in Figure 5.13, the curves in Figure 5.22 were corrected to subtract the anodic contribution. An exponential fit for the true cathodic currents was then done, thereby getting an expression of the form of equation 5.4.

$$k = k_0 e^{\frac{(1-\propto)F(E-E_0)}{RT}} \qquad 5.4$$

In which k_0 is a potential dependant rate constant. Natural logarithm (ln) of k_0 was then plotted against the inverse of temperature (Figure 5.23) and activation energy was determined as described in the methodology (Section 3.2.3). Activation energy of 15.13 kJ/mol was calculated suggesting the reaction was mass transfer controlled (the value is much lower than the 20 kJ/mol normally cited to be the upper boundary of purely mass transfer limited processes).

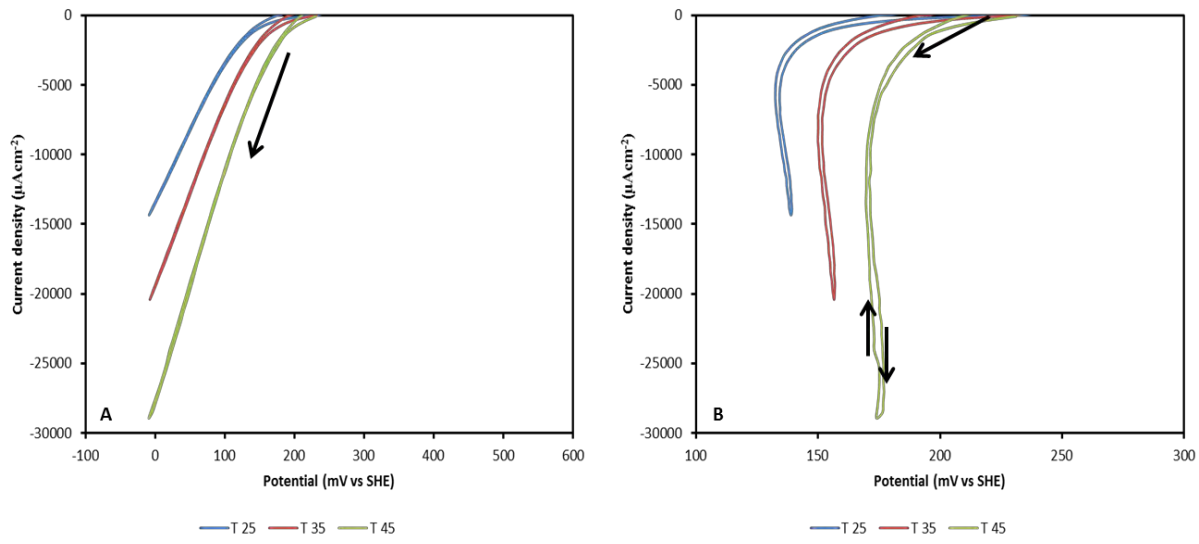

Figure 5.22. Cathodic sweep at scan rate 1 mv/sec in solutions of 1 M (NH_3+NH_4^+), 5g/L Cu(II), 25°C, pH 9.6±0.15 under nitrogen

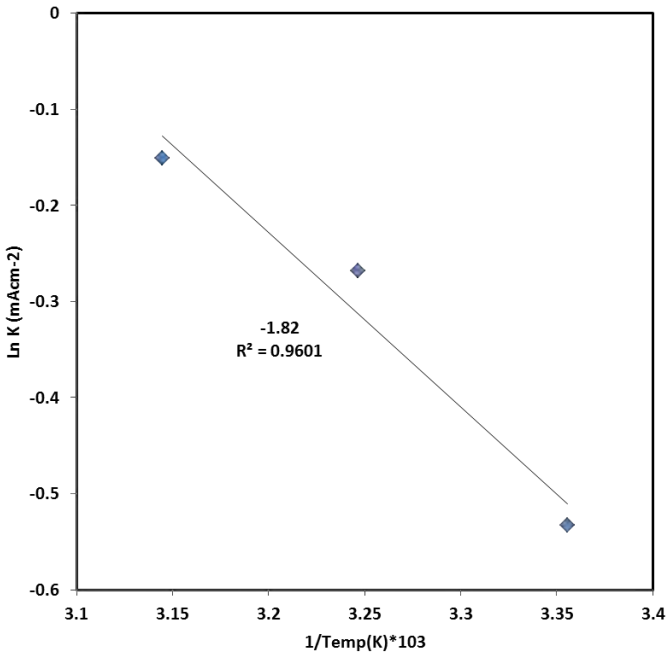

Figure 5.23. Arrhenius plots for the cathodic reaction.

5.7 Conclusion

Results from this section indicated that both the reduction of copper(II) and oxidation of copper(I) occur simultaneously at potentials close to mixed potentials of chalcopyrite under the conditions of this study. Contributions of the copper(I) oxidation currents to the overall measured current densities during cathodic tests lead to diffusion coefficient that is much lower than expected for mass transport of copper(II). At potentials close to the mixed potential, lowering of copper(I) concentrations on the mineral surface has been shown to result in increased measured cathodic currents. Lowering of these copper(I) concentrations is achieved by increasing agitation speed to increase the transport of copper(I) away from the electrode or by the introduction of oxygen to oxidise the copper(I) to copper(II) in situ. The reaction was not significantly affected by free ammonia in the concentration range studied and appears to be dependent on copper(II) at concentrations ≤1.5 g/L, a reaction order of 0.79 was calculated with respect to copper(II) at 1 g/L. The redox reaction of the copper(I)/copper(II) on the chalcopyrite surface appears highly reversible. The overall cathodic reaction was shown to be mass transport limited in terms of Cu(I), and this is supported by the calculated activation energy.

6 Bulk Leaching Studies

Electrochemical studies are used in hydrometallurgy to develop a fundamental understanding of the surface reactions of minerals in order to then apply this knowledge to elucidate mechanisms and or improve on reactor operation. The bulk leaching work presented in this section was carried out for two purposes:

1) To establish how leaching rates compare to those calculated from electrochemical studies and determine how effectively electrochemical studies can be used to predict the effects of leaching variables on the leaching kinetics.

2) To generate sufficient surface deposit for chemical analysis.

Chalcopyrite (96% passing 150 µm) was acid washed to remove any oxide layers (formed due to natural oxidation), dried in an oven at 85 °C then leached in varied solution conditions. The extraction of copper was measured over an 18 day period in ammonia-ammonium sulphate solutions at 1 M, 3 M and 6 M total ammonia, 25°C, starting pH of solution 9.6±0.15 in the presence of oxygen. Solution pH was routinely checked and adjusted by addition of ammonium hydroxide to the desired pH of 9.6 up until day 14. Beyond day 14, no further pH adjustments were made to all reactors. Figure 6.1 shows the leach curves obtained.

The results show what appears like a day of lag before commencement of leaching. The concentrations of copper in solution measured after 21 hours of leaching were 0.05 g/L, 0.1 g/L, and 0.13 g/L at 1 M, 3 M and 6 M total ammonia respectively. After one day, recoveries appeared to increase linearly with time for up to 50% extraction, thereafter appearing to slow down at the 3 M and 6 M total ammonia concentrations. The curves appeared to fit an S-shaped profile typical of autocatalytic reactions.

Increasing total ammonia concentration resulted in an increase in recoveries, with 73% extraction achieved after 14 days at 6 M total ammonia and 69% and 53% at 3 M and 1 M total ammonia, respectively. The rates of leaching were determined as the slopes of the linear part of the extraction curves (Table 6.1), and indicated that the rate of chalcopyrite leaching increased with an increase in total ammonia. Increasing total ammonia from 1 M to 3 M resulted in a 27% increase in rate of leaching while an increase in total ammonia form 3 M to 6 M only resulted in a 2% increase in the rate of leaching. A decrease in solution copper concentrations was observed in the 6 M reactor after day 14. This is unusual and is linked to a decrease in pH of the solution, which on day 15 was found to be below 8.5. At such pH values, copper(II) ammine is not stable in solution and has a tendency to

precipitate as basic copper sulphates. It was noted that the 6 M reactor had a small gas leak, resulting in continuous ammonia losses and hence more prone to pH drop due to continued dissociation of ammonium to maintain the equilibrium. Furthermore, Muzawazi (2013) reported, as expected, increased ammonia loses from solutions of high total ammonia concentrations compared to those of lower total ammonia concentration.

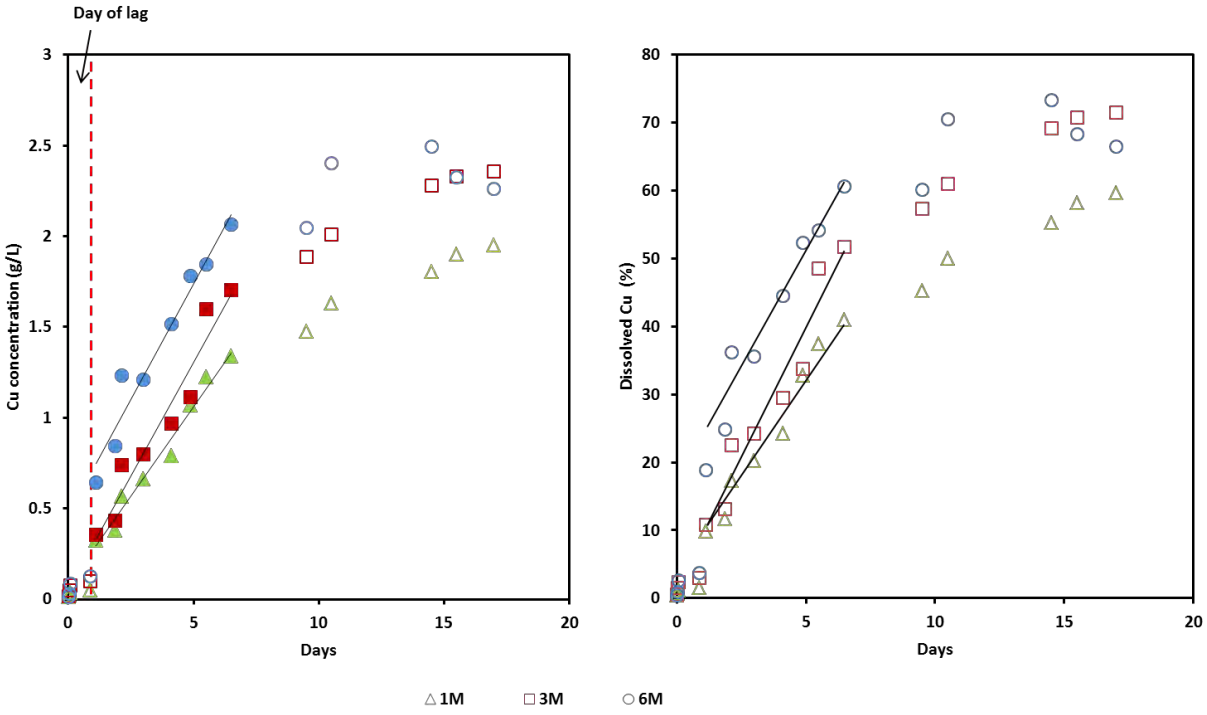

Figure 6.1. Leaching curves of copper from chalcopyrite in ammonia-ammonium sulphate solutions at 1, 3 and 6 M (NH_3+NH_4^+), 25°C, pH 9.6±0.15 (starting pH) in the presence of oxygen. Dissolved copper is given as a concentration in grams per litre and% dissolved copper respectively.

Table 6.1. Rate of leaching over the linear part of the copper extraction curves determined as the slope of the curves shown in Figure 6.1

Total ammonia(M)	Slope (g L^{-1} Day^{-1})	R squared	Slope (% L^{-1} Day^{-1})	R squared
1	0.197	0.953	6.046	0.975
3	0.25	0.941	7.605	0.941
6	0.255	0.975	7.491	0.953

The leaching tests were repeated for the first 8 days to check for reproducibility of results. Figure 6.2 shows the reproducibility of leaching results at 1 M (NH_3+NH_4^+). Sampling could not be carried out at similar times hence data points cannot be directly compared. The curves showed similar extraction

rates of 6% and 7% copper extraction per day. The data from leach test 1 showed slightly more variability and had a lower R^2 value. Based on Figure 6.2, the results from the leach study were accepted to be reasonably reproducible.

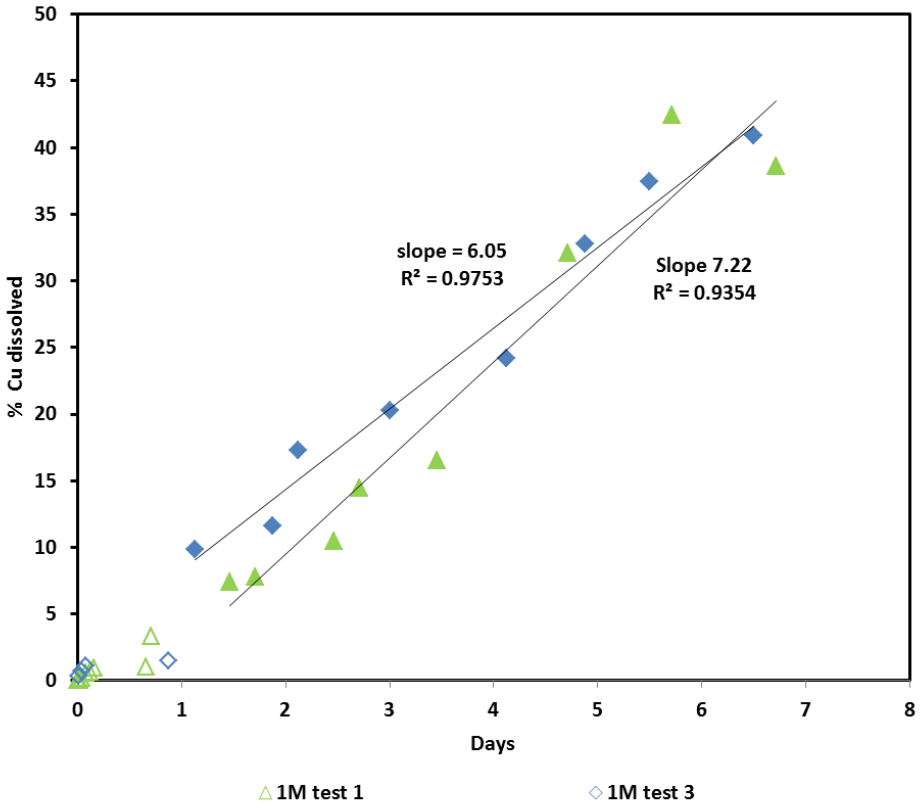

Figure 6.2. Leach curves of copper from chalcopyrite in ammonia-ammonium sulphate solutions showing% copper dissolved at 1 M (NH_3+NH_4^+), 25°C, pH 9.6±0.15 (starting pH) in the presence of oxygen.

Tests were done over 24 hours with more rapid sampling so as to populate the initial "lag" stage and investigate copper extraction over the initial leaching period. Figure 6.3a show a plot of the copper concentration in solution and Figure 6.3b shows the same data as percentage extraction of copper over day one of leaching at 1 M total ammonia, 25°C in solutions of pH 9.6±0.15 in the presence of oxygen. The curves appear to be linear, with slopes i.e. leaching rate shown in Table 6.2.

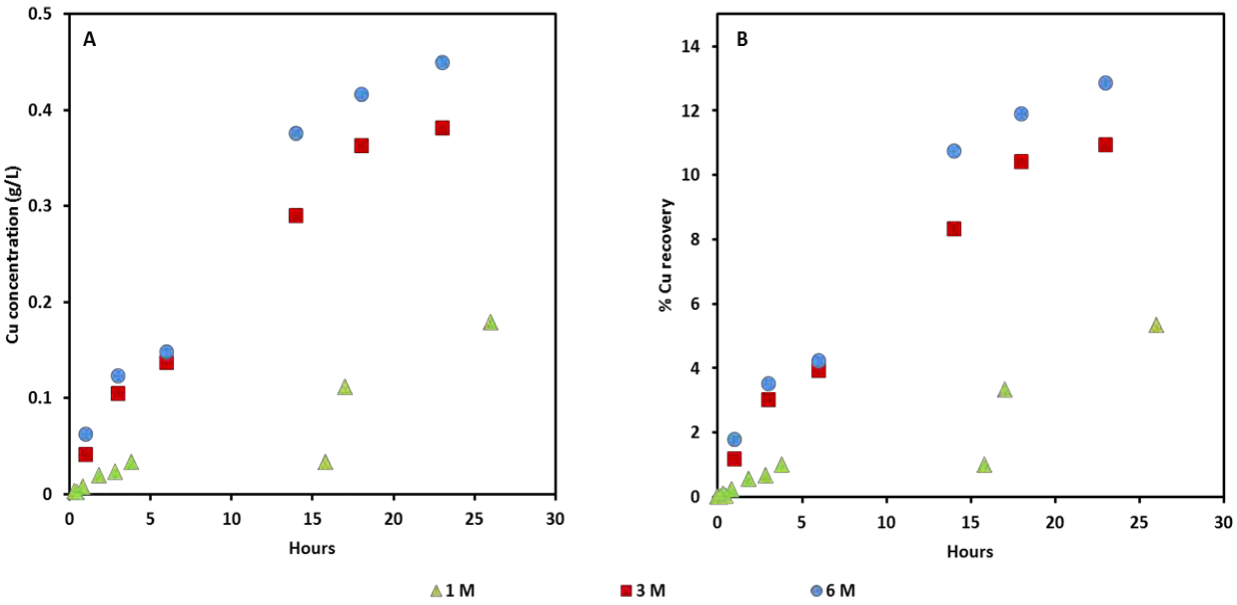

Figure 6.3. Extraction curve of copper from chalcopyrite in ammonia-ammonium sulphate solutions at 1 M, 3 M and 6 M (NH_3+NH_4^+), pH 9.6±0.15 (starting pH), 1% solids, in the presence of oxygen.

Table 6.2. Rate of leaching calculated as the slope of the curves presented in Figure 6.3

Total ammonia (M)	Slope ($molL^{-1}$ Day^{-1})
1	0.007
3	0.016
6	0.019

2 g and 1.76 g of chalcopyrite were leached at 1% solids in 3 M and 6 M (NH_3+NH_4^+) at temperatures 35°C and 45°C (Figure 6.4 and Figure 6.5), where copper concentrations in solution were up to 0.45 g/L. Data trends showed what appeared like a lag period during the first 3 hours; at 45°C the curves become linear after the three hours while at 35°C, they appear to follow an almost exponential trend. This is interesting in that, similar to Figure 6.1, these results suggest that the rate of reaction increased with an increase in dissolved copper(II).

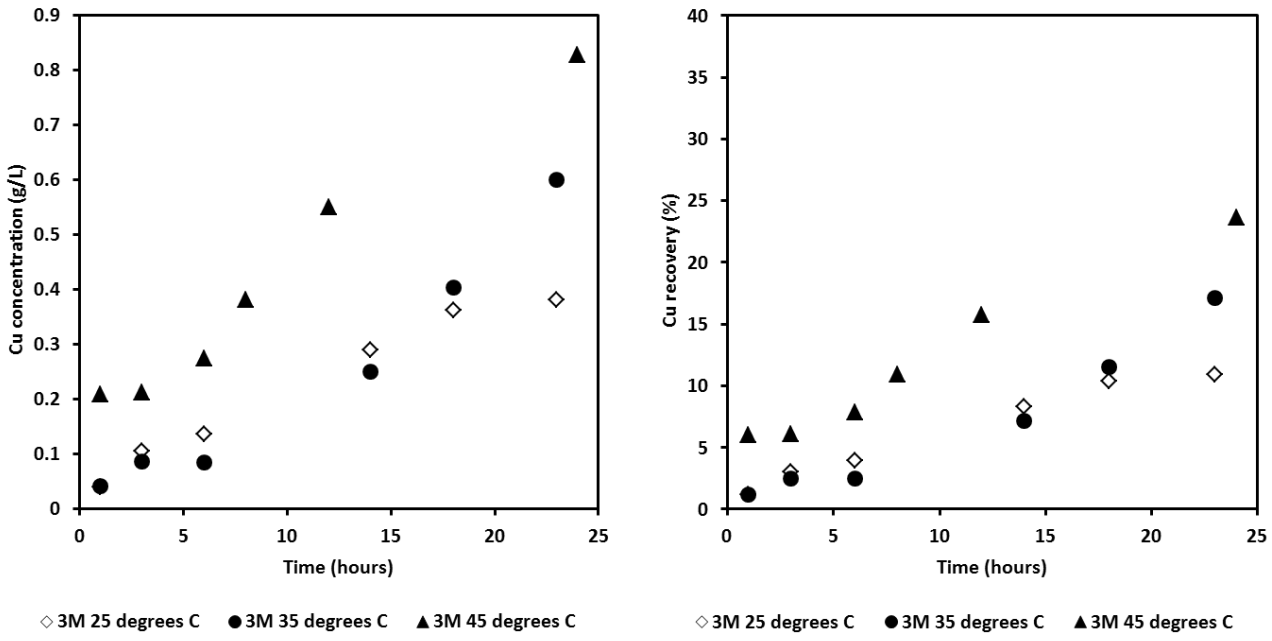

Figure 6.4. Extraction curve of copper from chalcopyrite in ammonia-ammonium sulphate solutions at 3 M (NH_3+NH_4^+), pH 9.6±0.15 (starting pH), 1% solids, at various temperatures in the presence of oxygen

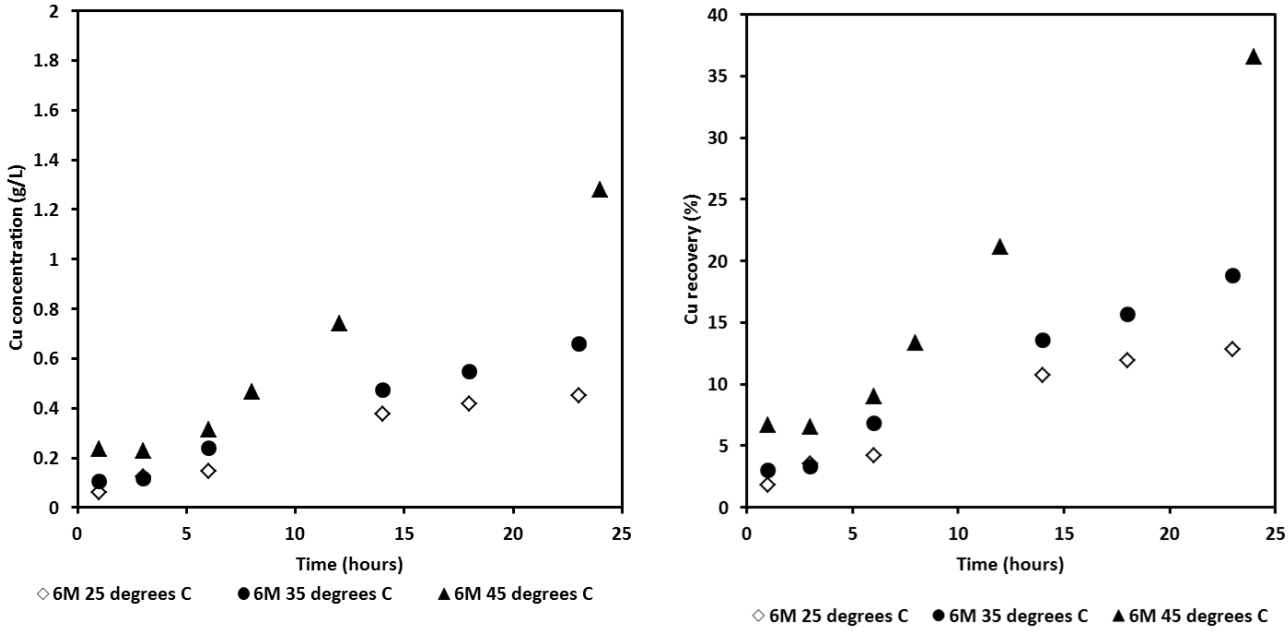

Figure 6.5. Extraction curve of copper from chalcopyrite in ammonia-ammonium sulphate solutions at 6 M (NH_3+NH_4^+), pH 9.6±0.15 (starting pH), 1% solid, at various temperatures in the presence of oxygen.

It is interesting to note that for all the total ammonia concentrations used, the calculated free ammonia concentration was in excess of that required to complex the copper at the concentrations at which copper was present in solution (Table 6.3). Despite this being the case, the rate of leaching increased with an increase in free ammonia and the order of the reaction was determined from the slopes of a 2^{nd} order polynomial fit to be 0.34 at 1 M total ammonia and decreased to 0.1 and 0 at 3

M and 6 M total ammonia respectively (Figure 6.6). The order of reaction at 3 M compares well to the 0.09 order with respect to ammonia calculated in the electrochemical tests. This increase in leaching rates with an increase in total ammonia is expected and has been discussed in detail in section 4.2.4.

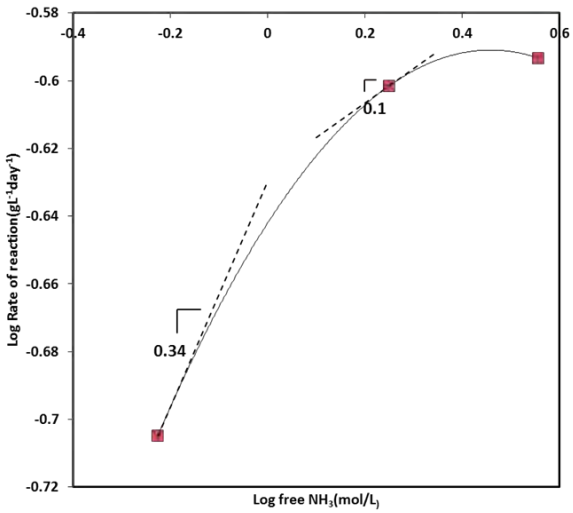

Figure 6.6. Log rate of reaction versus Log free ammonia plot for leaching reaction in ammonia-ammonium sulphate solutions in solutions of different total ammonium concentrations at pH 9.6±0.15 (starting pH), 1% solids, 25°C, and all reactors agitated using a magnetic stirrer set to the same speed.

Table 6.3. Free ammonia in solutions of different total ammonia concentrations after fixed periods of leaching

Total ammonia	In 24 hours		In 14.5 days	
	Cu in solution (mol/L)	Free Ammonia mol/L	Cu in solution (mol/L)	Free Ammonia mol/L
1	0.0008	0.6	0.0283	0.53
3	0.0015	1.8	0.0362	1.72
6	0.0020	3.6	0.0393	3.52

Evaluating the effect of oxygen was carried out by comparing the extraction curves generated in similar solution conditions in the presence and absence of oxygen. Figure 6.7 shows the chalcopyrite extraction curve in 1 M (NH_3+NH_4^+), 25°C, pH 9.6±0.15 (starting pH), the starting solution contained 50 ppm initial copper(II). Initial copper(II) was introduced into the solution because of the observed autocatalytic behaviour of the leaching reaction (Figure 6.1 and Figure 6.4) as well as the conclusion from the electrochemistry tests that found copper(II) to be the effective oxidant. The data presented in Figure 6.7 shows the copper(II) concentrations after subtracting the background or initial copper(II). In the absence of oxygen, copper concentrations increased from 0.001 g/L to 0.007 g/L

within the first hour and thereafter there was no further increase until day 2 when concentrations suddenly increased to about 0.05 g/L. It is expected that the chalcopyrite oxidation reaction would proceed through the reduction of the initial copper(II) present in solution and in the absence of oxygen, all the copper(II) would be reduced thereby generating copper(I) and the reaction would then stop. This is shown by the lack of further increase in copper concentration past the first hour on day 1. The increase in copper concentrations observed on day 2 is suspected to be due to contamination of the reactor by air leaks as well as oxygen accumulation from the nitrogen gas which contained traces of oxygen. Copper(I) ammonia complexes in solution are readily oxidised by dissolved oxygen even at trace concentration, thus solution contamination by oxygen could easily regenerate copper(II) allowing the chalcopyrite oxidation reaction to continue. Copper concentrations and recoveries in similar solutions in the presence of oxygen were obviously higher. In both tests the copper concentrations were up to 0.007 g/L within the same time frame of an hour, the reactor under oxygen increasing to 0.018 g/L thereafter while that under nitrogen remained at more or less the same concentration until day 2. This showed that that the leaching reaction can proceed when there is copper(II) in solution but oxygen is necessary to regenerate the oxidant.

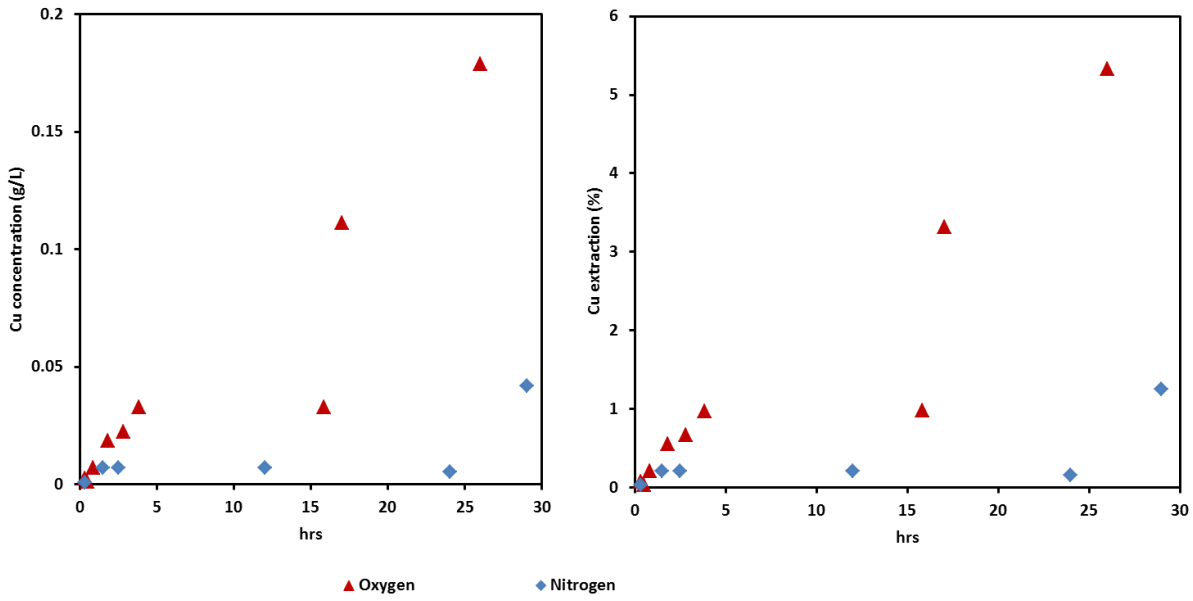

Figure 6.7. Extraction curve of chalcopyrite leaching in ammonia-ammonium sulphate solutions at 1 M (NH_3+NH_4^+), 25°C, pH 9.6±0.15 (starting pH) in the presence and absence of oxygen. Starting solution contained 50 ppm initial copper(II).

Effect of temperature

The effect of temperature was evaluated over a period of 24 hours at 3 and 6 M (NH_3+NH_4^+), pH 9.6±0.15 (starting pH). Since the reaction was found to be autocatalytic, initial kinetics were

determined from the linear parts of the extraction curves. Copper extractions were observed to increase with an increase in temperature (Figure 6.8 and Figure 6.9).

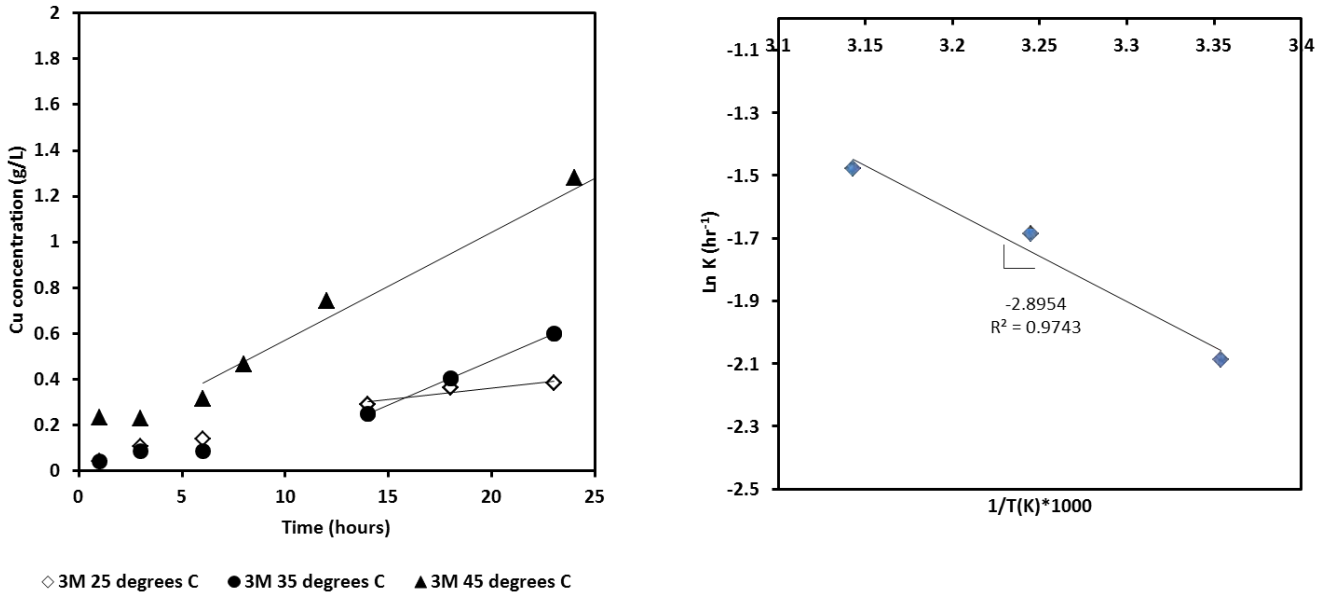

Figure 6.8. Copper extraction curve and corresponding Arrhenius plot in 3 M (NH_3+NH_4^+), pH 9.6±0.15 (starting pH), and 1% solids in the presence of oxygen.

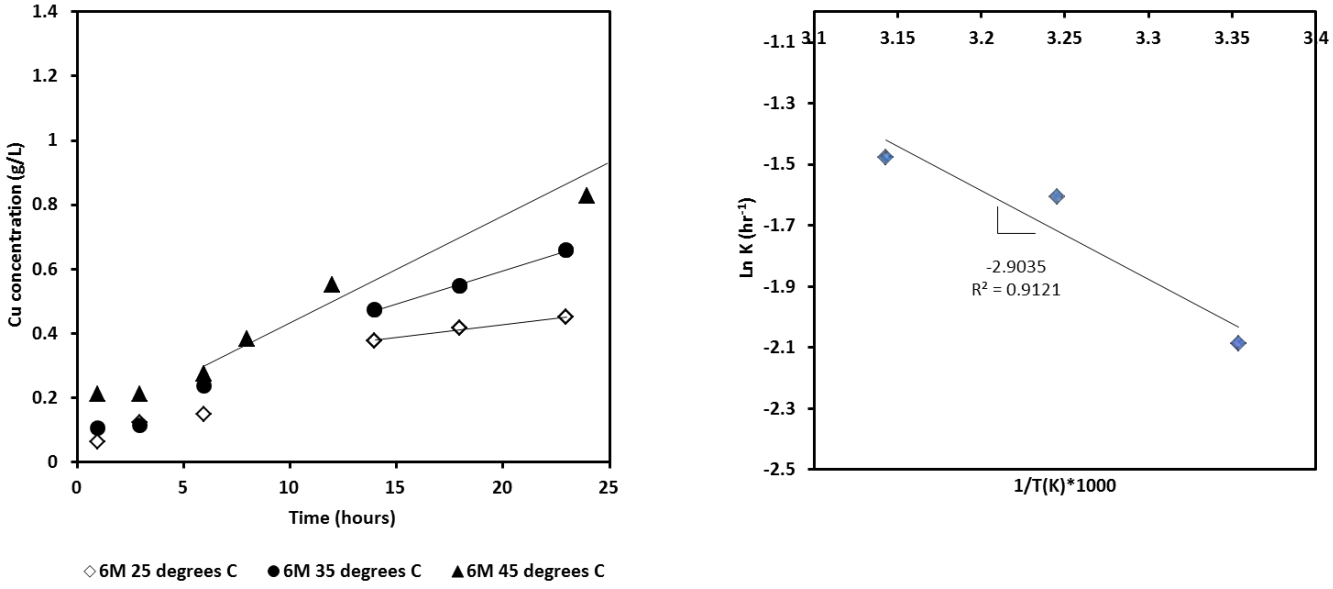

Figure 6.9. Copper extraction curve and corresponding Arrhenius plot in 6 M (NH_3+NH_4^+), pH 9.6±0.15 (starting pH), 1% solids in the presence of oxygen.

Activation energy was calculated from Arrhenius plots of Ln rate of reaction versus inverse of the absolute temperature. Activation energy was determined to be 24.07 kJ/mol and 24.14 kJ/mol for

the reaction at 3 M and 6 M (NH_3+NH_4^+) respectively. This suggests that the reaction is under mixed control.

6.1 Kinetic modelling of leaching results

The overall rate of leaching is usually measured by the rate of generation of the solubilised species of the desired metal in solution. This overall rate may be controlled by some individual rate process occurring as part of the overall leaching reaction. Different kinetic models for leaching or surface reactions have been developed and discussed in literature (Free, 2013; Cussler, 2009; Safari et al., 2009; Han, 2002; Levenspiel, 1999). Of these, the shrinking core model is more widely used to model the leaching of low grade sulphide ores. In many practical situations, the leaching of solids produces an insoluble permeable layer such that ions diffuse in and out (Han, 2002). The leaching of chalcopyrite has widely been linked to the formation of such a surface layer in both acid media (Viramontes-Gamboa et al, 2007; Hackl, 1995; Habashi and Toor, 1979) and alkaline media (Warren and Wadsworth, 1984; Beckstead and Miller, 1977a; Forward and Mackiw, 1955). While some researchers (Arbiter and McNulty, 1999; Bell et al, 1995; Duyvesteyn, 1995; Beckstead and Miller, 1977a; Beckstead and Miller, 1977b; Forward and Mackiw, 1955) have attributed the slow leaching kinetics of chalcopyrite to the presence of this surface film, Warren and Wadsworth (1984) observed the presence of the surface film but concluded it did not limit the rate of reaction of chalcopyrite. Furthermore, Crundwell (2013) presents an argument against the possibility of the passivation of minerals by presence of a surface film in hydrometallurgical processing stating that in electrochemical reactions such as those of the oxidation of chalcopyrite, direct physical contact between oxidant and mineral surface is not necessary for the reaction to occur. Studies have been carried out in conditions of high shear where formation of this surface film is said to be prevented from occurring (Beckstead and Miller, 1977a; Reilly and Scott, 1977; Arbiter and McNulty, 1999) and despite all this work in the subject, there is still no consensus whether or not it is a rate limiting factor.

Leaching results can be modelled using the shrinking core model provided the following the assumptions are valid.

i. The particle core shrinks uniformly during leaching leaving a layer of surface deposits and gangue.
ii. The small quantity of impurities found in the sample do not significantly affect the kinetics
iii. The particles are spherical in shape and uniform in size.
iv. The concentration of the leaching agent is constant through the reaction.

Results from the current study have shown the leaching reaction to be autocatalytic with the leaching agent, copper(II) being continuously generated, and hence assumption iv above is not valid. Furthermore, Malvern particle analysis results (Figure 3.7) clearly showed that the particle size distribution used in the current study was not uniform. Thus it was decided not to fit results from the current study to the shrinking core model.

7 Surface deposit effects

The surface of the chalcopyrite electrode as well as leach residue was analysed pre and post leaching in order to identify and characterise the surface deposit layer. It has already been mentioned that the slow leaching characteristic of chalcopyrite in ammoniacal solutions has been linked to the formation of this surface deposit layer (Li et al., 2013; Guan and Han, 1997; Warren and Wadsworth, 1984; Beckstead and Miller, 1977b; Reilly and Scott, 1977; Tozawa et al, 1976; Forward and Mackiw, 1955) which has been said to be formed by iron precipitation and/or sulphur disproportionation forming elemental sulphur on the mineral surface. It is known that ferrous ions are rapidly oxidised by oxygen or air to ferric state in alkaline solutions (Smythe, 1931), which explains why the iron released as ferrous from the chalcopyrite lattice is immediately oxidised and precipitates on the mineral surface. The work in this section explores the deportment of iron in the oxidative leaching and also touches on the deportment of sulphur.

The bulk of the work on surface deposits was done in ammonia-ammonium sulphate solutions and some additional tests were done in ammonia-ammonium carbonate and ammonia-ammonium perchlorate solutions for comparison.

7.1 Surface deposits in ammonia-ammonium sulphate solutions

The surface of the electrode was examined using SEM-EDS and optical microscopy prior to any oxidation tests. Figure 7.1 shows optical microscope images of the chalcopyrite electrode surface prior to (A) and post (B) oxidation for 22 hours in solutions of 1 M total ammonia at pH 9.6±0.15, under nitrogen and in the absence of initial copper, the potential set to 255 mV (corresponding to the mixed potential of chalcopyrite in similar solution conditions but in the presence of initial copper(II) at 5 g/L). The visual differences between the chalcopyrite surfaces after polarisation were apparent, even to the naked eye. Post oxidation the surface had lost its lustrous brass yellow colour, rather exhibiting a reddish brown coloration. The light microscope image of the oxidised chalcopyrite Figure 7.1B showed some grain patterns and existence of grain boundaries. SEM images were taken (Figure 7.2) and results from an EDS analysis prior to reaction on the bulk of the surface in atomic percentages indicated it to be 24.6% Cu, 25.7% Fe and 49.7% S which is consistent with that of clean chalcopyrite.

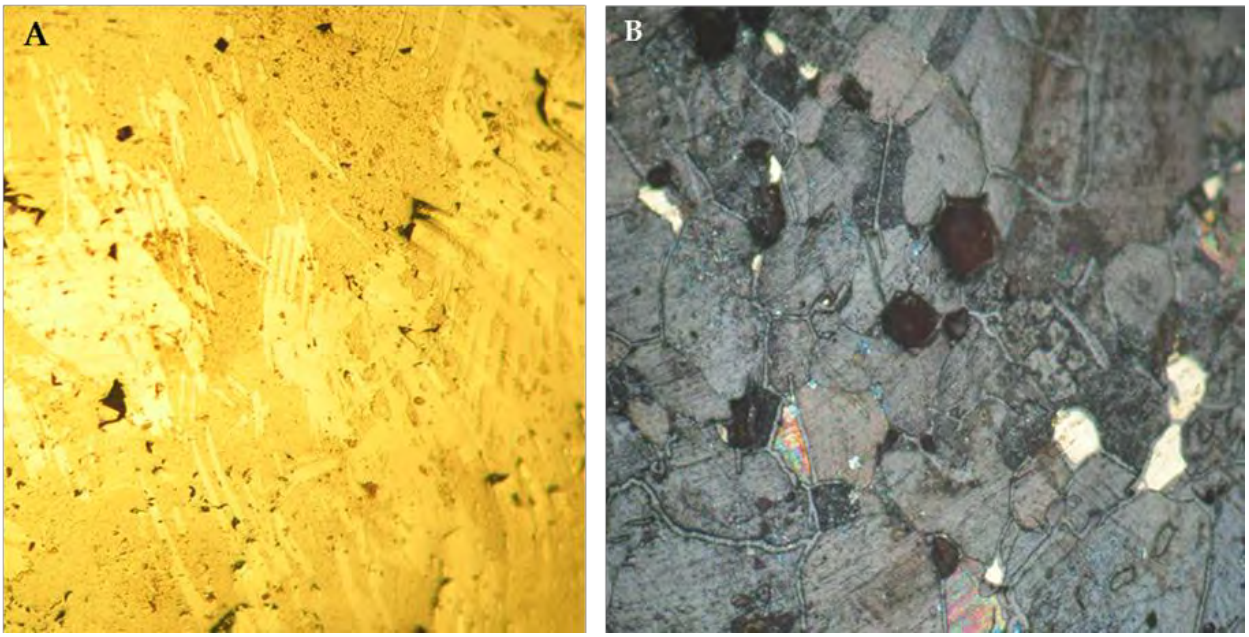

Figure 7.1. Optical microscope (A) and (B) images of a freshly polished chalcopyrite electrode surface magnification 10 times. Images show the surface prior and post oxidation but do not necessarily show identical areas.

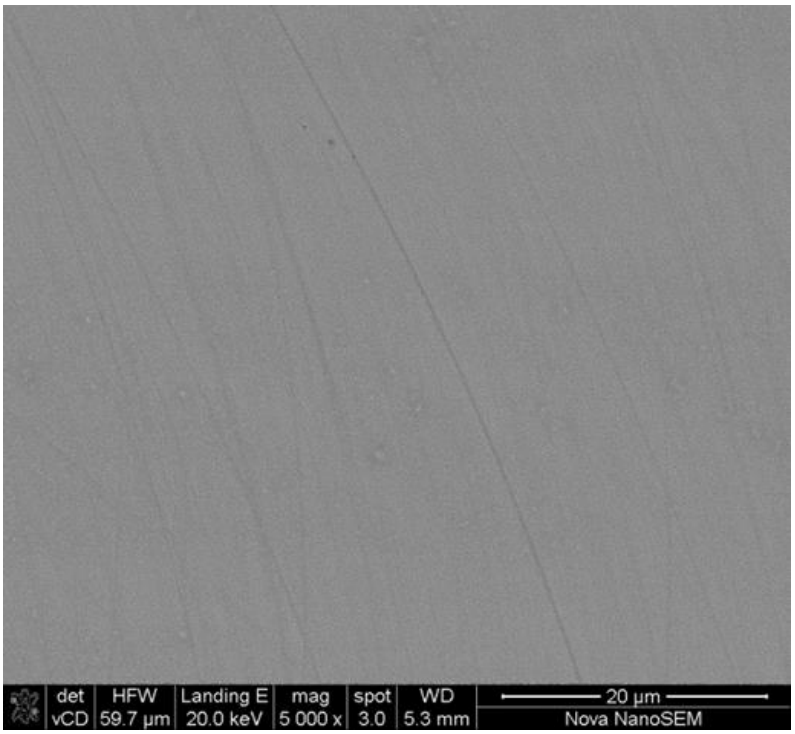

Figure 7.2. SEM image of freshly polished chalcopyrite prior to any leaching work. Results from an EDS analysis showed this (in atomic percentages) to be 24.6% Cu, 25.7% Fe and 49.7% S.

SEM images of the electrode surface shown in Figure 7.1B are presented in Figure 7.3 at two different resolutions and the results from EDS analysis is presented in Table 7.1. The surface was notably different from the clean, more or less smooth surface with visible polish marks seen prior to oxidation, to a surface which consisted of a cracked surface layer with some visible small globules on

top of the cracked bed. EDS results indicated a copper depleted bulk surface which had (spectrum A and B Table 7.1) an iron to sulphur atomic ratio of 1:1, an obvious deviation from the 1:2 atomic ratio expected of a pure chalcopyrite surface. The globules were shown to be sulphur rich, spectrum C indicating about 72% sulphur and only 1% iron. An analysis of the areas that did not contain any globules (spectrum D) showed it to contain both sulphur and iron but the iron to sulphur ratios showed a slight deviation from the 1:1 observed in the bulk area to 1:0.7 suggesting that the precipitate was not necessarily a stoichiometrically consistent iron-sulphur compound but possibly a mixture of iron, sulphur and iron-sulphur phases.

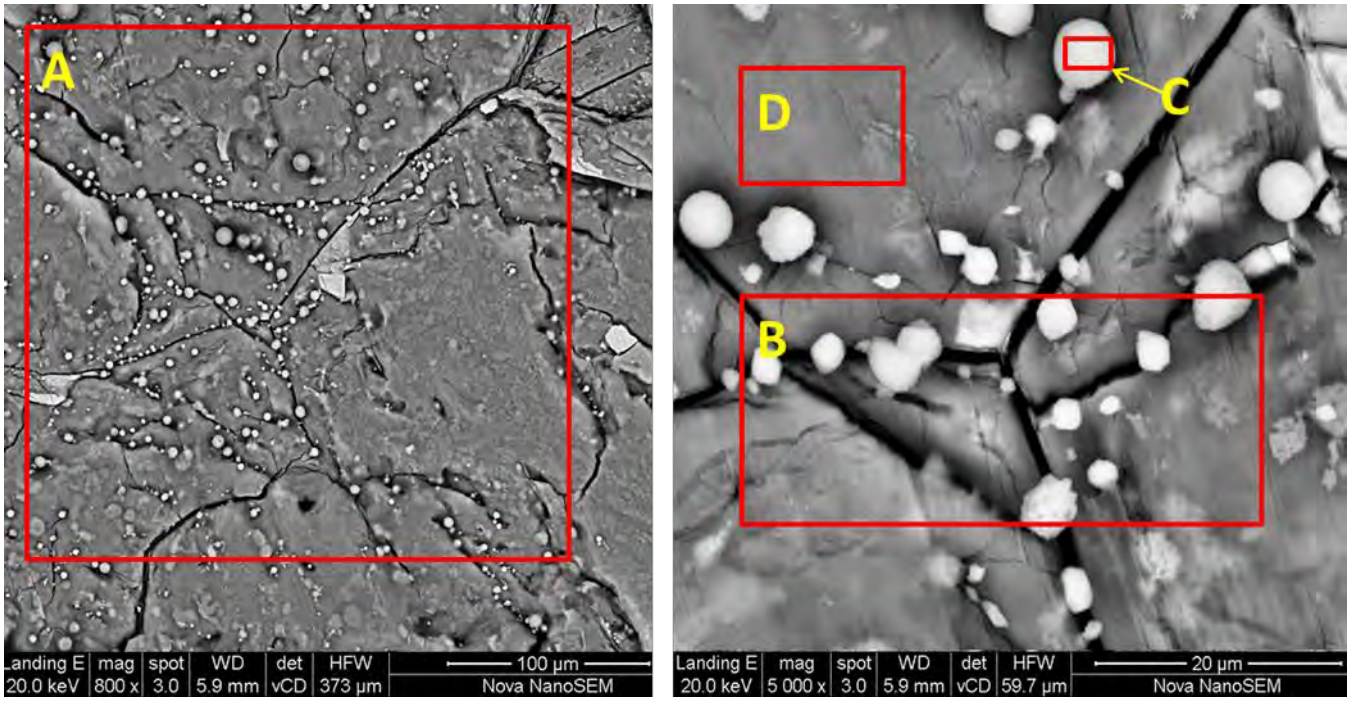

Figure 7.3. SEM images of chalcopyrite electrode surface after 22h of oxidation in ammonia-ammonium sulphate solutions at 255 mV in 1 M (NH_3+NH_4^+), 25°C, pH 9.6±0.15 under nitrogen. Results from EDS spectra summarised in Table 7.1

Table 7.1. Results in atomic percentages from EDS spectra of chalcopyrite electrode surface after 22h of oxidation in ammonia-ammonium sulphate solutions at 255 mV in 1 M (NH_3+NH_4^+), 25°C, pH 9.6±0.15 under nitrogen.

Spectrum	Oxygen	Silica	Sulphur	Iron
A	60.2	3.4	18.3	18.1
B	58.17	2.81	19.46	19.56
C	27.04	-	71.75	1.21
D	60.7	3.47	14.49	21.33

It was suspected that the white globules, predominantly sulphur in composition were formed by the crystallization of ammonium sulphate from the electrolyte. Thus, the electrode surface was rinsed in distilled water and dried under vacuum, procedures both which were expected to remove the ammonium sulphate if it was indeed what comprised the white globules on the electrode surface. Figure 7.4 shows images of the chalcopyrite electrode surface from Figure 7.3 after rinsing in distilled water and drying under vacuum. The surface is still visibly cracked but the globules appear to have been washed off. EDS analysis of the bulk area (Table 7.2 spectrum E) shows a high iron to sulphur atomic ratio of 1:0.2. Region F is a zoom in on the region around I thus spectrum G and I were found to be similar and show that after washing the electrode, copper was detected in some regions on the surface of the electrode. Spectrum H shows no copper and is similar to spectrum F. Figure 7.5 shows images of the chalcopyrite surface after oxidation in a repeat test of that shown in Figure 7.4, all conditions maintained to be similar. It appears the presence of copper on the mineral surface may have been an anomaly and was a localised effect. EDS results of the bulk areas in Figure 7.5a and Figure 7.5b indicated more or less similar surface compositions of 27% and 23% iron and 13% and 12% sulphur respectively, and these values are comparable to those of spectrum H which showed 25% iron but less sulphur at 5%. These observations support the suggestion that most of the sulphur observed came from crystallization of ammonium salt from solution onto the surface of the electrode. However, it is not possible to conclude that all the sulphur detected was due to crystallization of ammonium sulphate from solution considering that it is known that sulphur is released from the chalcopyrite lattice during oxidation. One cannot differentiate between sulphur that may be coming from solution and that coming from the oxidation of the mineral, using the analytical methods employed in this study.

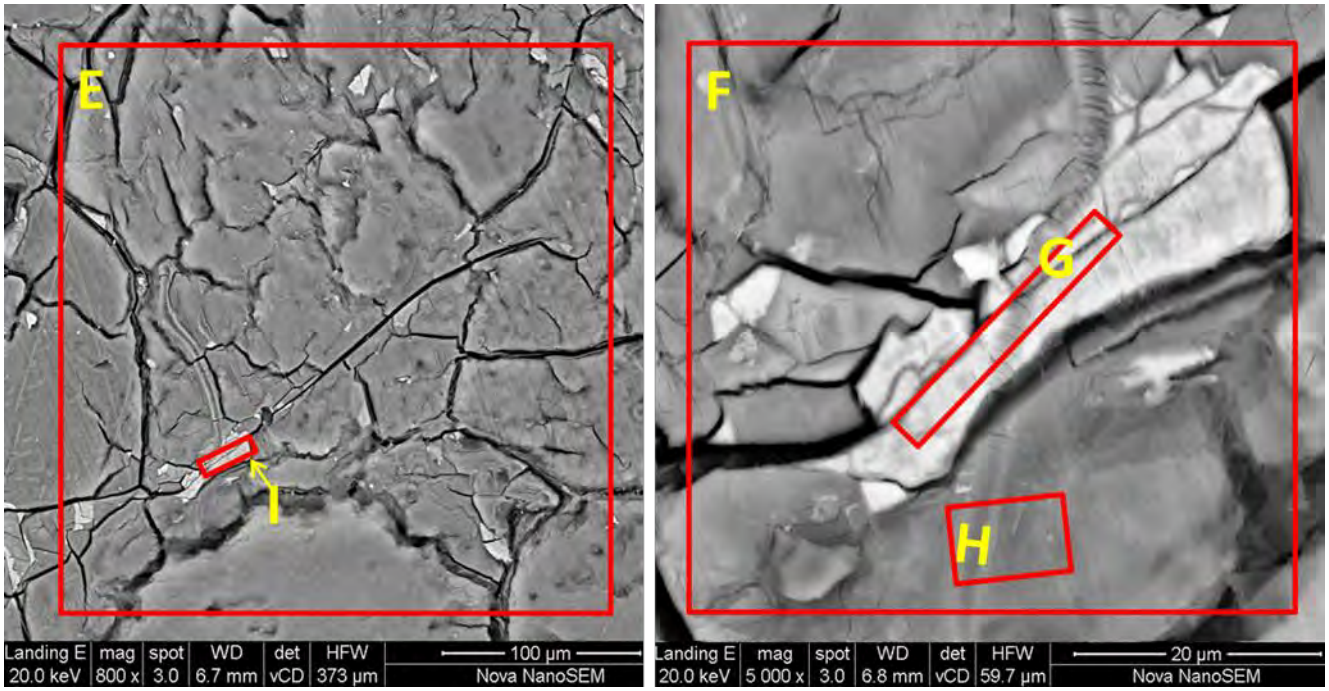

Figure 7.4. SEM images of chalcopyrite electrode surface after 22h of oxidation in ammonia-ammonium sulphate solutions at 255 mV in 1 M (NH_3+NH_4^+), 25°C, pH 9.6±0.15, 25°C under nitrogen. The electrode surface was washed in distilled water and dried under vacuum for 2.5 hours. Results from an EDS spectra summarised in Table 7.2

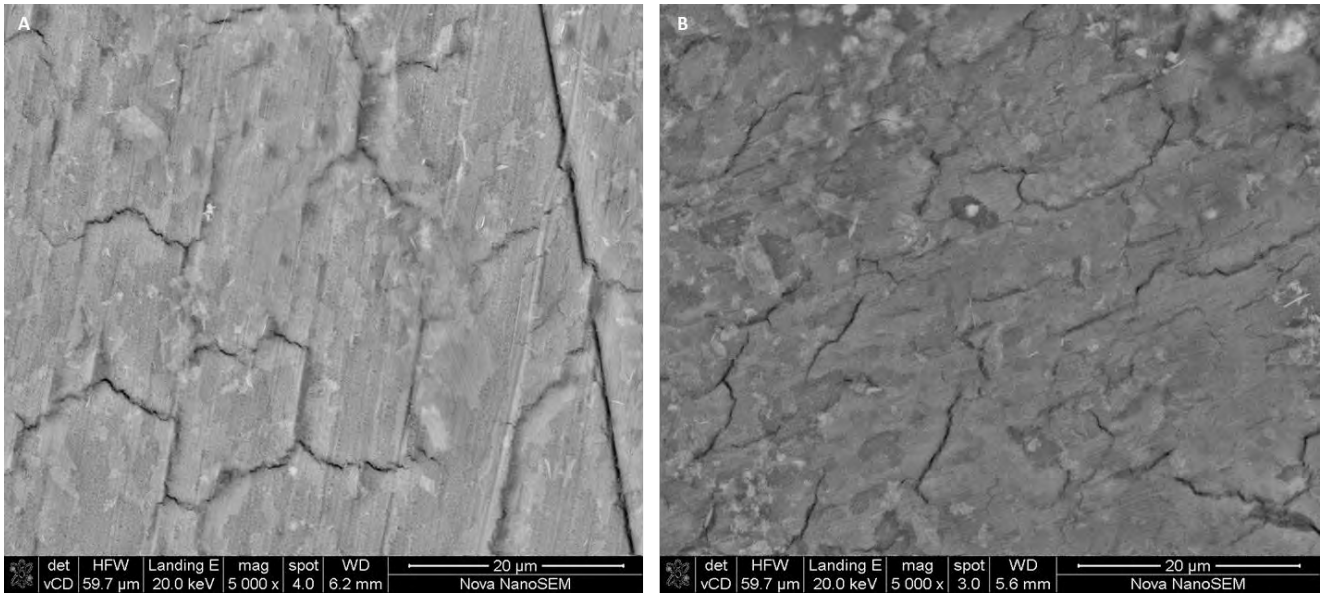

Figure 7.5. SEM images of chalcopyrite electrode surface after 22h of oxidation in ammonia-ammonium sulphate solutions at 255 mV in 1 M (NH_3+NH_4^+), 25°C, pH 9.6±0.15 25°C under nitrogen. The electrode surface was washed in distilled water and dried under vacuum for 2.5 hours. Results from an EDS spectrum over the entire image A- O 57%, Si 3%, S 13%, Fe 27%. B- O 62%, Si 2%, S 12%, Fe 23%.

Table 7.2. Results from an EDS spectra of chalcopyrite electrode surface after 22h of oxidation in ammonia-ammonium sulphate solutions at 255 mV in 1 M (NH_3+NH_4^+), 25°C, pH 9.6±0.15 under nitrogen. SEM image presented in Figure 7.4.

Spectrum	Oxygen	Silica	Sulphur	Iron	Copper
E	64.83	4	4.94	26.23	_
F	58.7	3.8	7.96	27	2.54
G	44.27	1.45	23	19.28	11.99
H	63.62	6.76	4.56	25.06	_
I	44.69	1.68	22.89	19.82	10.92

In general, the SEM-EDS results presented in Figure 7.4 and Figure 7.5 suggest the presence of an iron rich surface layer. Furthermore, the non-homogenous nature of this layer is evident from the cracked appearance of the surface (Figure 7.3, Figure **7.4** and Figure **7.5**) and it was also noted to be friable, easily cracking off the surface on attempts to scrape it off. These observations are consistent with those of Guan and Han (1997) who described the surface product after oxidation in ammonia-ammonia iodide solutions to be friable and porous.

A look at the electrode after only two hours of oxidation showed an only slightly tarnished electrode surface, and SEM-EDS analysis (Table 7.3) indicated some small deviations from the atomic ratios expected of freshly polished chalcopyrite in that time frame. Marginal accumulation of iron and sulphur was observed at ratio's Cu:Fe 1: 1.2 and Cu:S 2:2.2 and it appeared the distribution was similar across the mineral surface with no indication of preferential dissolution sites. It should be pointed out that although these deviations are very small they were found to be consistent when EDS analysis was done on different small areas of the electrode surface confirming that in the reported time frame of 2 hours, a surface deposit layer had started to build up. This also provides confirmation that this surface layer grows as oxidation proceeds and eventually no copper is detected as shown in Figure 7.3 and Table 7.1.

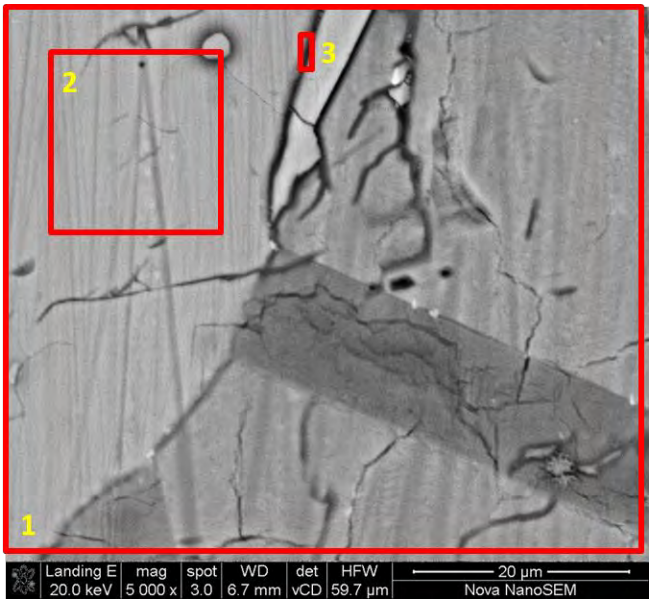

Figure 7.6. SEM image of chalcopyrite electrode surface after 2h of oxidation in ammonia-ammonium sulphate solutions at 255 mV in 1 M (NH_3+NH_4^+), 25°C, pH 9.6±0.15 25°C under nitrogen. Results from bulk EDS in atomic percentages, 30.83% S, 17.61% Fe, 14.3% Cu

Table 7.3. Results from bulk EDS spectra of chalcopyrite electrode surface after 2 h of oxidation in ammonia-ammonium sulphate solutions at 255 mV in 1 M (NH_3+NH_4^+), 25°C, pH 9.6±0.15 25°C under nitrogen. SEM images presented in Figure 7.7.

Spectrum	Oxygen	Silica	Sulphur	Iron	Copper
1	37.26	_	30.83	17.61	14.3
2	30.44	0.74	33.31	19.72	15.79
3	20.2	_	38.6	22.68	18.51

The oxidised electrode (Figure 7.4) was washed in 7 molar sulphuric acid for one minute, then rinsed in distilled water and dried in the vacuum chamber of the SEM before being once again examined. It appeared uniform, but with an etched appearance (Figure 7.8) and a bulk EDS indicated that its composition was similar to that of chalcopyrite.

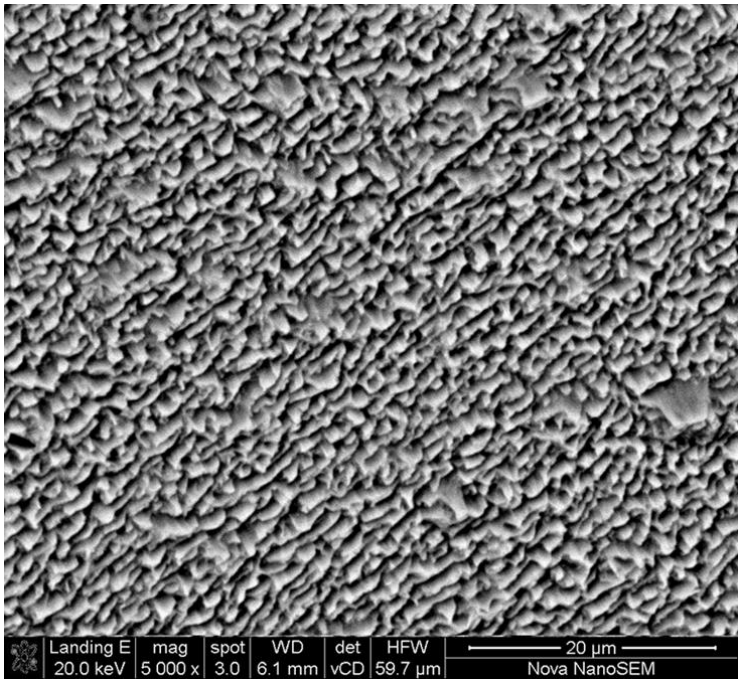

Figure 7.8. SEM image of chalcopyrite electrode surface that has been oxidised by fixing the potential for 22 hours then washed in 7 molar sulphuric acid and rinsed in distilled water. Results from a bulk EDS in atomic percentages, 49.48% S, 26.04% Fe, 24.48% Cu.

In general the appearance and composition of the surface layer did not appear to be affected by whether the tests were conducted in the presence or absence of oxygen. Sulphur was detected through all the tests; however this is not a widely reported phenomenon in literature with Warren and Wadsworth (1984) reporting to have identified some elemental sulphur on the mineral surface as well as in the electrolyte when leaching chalcopyrite in solution under conditions similar to those of this study. Considering Warren and Wadsworth (1984) were also working in ammonia-ammonium sulphate solutions, it was deemed necessary to work in non-sulphate solutions in order to rule out the possibility that the sulphur detected could be residual ammonium sulphate from the electrolyte which may have crystallized within the iron precipitate.

7.2 Surface deposits in ammonia-ammonium carbonate solutions

The electrode was oxidised for 22 hours in 1 M ammonia-ammonium carbonate solutions at pH 9.6±0.15, under nitrogen and in the absence of initial copper, the potential set to 231 mV (corresponding to the mixed potential of chalcopyrite in similar solution conditions but in the presence of initial copper(II) at 5 g/L). Figure 7.9 shows the surface of the electrode immediately after oxidation. A relatively clean looking surface (in comparison to that observed after oxidation in ammonia-ammonium sulphate) can be seen. The polish marks are still visible on the surface and

results of a bulk EDS analysis (Table 7.4, Spectrum J) show surface composition in atomic percentages to be 46.9% S, 27.06% Fe and 26.04% Cu approximating that of a freshly polished chalcopyrite surface. However, the cracks on the surface were found to be iron rich relative to sulphur, showing composition of 56.28% O, 1.54% Si, 10.69% S, 26.62% Fe and 4.87% Cu (spectrum K). This suggests preferential oxidation along the cracks. This is further supported by the fact that the charge was passed in quantities comparable to that passed in the presence of ammonium sulphate (Table 4.5 and Table 4.6) hence the apparent lack of surface layer build-up is not because the electrode was not oxidising but is likely to be due to preferential oxidation along the cracks. While it is makes sense to argue that the presence of iron deposits in the cracks could be due to poor mass transport in cracks compared to that in the bulk surface of the electrode, the fact that the bulk surface was clean and showed polish marks similar to a freshly polished electrode (Figure 7.2), supports the idea that oxidation preferentially occurred in the cracks and not on the bulk mineral surface.

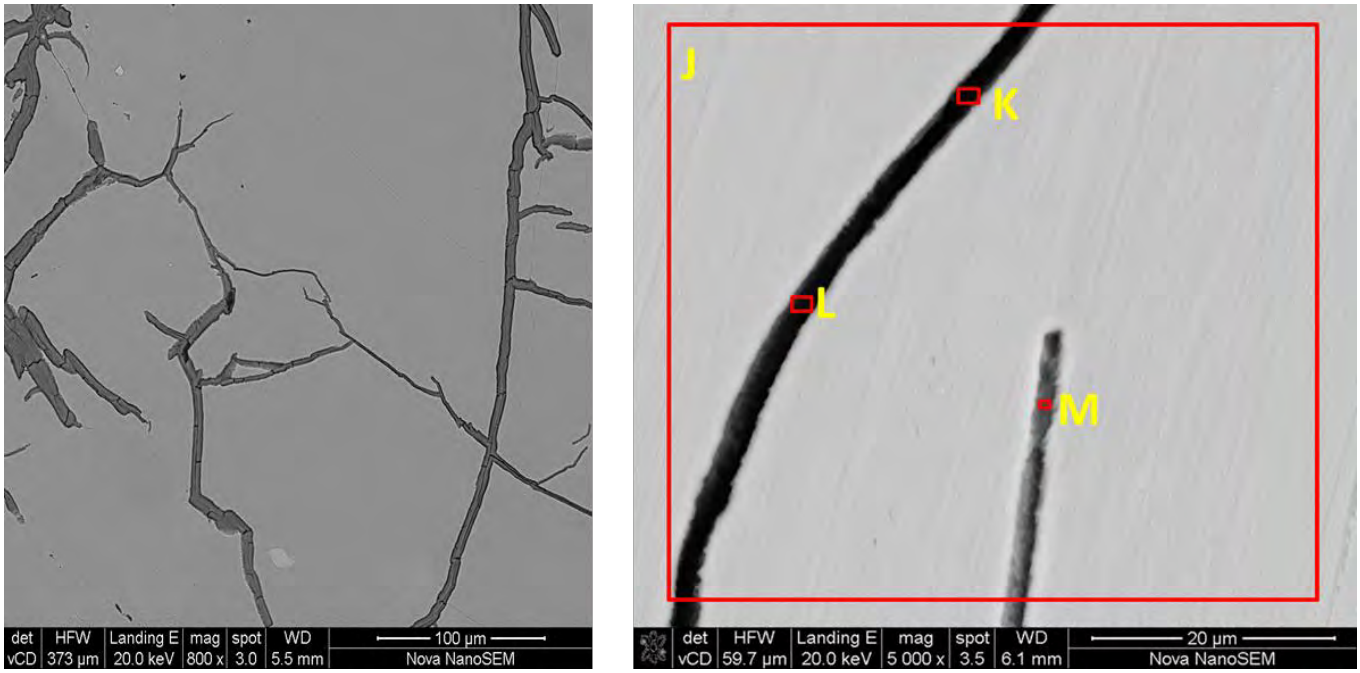

Figure 7.9. SEM images of chalcopyrite electrode surface after 22h of oxidation in ammonia-ammonium carbonate solutions at 225 mV in 1 M (NH_3+NH_4^+), 25°C, pH 9.6±0.15 25°C under nitrogen. Images are shown at x800 and x5000 magnification. The electrode surface was washed in distilled water and dried under vacuum. Results from an EDS spectra summarised in Table 7.4.

Table 7.4. Results from an EDS spectra of chalcopyrite electrode surface after 22h of oxidation in ammonia-ammonium carbonate solutions at 225 mV in 1 M (NH_3+NH_4^+), 25°C, pH 9.6±0.15 25°C under nitrogen. SEM image presented in Figure 7.9.

Spectrum	O	Si	S	Fe	Cu
J	_	_	46.9	27.06	26.04
K	56.28	1.54	10.69	26.62	4.87
L	51.54	1.5	10	32.12	4.85
M	50.36	0.76	17.93	22.87	8.08

Despite the coulometry of the reaction being similar to that determined in ammonia-ammonium sulphate solutions i.e. the number of electrons transferred per copper dissolved was determined to be 7.4 which is similar to the 7.2 calculated for the ammonia-ammonium sulphate solution (Section 4.2.6); the observations made on the electrode surface suggest that the dissolution differs in the presence of the carbonate anions. The deportment of the oxidation products also appears to be influenced by the choice of anion in solution.

The behaviour of iron in ammonium carbonate solutions has been explored by researchers, with a focus on improving leaching kinetics in the Caron process. Kim et al (1991) studied the active–passive behaviour of sintered iron in ammonia-ammonium carbonate solutions at pH 9.7 and reported that surface films were formed on the bulk iron during air exposure or immersion in ammoniacal solutions. The authors characterised the surface films using X-ray photoelectron spectroscopy (XPS) and ran cathodic polarisation transients; they reported that in the presence of air, Fe_3O_4 was formed. Caldeira et al. (2008) investigated the carbonate ion effect on pyrite oxidation in alkaline solutions and identified (using diffuse reflectance infrared spectroscopy) iron carbonate compounds as one of the products of pyrite oxidation. The authors explain that the increased oxidation rate typically observed on pyrite in carbonate solutions is possibly due to the formation of metastable Fe(II)–CO_3 complexes, the buffering effect of the carbonate and the fact that complexation with bicarbonate/carbonate provides a stronger Fe(III)/Fe(II) redox couple, increasing the Fe(III) solubility. Furthermore, it is known that ferrous can form stable complexes with ligands such as cyanide which are not readily oxidised by oxygen in alkaline solutions so the notion of forming metastable complexes is acceptable. Thus the formation of metastable Fe(II)–CO_3 complexes could provide an explanation for the apparent lack of significant surface layer formation

on the chalcopyrite electrode surface observed in ammonia-ammonium carbonate solution. It is proposed that solubilised iron species from the oxidising chalcopyrite form metastable Fe(II)–CO_3 complexes, which are then transported away from the vicinity of the mineral surface, thereby preventing immediate precipitation and growth of a deposit layer on the electrode surface. It is expected that some deposits will form in the cracks because of the relatively poor mass transport in such spaces. It should be noted that, although other studies of the carbonate system in the Caron process reported the presence of an oxide layer, the apparent lack of significant surface deposit layer reported in the current study could be attributed to the hydrodynamics around the electrode surface area. Rotation at 1600 rpm may be sufficient to allow for the transport of the metastable iron(II) carbonates away from the mineral surface and to undergo oxidation to iron(III) and subsequent nucleation and precipitation of iron hydroxides or carbonates in the bulk solution.

Effect of agitation speed on the extent of surface layer build-up and its morphology were reported for ammonia-ammonium sulphate solutions by Beckstead and Miller (1977b) who found chalcopyrite surfaces were much cleaner and relatively free of surface product at agitation speeds higher than 1100 rpm. They researchers went on to postulate that “as the rate of stirring is increased, the turbulence of the system abrades the mineral surface thus exposing fresh surface sites for reaction”. On the other hand, Arbiter and Kling (1999) in a leach study, speak of the major point of concern in the formation of the surface deposit in chalcopyrite ammoniacal leaching to be the rate of oxidation of iron from ferrous (as liberated from the chalcopyrite lattice) to ferric which subsequently hydrolyses and precipitates. The authors point out that if this occurs on the mineral surface then a surface film forms; however, if the iron migrates from the surface then the minerals surface remains active. The authors did not comment on the stability of ferrous in ammonia-ammonium sulphate solutions, neither did they demonstrate that that transport of the ferrous away from the surface prior to oxidation to ferric and not abrasion of the otherwise deposited ferric based surface layer were responsible for keeping the mineral surface active.

The deduction made from the analogy with this research, and applied to the ammonia-ammonium carbonate system under review, is that the stabilisation of the ferrous (as released from the chalcopyrite lattice) by carbonate ions and rapid transport can explain the lack of significant layer build up observed in the current study. Furthermore, the fact that charge was passed in relatively significant quantities yet a surface deposit layer was not observed uniformly across the electrode surface and the electrode surface still showed polished marks similar to a freshly polished surface, is indication of preferential oxidation sites along the cracks rather than homogeneous oxidation on the entire mineral surface.

7.3 Surface deposits in ammonia-ammonium perchlorate solutions

Examination of the surface after oxidation in ammonia-ammonium carbonate solutions did not provide clarity with regards to whether or not the sulphur observed in ammonia-ammonium sulphate solutions was a product of oxidation or a precipitate from solution. Thus, an alternative ammonium salt, i.e. ammonium perchlorate, which is expected not to react or complex with the products of chalcopyrite oxidation, was tested. The chalcopyrite electrode was once again oxidised for 22 hours in ammonia-ammonium perchlorate solutions at 254 mV (the mixed potential of chalcopyrite in 1 M (NH_3+NH_4^+) , pH 9.6±0.15, 5 g/L copper(II) under nitrogen) , solution conditions maintained similar to those in which mixed potentials were measured except that there was no initial copper(II) in solution.

The chalcopyrite electrode surface was observed to have a cracked, scaly look, similar to that seen after oxidation in ammonia-ammonium sulphate solutions but in this case no white globules were observed (Figure 7.10). EDS of the bulk area (Table 7.5, Spectrum N) showed the composition to be 52.3% O, 4.21% Si, 18.14% S, 17.55% Fe and 7.8% Cu. This gives an Fe:S atomic ratio of 1:1.1 and copper is present at a Cu:S of 1:2.25. Assuming that the copper detected is from unoxidised chalcopyrite beneath a relatively thin surface deposit layer then it seems that in perchlorate solutions only marginal accumulation of sulphur occurs, less than one atomic percent and iron is the major oxidation product found. The fact that copper was detected on the bulk of the surface is indication that although the surface was more or less similar to that observed in the sulphate system; in perchlorate solutions the surface deposit layer was distinctly thinner. It is tempting to attribute the presence of copper on the mineral surface to the relatively poor oxidation rates of chalcopyrite in perchlorate solutions, but the amount of charge passed in two hours was only 26% smaller than that passed in the sulphate system (Table 4.5).

The surface also showed what appeared to be ridges or what may have been cracks that had since filled up with some surface deposit material. Similar to the results from ammonium carbonate solutions, these regions had high iron and low copper (26.01% Fe and 2.38% S, Spectrum P) content relative to the bulk area (7.8%) and high iron content (26.01%) relative to the 17.55% detected in the bulk area. The regions of low copper may once again suggest preferential dissolution along the cracks or be due to poor mass transport in the cracks.

The atomic ratios of the sulphur and iron are not consistent with the stoichiometric ratios suggested by coulometry (Table 4.6) which indicated a 5 electron transfer reaction and this would require that the chalcopyrite oxidation reaction proceed through the formation of elemental sulphur. Since the

atomic ratio of iron to sulphur in chalcopyrite is 1:2, it would then have been expected that the amount or sulphur be twice that of iron in the surface deposit material.

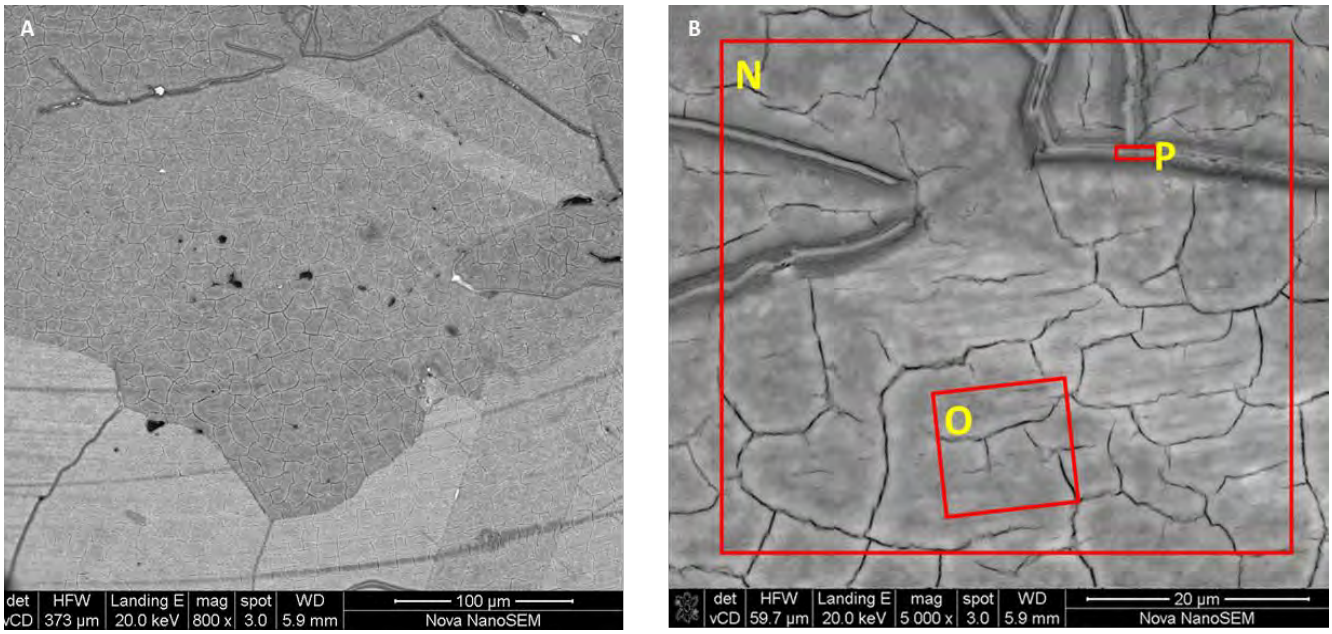

Figure 7.10. SEM images of chalcopyrite electrode surface after 22h of oxidation in ammonia-ammonium perchlorate solutions at 254 mV in 1 M (NH_3+NH_4^+), 25°C, pH 9.6±0.15 25°C under nitrogen. Images are shown at x800 and x5000 magnification. The electrode surface was washed in distilled water and dried under vacuum. Results from an EDS spectrum of entire area A O 52%, Si 4%, S 19%, Fe 17% and Cu 8%. EDS spectra of B is summarised in Table 7.5.

Table 7.5. Results from EDS spectra of chalcopyrite electrode surface after 22h of oxidation in ammonia-ammonium perchlorate solutions at 254 mV in 1 M (NH_3+NH_4^+), 25°C, pH 9.6±0.15 25°C under nitrogen. SEM image presented in Figure 7.10.

Spectrum	O	Si	S	Fe	Cu
N	52.3	4.21	18.14	17.55	7.8
o	49.59	4	20.65	17.78	7.97
P	60.97	5.02	5.62	26.01	2.38

Results from this test work confirm a marginal accumulation of sulphur but no deduction can be drawn as to whether this is in the form of some Fe–S matrix or elemental sulphur. Warren and Wadsworth (1984) studied chalcopyrite oxidation in ammonia-ammonium sulphate at solution pH above 9 and reported on the presence of elemental sulphur on the chalcopyrite electrode surface

and concluded that both the electrolyte and surface deposit film contained concentrations of intermediate sulphur species capable of forming elemental sulphur by disproportionation. Other researchers (Ahlberg et al, 1990; Gardner and Woods, 1979) reported on the formation of sulphur restricted to a monolayer in the pH range of 9.2-13 in a study of surface oxidation of pyrite in alkaline solutions and Buckley and Woods (1991) and Chander et al (1992) agree on that in pyrite oxidation, the initial reaction proceeds via the preferential removal of metal ions from the lattice leaving a sulphur rich layer. While the presence of sulphur on the mineral surface has previously been reported and explained, none of the explanations given are applicable to the current study. The results from this section show that a surface deposit layer containing iron and small quantities of sulphur was formed on the mineral surface and it can be concluded that the small quantities of sulphur are from the dissolving chalcopyrite since the tests were carried out in non-sulphate solutions. Disproportionation of intermediate sulphur species to form elemental sulphur as proposed by Warren and Wadsworth (1984) is not expected to occur under the conditions of the current study where dissolved oxygen is present in solution, and the stoichiometry of the reaction in ammonia-ammonium sulphate (Section 4.2.6) solutions indicates formation of a thiosulphate intermediate which does not support Buckley and Woods (1991) and Chander et al (1992) explanation for the sulphur they observed in their work. The marginal accumulation of sulphur on the chalcopyrite electrode surface in the current study remains an observation and will not be explained further in this study.

7.4 Surface deposits in leach tests

Controlled leaching tests allowed for the build-up surface of deposit layers of significant thickness which was analysed using;

- ICP-OS for a chemical analysis, samples were digested then analysed
- SEM-EDS
- QEMSCAN
- XRD
- BET and Malvern particle analysis

Table 7.6 summarises reactor configuration and observations from the surface deposit tests.

Table 7.6. Reactor configuration and observations in surface deposit tests

Reactor	Description of test and observations	Leaching conditions
A 2.8 g micronised chalcopyrite	Sample leached for 15 days at 1% solids. 70% recovery of the copper was achieved. Residue had a reddish-brown colour.	Ammonia-ammonium sulphate solutions at 3 M (NH3+NH4+), 25°C, pH 9.6±0.15, under oxygen. Agitation maintained at uniform speed across the reactors using magnetic stirrers.
B 3.3 g 5*5*5 mm chalcopyrite cubic shaped pieces	Sample leached for 5 days. Glass beads were placed in the reactor to aid with the abrasion. Solids to liquid ratio was maintained at 1% i.e. solids refers to the chalcopyrite and the glass beads. 54.9% recovery of copper, debris from abrasion was recovered, washed in distilled water, dried then sent for analysis. The remaining unleached pieces of mineral were visibly smooth and clean, appearing like pebbles.	
C 3.5 g 5*5*5 mm chalcopyrite cubic shaped pieces	Sample leached for 5 days. No glass beads were included in the reactor. Abrasion was due to collision of the coarse pieces during agitation. 14.7% copper recovery. Remaining pieces of chalcopyrite were washed in distilled water, dried and prepared for analysis. Sample had uneven distribution of reddish-brown patches on the surface.	

Figure 7.11 and Figure 7.12 show QEMSCAN and SEM images of the leach residue from reactor A (micronised chalcopyrite) which was leached for 15 days at 25°C, pH 9.6 with 70% recovery of the copper. It is apparent that an iron- and sulphur- based layer or rim was formed around a chalcopyrite core on many of the particles. The layer also contained iron which was not associated with sulphur and was identified as an iron oxy-hydroxide species. It is worth mentioning that all species that contained iron and sulphur in Fe:S ratios higher than 1: 0.5 reported as pyrite and pyrrhotite, but this classification does not in any way mean this phase is in actual fact pyrite or pyrrhotite.

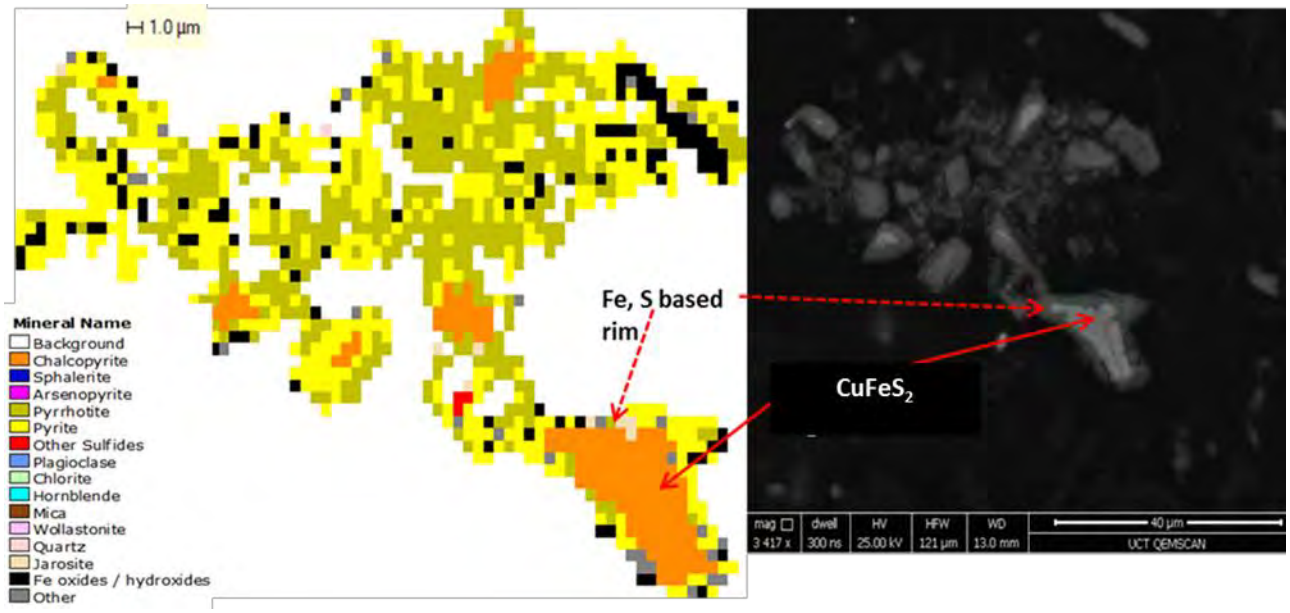

Figure 7.11. QEMSCAN and SEM images of chalcopyrite leach residue after 15 days of leaching in ammonia-ammonium sulphate solutions 3 M (NH_3+NH_4^+), 25°C, pH 9.6±0.15, 25°C under oxygen.

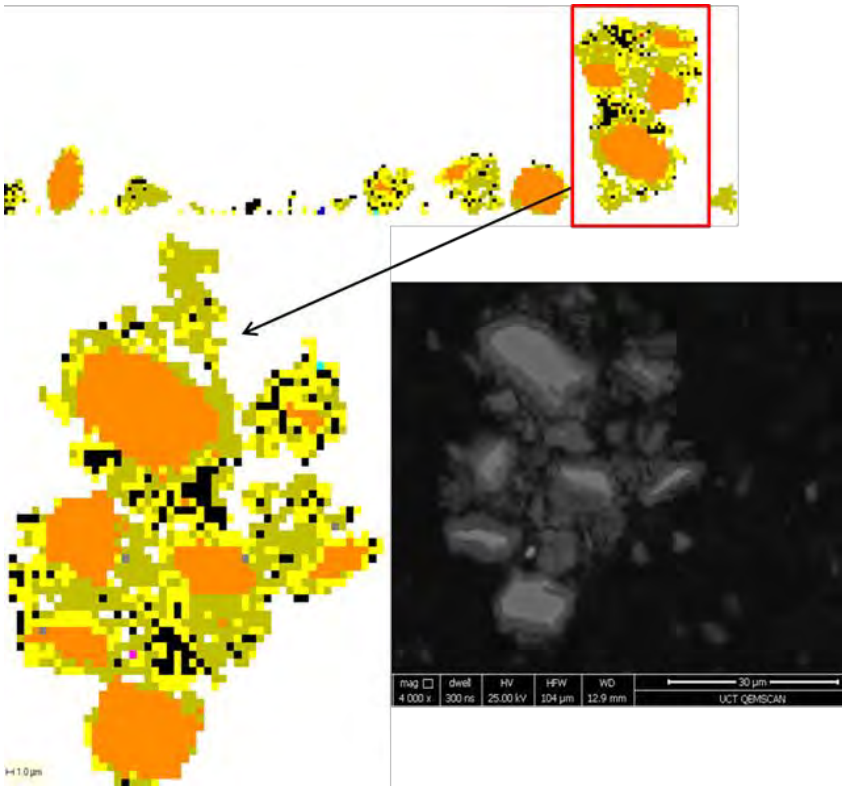

Figure 7.12. QEMSCAN and SEM images of chalcopyrite leach residue after 15 days of leaching in ammonia-ammonium sulphate solutions 3 M (NH_3+NH_4^+), 25°C, pH 9.6±0.15, 25°C under oxygen.

The debris from reactor B, in which cubic pieces of chalcopyrite were leached in the presence of glass beads (which were expected to abrade surface deposits), was washed, dried and analysed.

Results from a bulk EDS analysis (in atomic percentages) identified this to contain 31.73% Fe, 1.2% S, 4.02% Si and 63.04% O. QEMSCAN on the other hand (Figure 7.13a) identified the same sample to be 64.5% iron oxy-hydroxides with a significant number of pixels (34.7%) reporting as iron associated with sulphur. Both techniques did not identify any significant copper in the debris, this supports EDS results from the chalcopyrite electrode in similar solutions Table 7.2 which also indicated the absence of copper on the surface deposit. A chemical analysis of the sample indicated that it contained 44% iron and less than a percent each reported to copper and sulphur.

A portion of the sample was subjected to XRD analysis and was found to be mostly (90%) amorphous. Table 7.7 summarises the results of the remaining 10% non-amorphous content. Approximately 95% of the crystalline component reports to polymorphs of iron oxy-hydroxides the balance reporting to chalcopyrite (4.89%) and quartz (0.48%).

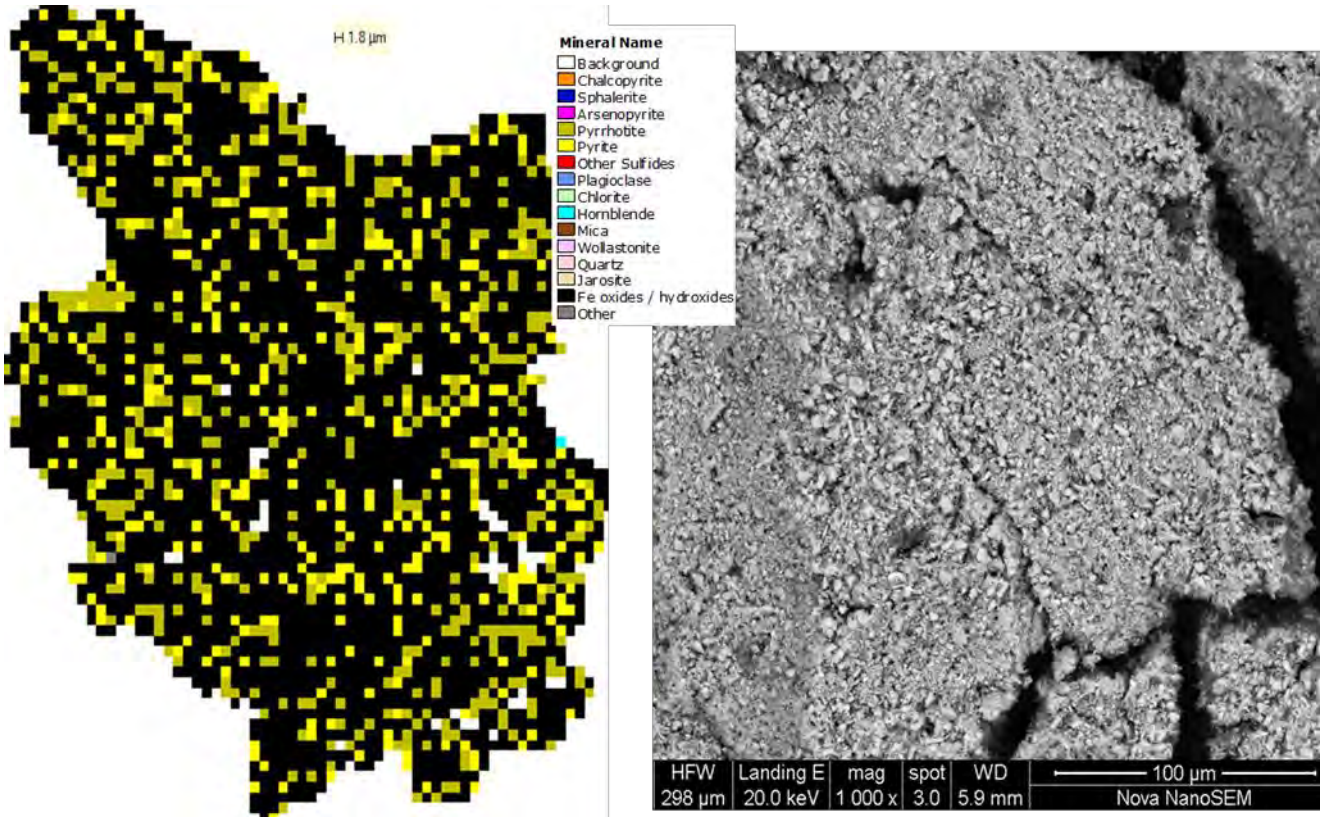

Figure 7.13. QEMSCAN and SEM images of chalcopyrite debris from reactor B after 5 days of leaching in ammonia-ammonium sulphate solutions 3 M (NH_3+NH_4^+), 25°C, pH 9.6±0.15, 25°C under oxygen.

Table 7.7. XRD results of the crystalline phases found in the chalcopyrite debris recovered from reactor B.

XRD results of the crystalline component of the leach residue	
Phase	**% Composition**
Chalcopyrite	4.89
Quartz	0.48
Geothite	5.8
Lepidocrite	51.5
Akaganeite	37.4

QEMSCAN defines the mineral map of a sample as a matrix of pixels each containing some chemical information. For each fixed point on the mineral surface, the number of pixels reporting to each element can be quantified. This data was plotted for iron and sulphur in an effort to determine the association of the elements; the graphs are shown in Figure 7.14 for the partially leached sample presented in Figure 7.11 and the completely leached sample presented in Figure 7.13. It can be seen that both samples had sites on which iron was detected but not sulphur. The bulk of the surface deposit was found to have high pixel counts for iron occurring together with sulphur, albeit at low pixel counts mostly at 225-375 pixel counts for iron associated with 40-60 pixel counts for sulphur. The partially leached sample is seen to show occurrences of high pixel counts for sulphur up to 250 with a slightly lower corresponding pixel count for iron. This is expected and is due to the presence of unleached chalcopyrite in which sulphur quantities would be expected to be more than the iron quantities. The completely leached samples were observed to show low pixel counts for sulphur, mostly below 100. This is indication that although sulphur was detected, it was only in small quantities.

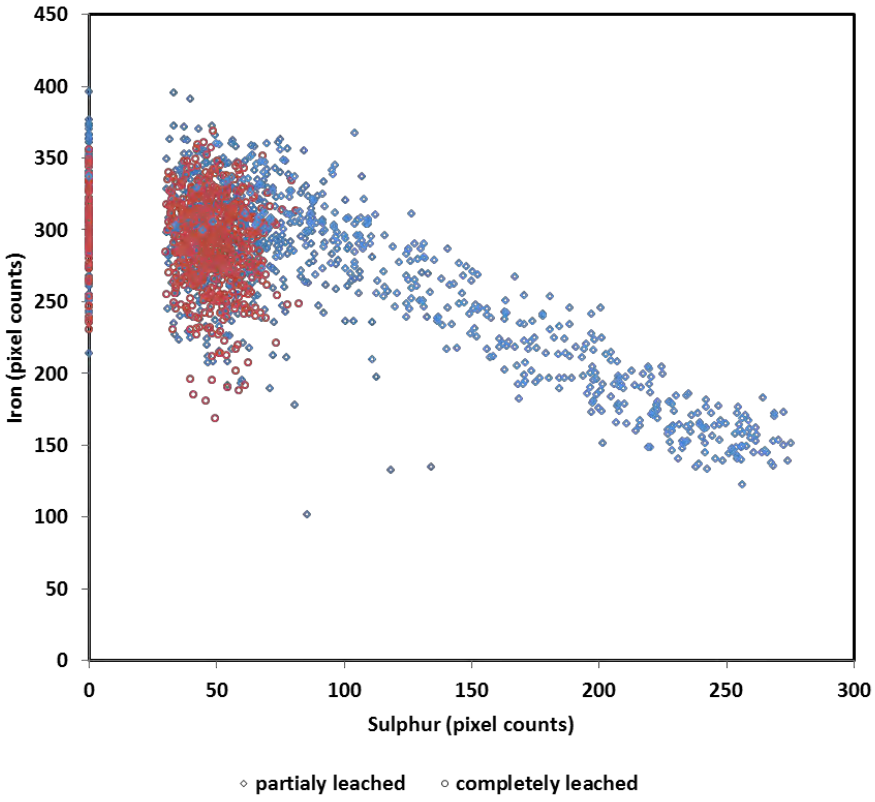

Figure 7.14. Pixel data for samples from reactor A (partially leached) and reactor B (completely leached) plotted as pixel counts for iron and sulphur.

The blocks from reactor C in which 5*5*5 mm pieces were leached in the absence of glass beads (meaning there was minimal mechanical abrasion) were retrieved, washed and prepared for QEMSCAN analysis. Figure 7.15 shows QEMSCAN and SEM images of a section of one of the blocks. The section was found to contain 75% chalcopyrite, 23% iron-sulphur phase, 2% iron oxy-hydroxides with only traces of less than 1% reporting as “other sulphides”.

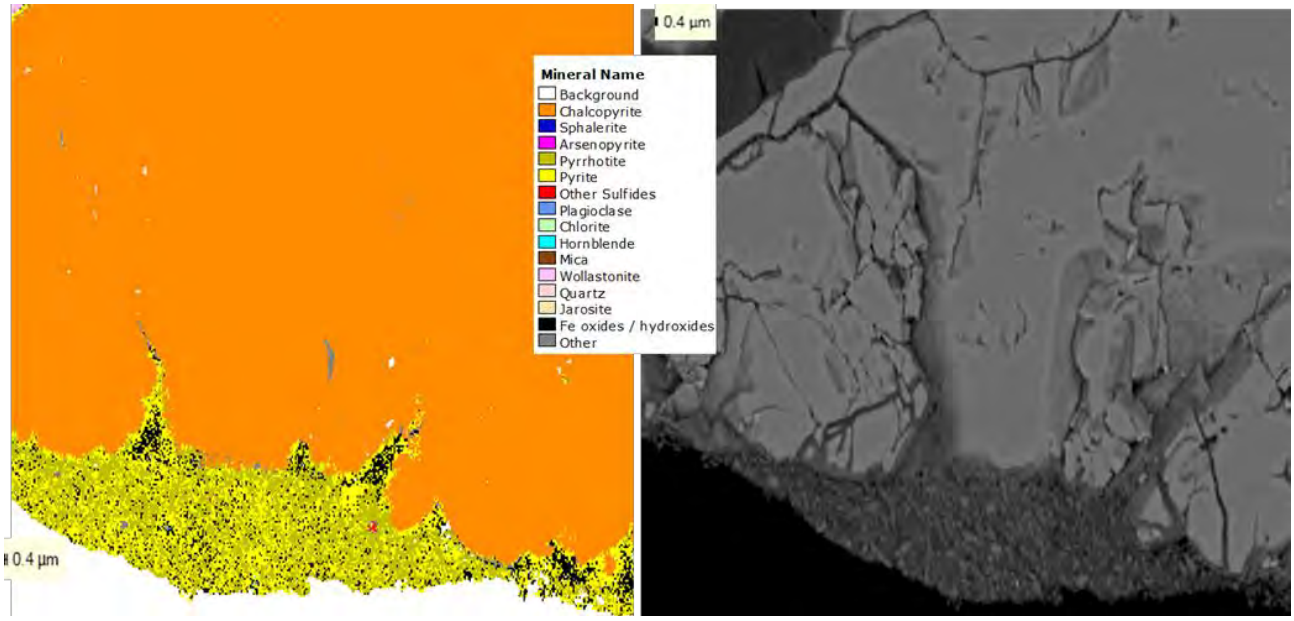

Figure 7.15. QEMSCAN and SEM images of chalcopyrite block after 5 days of leaching in ammonia-ammonium sulphate solutions 3 M (NH_3+NH_4^+), 25°C, pH 9.6±0.15, 25°C under oxygen.

From the SEM images (Figure 7.11, Figure 7.13 and Figure 7.15) the morphology of the surface product appears to be significantly different from that of the chalcopyrite mineral which can be seen as the core in Figure 7.11 and forms the bulk of Figure 7.15. The surface deposit appears to be composed of an agglomeration of smaller particles as opposed to the dense/compact solid images seen of chalcopyrite. As an agglomerate, it would be expected that it be relatively porous compared to chalcopyrite. Surface area and porosity were measured using the Brunauer-Emmett-Teller (BET) method on the micronised sample prior to and after leaching (Table 7.8). This is a non-penetrative method; therefore, it only gives information of the surface with minimal risk of reaching through to the otherwise non-leached mineral core. It is apparent that the surface area and surface-pore volume of leached particles increased significantly relative to that of the non-leached chalcopyrite, an increase from 1.275 m^2g^{-1} on non-leached chalcopyrite to 57.364 m^2g^{-1} on leach residue from a reactor at 1 M (NH_3+NH_4^+) leached for 17 days (leach curve presented in Figure 6.1). This is an increase of a factor of 44 in surface area.

Table 7.8. Surface analysis results of chalcopyrite prior to and post leaching tests in solutions of different total ammonia concentrations in similar leaching conditions (leach curves presented in Figure 6.1Figure 6.1**).**

Surface area and porosity results			
Sample	**surface area m^2/g**	**pore volume m^3/g**	**% passing 25µm**
chalcopyrite	1.275	0.0055	66.61
1M leached surface	57.346	0.0642	94.07
3M leached surface	57.734	0.0503	89.89
6M leached surface	59.526	0.0577	89.52

The observations made in the leach tests confirm the formation of a surface deposit layer during chalcopyrite leaching. This is in agreement with Forward and Mackiw's (1955) work on ammoniacal leaching of sulphide minerals which suggested the formation of a hydrated iron oxide layer enveloping a shrinking mineral sulphide core. The researchers went on to say that the hydrated iron oxide layer was pseudomorphic with the chalcopyrite; this suggests that the surface deposit had some form of crystallinity. Results from the current study contradict this inferred crystallinity of the surface deposit layer and it has been proven that 90% of the surface deposit layer was in fact amorphous. This finding was in agreement with Warren and Wadsworth (1984) who studied the surface deposit formed on a chalcopyrite electrode surface oxidised in ammonia-ammonium sulphate solutions and Gaun and Han (1997) who looked at the chalcopyrite electrode surface after oxidation in ammonia-ammonium iodide solutions and they all reported the presence of some form of iron oxide film which they found to be amorphous.

7.5 Discussion and conclusion

The influence of the surface deposit layer on the leaching reaction was explored through electrochemical tests. The observed rapid increase in mixed potentials on immersion of the electrode in the electrolyte suggests the spontaneous growth of an inhibiting surface deposit which then continues to grow gradually (Figure 4.1 and Figure 4.2). Potential sweeps in cyclic voltammetry tests did not indicate passivation (Figure 4.14, Figure 4.17, Figure 4.18 and Appendix 1) and hence did not support the otherwise widely accepted passivation phenomenon for chalcopyrite leaching reported for acid sulphate systems (Tshilombo et al, 2002; Lu et al, 2000; Parker et al, 1981; Ghahremaninezhad, 2012; Klauber, 2008). Passivation has been described as the situation in which the sulphide mineral is covered with an inhibiting layer of an oxide or other species which is formed at a so-called critical potential (Pugaev et al, 2011). According to this definition, it would be expected to see a point whereby an increase in potentials does not result in an increase in current densities, but this was not observed in the current study. This lack of defined passivation potentials was also contrary to the results presented by Warren and Wadsworth (1984), who reported some shoulders followed by decreased currents which then began to increase at potentials above 0.55 V vs SHE in solution conditions similar to the ones used in this study. Although this inconsistency in results could be a cause for concern considering the oxidation studies were done in similar solution conditions, we found this to be of no consequence in leach systems. This is so; taking into consideration that the reported passivation was observed in the high Tafel regions, at potentials which would not normally be achieved in a leaching plant and this makes it irrelevant to this study whose focus is on the leaching reactions at mixed potential and the potentials in the vicinity of mixed potentials. While findings from the current study support the formation of surface deposits, they do not support that this surface layer can be electrochemically controlled i.e. no critical passivation potential is defined. Furthermore, the increased pore volume and the ease with which the surface deposit can be dissolved are strong evidence that the surface deposit is formed through secondary precipitation, hence is not part of the surface electrochemical mechanism, which is what passivation at a critical potential implies.

The anodic current densities from constant potential tests were shown to decrease with time during the first half hour of the reaction and there after reached what appeared to be steady state values when observed over 2 hour periods. However, longer term potentiostatic test showed that steady state was in fact not attained and anodic currents gradually declined with time. According to (Bard and Faulkner, 2001), the shapes of a current-time transient show two limiting stages; diffusion limitation where current decays with time upon application of a potential step and the limitation of the rate by an electrochemical step on the surface of the reaction where by current remains fairly

constant with time. The same is not true for ammonia-ammonium carbonate solutions which showed no build-up of a surface deposit layer and also showed relatively steady state currents (Figure 4.23) there by suggesting a reaction controlled by an electrochemical step.

A surface deposit layer was shown to build-up in ammonia-ammonia perchlorate solutions (Figure 7.10 and Table 7.5) and the gradual decline of anodic currents with time indicated that this surface deposit layer was also growing in thickness as the reaction progressed. It makes sense that despite the tests running for the same duration, copper was still detected on the surface. This is because oxidation rates were lower in perchlorate solutions hence the rate of surface deposit build up was also low resulting in a thinner surface deposit layer relative to that which would be expected in sulphate solutions.

It is postulated that in the carbonate systems, chalcopyrite leaching proceeds mainly via preferential dissolution in the cracks. The carbonate system allows for the formation of metastable iron(II) complexes that can then be transported away before oxidation to iron(III) species and subsequent nucleation and growth away from the mineral surface. This postulation may be extended to the perchlorate system where evidence of deposits forming in the cracks was seen, however there is no further evidence to support this. If this preferential dissolution along cracks were true, then in perchlorate systems, where iron does not form metastable complexes, nucleation and growth of a surface deposit layer is proposed to occur, and the cracks would fill up with surface deposits, subsequently forcing the reaction to change from that of preferential dissolution along the cracks to uniform dissolution across the mineral surface. The sulphate system, there was no evidence of preferential leaching in the cracks, results after two hours of oxidation did not indicate for any preferential dissolution (Figure 7.6) while results after the extended oxidation tests (Figure 7.3) and (Figure 7.4) only showed a porous layer of surface deposit with no way of predicting preferential oxidation sites.

Conclusion

An inhibiting deposit layer is formed on the surface of chalcopyrite during oxidative dissolution in ammoniacal solutions. This surface layer is mostly an amorphous iron oxy-hydroxide which contains small quantities of crystalline polymorphs of iron oxy-hydroxides such as akaganeite, geothite and lepidocrite. Small quantities of sulphur were present in the surface layer after vacuum drying the electrode, and it is proposed that this sulphur was the oxidising chalcopyrite and its transport to the bulk solution was relatively slow. If the sulphur detected had been coming from solution, it would

have been expected that significant quantities of the sulphur be present on the leached mineral residue (Figure 7.13) had it been coming from solution.

Presence of this iron oxy-hydroxide surface deposit layer inhibits the oxidation reaction, but its formation is not through the electrochemical reaction mechanism. The formation of this surface layer and its stability is influenced by the anions present in solution.

8 Discussion

8.1 The mixed potential model

The potentials measured on the mineral surface at open circuit (Figure 4.1 to Figure 4.6) support that a mixed potential was established when the chalcopyrite electrode was immersed in oxidising ammoniacal solutions. The stoichiometry of the oxidation reaction was determined from coulometric studies (Equations 4.4 and 4.5) and the predominant cathodic reaction was shown to be that of the reduction of copper(II) (Equation 5.1).

The concept of mixed potential is discussed in the literature review (Section 2.3.1) and in the case of the present study, it has been shown that oxidation of chalcopyrite (Equations 4.4 and 4.5) occurs coupled to reduction of copper(II) (Equation 5.1). This can also be seen from the change in mixed potential when copper(I) was present (Figure 4.4), and it has been shown (Section 5.3) that the oxidation of copper(I) generated by the reduction reaction (Equation 5.2) takes place at the mixed potentials under the conditions of this study. The reduction of oxygen on the chalcopyrite surface, which is accepted in literature as the primary reduction reaction (Duyvesteyn, 1995; Duyvesteyn and Sabacky, 1993; Warren and Wadsworth, 1984; Beckstead and Miller, 1977a; Reilly and Scott, 1977; Tozawa et al, 1976; Kuhn et al, 1974; Forward and Mackiw, 1955) has been shown not to be the favoured reaction in the presence of copper(II) (Section 4.2.1). Thus, at the mixed potential, three reactions (Equations 4.5, 5.1 and 5.2) take place on the surface of chalcopyrite. The oxidation and reduction reactions (Equations 4.5, 5.1 and 5.2) are rewritten as equation 8.1 - 8.3 in terms of Cu(II) to refer to the cupric ammine species and Cu(I) to refer to the cuprous ammine for simplicity.

$$CuFeS_2 + 6OH^- = Cu(I) + Fe^{2+} + S_2O_3^{2-} + 3H_2O + 7e \quad 8.1$$

$$Cu(II) + e = Cu(I) \quad 8.2$$

$$Cu(I) = Cu(II) + e \quad 8.3$$

At the mixed potential, the oxidation and reduction reactions occur simultaneously on the chalcopyrite surface. The sum of the currents due to the oxidation of chalcopyrite (Equation 8.1) and Cu(I) (Equation 8.3) are equal to and opposite to the currents due to the reduction of copper(II) (Equation 8.2).

$$i_{CuFeS_2} + i_{Cu(I)} = -i_{Cu(II)} \quad 8.4$$

Writing the currents at the mixed potential in terms of the Butler-Volmer equation (Equation 2.18).

$$i_{CuFeS_2} = 7k_{CuFeS_2}Exp\ (\frac{\alpha_{CuFeS_2}FE_m}{RT}) \quad 8.5$$

$$i_{Cu(II)} = -Cu(II)k_{Cu(II)}Exp\ (\frac{-(1-\alpha_{Cu(II)}).F.E_m}{RT}) \quad 8.6$$

$$i_{Cu(I)} = Cu(I)k_{Cu(I)}Exp\ (\frac{(\alpha_{Cu(I)})FE_m}{RT}) \quad 8.7$$

in which k_{CuFeS2} , $k_{Cu(II)}$ and $k_{Cu(I)}$ are the rate constants of the anodic and cathodic reactions and may contain concentration terms for ions in solution and temperature. α is the so called charge transfer coeffient α_{CuFeS2} was calculated from the equation for Tafel slope (Equation 8.8) using the Tafel curves presented in (Figure 4.14) and was found to be 0.42 and this was accepted as reasonably close to the value of 0.5 commonly approximated in literature. $\alpha_{Cu(I)}$ and $\alpha_{Cu(II)}$ were not measured but assumed to be also equal to 0.5

$$\frac{-2.303RT}{\alpha F} = Tafel\ slope \quad 8.8$$

Substituting equations 8.5-8.7 into equation 8.4;

$$7k_{CuFeS_2}Exp\ \left(\frac{\alpha_{CuFeS_2}FE_m}{RT}\right) + Cu(I)k_{Cu(I)}Exp\ (\frac{(\alpha_{Cu(I)})FE_m}{RT}) = [Cu(II)]k_{Cu(II)}Exp\ (\frac{-(1-\alpha_{Cu(II)})FE_m}{RT} \quad 8.9a$$

$$Exp\ \left(\frac{0.5FE_m}{RT}\right) = \frac{[Cu(II)]k_{Cu(II)}}{\left(7k_{CuFeS_2}+[Cu(I)]k_{Cu(I)}\right)}Exp\ (\frac{-0.5*F.E_m}{RT}) \quad 8.9b$$

Solving for the mixed potential (E_m);

$$E_m = \frac{RT}{F}\ln(\frac{[Cu(II)]k_{Cu(II)}}{7k_{CuFeS_2}+[Cu(I)]k_{Cu(I)}}) \quad 8.10$$

It can also be shown that when copper(I) was present in sufficiently large quantities such as those in the results presented in **Table 4.1**, then at the mixed potential the potential was determined by the copper(I)/copper(II) redox couple by the following analysis.

The currents due to the oxidation of the mineral becomes negligibly small in comparison to those from the oxidation of copper(I), hence the current balance is reasonable approximated by equation 8.11

$$i_{Cu(I)} \approx -i_{Cu(II)} \quad 8.11$$

The expression for the mixed potential under such conditions is then defined by equation 8.12;

$$E_m = \frac{RT}{F}\ln(\frac{[Cu(II)]k_{Cu(II)}}{[Cu(I)]k_{Cu(I)}}) \quad 8.12$$

Equation 8.12 takes the form of the Nernst equation and the measured potentials are no longer mixed potentials but can be considered equilibrium potentials that equate to the solution potential (Figure 4.4) .

8.2 Derivation of the rate expression for the dissolution reaction

The anodic current for the oxidation of chalcopyrite at the mixed potential can be described by the Butler-Volmer equation (Equation 2.18) and is expressed by equation 7.5. A rate expression for the oxidation reaction can then be derived in accordance with the Faraday equation, relating current density and stoichiometry (Equation 8.13).

$$Rate = \frac{i}{nF} \tag{8.13}$$

Substituting the chalcopyrite oxidation (Equation 8.5) into 8.13 then equation 8.10 for E_m, where the number of electrons n =7

$$R_{CuFeS_2} = \frac{7k_{CuFeS_2} Exp\left(\frac{\alpha_{CuFeS_2} F \frac{RT}{F} ln\left(\frac{[Cu(II)]k_{Cu(II)}}{7k_{CuFeS_2}+[Cu(I)]k_{Cu(I)}}\right)}{RT}\right)}{7F} \tag{8.14}$$

After some mathematical manipulation and substituting for α = 0.5, equation 8.14 becomes;

$$R_{CuFeS_2} = \frac{k_{CuFeS_2}}{F} . \left(\frac{[Cu(II)]k_{Cu(II)}}{7k_{CuFeS_2}+[Cu(I)]k_{Cu(I)}}\right)^{0.5} \tag{8.15}$$

The rate expression (Equation 8.15) implies that the order of reaction with respect to copper(II) is 0.5 and this has been shown to be true in section 4.2.3 where the effect of copper(II) on the anodic reaction was discussed.

As stated earlier in section 8.1, the rate constants k_{CuFeS2}, $k_{Cu(II)}$ and $k_{Cu(I)}$ may contain concentration terms for ions in solution thus will vary with solution conditions. Looking at the anodic reaction (Equation 4.5), the concentration terms for ammonia and pH can be unbundled from the rate constant such that an expression for k_{CuFeS2} is as follows;

$$k_{CuFeS_2} = k^*_{CuFeS_2}[OH^-]^A[NH_3]^B \tag{8.16}$$

In which A and B refer to the order of reaction with respect to hydroxyl and free ammonia respectively. The order(s) of reaction with respect to free ammonia and pH was determined in section 4.2.4. At 1 M total ammonia and pH 9.6, the solution conditions under which most of the electrochemistry test work was done, the reaction order was 1.76 with respect to free ammonia and 0.22 with respect to hydroxyl ions. The value for k_{CuFeS2} has been calculated from a log current

density-potential plot (Figure 4.13) by taking the antilog of the y intercept and it was found to be $1.96*10^{-3}$ µAcm^{-2}. Equation 8.16 can then be solved for k^*_{CuFeS2} (Equation 8.17).

$$1.96 * 10^{-3}\ \mu Acm^{-2} = k^*_{CuFeS_2}[3.98 * 10^{-5} molL^{-1}]^{0.22}[0.602\ molL^{-1}]^{1.7} \quad 8.17$$

$$\frac{1.96*10^{-3}\ \mu Acm^{-2}}{[3.98*10^{-5} molL^{-1}]^{0.22}[0.602\ molL^{-1}]^{1.7}} = k^*_{CuFeS_2} \quad 8.18$$

$$k^*_{CuFeS_2} = 0.0431\ \mu Acm^{-2} \quad 8.19$$

The rate constant for the anodic reaction is k^*_{CuFeS2} is thus 0.0431 cms^{-1}. It should be pointed out that k^*_{CuFeS2}, was calculated using data from contestant potential tests that ran for 2 hours at each set potential and current density values after the 2 hours were used (Figure 4.9 and 4.12). To validate this method of calculating the rate constant for the anodic reaction, a similar approach was taken using cyclic voltammetry data in 1 M and 3 M total ammonia solutions in the absence of copper at 25°C (Figure 4.17), the results were corrected for IR drop following the method described in the methodology (Section 3.2.3) and an exponential fit to the data is presented below.

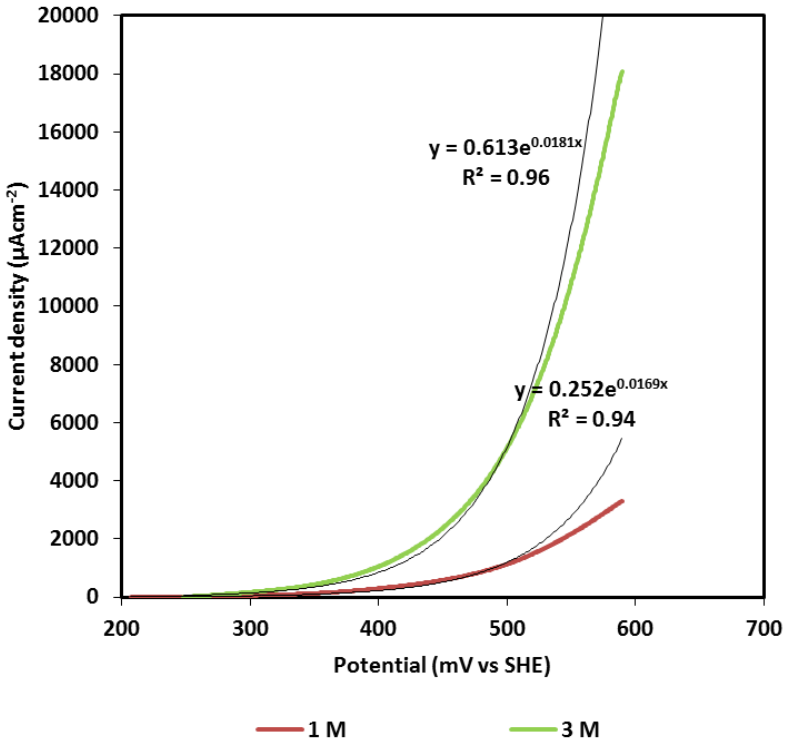

Figure 8.1. Exponential fit to the back sweeps in cyclic voltammograms on a chalcopyrite electrode surface measured in solutions of 1 M and 3 M total ammonia, 25°C, pH 9.6±0.15, no initial Cu(II), under nitrogen at a scan rate of 1 mV sec^{-1}.

Using equation 8.16, the order of reaction A and B determined from Figure 4.20 and Figure 4.21 the values of k^*_{CuFeS2} were calculated. Table 8.1 shows the k^*_{CuFeS2} values calculated and these were

found to be 5.55 cms^{-1} in 1 M (NH_3+NH_4^+) and 5.4 cms^{-1} in 3 M (NH_3+NH_4^+) which is reasonably similar, as would be expected for a rate constant. Notably, the rate constants determined from cyclic sweeps are larger than those determined from constant potential tests. This is due to that in the constant potential tests, surface deposits had been growing over the 2 hour course of the experiment on the mineral surface while in the cyclic sweep tests, a forward sweep from mixed potentials at scan rate 1 mV/sec lasted a mere 5 min. Thus, it is unlikely that a significant surface deposit layer was formed in cyclic sweeps in comparison to that formed in the 2 hour constant potential test.

Table 8.1. k^*_{CuFeS2} values in 1 and 3 M (NH_3+NH_4^+) solutions at 25°C, pH 9.6±0.15 under nitrogen.

Solution conditions			Exponential fit	Order of reaction		Rate expression	k^*_{CuFeS2}
NH_3+NH_4^+	Free NH_3	OH^-		A	B		
1	0.60	3.98E-05	$y=0.252e^{18.08}$	0.22	1.7	$0.244=k^*[3.98\cdot10^5]^{0.22}[0.602]^{1.7}$	5.55
3	1.81	3.98E-05	$y=0.613e^{16.93}$	0.22	0.09	$0.618=k^*[3.98\cdot10^5]^{0.22}[1.81]^{0.09}$	5.4

The term was $K_{Cu(I)}Cu(I)$ in equation 8.14 was assumed to be negligible when determining the initial rate of reaction. It should be pointed out that $K_{Cu(I)}$ may well not be negligible but the lack of copper(I) in solution renders the term $K_{Cu(I)}Cu(I)$ negligible. The term $K_{Cu(II)}$ was determined from cyclic sweep data presented in Figure 5.9 using the same approach as that used to obtain Table 8.1. A detailed derivation of the cathodic expression can be found in appendix 1. Figure 8.2 shows the exponential fit and the pre-exponential term $K_{Cu(I)}$ to be $2x10^6$ cms^{-1} which is over 5 orders of magnitude higher than the rate constant for the anodic reaction (k_{CuFeS2}) which was found to be 0.252 (Figure 8.1). This indicates that kinetically, the anodic reaction proceeds slower than the cathodic reaction.

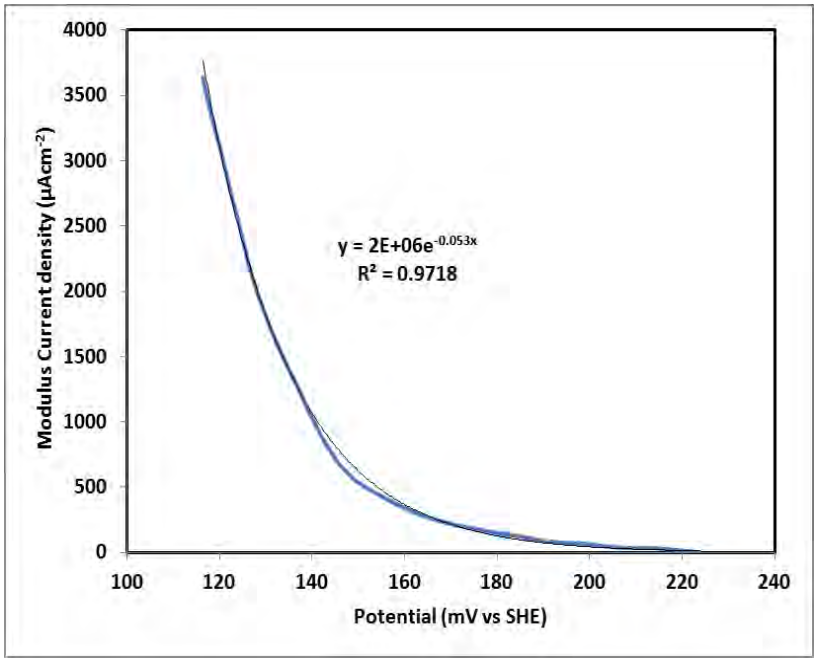

Figure 8.2. Exponential fit to the modulus of cathodic current densities from cyclic voltammetry data measured in solutions of 1 M (NH_3+NH_4^+), 25°C, pH 9.6±0.15, 5 g/L initial Cu(II), under nitrogen at a scan rate of 1 mV sec^{-1}.

8.3 Towards a physical model

Electrochemical experiments have shown that the dissolution of chalcopyrite proceeds through the anodic oxidation of the chalcopyrite and cathodic reduction of copper(II). The oxidation reaction has been found to approximate half order dependence on copper(II) (Sections 4.2.3 and 4.2.3) as would be expected of a reaction following the electrochemical theory of dissolution. The effects of pH and free ammonia on the chalcopyrite oxidation reaction are also adequately explained by the electrochemical leaching mechanism (Section 4.2.6). The rate constant for the cathodic reaction was found to be over 5 orders of magnitude higher than that of the anodic reaction (Section 8.2). A high rate constant is an indication of a very fast reaction while a low rate constant indicates the opposite. Since the overall leaching reaction occurs as the two coupled reactions, and the cathodic reaction is seen to be very fast relative to the anodic reaction, it is seen as proven that under the conditions in which the tests were carried out, the overall leaching reaction is limited by the anodic reaction.

The chalcopyrite oxidation reaction, like many other corrosion processes, occurs through the transfer of electrons from solid phase to liquid phase. The rate of transfer of these electrons is dependent on the potential difference across the electrode-electrolyte interface and this has been discussed in detail by Stojek (2005) and Srinivasan (2006). The electrical double layer, formed when the chalcopyrite electrode is placed into solution, is important in that aside from the potential difference across this double layer being the driving force for the reaction, the composition of the double layer also influences electron transfer rates. This implies that under free dissolution

conditions, changes in solution conditions or nature of the surface would result in changes on potentials measured on the mineral surface. Some of the interesting results from this study were from the potential-time and current-time transients, as these reveal further insights on the processes at the surface. Increasing the concentration of the oxidant resulted in increased mixed potentials which in a leaching system translate to increased dissolution rates as discussed in Chapter 4. Mixed potentials increased with time indicating that the mineral surface was becoming more noble, and current densities at fixed potentials decreased with time, suggesting that some form of resistance to the oxidation reaction was building up. A porous and amorphous surface deposit layer of relatively high surface area was shown to be formed on the mineral surface in ammonia-ammonium sulphate (Section 7.1) and in ammonia-ammonium perchlorate solutions (Section 7.3). Ammonia-ammonium carbonate solutions did not show presence of surface deposits except along cracks were mass transport of oxidation products is expected to be poor. These observations indicate that anions in solution played a critical role with regards to the deportment of solubilised oxidation products and in turn on the formation and growth of a surface deposit layer. It is logical to postulate that the increasing mixed potentials and the suggested resistance to oxidation are directly related to the build-up of the observed surface deposit.

Figure 8.3 and Figure 8.4 show schematics of the electrochemical cell prior to and post, the growth of a surface deposit layer. At mixed potential there is no net flow of current, but equal and opposite anodic and cathodic currents exists between the oxidising chalcopyrite and the reducing copper(II). On Figure 8.3 and Figure 8.4, the activities occurring in the cell at mixed potential are limited to the dashed line box showing that the potential on the mineral surface is measured against that of a reference electrode. In both instances, equivalent electrical circuits of the cell are shown beneath the cell schematic, with the mixed potential established on the mineral surface being perceived as the battery or voltage source. A dotted line is shown on the equivalent cell, closing the circuit; this is because despite the measured potentials being known to be at open circuit against the reference electrode, it is known that the steady-state established on the solid-liquid interface involves charge transfer between the oxidising and reducing species. The difference between the two figures is that Figure 8.3 illustrates mixed potentials as would be measured on a “clean/pristine” mineral surface prior to nucleation and growth of surface deposit, and Figure 8.4 shows potentials measured on a mineral surface that has some surface deposits growing on it. A capacitor is shown on both figures and caters for the charging of the electrical double layer. Since it has been pointed out that charge transfer occurs between the chalcopyrite and the copper(II), thus presence of a surface deposit layer can be said to cause a potent drop (δV). The potential drop δV is contributed by this surface deposit layer, and as this surface deposit layer grows in thickness so does δV. The total potential measured

(V_T) in each case is given by equations 8.20 on a clean surface and 8.21 on a surface with some surface deposits.

$$V_T = V_0 \quad 8.20$$

$$V_T = V_0 + (\delta V) \quad 8.21$$

In which V_o refers to potentials established on the mineral surface and δV is the voltage drop across the surface deposit layer. This is illustrated in Figure 8.5 which shows a schematic of the mixed potential measurements in the presence and absence of a surface deposit layer. It needs to be pointed out that Figure 8.5 is for illustrative purposes and it should not be understood to mean that the actual system would exist as such separate layers.

If it is assumed that presence of a surface deposit layer poses a diffusion barrier for the oxidant and the products of the oxidation reaction, a localised depletion of copper(II) and accumulation of copper(I) should follow, and this should cause a decline in mixed potentials V_0. However, if the surface deposit layer imposes a potential drop δV larger than the margin by which V_0 is decreasing, then the net effect of this change in ion concentration and potential drop would be an increase in measured potentials V_T. It was established that the surface deposit layer was porous thus copper(II) and copper(I) can diffuse to and from the chalcopyrite surface. The value of δV and the fact that this δV parameter increases with time have implications on tests in which a potential is applied to drive the reaction. This is explained by using an example of a fixed potential test where, as the oxidation reaction occurs, it is accompanied by growth of the surface deposit layer. In such instances, while the set potential V_{app}(as controlled by the instrument) remains fixed, δV is increasing thus the effective potential ($V_{effective}$) driving the reaction on the mineral surface is in fact given by ;

$$V_{effecive} = V_{app} - (\delta V) \quad 8.22$$

It is apparent from equation 8.22 that, as the surface deposit layer grows (which translates to an increase in δV) the effective potential on the mineral surface decreases. Thus it would be expected that growth of a surface deposit layer be accompanied by lowered oxidation current densities, which is exactly what has been observed in the current study (see for example Figure 4.11).

Iron oxy-hydroxides are known to interact strongly with their surrounding media especially in the form of adsorption (Chesne and Kim, 2014; Kozin, 2014; Mohapatra et al, 2010), thus the illustrated inner layer in the electric double layer shown in Figure 8.5b could well be adsorbed onto the iron oxy-hydroxide surface deposit layer.

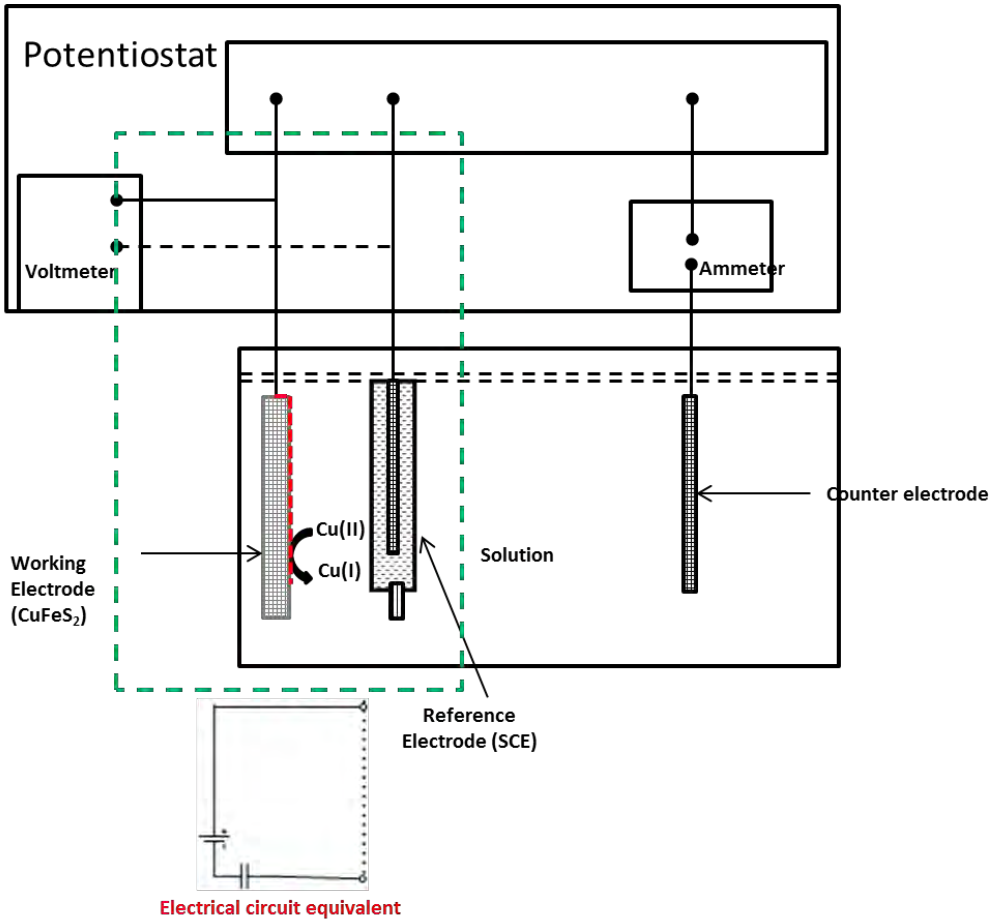

Figure 8.3. Electrochemical set up on a "pristine" electrode, i.e. before growth of surface deposits

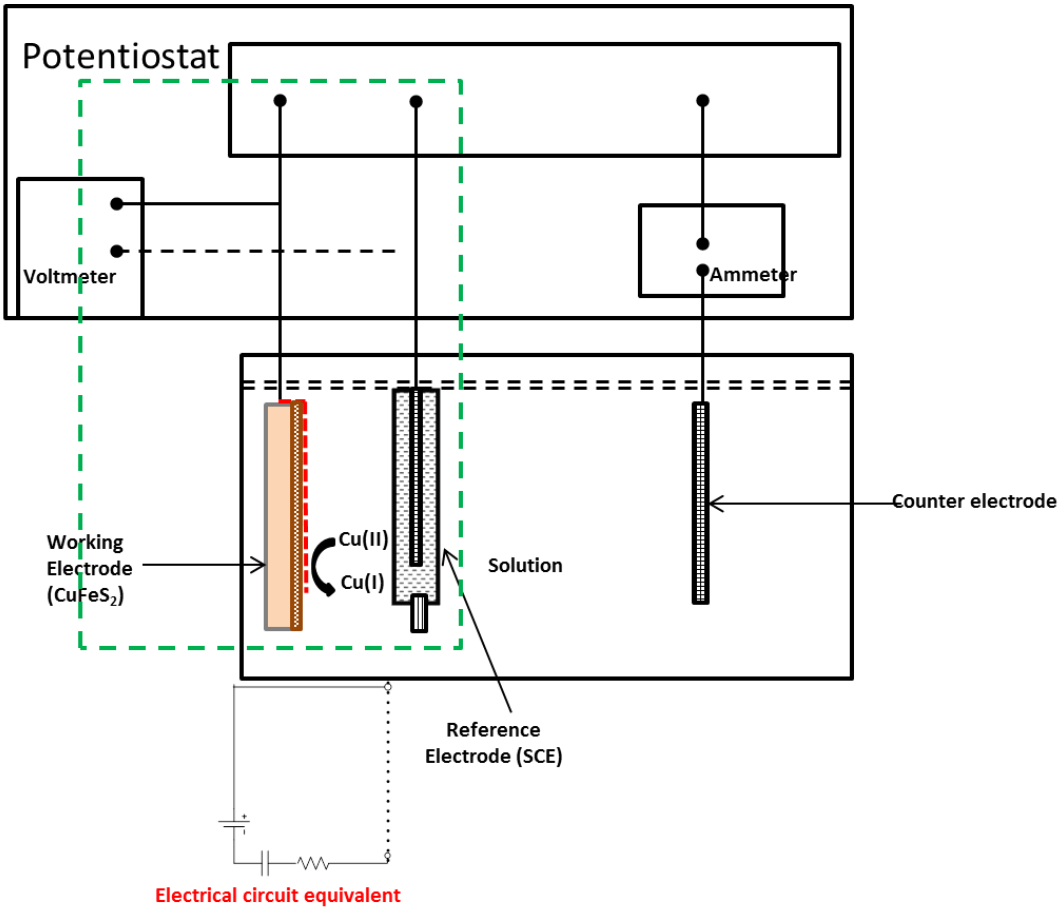

Figure 8.4. Electrochemical set up after growth of surface deposits

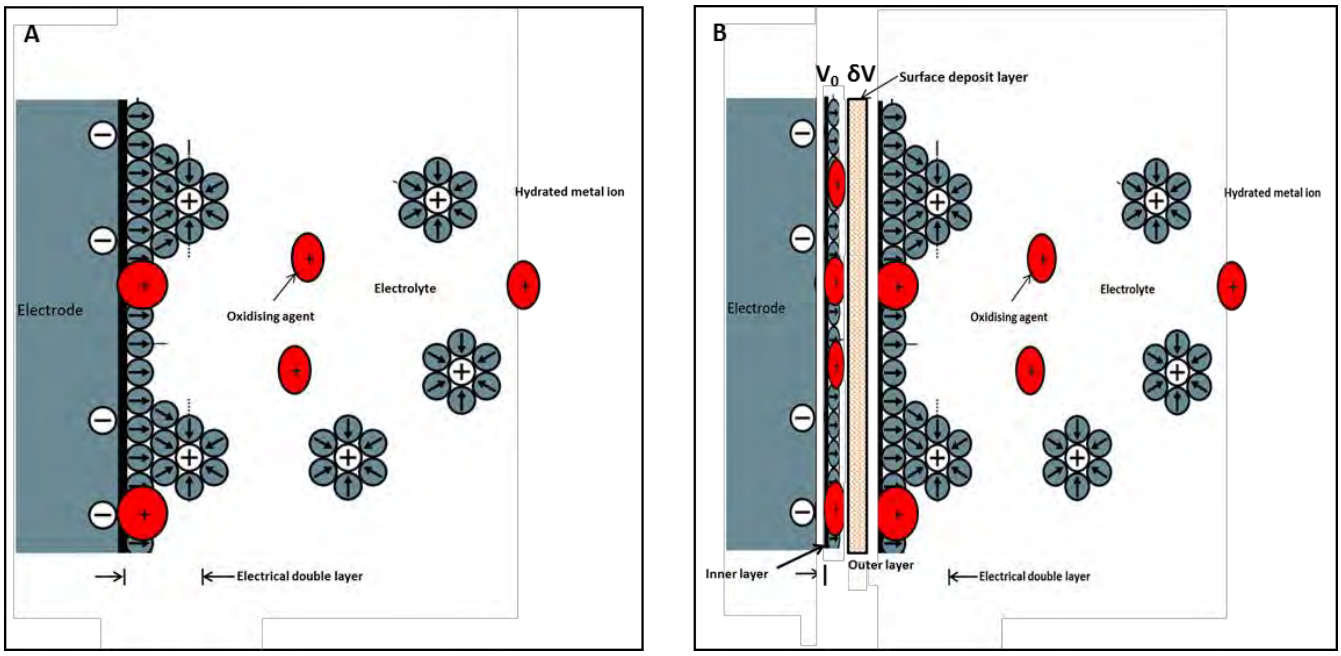

Figure 8.5. Illustration of the electric double layer before and after formation of surface deposits.

The oxidative leaching reaction showed half order dependence on the concentration of copper(II), the oxidant (Figure 4.25). This is evidence of a reaction controlled by an electrochemical surface reaction and is further supported by the activation energies of 67.6 kJ/mol calculated for the dissolution currents. Notice should be taken that this is true for tests run for relatively short periods of time, i.e. the half-order dependence on oxidant concentration was determined using dissolution current densities measured after 2 hours. Constant potential versus time plots showed current densities appeared to reach steady state over such short periods of time but, longer term experiments showed a continued gradual decline of current densities with time. This ties in well with the analogy drawn from the mixed potential time plots which also appeared to reach steady state over short term tests, but showed an apparent continued increase with time over longer term tests (Figure 4.1 and Figure 4.2). Analysis of the slopes of Figure 4.6 and Figure 4.10 from 10 minutes into the reaction (time at which Figure 4.6 indicates currents to be at steady state) showed a gradient of less than -0.1 $\mu Acm^{-2}hr^{-1}$ in the first 2 hours (Figure 4.6) and -3.1 $\mu Acm^{-2}hr^{-1}$ over 20 hours (Figure 4.10). This suggests that although growth of a surface deposit layer is spontaneous, its effects on the kinetics of the reaction were not immediately observed thus tend not to be accounted for when the leaching reaction is modelled based on data collected over such short periods. Warren and Wadsworth (1984) observed the presence of an iron oxide layer but concluded that due to the porous nature of the layer, it was not protective and did not affect the leaching reaction. The researchers drew this conclusion based on fixed potential tests that ran for 160 minutes and in that time frame, currents were observed to have had reached steady state. Their observations are in agreement with those made in this study for tests run for similar durations and as already mentioned, are unlikely to be true for situations were a surface deposit layer of significant thickness has formed.

Results from the current study, supported by literature (Kozin, 2014; Warren and Wadsworth, 1984; Kaneko and Inouye, 1974) show iron oxy-hydroxides to be porous, thus, it is expected that when present only as thin layer, such as in initial leaching, ions can easily migrate through it, not experiencing mass transfer limitations which cause a low rate of reaction. This has been illustrated in Figure 8.6 which shows a schematic of a chalcopyrite surface with a porous surface deposit layer on it. However, as the reaction proceeds, the iron oxy-hydroxide deposit layer grows in thickness, and this would likely pose either as a diffusion barrier to the leachate (Weisener et al, 2003) or a barrier to electron transfer (Munoz, 1979). The exact thickness of the surface deposit layer was not measured in the current study. However, in some instances such, as shown in Figure 7.3 in which no copper was detected in the surface analysis, it is inferred that the surface deposit layer was more than 30.1 μm thick, which was calculated to be the electron penetration (Section 3.2.2) of the

instrument at the settings used. Similarly, in instances in which copper was detected, it was assumed that this was due to the detection of chalcopyrite and the surface deposit layer was inferred to be less than 30.1 µm thick. Biegler and Horne (Biegler and Horne, 1985) in acid leach studies reported the chalcopyrite surface to be passivated by a copper sulphide layer 2.9 nm thick, and the copper sulphide passivating layer was said to remain stable under open circuit for many hours.

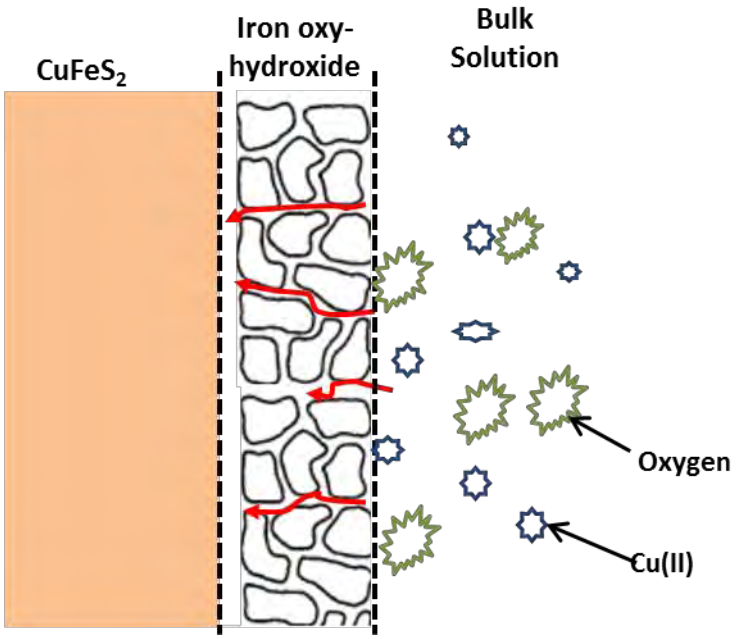

Figure 8.6. Illustration of copper(II) transport through a porous iron oxy-hydroxide surface deposit layer

Both ion and electron transport through oxides can be slow. Metal ions and oxygen anions tend to be the hardest species to move as both are large and can firmly attach to the oxide lattice (Bunker and Casey, 2016). Crundwell (2013) highlighted a significant difference between the transport of electrons and atomic ions pointing out that electrons are quantum particles which do not need to rise over some activation barrier like atomic ions. The author (Crundwell, 2013) went on to argue against the passivation of mineral surfaces by surface deposit layers of small thickness (such as the 2.9 nm indicated to be the thickness of the passivating layer by Biegler and Horne (1985)), pointing out that electrons could tunnel across distances up to 3 nm thick. This was supported by Fisher and Giaever (1961) who reported on electron tunnelling through thin insulating layers pointing out that oxide films showed ohmic behaviour, and Duke (1969), who illustrated the features of current-voltage characteristics through insulating layers less than 5 nm thick, indicating that at such thickness, electron tunnelling satisfactorily accounted for the observed conductivity. Doblhofer and Ulstrup (1977) reported that electrons were transported across insulating films on stainless steel and platinum through tunnelling and/or through electron hopping. Crundwell (2015) went further and

proposed electron tunnelling and hoping as part explanation for a semiconductor mechanism of dissolution of chalcopyrite in which he refuted the passivation theory.

Electron transport through iron oxy-hydroxides at 25°C was evaluated by Alexandrov and Rosso (2014) using density functional theory based calculations, they reported that electrons moved through small polaron hopping. This is in agreement with Larese-Casanova (2006) who reported on a similar mechanism i.e. facile electron hopping and that adsorption of soluble iron from solution created centres migrating through the bulk iron oxy-hydroxide lattice. Xu et al (2013) demonstrated how the large surface area of amorphous iron oxy-hydroxide increased the capacity for lithium storage thus increasing the discharge capacity of anodes in lithium batteries. In general, the "doping" of amorphous iron oxide to improve current discharge is a well-researched area (Yang et al, 2014; Wang and Hebert, 1999; Cahan and Chen, 1982) and an attempt will be made to explain some of the phenomena of surface deposit effects on chalcopyrite leaching based on this.

In the current study, copper(II) can both diffuse through, as well as adsorb onto the iron-oxy-hydroxide surface layer. This allows for electron migration to take place directly on the mineral surface as it would occur on pristine chalcopyrite surfaces, and this "direct" electron transfer is expected to increase with an increase in extent of prior oxidation of the electrode because oxidation roughens the mineral surface there by increasing its surface area. It could also be considered that by adsorbing onto the surface deposit layer (which has been established to have a large surface area), concentrations copper(II) ions near the mineral surface build up there by allowing for increased reaction rates. Furthermore, apart from these "direct" transfer methods, electron transfer could proceed indirectly through electron tunnelling and the electron hopping mechanism (Crundwell, 2015; Alexandrov and Rosso, 2014; Larese-Carsanova and Scherer, 2007) in the surface deposit layer. This offers plausible explanation for the increases in cathodic currents observed in the presence of surface deposit layers in that as the iron oxy-hydroxide layer grew in thickness, more copper(II) was adsorbed and electron migration was promoted. In such a case, the adsorption of copper(II) onto the surface deposit layer counters the surface deposit layer's otherwise resistor-like properties and electron migration is promoted. Also, at a fixed agitation speed, current densities reached steady state within the initial 10 min of the reaction, which is an indication there were no further changes on the steady-state established on the mineral-electrolyte interphase.

Considering that the same electron migration pathways could well be employed in the anodic reaction, it is thought that the decrease in anodic currents observed in the extended duration polarisation tests carried out in solutions that did not contain copper(II), is due to the poor electrical conductive nature of the surface deposits. Iron oxy-hydroxides are typically described as wide band

conductors to insulators (Alexandrov and Rosso, 2014). There is an apparent contradiction in the effects of the surface deposit layer on the anodic and cathodic currents; with the former decreasing while the later increased with growth of the surface deposits. Thus, it must be pointed out that although the leading discussion has argued against the notion of passivation of the mineral surface, pointing out that electron transport could still proceed through a surface deposit layer, the thickness of this surface deposit layer and possible adsorption of ions from the electrolyte influence the overall "ohmic" behaviour of the surface deposit layer. Hence, the effect of the surface deposit layer on current densities in constant potential tests differed between anodic and cathodic tests and this is thought to be due to the absence and presence of copper(II) ions in test solutions respectively. It is emphasised that electrochemistry results from the current study in both cyclic sweeps (Figure 4.19 and 4.2) and constant potential tests (Figure 4.13b) did no exhibit the trends typical of passivation or pseudo-passivation as described by Viramontes-Gamboa et al (2007) and Ghahremaninezhad et al (2010).

To explain the effect of the surface deposit layer on anodic current densities, an equivalent electrical circuit for the electrochemical cell with an external potential source (Figure 8.7) will be referred to. The circuit shows the cell to have two resistors in series, with R_1 thought to be the resistance on the mineral surface due to the surface deposit layer and R_2 being the resistance due to the electrolyte which was found to be negligible at low current densities such as those measured in the anodic reaction but was significant at the high current densities measured for the cathodic reaction. A capacitor is shown and this accounts for the overall capacitance on the mineral surface. It must be pointed out that constant potential-time transients showed initial spikes in both anodic and cathodic currents and these are accepted to be due to the charging of the electric double layer which behaves like a capacitor. Ghahremaninezhad et al (2010) also made reference to the capacitance of the surface deposits formed on the chalcopyrite surface during acid leaching where he employed Electrochemical Impedance Spectroscopy (EIS) to study surface deposits in sulphuric acid solutions. Furthermore, the aspect on the use of iron oxy-hydroxides for their large capacitance properties was mentioned above and is supported by several other reports (Shiue et al, 2003; Kozin, 2014; Chen et al, 2013) with Shiue et al (2003) having patented a method which can see the iron oxy-hydroxides used as supercapacitors with a capacitance, as high as 0.5 Fcm^{-2} in lithium battery making. Hence, it is reiterated that the iron oxy-hydroxides capacitance properties are emphasised in the presence of adsorbed copper(II) ions thus this capacitance is not expected to change significantly in test solutions that do not contain copper(II) ions. Furthermore it is postulated that copper(I) is also adsorbed hence remains available for re-oxidation through faradaic reactions, in the absence of effective mass transport.

Referring back to Figure 8.7, as the surface deposit layer grows in thickness, so does the potential drop associated with R1. It is therefore logical that the measured current density response decreases with an increase in thickness of the surface deposit layer. If the anode was polarised in solutions that contain initial copper(II) as done in the constant potential tests (Figure 4.16) and the cyclic sweeps (Figure 4.17, and Figure 4.18), it would have been expected that the copper(II) in solution would adsorb onto the growing surface deposit layer such that the overall effect would be an increasing resistance and continuous charging of the increasing capacitor size. Since the true effect of surface deposit layer on anodic currents could only be observed in long term tests, the results generated in the current study do not adequately show what impact the surface deposit layer would have on anodic current densities in solutions that contained copper(II). However, this can be inferred from the cyclic voltammograms (Figure 4.17, Figure 4.18 and Figure **5.9**) which consistently showed hysteresis between the forward and backward sweeps. It is proposed that in the forward sweep, as currents increased the surface deposit layer, albeit at a few atoms in thickness, would be charging hence slightly over estimating the current response of the mineral surface and on the reverse sweep as potentials decrease, this surface deposit layer capacitor would be discharging hence underestimating the current response of the mineral surface. Thus, it is thought that the true current response of the mineral surface lies somewhere between the forward and reverse anodic curve. Hysteresis was also observed on the cathodic branches, in which the cyclic sweep started at anodic potentials thereby generating surface deposits (Figure 5.9). By contrast, sweeps that started in the cathodic direction and hence had no surface deposits formed on them (Figure 5.4), exhibited negligible hysteresis.

It is reiterated that in solutions that contain copper(II), such as those in which cathodic tests were carried out, the iron oxy-hydroxide surface deposit was allowed to build up prior to starting the experiment during prior oxidation. It is assumed that there was negligible further growth, if any, of this surface deposit layer during cathodic tests, since potentials where at that stage set to be negative. Thus, current densities would be expected to reach steady state unless other factors, either than the gradual growth of a surface deposit layer, were of influence. In the anodic tests, the surface deposit layer gradually grows as the chalcopyrite is being oxidised during the test; also there are no copper(II) ions in solution to adsorb onto the “typically wide band conductors to insulators” (Alexandrov and Rosso, 2014) surface deposit and improve its electron conductivity.

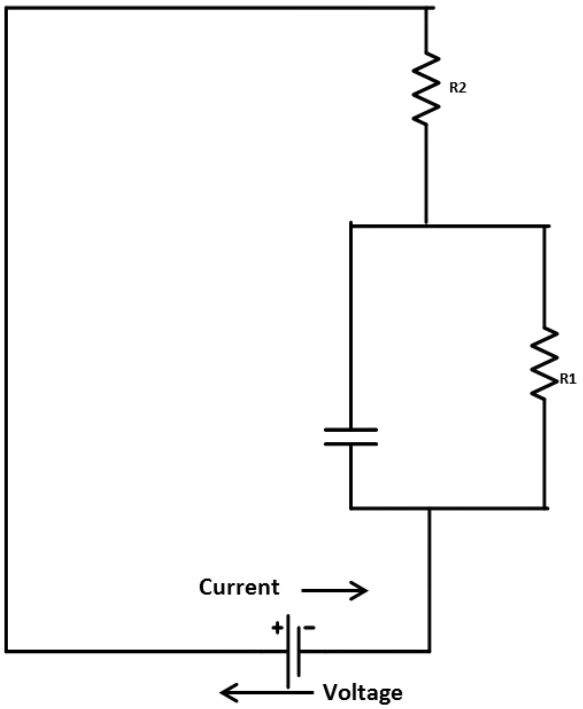

Figure 8.7. Electrical cell equivalent of an electrochemical cell when a surface deposit layer has formed.

In leach tests, the reaction takes place at open circuit, i.e. the reaction is not driven by an externally imposed potential, rather, the reaction proceeds through

i. The transport of electrons from the sulphur in the mineral lattice to the copper(II) in solution.
ii. The transport of the oxidant copper(II) to the mineral surface

Transport of electrons through a surface deposit layer growing on the mineral surface has been proposed to be able to proceed through electron tunnelling and hoping which are promoted by the adsorption of copper(II) onto the iron oxy-hydroxide surface product which is also known to be of a large surface area. Despite the fact that no direct contact is necessary between the mineral surface and the oxidant, it is still necessary that copper(II) be present on the mineral surface and in the vicinity of the mineral surface. This concentration of copper(II) can be lowered by its consumption by the oxidation reaction which results in the build-up copper(I). It was shown (section 5.4) that although the reduction of copper (II) was favoured in a kinetic sense, this reaction was limited by the transport of copper(I) away from the mineral surface.

In electrochemical tests where oxygen was introduced, it was shown to promote the cathodic reaction and this was thought to be due to the fact that oxygen could then oxidise some of the copper(I) which was responsible for contributions of anodic currents to the overall cathodic reaction (section 5.4). In bulk leach tests, presence of oxygen was also shown to promote the leaching

reaction (Figure 6.7). Thus, it is proposed that the overall leaching of chalcopyrite is both kinetically controlled in terms of the anodic charge transfer reaction and mass transport controlled with regards to the transport of copper(I) away from the mineral surface and possibly its desorption from the surface deposit layer. Presence of oxygen and its mass transport is likely to impact on the aspects to do with the mass transport of copper (I). It is expected that with adequate oxygen mass transport into the surface layer, the copper(I) would be oxidised in situ. In iron oxy-hydroxides, the hydroxyl groups represent a broken metal-oxygen bond, facilitating the transport of both cations and anions in the lattice (Bunker and Casey, 2016), so both copper and oxygen can be transported through the surface deposit layer. Wang et al (Wang and Hebert, 1999) studied metal and oxygen transport in amorphous anodic oxide films and reported that vacancy clusters were created by the inward displacement of oxygen ions and proposed the rate limiting step to be the jump of the oxygen vacancy cluster. Thus it can be assumed that in situ oxidation of the copper(I) would be slower than its transport to the bulk solution where it can then be oxidised. It is appreciated that oxygen is crucial in the leaching reaction because of its role not only in the regeneration of the oxidant but also in preventing the accumulation of copper(I) which would otherwise affect potentials (Section 4.1)and hence the overall leaching reaction.

Comparison of leaching rates determined from bulk leach tests to that of chronoamperometry tests has been done using the 1 M (NH_3+NH_4^+) chronoamperometric tests with potentials set to the equivalent of chalcopyrite's mixed potential in similar solutions but that did not contain initial copper(II) (data presented in Figure 4.1a) and the leach rates from the 1 M (NH_3+NH_4^+) over the first 4 hours (data presented in Figure 6.3). Both rates were converted to current densities using the method described in section 3.2.3 and bulk leach tests gave a leaching rate of 5.33 μAcm^{-2} while the constant potential test gave a rate of 5.87 μAcm^{-2}. Thus it is demonstrated that under the test condition for which this comparison was done, electrochemical tests gave a good approximation of the bulk leaching rates of chalcopyrite under similar solution conditions. It should be emphasised that this comparison was done only for initial leaching rates for periods of time in which surface deposits were not significant enough to affect the reaction kinetics, as well as where solution conditions had not changed substantially in either reactor. It is not expected that these results would have such consistency when compared for tests in which the reaction had progressed such that in either test, surface deposit layers were interfering with the reaction. It is thought that maintaining reaction conditions as the reaction proceeds between electrochemistry and bulk leaching tests may be increasingly difficult because;

- differences in hydrodynamics between the two reactors may come into effect with possible particle collision and abrasion in bulk leach tests, and
- bulk leach tests usually use larger sample and will thus have higher concentrations of copper(II) in solution. The copper(II) has been shown to be the oxidant thus at larger concentrations, which implies the reaction would have a larger driving force compared to one running at a fixed potential. Furthermore, increasing copper concentrations in solution take up free ammonia, which will result in changes in the ammonia-ammonium equilibrium and hence the pH, which are all parameters which have been shown to affect the reaction at certain concentrations.

9 Conclusion

This study has made significant contributions to understanding the fundamental reactions in the free dissolution of chalcopyrite in ammoniacal solutions. Electrochemical tests through measuring mixed potentials; then using constant potential tests to determine the dissolution current density of chalcopyrite at the measured mixed potentials, have been shown to adequately predict the initial leaching rates of bulk leach tests. This approach of measuring mixed potentials, then using constant potential tests to establish dissolution current densities at mixed potential and potentials in the vicinity of mixed potential (±50 mV within the vicinity of the mixed potential) has been demonstrated to be an effective way of evaluating the reactions that take place on chalcopyrite surfaces during free dissolution. By so doing, the importance of the mixed potential theory has been reiterated.

The role of copper(II) ions which was in question at the onset of this study has been established. A mixed potential was shown to be established between the chalcopyrite surface and copper(II) in solution in the presence and absence of oxygen. The ammoniacal leaching of chalcopyrite has been established to proceed via the copper(I)/Copper(II) couple, which is highly reversible on the chalcopyrite surface. Mixed potentials of chalcopyrite in ammoniacal solutions were seen to increase gradually with time while anodic current densities showed continuous gradual decrease with time. These trends were linked to the precipitation and growth of an iron oxy-hydroxide surface deposit layer on the mineral surface. The oxidation reaction was determined to be a 7 - 8 electron transfer reaction (Section 4.2.6), resulting in the formation of intermediate $S_2O_3^{2-}$, Fe(II) and Cu(I)/Cu(II). Further oxidation of these intermediate species has been proposed to take place in solution as non-Faradaic reactions.

The cathodic reaction was shown to be that of the reduction of copper(II) on the chalcopyrite surface, generating copper(I). Thus, in the overall surface reaction, copper(I) is generated by the cathodic reaction through copper(II) reduction (Equation 5.1) and the anodic reaction through chalcopyrite oxidation (Equation 4.5). It was shown through cathodic tests, that this copper(I), if not immediately transported away from the mineral surface, was oxidised at the potentials in which the cathodic reaction study was carried out. This resulted in positive currents being contributed to the overall currents measured at cathodic potentials. The observation that the magnitude of these positive currents was dependant on the rate of the transport of copper(I) away from the electrode surface (Figure 5.21), gave the overall measured cathodic currents Levich-like characteristics. Despite the observed dependence of the overall cathodic reaction on mass transport, it was established to be kinetically faster than the anodic reaction.

Since the cathodic reaction was found to be highly reversible, the overall chalcopyrite dissolution reaction was concluded to be anodically controlled in conditions where a surface deposit layer had not built-up to a thickness of any consequential bearing on the reaction. This was proven by the high rate constant of the cathodic reaction which was determined to be over 5 orders of magnitude higher than that of the anodic reaction. The presence or absence of oxygen was found to have no significant effect on the anodic reaction but to promote the cathodic reaction. It was shown that in the *absence* of copper(II), cathodic currents measured in the presence of oxygen were not significant. However, oxygen caused increased cathodic currents in solutions that contained copper(II). Thus the role of oxygen was concluded to be that of regenerating copper(II), by oxidising the copper(I) generated as a product of the chalcopyrite oxidation and the copper(II) reduction reactions. This disproves the hypothesis presented at the beginning of the study that an intermediate copper(II)-oxygen species is formed. However, copper(II) and oxygen are concluded to have synergistic effects on the overall reaction.

A surface deposit layer is formed during the oxidation reaction and it comprises 90% amorphous iron oxy-hydroxide and 10% crystalline polymorphs of iron-oxy-hydroxides. Sulphur was found to be present in very small quantities on the surface deposit layer and this is concluded to have been sulphur from the oxidising chalcopyrite which was still to migrate out of the surface deposit layer. This observation was supported by the apparent absence of sulphur on the residue of completely leached chalcopyrite while surface deposits on partially leached chalcopyrite and that on the chalcopyrite electrode showed presence of small quantities of sulphur. The surface deposit layer was found to be porous and of large surface area. It was concluded that while presence of the surface deposit layer influenced the overall reaction, it did not passivate the mineral surface.

The mechanism of reaction was proposed to proceed via the transfer of electrons from the chalcopyrite to the copper(II) at the electrode electrolyte interphase. The iron oxy-hydroxide that nucleates and grows on the surface of the mineral adsorbs copper(II)/copper(I) ions and this allows it to have some form of ohmic behaviour. Thus, electron transfer proceeds on the mineral surface either directly to the copper(II) that diffuses through the porous iron oxy-hydroxide surface deposit layer and through electron hopping and tunnelling across the surface deposit layer to the solid-electrolyte interphase.

Chalcopyrite was concluded to dissolve preferentially along grain boundaries and cracks in ammonia-ammonium carbonate solutions and in ammonia-ammonium perchlorate solutions while in the ammonia-ammonium sulphate solutions there was no apparent indication of such preferential dissolution. Thus, the mineral was concluded to dissolve uniformly across the mineral surface in

ammonia-ammonium sulphate solutions. The formation and growth of the surface deposit layer was influenced by the anion in solution, in the case of this study, the anion was introduced as an ammonium salt to make ammoniacal buffer solutions. The hydrodynamic environment, in the sense of allowing for the leaching particles to swirl around the rector and hence, allow for abrasion, was of consequence to the formation of surface deposits and hence the kinetics of the leaching reaction. This was evident from the low copper extraction rate (14.7%) in a reactor in which no abrasion agent i.e. glass beads were incorporated into the feed compared to a 54.9% extraction in a reactor operating under similar conditions but with glass beads.

Electrochemistry tests were able to adequately predict the bulk leaching of chalcopyrite only in the early stages, prior to the growth of significant surface deposit layers, as well as before any appreciable changes in solution conditions. In long term tests, solution conditions change due to differences in quantities of copper in solution; differences in thickness of surface deposit layer as well as the differences in hydrodynamic environment around leaching chalcopyrite, which makes it difficult to correlate long term bulk leaching tests to electrochemical tests. While electrochemistry tests cannot adequately predict the long term leaching of chalcopyrite, the tests adequately predict initial kinetics and thus can be used to understand surface reactions taking place on the chalcopyrite surface during leaching. However, electrochemistry results should be used in conjunction with equally detailed bulk leaching tests when it is desired to formulate a comprehensive leaching model.

10 Future Work

While this study made known the role of the copper redox couple in ammoniacal chalcopyrite leaching and how surface deposits affect the rate of reaction, it also brought to attention several aspects of electrochemical studies of chalcopyrite leaching that limit its use as a reliable means to predict leaching kinetics and mechanisms.

Longer term electrochemical anodic oxidation tests with the build-up of surface deposit layers of significant thickness need to be carried out. Results from these can then be modelled and compared to bulk leach tests. It is recommended that more comprehensive bulk leach tests using mono-sized particles be done for effective comparisons. Furthermore, it is recommended that further work be done on the analysis of the surface deposit layer and the inferred ohmic behaviour be validated as well as the influence of adsorbed ions on this “ohmic” behaviour.

Results from the influence of the choice of anion were quite interesting and more comprehensive tests are recommended for the carbonate system which appears promising as it can potentially overcome the surface deposit problems encountered in the sulphate system. While the surface deposit analysis reported on the presence of sulphur, it should be pointed out no further work was done to track the deportment of sulphur in this thesis and thus it is recommended that future studies in this area look into the deportment of sulphur. Furthermore, it is recommended that electrochemistry tests should be accompanied by some bulk leach tests to validate the results at it has been demonstrated that these can easily give false impressions as they can potentially address only what happened at the onset of reaction but not factor in changes which take place with progression of the reaction to scales typically experienced in industrial plants.

List of references

Ahlberg, E., Forseeberg, K.S.E. and Wang, X. 1990. The Surface Oxidation of Pyrite in Alkaline Solution. *Journal of Applied Electrochemistry.* 20(6):1033-1039.

Alexandrov, V. and Rosso, K.M.x. 2014. Electron transport in pure and substituted iron oxyhydroxides by small-polaron migration. *The Journal of Chemical Physics.* 140(23):234701.

AQM Copper Inc 2015. *Copper Fundamentals.* Available: http://www.aqmcopper.com/s/copperfundamentals.asp.

Arbiter, N. and McNulty, T. 1999. Ammonia leaching of copper sulphide concentrates. *Proceedings of Copper 99-Hydrometallurgy of Copper.* 4:197-212.

Asselin, E. 2011. Thermochemistry of the Fe, Ni and Co-NH3-H2O system as they relate to the Caron process: a review. *Minerals and Metallurgical Processing.* 28(4):169-175.

Aylmore, M.G. and Muir, D.M. 2001. Thiosulphate leaching of gold - A review. *Minerals Engineering.* 14(2):135-174.

Bard, A.J. and Faulkner, L.R. 2001. *Electrochemical Methods. Fundamentals and Applications.* 2nd edition. John Wiley and Sons Inc, USA.

Bbaba, A.A., Ghosh, M.K., Pradhan, S.R., Rao, D.S., Baral, A. and Adekola, F.A. 2014. Characterization and kinetic study on ammonia leaching of complex copper ore. *Transactions of Nonferrous Metals Society of China.* 24:1587-1595.

Beckstead, L. and Miller, J. 1977a. Ammonia, oxidation leaching of chalcopyrite —reaction kinetics. *Metallurgical and Materials Transactions B.* 8(1):19-29.

Beckstead, L. and Miller, J. 1977b. Ammonia, oxidation leaching of chalcopyrite —surface deposit effects. *Metallurgical and Materials Transactions B.* 8(1):31-38.

Bell, S.L., Welch, G.D. and Bennett, P.G. 1995. Development of ammoniacal lixiviants for the in-situ leaching of chalcopyrite. *Hydrometallurgy.* 39(1–3):11-23.

Bertini, M.M. and Duby, P.F. 2003. Leaching of chalcopyrite in ammoniacal solutions sparged with SO_2/O_2 gas mixture. *Hydrometallurgy 2003 - Fifth International Conference in Honour of Professor Ian Ritchie, Volume 1: Leaching and Solution Purification.* August 24-27. C. Young, A. Alfantazi, C. Anderson, D. Dreisinger, B. Harris and A. James, Eds. Vancouver, Canada: Met Society. 431.

Biegler, T. and Horne, M.D. 1985. The Electrochemistry of Surface Oxidation of Chalcopyrite. *Journal of the Electrochemical Society.* 132(6):1363-1369.

Biegler, T. and Swift, D.A. 1979. Anodic electrochemistry of chalcopyrite. *Journal of Applied Electrochemistry.* 9(5):545-554.

Black, Silvia Beatriz. 2006. The thermodynamic chemistry of the aqueous copper-ammonia thiosulfate system. PhD thesis, Murdoch University

Bockris, J.O., Reddy, A.K.N. and Gamboa-Aldeco, M. 2000. *Modern Electrochemistry 2A.* 2nd edition. New York: Academic Publishers.

Breuer, P.L. and Jeffrey, M.I. 2003. The reduction of copper(II) and the oxidation of thiosulfate and oxysulfur anions in gold leaching solutions. *Hydrometallurgy.* 70(1–3):163-173.

Buckley, A.N. and Woods, R. 1987. The surface oxidation of pyrite. *Applied Surface Science.* 27(4):437-452.

Buckley, A.N. and Woods, R. 1991. Electrochemical and XPS studies of the surface oxidation of synthetic heazlewoodite (Ni3S2). *Journal of Applied Electrochemistry.* 21(7):575-582.

Bunker, B.C. and Casey, W.H. 2016. *The Aqueous Chemistry of Oxides.* 1st ed. UK: Oxford University Press.

Byerley,J., Founda, S. and Rempel, G. 1975. Activation of Copper(II) Ammine Complexes by Molecular Oxygen for the Oxidation of Thiosulphate Ions. *Journal of the Chemical Society, Dalton Transactions.* (13):1329-1338.

Byerley, J.J., Fouda, S.A. and Rempel, G.L. 1973. Kinetics and mechanism of the oxidation of thiosulphate ions by copper(II) ions in aqueous ammonia solution. *Journal of the Chemical Society, Dalton Transactions.* (8):889-893.

Cahan, B.D. and Chen, C. 1982. The Nature of the Passive Film on Iron III . The Chemi-Conductor Model and Further Supporting Evidence. *Journal of the Electrochemical Society.* 129(5):921-925.

Caldeira, C.L., Ciminelli, V.S.T. and Osseo-assare, K. 2008. Pyrite Oxidation in Alkaline Solutions: The Carbonate Effect. *Hydrometallurgy 2008: Proceedings of the Sixth International Symposium.* 17th-20th August 2008. C.A. Young, P.R. Taylor, C.G. Anderson and Y. Choi, Eds. Colorado, USA: Society for Mining,Metallurgy and Exploration, Inc. 990.

Caron, M.H. 1950. Fundamental and Practical Factors in Ammoniacal Leaching of Nickel and Cobalt Ores. *Journal of Metals.* 188:67-90.

Chander, S., Briceno, A. and Pang, J. 1992. On the mechanism of sulphur oxidation in pyrite. February 24-27, 1992.

Chandra, Y.L.A.P. and Gerson, A.R. 2014. Scanning photoelectron microscopy studies of freshly fractured chalcopyrite exposed to O2and H2O. *Geochemica Et Cosmochimica Acta.* 133:372-386.

Chao, C.W., Lan, Y.P., Shiue, L.R., Wu, D.S. and Wu, N.L. - *Electrochemical capacitor with electrode material for energy storage.* - Google Patents.

Chen, X., Yi, Z., Xianhong, R., Jixin, Z., Huiteng, T., Antonio, G.C., Toribio, J., Juan, B. 2013. Amorphous Iron Oxyhydroxide Nanosheets: Synthesis, Li Storage, and Conversion Reaction Kinetics. *The Journal of Physical Chemistry.* 117(34):17462-17469.

Cheng, L. 2003. Fundamental Aspects of Gold Leaching in Thiosulphate Solutions. MSc Thesis. University of British Columbia.

Chesne, R.B. and Kim, C.S. 2014. Zn(II) and Cu(II) adsorption and retention onto iron oxyhydroxide nanoparticles: effects of particle aggregation and salinity. *Geochemical Transactions.* 15(6).

Chmielewski, T., Wodka, J. and Iwachow, L. 2009. Ammonia Pressure Leaching for Lubin Shale Middlings. *Physicochemical Problems of Mineral Processing.* 43:5-20.

Christie, T. and Brathwaite, B. *Mineral Commodity Report 4-Copper.* Available: http://www.nzpam.govt.nz/cms/pdf-library/minerals/publications/Commodity%20Reports/report04_copper.pdf.

Coelho, A. 2007. *TOPAS-Academic, Coelho Software.* Brisbane, Australia

Córdoba, E.M., Muñoz, J.A., Blázquez, M.L., González, F. and Ballester, A. 2009. Passivation of chalcopyrite during its chemical leaching with ferric ion at 68 °C. *Minerals Engineering.* 22(3):229-235.

Crundwell, F.K. 2013. The dissolution and leaching of minerals: Mechanisms, myths and misunderstandings. *Hydrometallurgy.* 139:132-148.

Crundwell, F.K. 2015. The Semiconductor mechanism of dissolution and the pseudo-passivation of chalcopyrite. *Canadian Metallurgical Quarterly.* 54(3):279-288.

Cussler, E.L. 2009. *Diffusion - Mass Transfer in Fluid Systems.* 3rd edition. Cambridge: Cambridge University Press.

D'Aloya, A. and Nikoloski, A.N. 2012. The passivation of iron in ammoniacal solutions containing copper (II) ions. *Hydrometallurgy.* 111–112(0):58-64.

Das, R.P., Anand,S. 1995. Precipitation of iron oxides from ammonia-ammonium sulphate solutions. *Hydrometallurgy.* 38(2):161-173.

Dixon, C.J. 1979. *Atlas of Economic Mineral Deposits.* London: Chapman and Hall.

Doblhofer,K., Ulstrup,J. 1977. Effectof Localised Electronic States on Simple Electron Transfere Reactions at Film-Covered Electrodes. *Journal De Physique Colloques.* 38(C5):C5-49-C5-55.

Doebrich, J. 2009. *Copper-A metal for the ages.* USA: USGS.

Dreisinger, D. 2006. Copper leaching from primary sulfides: Options for biological and chemical extraction of copper. *Hydrometallurgy.* 83(1–4):10-20.

Duke, C.B. 1969. Theory of Metal-Barrier-Metal Tunneling. In *Tunneling Phenomena in Solids.* E. Burstein and S. Lundqvist, Eds. USA: Springer US. 31-46.

Dutrizac, J.E. 1992. The leaching of sulphide minerals in chloride media. *Hydrometallurgy.* 29(1–3):1-45.

Dutrow, B.L. and Clark, C.M. *X-ray Powder Diffraction (XRD).* Available: http://serc.carleton.edu/research_education/geochemsheets/techniques/XRD.html.

Duyvesteyn, P.C. and Sabacky, B.J. 1993. The Escondida Process for Copper Concentrates. *The Paul Queneau International Symposium, Fundamental Aspects.* 1:881-910.

Duyvesteyn, P.C.W. 1995. The development of the Escondida Leach Process and its Implementation in the Escondida Copper Cathode Plant. *World's Best Practice in Mining and Processing Conference.* 17-18May 1995. Sydney: Carlton, Vic. : The Institute, ©1995. 29-42.

Ek, C., Frenay, J. and Herman, J. 1982. Oxidized copper phase precipitation in ammoniacal leaching — the influence of ammonium salt additions. *Hydrometallurgy.* 8(1):17-26.

Elsherief, A.E. 2002. The influence of cathodic reduction, Fe2+ and Cu2+ ions on the electrochemical dissolution of chalcopyrite in acidic solution. *Minerals Engineering.* 15(4):215-223.

Everret D.H. and Wynn-Jones, W.F. 1938. The Dissolution of the Ammonium Ion and the Basic Strength of Ammonia in Water. *Proceedings of the Royal Society of London. Series A.* 169(937):190-204.

Feng, D. and Van Deventer, J.S.J. 2002. Leaching behaviour of sulphides in ammoniacal thiosulphate systems. *Hydrometallurgy.* 63(2):189-200.

Filmer, A.O., Parker, A.J. and Wadley, L.G.B. 1979. Oxidation of copper sulphides in aqueous ammonia. 1 formation of sulphur. *Australian Journal of Chemistry.* 32:961-973.

Fisher, J.C. and Giaever, I. 1961. Tunnelling Through Thin Insulating Layers. *Journal of Applied Physics.* 32(2):172.

Forward, F.A. and Mackiw, V.N. 1955. Chemistry of Ammonia Pressure Process for Leaching Ni, Cu, and Co from Sherritt Gordon Sulphide Concentrates. *Transactions AIME, Journal of Metals.* :457-463.

Free, M.L. 2013. *Hydrometallurgy Fundamentals and Applications.* Canada: John Wiley and Sons.

Fuentes-Aceituno, J.C., Lapidus, G.T. and Doyle, F.M. 2008. A kinetic study of the electro-assisted reduction of chalcopyrite. *Hydrometallurgy.* 92(1–2):26-33.

Gardner, J.R. and Woods, R. 1979. An electrochemical investigation of the natural flotability of chalcopyrite. *International Journal of Mineral Processing.* 6(1):1-16.

Geology.com 2016. ***Chalcopyrite-***
The world's most important ore of copper for at least five thousand years.. Available: http://geology.com/minerals/chalcopyrite.shtml.

Geng, M. and Duan, Z. 2010. Prediction of oxygen solubility in pure water and brines up to high temperatures and pressures. *Geochimica Et Cosmochimica Acta.* 74(19):5631-5640.

Ghahremaninezhad, A. 2012. The surface chemistry of chalcopyrite during electrochemical dissolution. PhD Thesis. University of British Colombia.

Ghahremaninezhad, A., Asselin, E. and Dixon, D.G. 2010. Electrochemical evaluation of the surface of chalcopyrite during dissolution in sulfuric acid solution. *Electrochimica Acta.* 55(18):5041-5056.

Goodge, J. 2016. *Energy-Dispersive X-Ray Spectroscopy (EDS).* Available: http://serc.carleton.edu/research_education/geochemsheets/eds.html

Guan, Y. and Han, K. 1997. The leaching kinetics of chalcopyrite (CuFeS2) in ammonium iodide solutions with iodine. *Metallurgical and Materials Transactions B.* 28(6):979-985.

Guidelli, R., Compton, R.G., Feliu, J.M. and Gileadi, E. 2014. Defining the transfer coefficient in electrochemistry: An assessment (IUPAC Technical Report). *Pure Applied Chemistry.* 86(2):245-258.

Habashi, F. and Toor, T. 1979. Aqueous Oxidation of Chalcopyrite in Hydrochloric Acid. *Metallurgical and Materials Transactions B.* 10(1):49-56.

Habashi, F.2007. Abandoned but not forgotten. The Recent History of Copper Hydrometallurgy. *Copper 2007 - Cu2007 - Volume 4- 4 - the John E. Dutrizac International Symposium on Copper Hydrometallurgy.* August 25-30. Riveros,P., Dixon, D., Dreisinger,D., Collins,M., Ed. Toronto, Canada: The Canadian Institute of Mining, Metallurgy and Petroleum.

Habashi, F. and Bas, A.D. 2014. Evidence of the existence of cathodic and anodic zones during the leaching of minerals and metals. *Hydrometallurgy.* 144–145:148-150.

Hackl, R.P. 1995. Passivation of chalcopyrite during oxidative leaching in sulphate media. *Hydrometallurgy.* 39(1-3):25.

Hall, S.R. and Stewart, J.M. 1973. The Crystal Structure Refinement of Chalcopyrite, CuFeS2*. *Acta Crystallographica.* B29:579-585.

Hamilton, I.C. and Woods, R. 1981. An investigation of surface oxidation of pyrite and pyrrhotite by linear potential sweep voltammetry. *Journal of Electroanalytical Chemistry and Interfacial Electrochemistry.* 118(0):327-343.

Han, K.N. 2002. *Fundamentals of Aqueous Metallurgy.* Littleton Colorado, USA: Society of Mining, Metallurgy and Exploration.

Hathaway, B.J. and Tomlinson, A.A.G. 1970. Copper(II) ammonia complexes. *Coordination Chemistry Reviews.* 5(1):1-43.

Haver, R., Wang, M. 1971. Recovery of copper, iron, and sulphur from chalcopyrite concentrates using a ferric chloride leach. *Journal of Metals.* 23(2):25-29.

Havlik, T. 2008. *Hydrometallurgy- Principles and applications.* England: Cambridge International Science Publishing Limited in association with Woodhead Publishing Limited.

Hem, J.D. 1960. Some chemical relationships among sulphur species and dissolved ferrous iron. United States of America: United States Government Printing Office, Washington.

Hill, C.M., Kim, J. and Bard, A.J. 2015. Electrochemistry at a Metal Nanoparticle on a Tunnelling Film: A Steady-State Model of Current Densities at a Tunnelling Ultramicroelectrode. *Journal of the American Chemical Society.* 137(35):11321-11326.

Hinatsu, J.T. and Foulkes, F.R. 1989. Diffusion Coefficients for Copper (II) in Aqueous Cupric Sulphate-Sulfuric Acid Solutions. *Journal of the Electrochemical Society.* 136(1):125-132.

Hirato, T., Kinoshita, M., Awakura, Y. and Majima, H. 1986. The leaching of chalcopyrite with ferric chloride. *Metallurgical Transactions B.* 17(1):19-28.

Hirato, T., Majima, H. and Awakura, Y. 1987. *The leaching of chalcopyrite with ferric sulfate.* Springer Boston.

Hiroyoshi, N., Kuroiwa, S., Miki, H., Tsunekawa, M. and Hirajima, T. 2004. Synergistic effect of cupric and ferrous ions on active-passive behaviour in anodic dissolution of chalcopyrite in sulfuric acid solutions. *Hydrometallurgy.* 74(1–2):103-116.

Hiskey, J.B. 1993. Chalcopyrite Semiconductor Electrochemistry and Dissolution. In *The Paul E. Queneau International Symposium, Extractive Metallurgy of Copper, Nickel and Cobalt, Vol 1. Fundamental Aspects.* R.N.W. R.G.Reddy, Ed. Warrendale: TMS. 949-969.

Hiskey, J.B. and Wadsworth, M.E. 1981. Electrochemical processes in the Leaching of Metal Sulphides and Oxides. *Process and Fundamental Considerations of Selected Hydrometallurgical Systems. SME-AIME.* M.C. Kuhn, Ed. New York: SME. 303.

Holmes, P.R. and Crundwell, F.K. 2000. The kinetics of the oxidation of pyrite by ferric ions and dissolved oxygen: An electrochemical study. *Geochimica Et Cosmochimica Acta.* 64(2):263-274.

Itoh, T., Hisada, H., Usui, Y. and Fujii, Y. 1998. Hydrolysis of phosphate esters catalysed by copper(II)-triamine complexes. The effect of triamine ligands on the reactivity of the copper(II) catalysts. *Inorganica Chimica Acta.* 283(1):51-60.

Jansen, M. and Taylor, A. 1999. Overview of Gangue Minerology Issues in Oxide Copper Heap Leaching. (Unpublished).

Jones, D.L. 1974. The Leaching of Chalcopyrite. PhD. University of British Columbia.

Jones. D.L, P.E., 1976. The leaching of chalcopyrite with ferric sulphate and ferric chloride. *Extractive Metallurgy of Copper AIME.* :633-653.

Kametani, H. and Aoki, A. 1985. Effect of suspension potential on the oxidation rate of copper concentrate in a sulfuric acid solution. *Metallurgical and Materials Transactions B.* 16(4):695-705.

Kawashima, J.L.N., Kaplun, K., Absolon, V.J. and Gerson, A.R. 2010. Chalcopyrite leaching: The rate controlling factors. *Geochemica Et Cosmochimica Acta.* 74:2881-2893.

Kim, H.S., Kho, Y.T., Osseo-Assare, K. and Pickering, H.W. 1991. Active and Passive Behaviour of Sintered Iron in ammoniacal ammonium carbonate solution. *Metallurgical Transactions B.* 22(3):323-332.

Kim, J. and Bard, A.J. 2016. Application of the Koutecký-Levich Method to the Analysis of Steady State Voltammograms with Ultramicroelectrodes. *American Chemical Society Publications; Analytical Chemistry.* 88(3):1742-1747.

Kinoshita, K. 1992. *Electrochemical Oxygen Technology.* New Jersey: John Wiley and Sons Inc.

Klauber, C. 2008. A critical review of the surface chemistry of acidic ferric sulphate dissolution of chalcopyrite with regards to hindered dissolution. *International Journal of Mineral Processing.* 86(1–4):1-17.

Klocke,D.J. and Hixson,A.N. 1972. Solubility of Ferrous Iron in Aqueous Ammoniacal Solutions. *Industrial and Engineering Chemistry Process Design and Development.* 11(1):141-146.

Koyama, K., Tanaka, M. and Lee, J. 2006. Copper Leaching Behaviour from Waste Printed Circuit Board in Ammoniacal Alkaline Solution. *Materials Transactions.* 47(7):1788-1792.

Kozin, P.A. 2014. Charge Development at Iron Oxy-Hydroxide surface. The Interplay Between Surface Structure, Particle Morphorlogy and Counter Ion Identity. PhD. Umea University.

Kuhn, M.C., Arbiter, N. and and Kling, H. 1974. Anaconda's Arbiter process for copper. *CIM Bulletin.* 67:62-73.

Lee, J.W., Osseo-Assare, K. and Pickering, H.W. 1985. Anodic Dissolution of Iron in Ammoniacal Ammonium Carbonate Solution. *Journal of the Electrochemical Society.* 132:550-555.

Leussing, D.L. and Kolthoff, I.M. 1952. The Solubility Product of Ferrous Hydroxide and the Ionisation of the Aquo-Ferrous Ion. *American Chemical Society Journal.* 75:2476-2479.

Levenspiel, O. 1999. *Chemical Reaction Engineering.* Third edition ed. Wiley: New York.

Li, Y., Kawashima, N., Li, J., Chandra, A.P. and Gerson, A.R. 2013. A review of the structure, and fundamental mechanisms and kinetics of the leaching of chalcopyrite. *Advances in Colloid and Interface Science.* 197–198(0):1-32. Litch, S. and Davis, J. 1997. Disproportionation of Aqueous Sulphur and Sulphide: Kinetics of Polysulphide Decomposition. *Journal of Physical Chemistry B.* 101(14):2540-2545.

Liang, Y., Li, Y., Wang, H., Zhou, J., Wang, J., Regier, T. and Dai, H. 2011. Co_3O_4 nanocrystals on graphene as a synergistic catalyst for oxygen reduction reaction. *Nature Materials.* (10):780-786.

Litch, S. and Davis, J. 1997. Disproportionation of Aqueous Sulphur and Sulphide: Kinetics of Polysulphide Decomposition. *Journal of Physical Chemistry B.* 101(14):2540-2545.

Lu, Z.Y., Jeffrey, M.I. and Lawson, F. 2000. An electrochemical study of the effect of chloride ions on the dissolution of chalcopyrite in acidic solutions. *Hydrometallurgy.* 56(2):145-155.

Lundström, M., Aromaa, J., Forsén, O., Hyvärinen, O. and Barker, M.H. 2005. Leaching of chalcopyrite in cupric chloride solution. *Hydrometallurgy.* 77(1–2):89-95.

Lundström, M., Aromaa, J., Forsén, O., Hyvärinen, O. and Barker, M.H. 2007. Cathodic reactions of Cu2+ in cupric chloride solution. *Hydrometallurgy.* 85(1):9-16. Marianne, S. 2005. A Brief History of Copper.

Majima, H., Awakura, Y., Hirato, T. and Tanaka, T. 1985. The Leaching of Chalcopyrite in Ferric Chloride and Ferric Sulphate Solutions. *Canadian Metallurgical Quarterly.* 24(4):283-291.

Marianne, S. 2005. A Brief History of Copper. Unpublished work. (Unpublished).

Marsden, J.O. & Ian House, C. 2006. *The Chemistry of Gold Extraction.* Second ed. Colorado, USA: Society of Mining and Metallurgy.

Meng, X. and Han, K.N. 1996. The principles and applications of ammonia leaching of metals-A review. *Mineral Processing and Extractive Metallurgy Review.* 16:23-61.

mindat.com 2015. ***Chalcopyrite***. Available: http://www.mindat.org/min-955.html.

Mohapatra, M., Mohapatra, L., Singh, P., Anand, S. and Mishra, B.K. 2010. A comparative study on Pb(II), Cd(II), Cu (II), Co(II) adsorption from single and binary aqueous solutions on additive assisted nano-structured goethite. *International Journal of Engineering, Science and Technology.* 2(8):89-103.

Morgan, B. and Lahav, O. 2007. The effect of pH on the kinetics of spontaneous Fe(II) oxidation by O2 in aqueous solution – basic principles and a simple heuristic description. *Chemosphere.* 68(11):2080-2084.

Munoz.P.B., Miller,J.D. and Wadsworth.M.E. 1979. Reaction Mechanisms for the acid ferric sulphate leaching of chalcopyrite. *Metallurgical Transactions B.* 10B(2):149-158.

Muzawazi, C. 2013. Base Metal Heap and Tank Leaching of a Platreef Flotation Concentrate using Ammoniacal Solutions. MSc Thesis. University of Cape Town.

Muzawazi, C. and Petersen, J. 2015. Heap and tank leaching of copper and nickel from a Platreef flotation concentrate using ammoniacal solutions. *Canadian Metallurgical Quarterly.*

Mwase, J.M., Petersen, J. and Eksteen, J.J. 2012. A conceptual flowsheet for heap leaching of platinum group metals (PGMs) from a low-grade ore concentrate. *Hydrometallurgy.* 111–112:129-135.

Nabizadeh, A. and Aghazadeh, V. 2015. Dissolution study of chalcopyrite concentrate in oxidative ammonia/ammonium carbonate solutions at moderate temperature and ambient pressure. *Hydrometallurgy.* 152:61-68.

Narita, E., Lawson, F. and Han, K.N. 1983. Solubility of oxygen in aqueous electrolyte solutions. *Hydrometallurgy.* 10(1):21-37.

Needes, C.R.S., Nicol, M.J. and Finkelstein, N.P. 1975. An electrochemical model for the leaching of uranium dioxide. In *Leaching and Reduction in Hydrometallurgy.* A.R. Burkin, Ed. Institute of Mining and Metallurgy, London,. 1-11.

Nicol, M.J. Hydrometallurgy Notes. (Unpublished).

Nicol, M.J. 2013. Excel spreadsheet. Personal communication. (Unpublished).

Nicol, M.J., Nikoloski, A.N. and Fittock, J.E. 2004. A fundamental study of the leaching reactions involved in the Caron process. *Proceedings of the International Laterite Sympossium; 2004.* March 14-18, 2004. W.P. Imrie and D.M. Lane, Eds. North Carolina: TMS Wareendale. 369-384.

Nicol, M.J. 1993. The role of electrochemistry in hydrometallurgy. *Hydrometallurgy Fundamentals, Technology and Innovation. .* 1-5 August. M.E. Wadsworth, J.B. Hiskey and G.W. Warren, Eds. Littleton, Colo.: Society for Mining, Metallurgy, and Exploration. 43.

Nicol, M.J. and Lázaro, I. 2002. The role of EH measurements in the interpretation of the kinetics and mechanisms of the oxidation and leaching of sulphide minerals. *Hydrometallurgy.* 63(1):15-22.

Nicol, M., Miki, H. and Velásquez-Yévenes, L. 2010. The dissolution of chalcopyrite in chloride solutions: Part 3. Mechanisms. *Hydrometallurgy.* 103(1–4):86-95.

Nikoloski, A.,N. 2002. The Electrochemistry of the Leaching of Pre-reduced Nickel Laterites in Ammonia-Ammonium Carbonate Solution. PhD Thesis. Murdoch University.

Nikoloski,A,N. and Nicol,M,J. 2006. The electrochemistry of the Leaching Reactions in the Caron Process.1. Anodic Processes. *ECS Transactions.* 2:197-207.

Oldham, K.B. and Myland, J.C. 1994. *Fundamentals of Electrochemical Science.* United Kingdom: Academia Press Inc.

Olvera, O.G., Rebolledo, M. and Asselin, E. Atmospheric ferric sulphate leaching of chalcopyrite: Thermodynamics, kinetics and electrochemistry. *Hydrometallurgy.*

Osseo-Asare, K. and Asihene, S.W. 1979. Heterogeneous equilibria in ammonia laterite leaching systems. *Proceedings of the International Laterite Symposium. New Orleans Louisiana, AIME.* February 19-21. D.J.I. Evans, R.S. Shoemaker and H. Vetman, Eds. New York: Society of Mining Engineers of the American Institute of Mining, Metallurgical, and Petroleum Engineers.

Park, K., Mohapatra, D., Nam, C. and Kim, H. 2007a. A comparative study of different leaching processes for the extraction of Cu, Ni and Co from a complex matte. *Korean Journal of Chemical Engineering.* 24(5):835-842.

Park, K., Mohapatra, D., Reddy, B.R. and Nam, C. 2007b. A study on the oxidative ammonia/ammonium sulphate leaching of a complex (Cu–Ni–Co–Fe) matte. *Hydrometallurgy.* 86(3–4):164-171.

Parker, A., Paul, R. and- Power, G. 1981. Electrochemical aspects of leaching copper from chalcopyrite in ferric and cupric salt solutions. - *Australian Journal of Chemistry.* (1):-13-34.

Pavelka, M. and Burda, J.V. 2005. Theoretical description of copper Cu(I)/Cu(II) complexes in mixed ammine-aqua environment. DFT and ab initio quantum chemical study. *Chemical Physics.* 312(1–3):193-204.

Paynter, J.C. 1973. Review of Copper Hydrometallurgy. *Journal of South African Institute of Mining and Metallurgy.* 74:158-170.

Pearce, C.I., Pattrick, R.A.D., Vaughan, D.J., Henderson, C.M.B. and van der Laan, G. 2006. Copper oxidation state in chalcopyrite: Mixed Cu d9 and d10 characteristics. *Geochimica Et Cosmochimica Acta.* 70(18):4635-4642.

Peters, E. 1987. Oxygen Utilisation in Hydrometallurgy: Fundamental and Practical Issues. *The Impact of Oxygen on the Productivity of Non-Ferrous Metallurgical Processes. Vol.2. Proceedings of the Metallurgical Society of the Canadian Institute of Mining and Metallurgy.* August 23-26. G. Kachaniwsky and C. Newman, Eds. New York: Pergamon Press. 151.

Peters, E. 1976. Direct Leaching of sulphides: Chemistry and applications. *Metallurgical and Materials Transactions B.* 7(4):505-517. DOI:10.1007/BF02698582.

Power, G.P. and Ritchie, I.M. 1983. Mixed Potentials-Experimental Illustrations of an Important Concept in Practical Electrochemistry. *Journal of Chemical Education.* 60(12):1022-1026.

Pridmore, D.F. and Shuey, R.T. 1976. The electrical resistivity of galena, pyrite, and chalcopyrite. *American Mineralogist.* 61:248-259.

Pugaev, D. 2011. The Mechanisms of the Dissolution and Passivation of Base Metal Sulphide Minerals. PhD Thesis. Murdoch University.

Pugaev, D., Nicol, M.J. and Senanayake, G. 2011. The Mechanisms of the Passivation of Sulphide Minerals in Oxidative Leaching Processes. *6th Southern African Base Metals Conference 2011. Symposium Series S66.* 18-21 July 2011. RSA: The Southern African Institute of Mining and Metallurgy. 39.

Radmehr, V., Koleini, S.M.J., Khalesi, M.R. and Mohammadi, M.R.T. 2013. Ammonia Leaching: A New Approach of Copper Industry in Hydrometallurgical Processes. *Journal of the Institution of Engineers (India): Series D.* 94(2):95-104.

Rajib Dasguota, Y., Gaun, C. and Han, K.N. 1997. The electrochemical behaviour of gold in ammoniacal solutions at 75 degrees celsius. *Metallurgical and Materials Transactions B.* 28B(1):5-12.

Rand, D.A.J. and Woods, R. 1984. Eh measurements in sulphide mineral slurries. *International Journal of Mineral Processing.* 13(1):29-42.

Reilly, I.G. and Scott, D.S. 1977. The Leaching of Chalcopyrite Concentrate in Ammonia. *The Canadian Journal of Chemical Engineering.* 55:527-533.

Richardson, H.W. 1997. *Handbook of Copper Compounds and Applications.* USA: Marcel Dekker Inc.

Roman, R.J. and Benner, B.R. 1973. The Dissolution of Copper Concentrates. *Mineral Science Engineering.* 5(1):3.

Sadowski, Ł. 2010. New non-destructive method for linear polarisation resistance corrosion rate measurement. *Archives of Civil and Mechanical Engineering.* 10(2):109-116.

Safari, V., Arzpeyma, G., Rashchi, F. and Mostoufi, N. 2009. A shrinking particle—shrinking core model for leaching of a zinc ore containing silica. *International Journal of Mineral Processing.* 93(1):79-83.

Santos, L.G.R., Souza, A.D. Leao, V.A. 2008. Galvanic interactions during the bioleaching of mixed nickel sulphides. *Hydrometallurgy 2008 Proceedings of the Sixth International Symposium.* C.A. Young, P.R. Taylor, C.G. Anderson and Y. Choi, Eds. USA: Society for Mining, Metallurgy and Exploration Inc. 514.

Sarveswara Rao, K. and Ray, H.S. 1998. A new look at characterisation and oxidative ammonia leaching behaviour of multimetal sulphides. *Minerals Engineering.* 11(11):1011-1024.

Saveant, J. and Tessier, D. 1982. Variation of the Electrochemical Transfer Coefficient with Potential. *Faraday Discussions of the Chemical Society.* 74:57-72.

Senanayake, G. 2005a. The role of ligands and oxidants in thiosulphate leaching of gold. *Gold Bulletin.* 38(4):170-179.

Senanayake, G. 2005b. Role of copper(II), carbonate and sulphite in gold leaching and thiosulphate degradation by oxygenated alkaline non-ammoniacal solutions. *Minerals Engineering.* 18(4):409-426.

Shao-hua, J., Mo-tang, T., Sheng-hai, Y. and Chao-bo, T. 2005. Thermodynamics of Cu (n) - NH3 - NH4 CI-H2 0 system①. *Transactions of Nonferrous Metals Society of China.* 15(6):1414-1419.

Smythe, C.V. 1931. The mechanism of iron catalysis in certain oxidations. *Journal of Biological Chemistry.* (90):251-265.

Song, C. and Zhang, J. 2008. Electrocatalytic oxygen reduction reaction. In *PEM Fuel Cell Electrocatalysts and Catalyst Layers.* J. Zhang, Ed. London: Springer-London. 89-134.

Srinivasan, S. 2006. Electrode/Electrolyte Interfaces: Structure and Kinetics of Charge Transfer. In *Fuel Cells : From Fundamentals to Applications.* S. Srinivasan, Ed. USA: Springer. 27-92.

Stanczyk, M.H.:.R.C. 1966. *Oxidation Leaching of Copper Sulphides in Ammonia Pulps at Elevated Temperatures and Pressures.* (6808). US Bureau of Mines: USA.

Stojek, Z. 2005. The Electrical Double Layer and Its Structure. In *Electroanalytical Methods Guide to Experiments and Applications.* F. Scholz, and others, Eds. 2nd ed. Springer Berlin Heidelberg. 3-9.

Roy, S., 2010. Electrochemical Dissolution and Passivation Behaviour of Iron in Ammoniacal Caron Leaching Solution. MSc Thesis . The University of British Columbia.

Tomlinson, A.A.G. and Hathaway, B.J. 1968. The electronic properties and stereochemistry of the copper(II) ion. Part III. Some penta-ammine complexes. *Journal of the Chemical Society A: Inorganic, Physical, Theoretical.* :1905-1909.

Tomlinson, A.A.G., Hathaway, B.J., Billing, D.E. and Nichols, P. 1969. The electronic properties and stereochemistry of the copper(II) ion. Part V. The tetra-ammine complexes. *Journal of the Chemical Society A: Inorganic, Physical, Theoretical.* :65-71.

Tozawa, K., Umetsu, Y. and Sato, K. 1976. On Chemistry of Ammonia Leaching of Copper Concentrates. In *Extractive Metallurgy of Copper Vol 2.* J.C.A. J.C.Yannopoulos, Ed. AIME. 706.

Tromans, D. 1999. Oxygen solubility modelling in aqueous solutions. *Intelligent Processing and Manufacturing of Materials, 1999. IPMM '99. Proceedings of the Second International Conference on (Volume:1).* 10 -15 July 1999. Honolulu, HI: IEEE. 411.

Tromans, D. 2000. Oxygen solubility modelling in ammoniacal leaching solutions: Leaching of sulphide concentrates. *Minerals Engineering.* 13(5):497-515

Tshilombo, A.F. and Dixon, D.G. 2003. Kinetic Study of Chalcopyrite Passivation During Electrochemical and Chemical Leaching. *Proceedings- Electrochemical Society. Electrochemistry in Mineral and Metal Processing International Symposium; 6th, Electrochemistry in Mineral and Metal Processing.* (6):108-119.

Tshilombo, A.F., Petersen, J. and Dixon, D.G. 2002. The influence of applied potentials and temperature on the electrochemical response of chalcopyrite during bacterial leaching. *Minerals Engineering.* 15(11):809-813.

Tyma, P.D. and Weaver, M.J. 1980. Further observations on the dependence of the electrochemical transfer coefficient upon the electrode potential. *Journal of Electroanalytical Chemistry and Interfacial Electrochemistry.* 111(2):195-210.

U.S. Congress, Office of Technology Assessment 1987. *Copper production Technology OTA-E-367.* Washington DC: U.S. Government Printing Office.

Van Wensveen.C 2010. The kinetics of the oxidation of thiosulphate in copper-ammonia solutions. PhD Thesis. Murdoch University.

Vasquez, B.R., Viramontes-Gamboa, G. and Dixon, D.G. 2011. Transpassive Electrochemistry of Chalcopyrite Microparticles. *Journal of the Electrochemical Society.* 159(1):C8-C12.

Vegliò, F., Trifoni, M., Pagnanelli, F. and Toro, L. 2001. Shrinking core model with variable activation energy: a kinetic model of manganiferous ore leaching with sulphuric acid and lactose. *Hydrometallurgy.* 60(2):167-179.

Velásquez-Yévenes, L. (2009). *The Kinetics of the Dissolution of Chalcopyrite in Chloride Media.* Perth, Australia: Murdoch University.

Venkatachalam S 1991. Treatment of chalcopyrite concentrates by hydrometallurgical techniques. *Minerals Engineering.* 4(7-11):1115-1126.

Viramontes-Gamboa, G. Rivera-Vasquez, B. F. Dixon, D. G. 2007. The Active-Passive Behaviour of Chalcopyrite Comparative Study Between Electrochemical and Leaching Responses. *Journal- electrochemical society.* 154(6):C299-C311.

Wan, R.Y., Miller, J.D. and Simkovich, G. 1984. *Enhanced Ferric Sulphate Leaching of Copper from CuFeS2 and C Particulate Aggregates.* (ADA148661). Utah: Defence Technical Information Centre.

Wang, H., Bigham, J.M., Jones, F.S. and Tuovinen, O.H. 2007. Synthesis and properties of ammoniojarosites prepared with iron-oxidizing acidophilic microorganisms at 22–65 °C. *Geochimica Et Cosmochimica Acta.* 71(1):155-164.

Wang, M. and Hebert, K.R. 1999. Metal and Oxygen Ion Transport during Ionic Conduction in Amorphous Anodic Oxide Films. *Journal of Electroanalytical Society.* 146(10):3741-3749.

Wang, S. 2005. Copper leaching from chalcopyrite concentrates. *JOM Journal of the Minerals, Metals and Materials Society.* 57(7):48-51..

Warren, G. and Wadsworth, M. 1984. The electrochemical oxidation of chalcopyrite in ammoniacal solutions. *Metallurgical and Materials Transactions B.* 15(2):289-297.

Warren, G., Wadsworth, M. and El-Raghy, S.M. 1982. Passive and Transpassive anodic behaviour of chalcopyrite in acid solutions. *Metallurgical Transactions B.* 13(4):571-579.

Weisener, C.G., Smart, R.S.t.C. and Gerson, A.R. 2003. Kinetics and mechanisms of the leaching of low Fe sphalerite. *Geochimica Et Cosmochimica Acta.* 67(5):823-830.

Wy, Z., Yang, S., Sun, Y., Parvez, K., Feng, X. and Mullen, K. 2012. 3D Nitrogen-Doped Graphene Aerogel-Supported Fe3O4 Nanoparticles as Efficient Electrocatalysts for the Oxygen Reduction Reaction. *Journal of the American Chemical Society.* 134:9082-9085.

Xi, W., Qi-yuan, C., Zhou-lan, Y., Hui-ping, H. and Zhong-liang, Z. 2011. Real-solution stability diagrams for copper-ammonia-chloride-water system. *Journal of Central South University.* 18:48-55.

Xu, C., Zeng, Y., Rui, X., Zhu, J., Tan, H., Guerrero, A., Toribio, J., Bisquert, J. et al. 2013. Amorphous Iron Oxyhydroxide Nanosheets: Synthesis, Li Storage, and Conversion Reaction Kinetics. *The Journal of Physical Chemistry.* C117:17462.

Yang, Y., Zhang, J., Wu, X., Fu, Y., Wu, H. and Guo, S. 2014. Composites of boron-doped carbon nanosheets and iron oxide nanoneedles: fabrication and lithium ion storage performance. *Royal Society of Chemistry.* 2:9111-9117.

Yin, Q., Vaughan, D.J., England, K.E.R., Kelsall, G.H. and Brandon, N.P. 2000. Surface Oxidation of Chalcopyrite (CuFeS2) in Alkaline Solutions. *Journal of the Electrochemical Society.* 147(8):2945-2951.

Zhang, J., Vukmirovic, M.B., Xu, Y., Mavrikakis, M. and Adzic, R.R. 2005. Controlling the Catalytic Activity of Platinum-Monolayer Electrocatalysts for Oxygen Reduction with Different Substrates. *Angewandte Chemie.* 44(14):2132-2135.

Appendices

APPENDIX 1. Cathodic reaction rate model

Rate expression for the cathodic reaction

The rate expression for the cathodic reaction is derived based on the same principles as those used in section 8.2 on anodic reactions. The measured cathodic currents are due to the reduction of copper(II) and have been shown to be influenced by the oxidation of the resultant copper(I). It is pointed out that in anodic tests carried out in solutions that did not contain any initial copper (as copper(II) or copper(I)), it was reasonable to assume rate of copper(I) oxidation to be negligible. The measured cathodic current can be described by the Butler-Volmer equation and is written as shown in equation A1.1.

$$i = -F\{k_{cf}[Cu(II)]_s e^{-\frac{\alpha F\left(E-E_f\right)}{RT}} - k_{cr}[Cu(I)]_s e^{\frac{(1-\alpha)F\left(E-E_f\right)}{RT}}\} \quad \text{A1.1}$$

Where i is the measured current density (Acm^{-2}) and the negative sign denotes that it is cathodic currents, k_{cf} and k_{cr} are the potential independent electrochemical rate constant (cms^{-1}) for the forward and reverse reaction respectively, E the potential with respect to a reference electrode (V), E_f is the formal potential for the reaction in solution condition of study at equilibrium(V), F Faraday number 96485 $A.s.mol^{-1}$) and α the transfer coefficient usually assumed to be 0.5. The negative sign is convention for denoting cathodic currents and subscripts "s" denotes surface concentrations.

When the reaction takes place at the formal potential i.e. $E=E_f$

$$i = -F\{k_{cf}[Cu(II)]_s - k_{cf}[Cu(I)_s]\} \quad \text{A1.2}$$

When the reaction is at equilibrium i.e. i =0, then

$$-Fk_{cf}[Cu(II)]_s = Fk_{cr}[Cu(I)]_s = i_{O.F} \quad \text{A1.3}$$

Where $i_{O.F}$ is the exchange current density at formal potential.

For ongoing reactions, the surface concentration will not be equal to the bulk concentrations due to the consumption and generation of the reacting species and product species by electrochemical reactions. The surface concentrations of the species involved in the faradaic reactions are related to the electrode potential by an equation of the Nernst form. For the cathodic reaction (Equation 5.1), at the start of the reaction, concentration of the oxidised species [copper(II)] at the electrode surface $C_s(x=0)$ becomes smaller than the bulk concentration C_b in the bulk of the solution. If we assume a Nernst diffusion layer of thickness δ exists between the bulk of the solution and the mineral surface and that agitation maintains the concentration of copper(II) at C_b beyond x=δ. Assuming a linear concentration gradient within the diffusion layer, the rate of mass transfer of

copper(II) from the bulk solution to the mineral surface is given by equation A1.4, derived from Fick's first law .

$$\frac{i}{nF} = J = \frac{D[C_b - C_s]}{\delta} molm^{-2}s^{-1} \quad \text{A1.4}$$

J mass transfer rate, D diffusion coefficient of the transferred ion, C_s concentration of the ion on the surface of the electrode, C_b concentration of the ion in the bulk of the solution and δ the thickness of the diffusion layer. δ is not known, so the expression is conveniently expressed by combining it with the diffusion coefficient to give a single constant K_L=D/δ also referred to as the mass transfer coefficient and rewriting equation A1.4;

$$i = nFk_L[C_b - C_s]molm^{-2}s^{-1} \quad \text{A1.5}$$

At limiting currents, Cs = 0 and equation A1.5 can be written out as

$$i_L = nFk_L C_b \quad \text{or} \quad \frac{1}{i_L} = \frac{1}{nFk_L C_b} \quad \text{A1.6}$$

Notice that while equation A1.3 and A1.6 appear to be similar, K_L in equation A1.6 is a mass transfer coefficient and, k_{cf} and k_{cr} in equation A1.3 are the potential independent electrochemical rate constants.

The concentration of species on the surface can be written as;

$$\frac{C_s}{C_b} = 1 - \frac{i}{i_L} \quad \text{A1.7}$$

The concentrations of the oxidised and reduced species on the surface of the electrode can then be written out by combining equation A1.6 and 8.26. The concentrations of copper(II) and copper(I) on the surface are given by equations A1.8 and A1.9.

$$[Cu(II)]_s = [Cu(II)]_b - \frac{i}{nFK_{L_{Cu(II)}}} \quad \text{A1.8}$$

$$[Cu(I)]_s = [Cu(I)]_b + \frac{i}{nFK_{L_{Cu(I)}}} \quad \text{A1.9}$$

Substituting equations A1.8 and A1.9 into equation A1.1, letting $F(E-E_f)/RT = f(E)$ and n=1. For ease of calculations the negative sign denoting direction of flow of current will be omitted in the derivation and only replaced in the final equation.

$$i = Fk_{cf}\{[Cu(II)]_b - \frac{i}{FK_{L_{Cu(II)}}}\}e^{-\alpha f(E)} - Fk_{cr}\{[Cu(I)]_b + \frac{i}{FK_{L_{Cu(I)}}}\}e^{(1-\alpha)f(E)} \quad \text{A1.10}$$

Making i the subject;

$$i = \frac{Fk_{cf}[Cu(II)]_b e^{-af(E)} - Fk_{cr}[Cu(I)]_b e^{(1-a)f(E)}}{1+\frac{k_{cf}e^{-af(E)}}{k_{LCu(II)}}+\frac{k_{cr}e^{(1-a)f(E)}}{k_{LCu(I)}}} \quad \text{A1.11}$$

In the current study, there was no copper(I) in the bulk solution so that term is assumed to be zero and equation A1.11 simplifies to equation A1.12 below.

$$\mathrm{i} = -\frac{\mathrm{F}\{[\mathrm{Cu(II)}]_\mathrm{B}\mathrm{e}^{-\alpha f(E)}\}}{\frac{1}{\mathrm{k_{cf}}}+\frac{\mathrm{e}^{-\alpha f(E)}}{\mathrm{k}_{LCu(II)}}+\frac{k_{cr}e^{(1-a)f(E)}}{k_{cf}k_{LCu(I)}}} \quad \text{A.12}$$

From equation A1.12, it can be seen that the measured cathodic currents can be influenced by three parameters or "resistances", i.e. the kinetics of copper(II) reduction, mass transport restrictions (which are measured as the limiting currents on the reduction reaction) and the oxidation of copper(I) the product of the reduction reaction. If these were regarded as resistances then according to Ohms law, the measured current is the voltage divided by the sum of the resistances, therefore

$$i_t = \frac{V}{R} = \frac{V}{R_c+R_{ap}+R_L} \quad \text{A1.13}$$

in which R_c, $R_{ap}$and R_L are the specified "resistances" i.e. kinetic limitations, oxidation of copper(I) and mass transfer limitations.

The measured currents can be expressed in the form analogous to the Koutecky-Levich format (Guidelli et al., 2014; Bard and Faulkner, 2001) (Equation A1.14) with an additional term i_{ap} to account for the contributions of the back reaction in the form of oxidation of copper(I). This approach of using the Koutecky-Levich model to analyse current densities is used where the rotation rate or angular velocity is varied to adjust the mass transfer coefficient (Kim and Bard, 2016; Bard and Faulkner, 2001).

$$\frac{1}{i_t} = \frac{1}{i_c} + \frac{1}{i_{ap}} + \frac{1}{i_L} \quad \text{A1.14}$$

In which,

i_t = the (total) measured cathodic currents

i_c is the contribution for the reduction of Cu(II) in the absence of mass transport restrictions i.e. kinetic of the reduction reaction

i_{ap} is the contribution of the back reaction i.e. oxidation of Cu(I)

i_L is the limiting current density for the reduction of Cu(II) i.e. mass transfer limitation

$$\frac{1}{i} = \frac{1}{\frac{Fe^{-\alpha f(E)}[Cu(II)]_B}{\frac{1}{k_{cf}} + \frac{e^{-\alpha f(E)}\}}{k_{LCu(II)}} + \frac{k_{cr}e^{(1-a)f(E)}}{k_{cf}k_{LCu(I)}}}} \quad \text{A1.15}$$

On simplifying equation A1.15, and taking the inverse of each term. It can be seen that

$$i_c = -Fk_{cf}[Cu(II)_B]e^{-\alpha\frac{f(E)}{RT}} \quad \text{A1.16}$$

$$i_{ap} = -\frac{k_{cf}}{k_{cr}}Fk_{L_{Cu(I)}}[Cu(II)_B]e^{-\frac{f(E)}{RT}} \quad \text{A1.17}$$

$$i_L = -Fk_{L_{Cu(II)}}[Cu(II)]_b \quad \text{A1.18}$$

Consider a case in which mass transfer of Cu(II) (i_L) is very fast relative to the electrochemical reduction of the Cu(II) (i_C), then $1/i_L >> 1/i_c$. If we assume there is no back reaction (oxidation of Cu(I)) the process is governed by i_c and this would be referred to as a kinetically limited reaction. In another case, (still assumed zero contribution from the back reaction) where mass transfer is very slow such that $1/i_C >> 1/i_L$, this gives the mass-transfer limited reaction. Mixed control arises when the current is affected by both the potential (charge transfer reaction) and the mass transport. The relative contributions of each term to the overall cathodic currents (Equation 8.36 and Equation 8.38) to the overall current density will depend on the magnitude of each term, with the one contributing the smallest currents being the rate limiting step (Nicol, unpublished; Hill et al, 2015). This was partially demonstrated in section 5.5 where it was shown that at potentials close to mixed potential where rate of the electrochemical reaction(i_c) is small relative to rate of mass transfer (i_L). However, the inverse relationship between the current densities due to the reverse reaction and agitation speeds observed as differences of first peak sizes on the reverse sweep in section 5.5, provided evidence that under the conditions of the study, the anodic oxidation of copper(I) can take place.

APPENDIX 2. Simulation of cathodic currents

Simulation of the cathodic current density potential curve

In the measurement of cathodic currents under the conditions of the current study, the output results from the instrument are a summation of the currents due to the reduction of copper(II) (Equation 5.1), which are negative, and the currents due to the oxidation of copper(I) (Equation 5.2), which are positive. Also possible, are very small contributions of anodic currents due the oxidation of chalcopyrite considering the instrument was set to potentials in the vicinity of the chalcopyrite-copper(II) mixed potentials. Because of this, the true cathodic currents are understated and the extent of understating is dependent on the mass transport of copper(I) from the mineral surface as shown in section 5.6. The simulation presented here was developed in order to isolate the true cathodic currents from the positive oxidation currents.

The reactions considered to occur on the chalcopyrite surface at negative potentials in the vicinity of mixed potentials are tabulated and categorised in Table A.1.

Table A.1. Reactions taking place at the mineral surface at potentials below mixed potentials but in the vicinity of mixed potentials

Reaction	Process
1. Cu(II) + e- = Cu(I)	Cathodic
2. Cu(I) = Cu(II) + e	Anodic
3. CuFeS2+ 3H2O = Cu(I) + Fe(II) + S2O3(-2a) + 6H(+a) + 7e	Anodic
4. O2 + 4H(+a) + 4e = 2H2O (pH 9)	Cathodic

Current contributions by reactions 3 and 4 are considered to be negligibly small relative to that from 1 and 2, and thus will not be considered in the calculations. The currents are calculated from equations 8.36-8.37 whose derivation was explained in appendix 1. The formal potential for the copper(I)/ copper(II) redox reaction used for the simulation was 100 mV (Bard et al) and α was assumed to be 0.5. The mass transfer coefficient was estimated from a form of the Levich equation A2.1.

$$k_l = 0.62 D^{\frac{2}{3}} v^{-\frac{1}{6}} w^{\frac{1}{2}} \qquad \text{A2.1}$$

Table A.2 shows an extract from the spread sheet used for the simulation.

Table A.2. Extract from the spreadsheet used for the simulation

Reaction	Process	E_f(1MNH3-NH4) V	Alpha	kf cm/s	kL cm/s	w rpm	kL cm/s	w rpm
1. Cu(II) + e- = Cu(I)	Cathodic	0.100	0.5	0.0020	0.00610	1600	0.00193	100
2. Cu(I) = Cu(II) + e	Anodic	0.100	0.5	0.0020	0.00915	1600	0.00290	100
3. CuFeS2+ 3H2O = Cu(I) + Fe(II) + S2O3(-2a) + 6H(+a) + 7e	Anodic	0.150	0.5					
4. O2 + 4H(+a) + 4e = 2H2O (pH 9)	Cathodic	0.935	0.5					

[Cu(II)]	0.0787	mole/L
[Cu(I)]	0	mole/L
[O2]	0.00E+00	mole/L
F	96500	As/mole

Copper **1M NH3/NH4**

E (V vs SHE)	$F(E-E_f)/RT$	i ($mAcm^{-2}$)	$i_{a(p)}$	i_L ($mAcm^{-2}$)	i_c	[Cu(I)] at electrode mol/L	100rpm i_c and I_L ($mAcm^{-2}$)	i_a ($mAcm^{-2}$)	current from column 3 in A	IR drop (V)	Effective potential (V)
0.236	5.29	-1.08	-0.349	-29	-26.1	0.000296	-1.04	0.777	0.00028	0.008	0.228
0.231	5.10	-1.19	-0.424	-29	-30.9	0.000350	-1.14	0.831	0.000299	0.00855	0.222
0.226	4.91	-1.31	-0.515	-29	-36.5	0.000413	-1.25	0.886	0.000319	0.00912	0.217
0.221	4.71	-1.44	-0.625	-29	-43	0.000486	-1.37	0.943	0.00034	0.00971	0.211
0.216	4.52	-1.59	-0.759	-29	-50.5	0.000571	-1.5	1	0.00036	0.0103	0.206

APPENDIX 3. Additional Results

Mixed potential curves

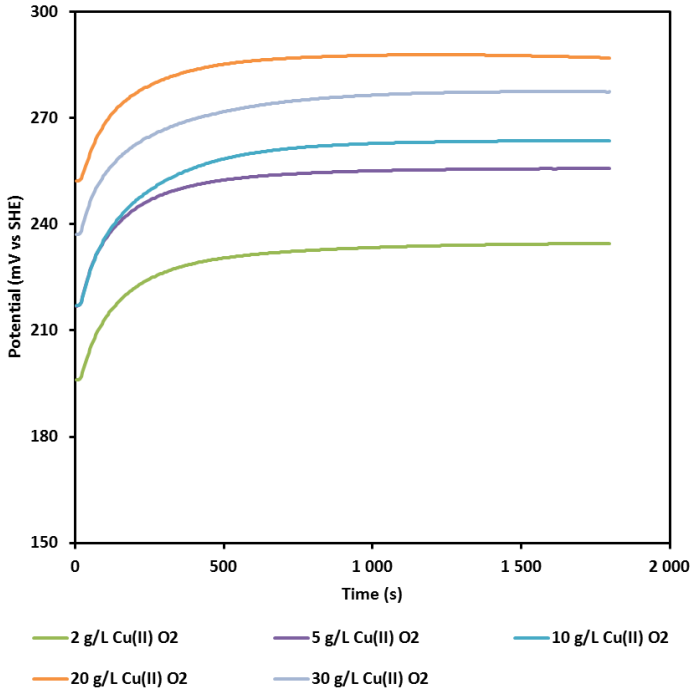

Figure A.1. Mixed potential of chalcopyrite in ammonia-ammonium sulphate solutions at 1 M (NH_3+NH_4^+), 25°C, 1600 rpm, pH 9.6±0.15 in the presence of oxygen at varied initial Cu(II) concentrations. Over a period of 30 minutes.

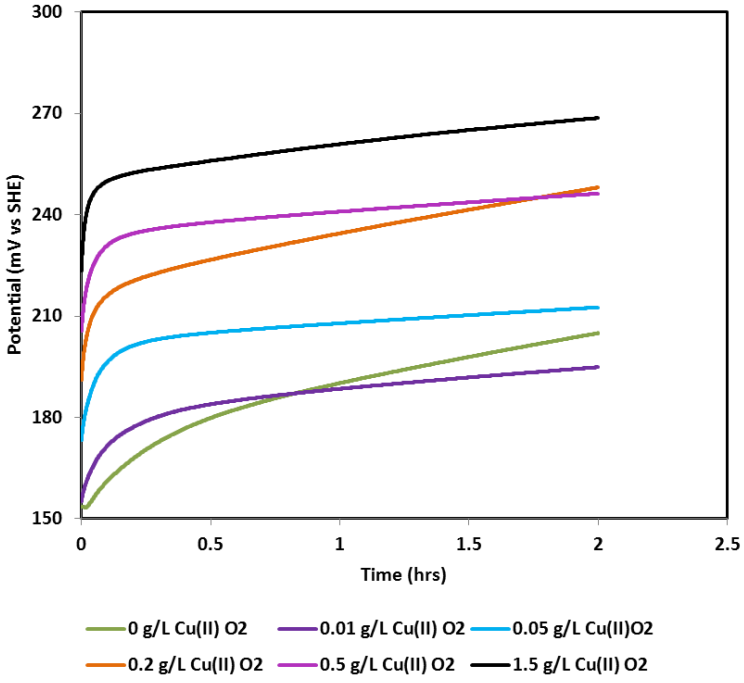

Figure A.2. Mixed potential of chalcopyrite in ammonia-ammonium sulphate solutions at 1 M (NH_3+NH_4^+), 25°C, 1600 rpm, pH 9.6±0.15 in the presence of oxygen at varied initial Cu(II) concentrations. Over a period of 2 hours.

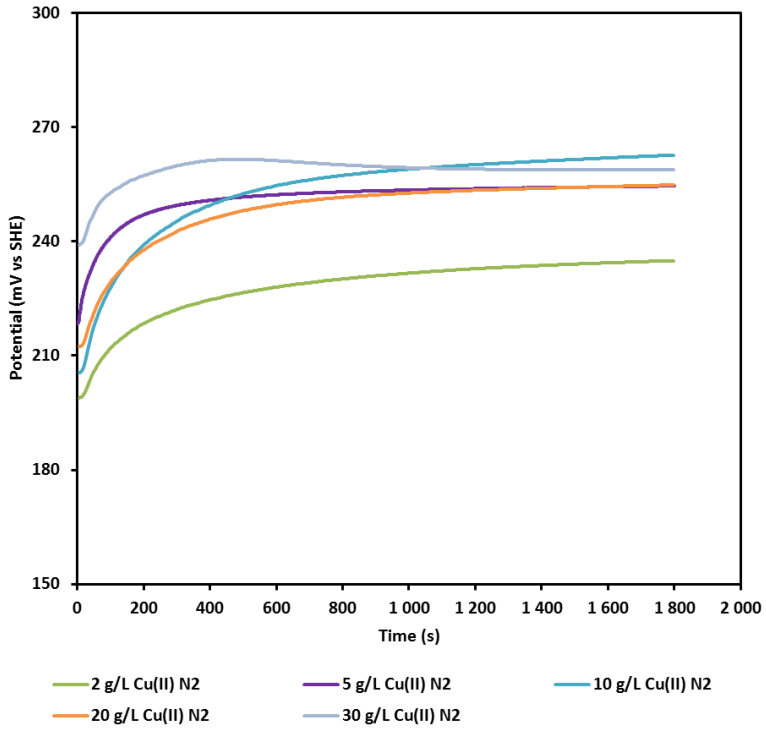

Figure A.3. Mixed potential of chalcopyrite in ammonia-ammonium sulphate solutions at 1 M (NH_3+NH_4^+), 25°C, 1600 rpm, pH 9.6±0.15 under nitrogen at varied initial Cu(II) concentrations. Over a period of 30 minutes.

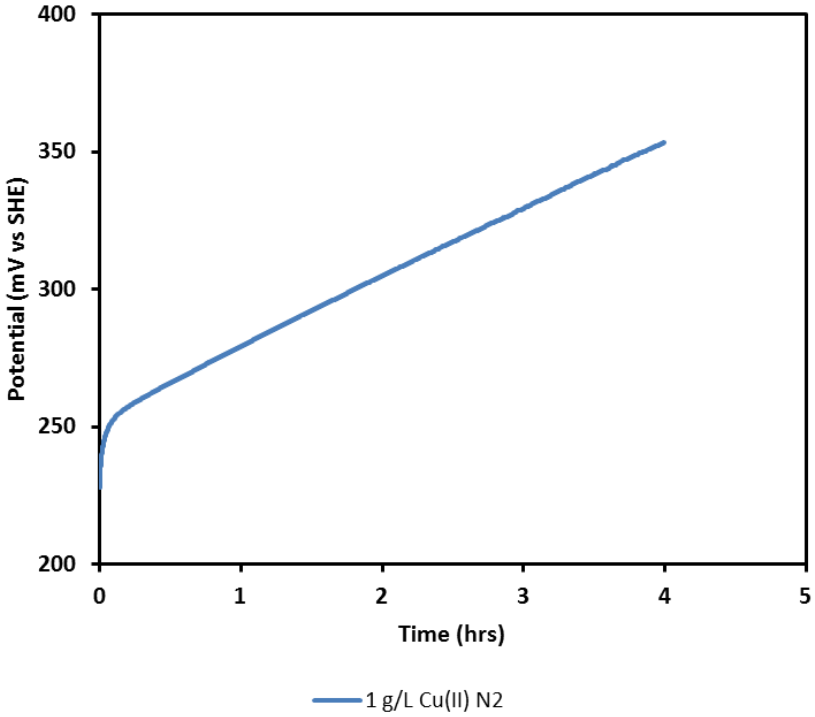

Figure A.4. Mixed potential of chalcopyrite in ammonia-ammonium sulphate solutions at 1 M (NH_3+NH_4^+), 25°C, 1600 rpm, pH 9.6±0.15 under nitrogen at varied initial Cu(II) concentrations. Over a period of 4 hours.

Table A.3. Chalcopyrite's mixed potentials (E_0) and the solution potentials(E_h) in ammonia-ammonium sulphate solutions at 1 M (NH_3+NH_4^+), 45°C, 1600 rpm, pH 9.6±0.15 in the and absence of oxygen at varied initial Cu(II) concentrations. Potentials recorded after 30 minutes.

T45	Oxygen		Nitrogen	
Cu(II) conc	E_m versus SHE	E_h	E_m versus SHE	E_h
0	144	300	162	214
0.01	182	309	185	234
0.05	185	299	178	227
0.1	209	308	193	238
0.2	200	299	233	281
0.5	236	305	241	295
1	236	310	263	319
1.5	233	330	251	303
2	239	339	263	315
5	260	365	266	319
10	250	359	267	328

Chronoamperometric curves

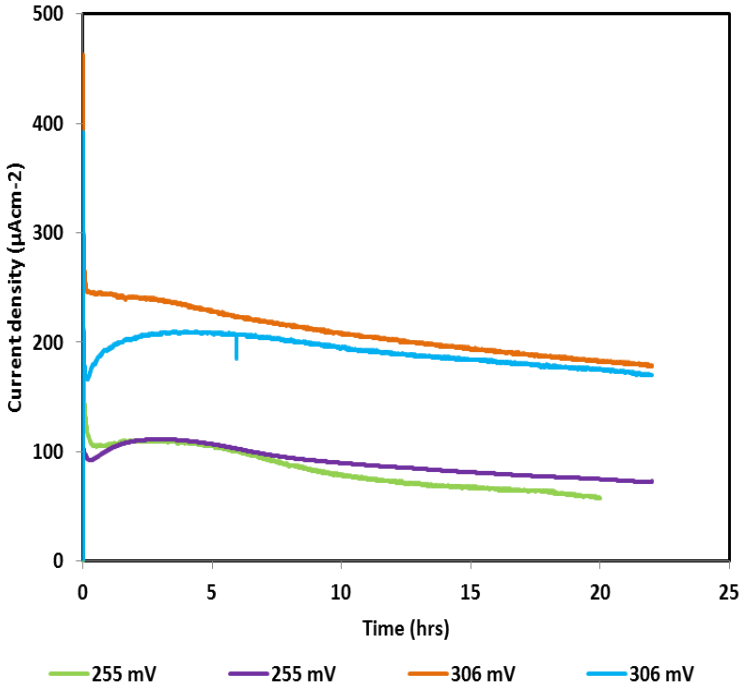

Figure A.5. Constant potential plots showing current density versus time when potential was set at 255 mV and 306 mV (versus SHE) in 1 M (NH_3+NH_4^+) in ammonia-ammonium sulphate , 25°C, 1600 rpm, pH 9.6±0.15 under nitrogen.

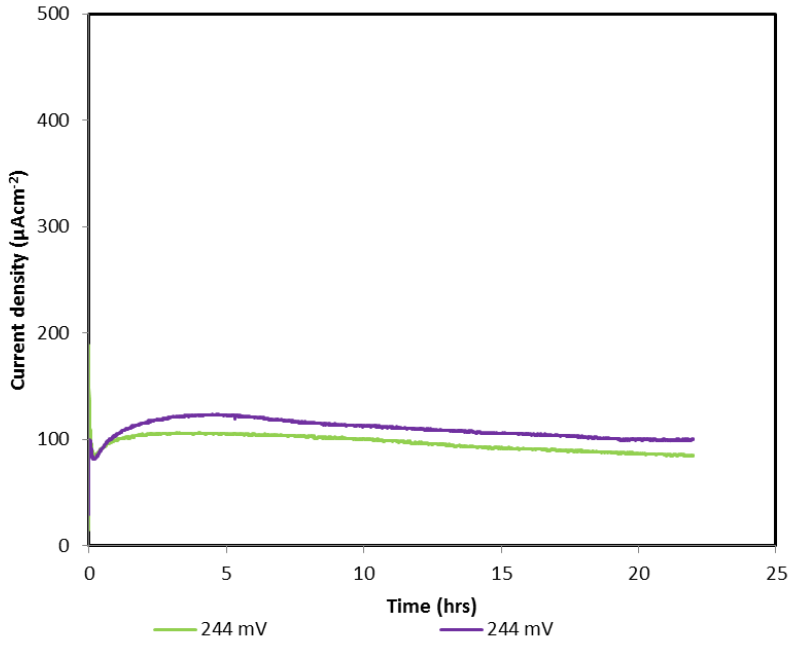

Figure A.6. Constant potential plots showing current density versus time when potential was set at 244 mV (versus SHE) in 1 M (NH_3+NH_4^+) in ammonia-ammonium sulphate, 25°C, 1600 rpm, pH 9.6±0.15 under oxygen.

Cyclic Voltammetry

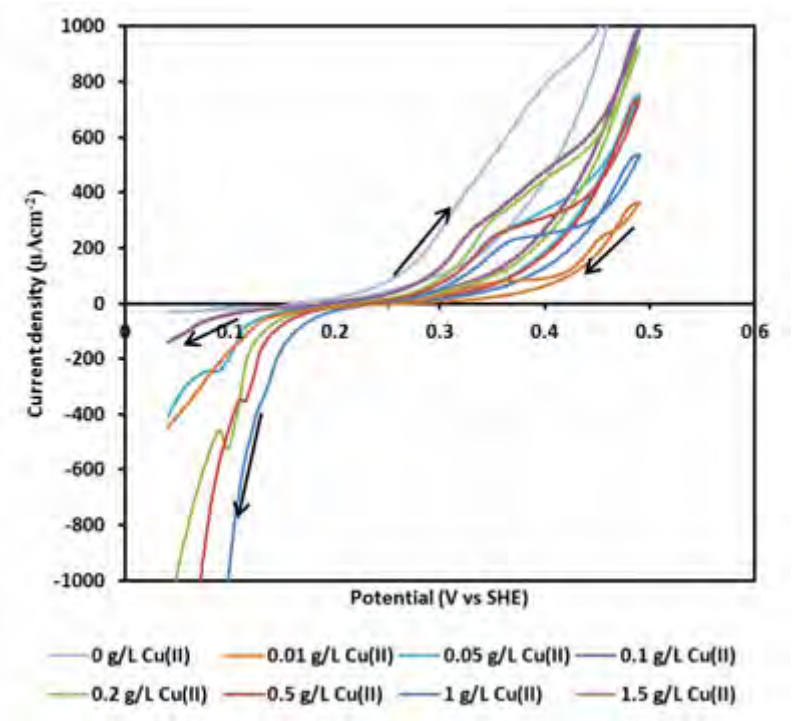

Figure A.7. Cyclic voltammograms of a chalcopyrite electrode surface measured in in ammonia-ammonium sulphate solutions of varied initial copper(II) concentrations, at 1 M (NH_3+NH_4^+) 25°C, pH 9.6±0.15, under *oxygen* at a scan rate of 1 mV/sec.

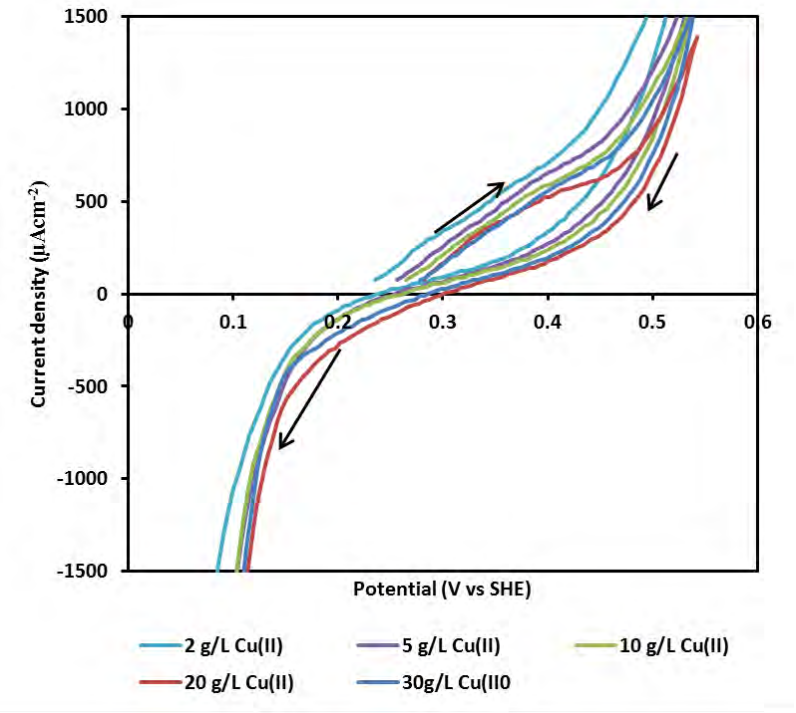

Figure A.8. Cyclic voltammograms of a chalcopyrite electrode surface measured in in ammonia-ammonium sulphate solutions of varied initial copper(II) concentrations, at 1 M (NH_3+NH_4^+) 25°C, pH 9.6±0.15, under *oxygen* at a scan rate of 1 mV/sec.

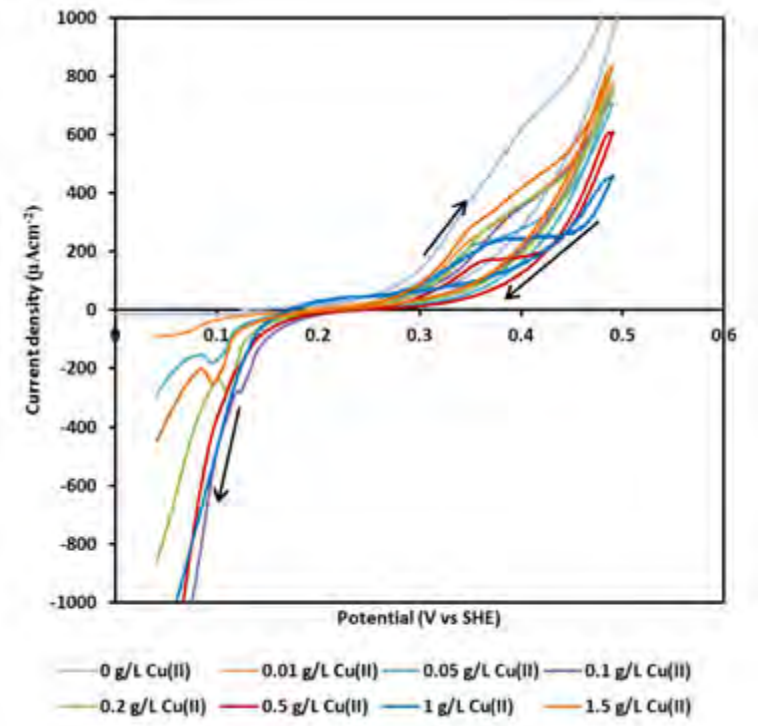

Figure A.9. Cyclic voltammograms of a chalcopyrite electrode surface measured in in ammonia-ammonium sulphate solutions of varied initial copper(II) concentrations, at 1 M (NH_3+NH_4^+) 25°C, pH 9.6±0.15, under *nitrogen* at a scan rate of 1 mV/sec.

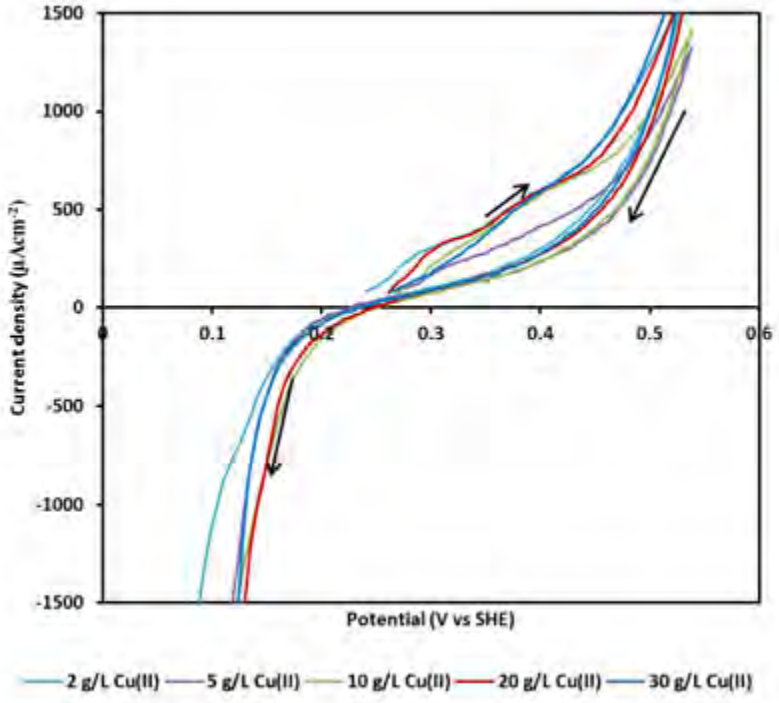

Figure A.10. Cyclic voltammograms of a chalcopyrite electrode surface measured in in ammonia-ammonium sulphate solutions of varied initial copper(II) concentrations, at 1 M (NH_3+NH_4^+) 25°C, pH 9.6±0.15, under *nitrogen* at a scan rate of 1 mV/sec.

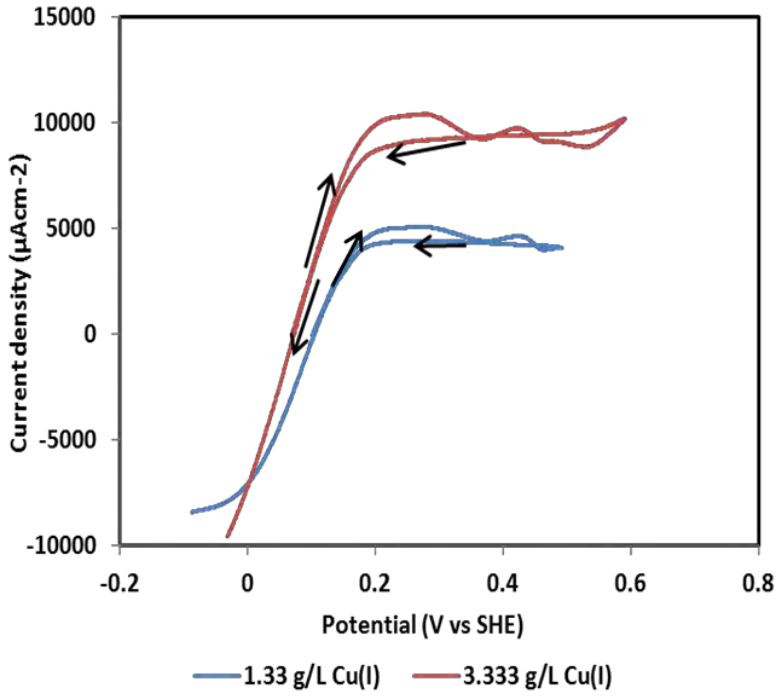

Figure A.11. Cyclic voltammograms of a chalcopyrite electrode surface measured in the presence of copper (I) at equimolar ratios with copper(II) in in ammonia-ammonium sulphate at 1 M (NH_3+NH_4^+) 25°C, pH 9.6±0.15, under *nitrogen* at a scan rate of 1 mV/sec.

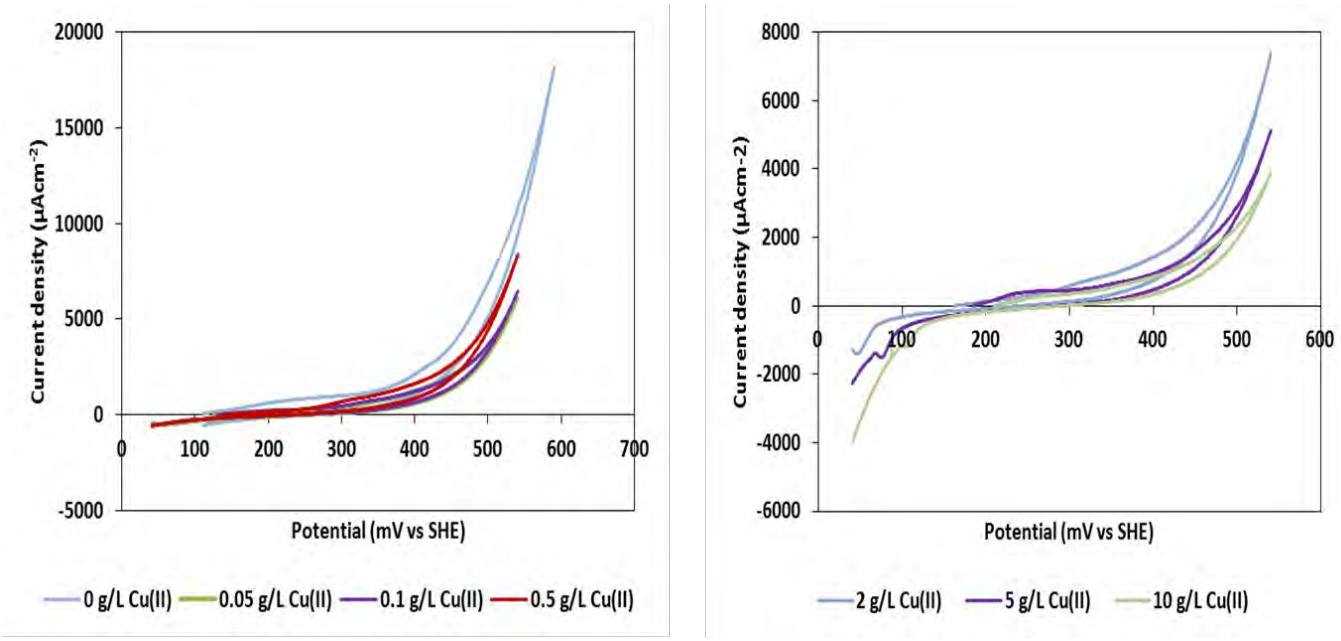

Figure A.12. Cyclic voltammograms of a chalcopyrite electrode surface measured in in ammonia-ammonium sulphate solutions of varied initial copper(II) concentrations, at 3 M (NH_3+NH_4^+) 25°C, pH 9.6±0.15, under *nitrogen* at a scan rate of 1 mV/sec.

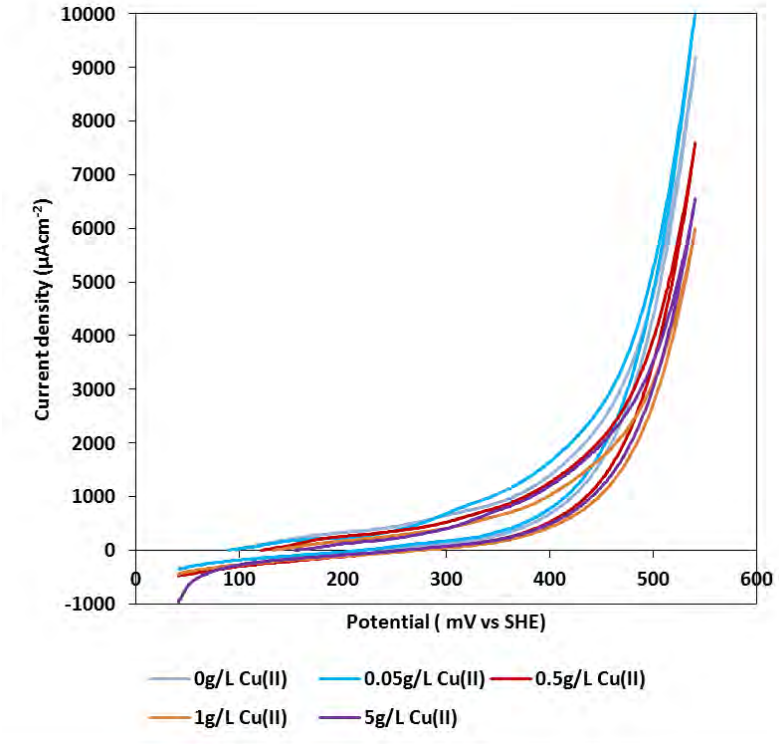

Figure A.13. Cyclic voltammograms of a chalcopyrite electrode surface measured in ammonia-ammonium sulphate solutions of varied initial copper(II) concentrations, at 6 M (NH_3+NH_4^+) 25°C, pH 9.6±0.15, under *nitrogen* at a scan rate of 1 mV/sec.

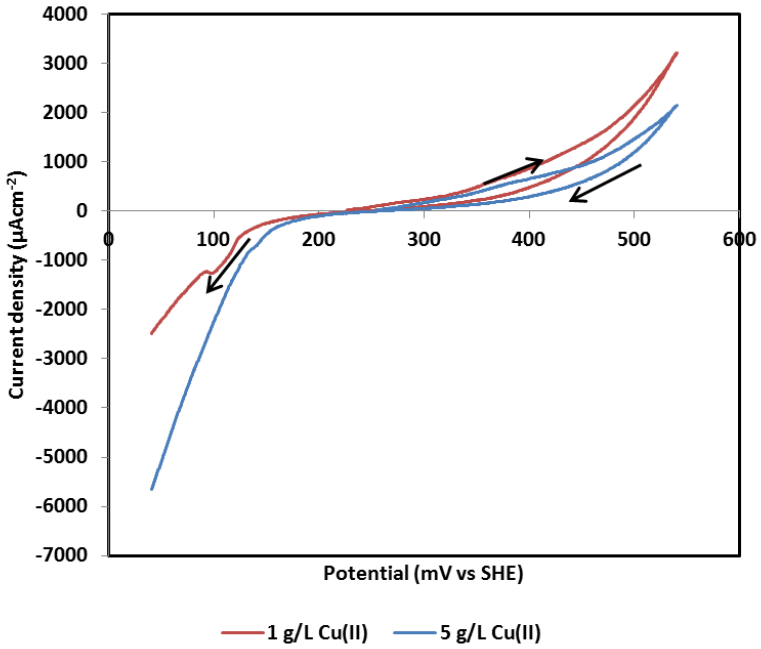

Figure A.14. Cyclic voltammograms of a chalcopyrite electrode surface measured in ammonia-ammonium perchlorate solutions at 1 and 5 g/L initial copper(II) concentrations, at 1 M (NH_3+NH_4^+) 25°C, pH 9.6±0.15, under *nitrogen* at a scan rate of 1 mV/sec.

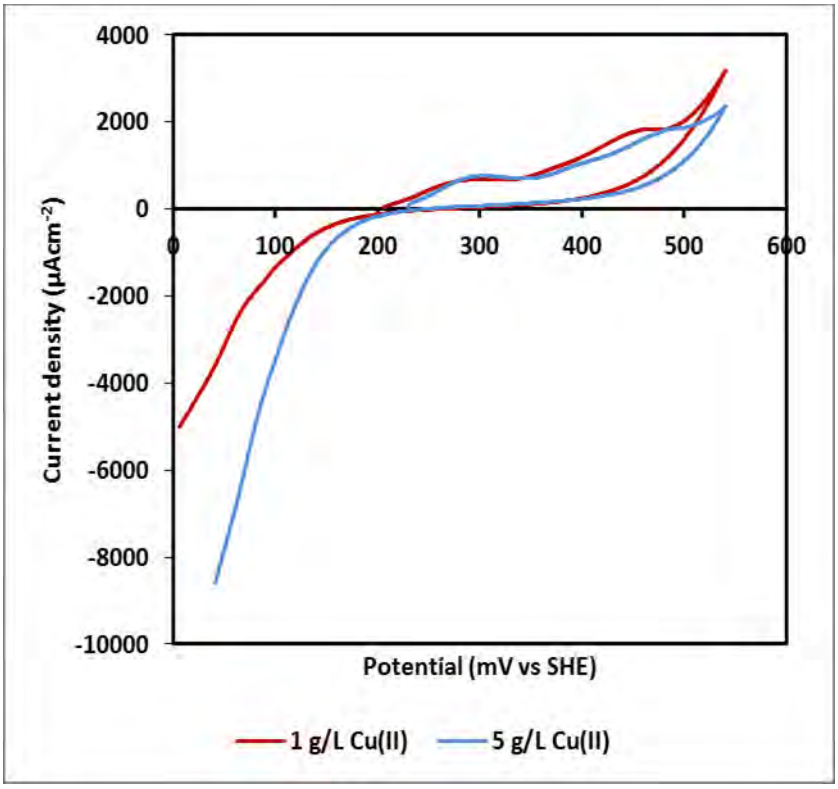

Figure A.15. Cyclic voltammograms of a chalcopyrite electrode surface measured in ammonia-ammonium carbonate solutions at 1 and 5 g/L initial copper(II) concentrations, at 1 M (NH_3+NH_4^+) 25°C, pH 9.6±0.15, under *nitrogen* at a scan rate of 1 mV/sec.

SEM images

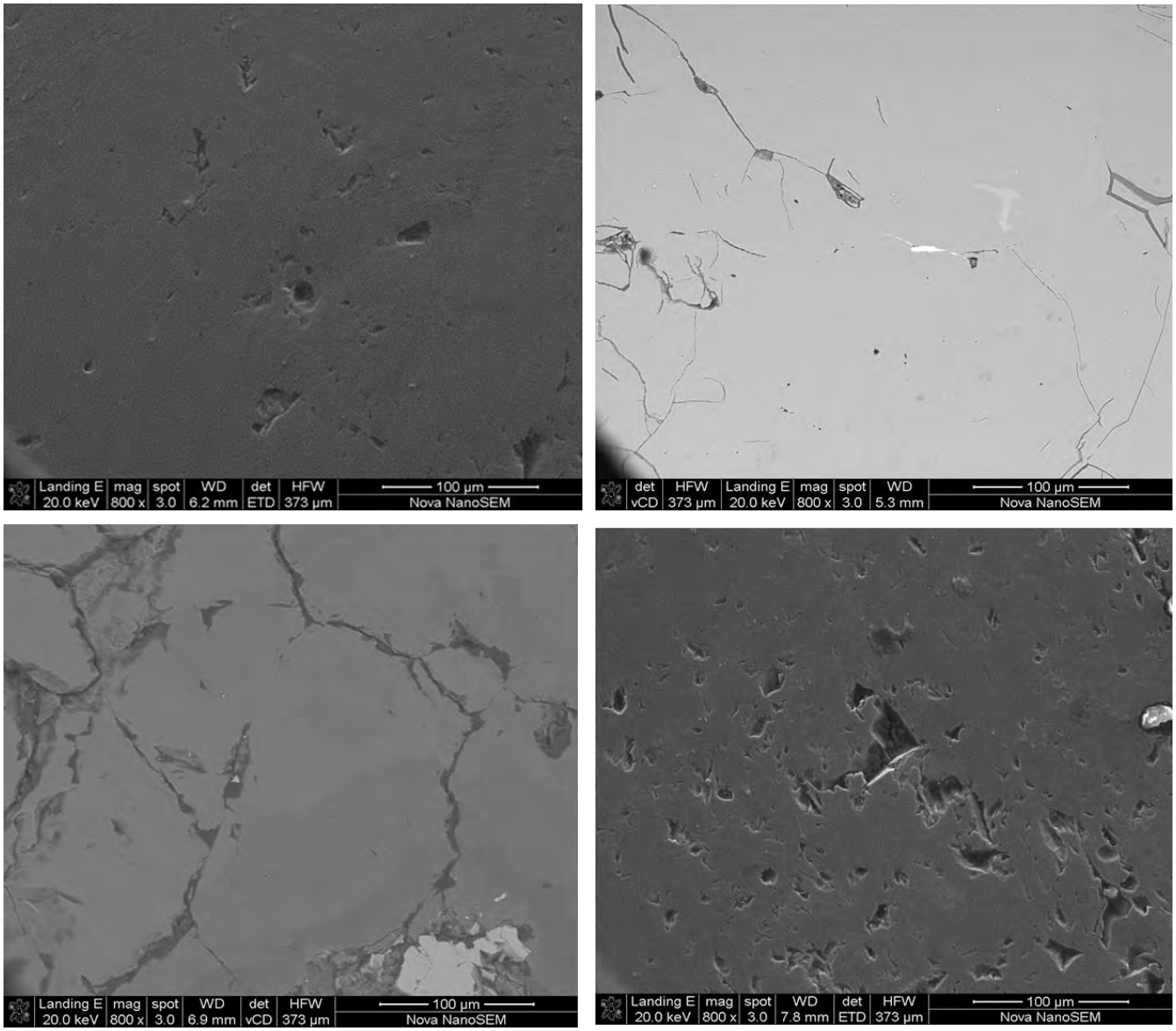

Figure A.16. SEM images of freshly polished chalcopyrite prior to exposure to electrolyte and/or oxidation. Image at x 800 magnification.

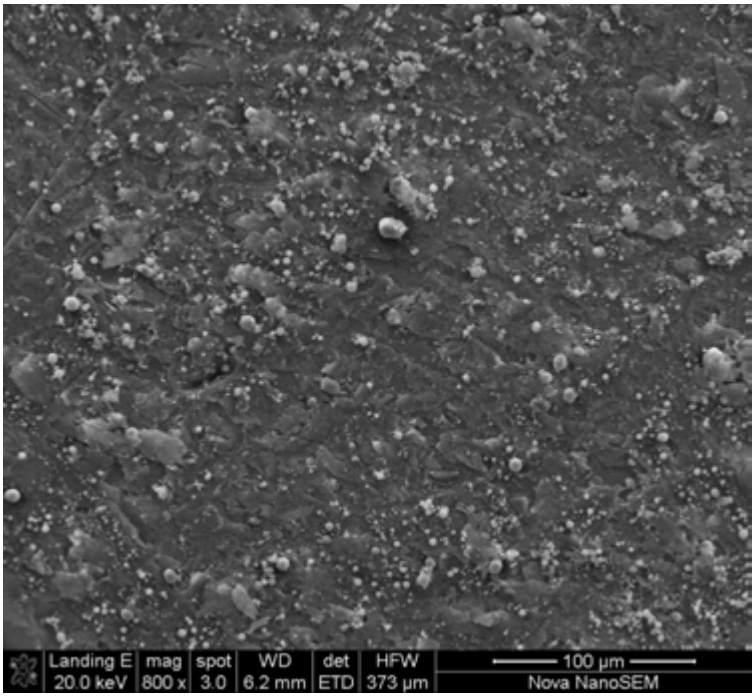

Figure A.17. SEM images of chalcopyrite (X 800) electrode surface after 22h of oxidation in ammonia-ammonium sulphate solutions at 246 mV in 1 M (NH_3+NH_4^+), 25°C, pH 9.6±0.15, 25°C under oxygen.

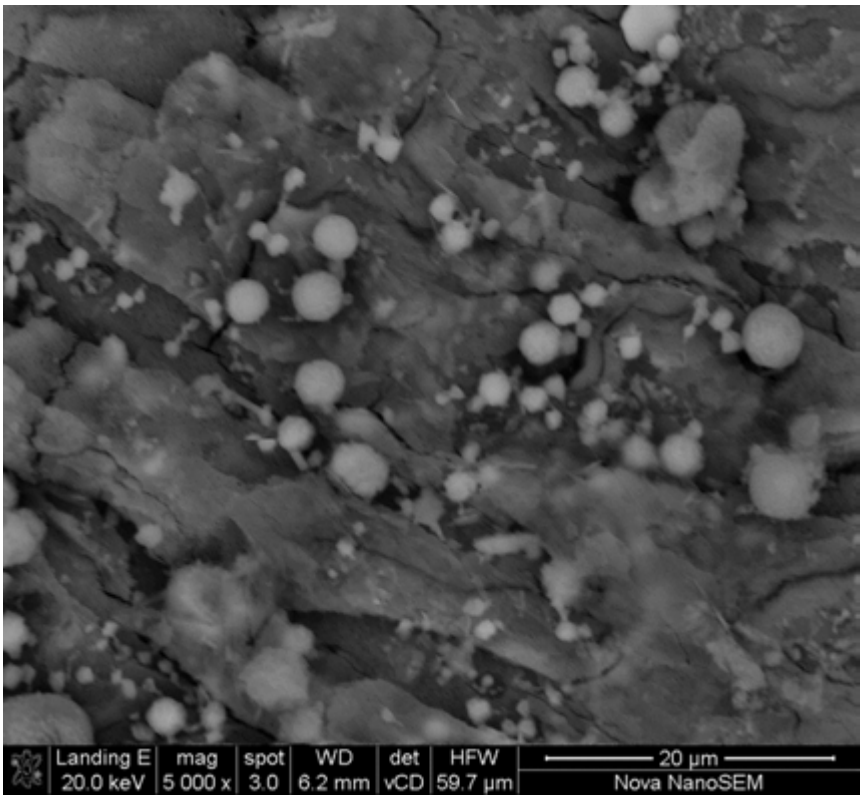

Figure A.18. SEM images of chalcopyrite (X 5000) electrode surface after 22h of oxidation in ammonia-ammonium sulphate solutions at 246 mV in 1 M (NH_3+NH_4^+), 25°C, pH 9.6±0.15, 25°C under oxygen.

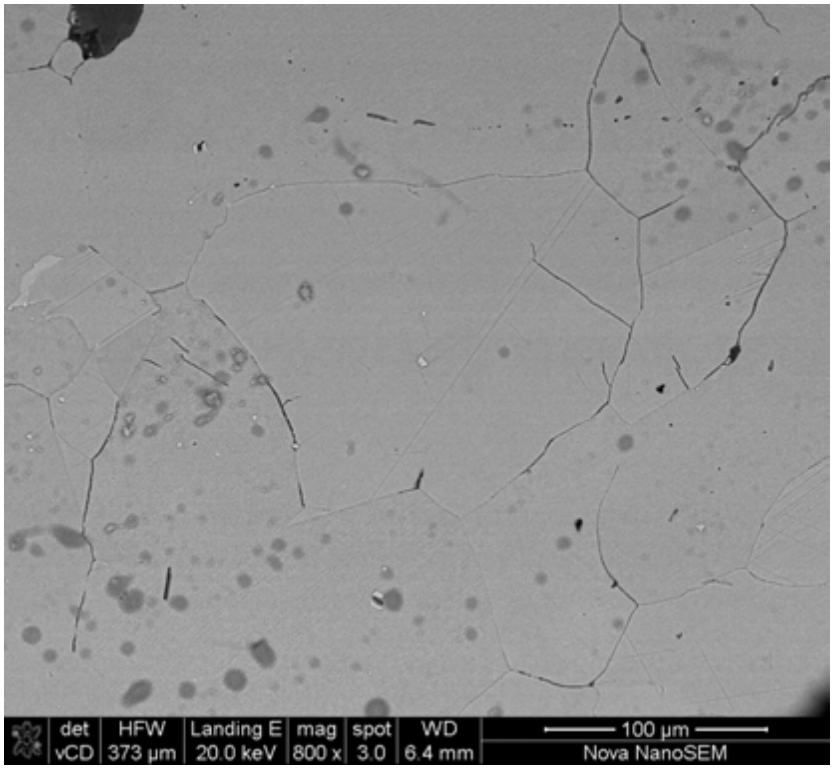

Figure A.19. . SEM images of chalcopyrite electrode surface (X800), after 22h of oxidation in ammonia-ammonium carbonate solutions at 225 mV in 1 M (NH_3+NH_4^+), 25°C, pH 9.6±0.15, 25°C under nitrogen.

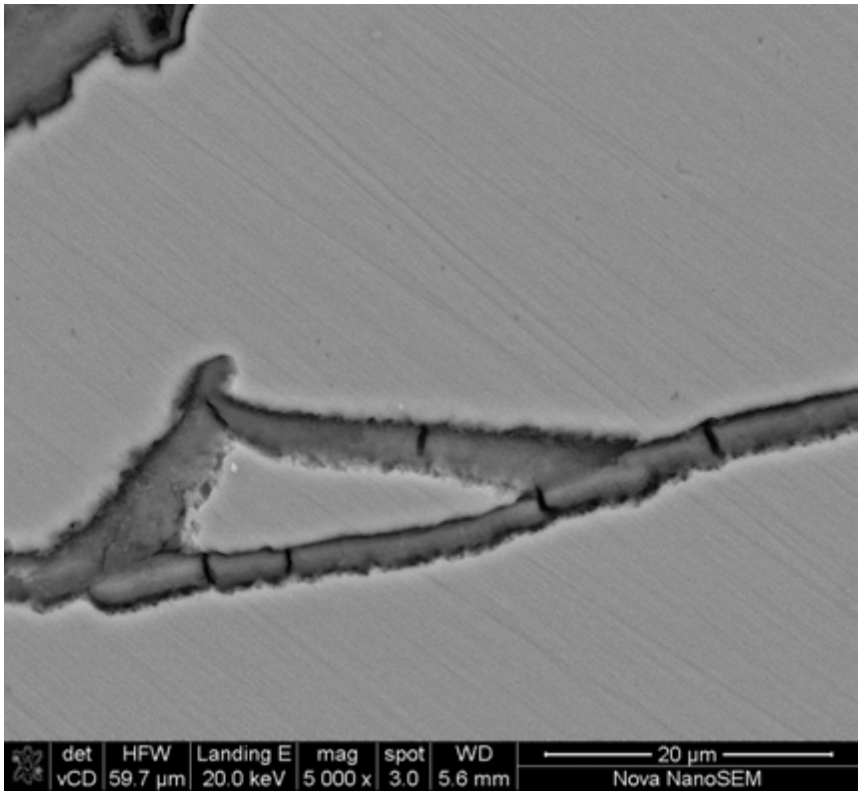

Figure A.20. SEM images of chalcopyrite electrode surface(X5000), after 22h of oxidation in ammonia-ammonium carbonate solutions at 225 mV in 1 M (NH_3+NH_4^+), 25°C, pH 9.6±0.15, 25°C under nitrogen.

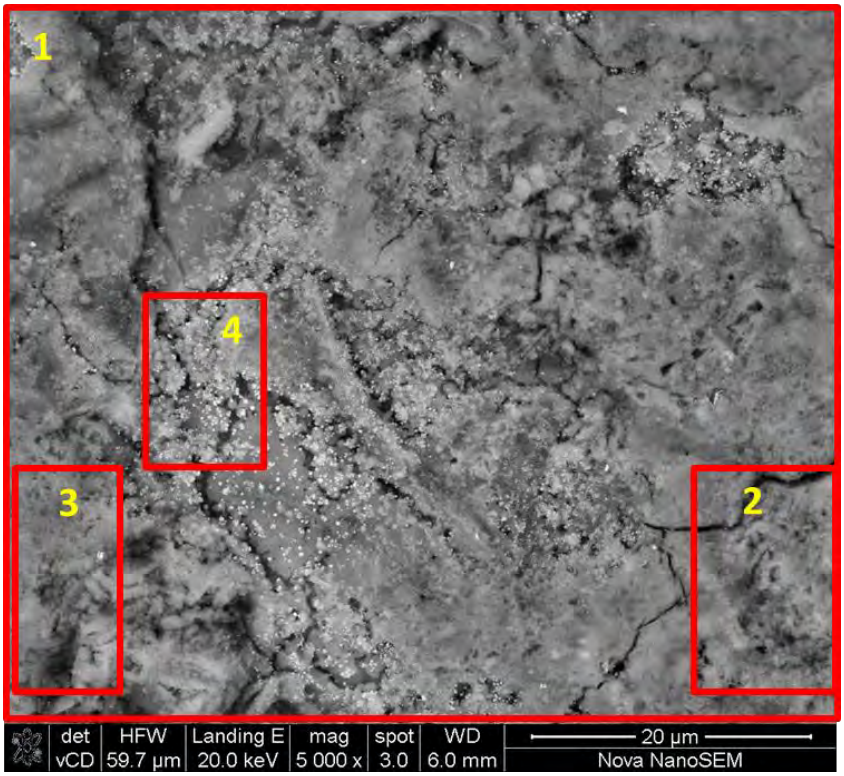

Figure A.21. SEM image of a chalcopyrite cube described in Table 7.6 reactor C, in which there were no glass beads in the reactor. This block was left in the reactor after completion of the experiment and pH was not controlled. At time of sampling, solution pH was 8.8, 25°C, under oxygen.

Table A.4. EDS spectrum for Figure A.21.

Spectrum	O	Si	S	Fe	Cu
1	58.9	1.6	7.8	27.8	3.9
2	62.3	1.6	3.9	31	1.2
3	60.4	2.1	3.3	33.3	0.9
6	45.8	1.6	17.7	25.4	9.6

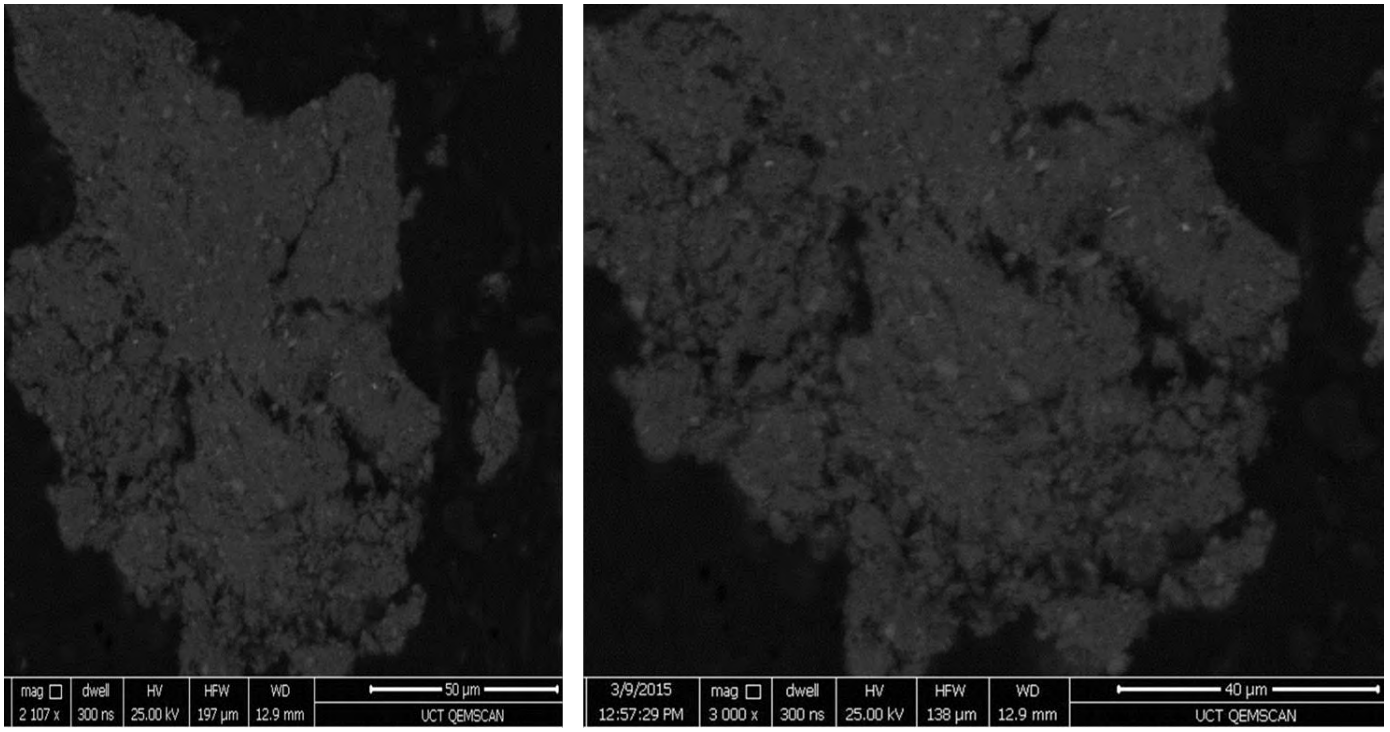

Figure A.22. Debris from reactor B Table 7.6, leaching chalcopyrite cubes in a reactor with glass beads. Debris collected after 4 days of leaching in in ammonia-ammonium sulphate solutions 3 M (NH_3+NH_4^+), 25°C, pH 9.6±0.15 25°C under oxygen